JAERI-M
82-175

JAPANESE CONTRIBUTIONS TO IAEA INTOR WORKSHOP, PHASE IIA

CHAPTER VIII : TRITIUM AND BLANKET

November 1982

Yuji NARUSE, Toru HIRAOKA, Kichizo TANAKA,
Yuji MATSUDA, Hiroshi YOSHIDA, Kenji OKUNO,
Satoshi KONISHI, Ken TOMABECHI, Hitoshi WATANABE,
Tadashi TAKAHASHI, Toshiaki KURASAWA, Kenji NODA,
Hidefumi TAKESHITA, Hiroji KATSUTA, Hiroshi KUDO,
Yoshikazu YOSHIDA, Morinobu KOKUBU, Hiroshi KATAGIRI,
Junichi ADACHI*, Toshiichi AOTA*, Shingo HIRATA*,
Takeshi KOBAYASHI*, Toshimasa KURODA*, Masahiro MISUMI*,
Kensuke MOHRI*, Seiji MORI*, Tatsushi SUZUKI*,
Nobuyuki TAKAHASHI*, Yoshihisa TANAKA* and Seiichiro YAMAZAKI*

日本原子力研究所
Japan Atomic Energy Research Institute

JAERI-M レポートは，日本原子力研究所が不定期に公刊している研究報告書です。
入手の問合わせは，日本原子力研究所技術情報部情報資料課（〒319—11 茨城県那珂郡東海村）あて，お申しこしください。なお，このほかに財団法人原子力弘済会資料センター（〒319—11 茨城県那珂郡東海村日本原子力研究所内）で複写による実費頒布をおこなっております。

JAERI-M reports are issued irregularly.
Inquiries about availability of the reports should be addressed to Information Section, Division of Technical Information, Japan Atomic Energy Research Institute, Tokai-mura, Naka-gun, Ibaraki-ken 319—11, Japan.

© Japan Atomic Energy Research Institute, 1982

編集兼発行　日本原子力研究所
印　　刷　日立高速印刷株式会社

Japanese Contributions To IAEA INTOR Workshop, Phase IIA Chapter VIII : Tritium and Blanket

Yuji NARUSE, Toru HIRAOKA, Kichizo TANAKA, Yuji MATSUDA, Hiroshi YOSHIDA, Kenji OKUNO, Satoshi KONISHI, Ken TOMABECHI, Hitoshi WATANABE[+1], Tadashi TAKAHASHI[+1], Toshiaki KURASAWA[+1], Kenji NODA[+1], Hidefumi TAKESHITA[+1], Hiroji KATSUTA[+1], Hiroshi KUDO[+2], Yoshikazu YOSHIDA[+3], Morinobu KOKUBU[+3], Hiroshi KATAGIRI[+3], Junichi ADACHI*, Toshiichi AOTA*, Shingo HIRATA*, Takeshi KOBAYASHI*, Toshimasa KURODA*, Masahiro MISUMI* Kensuke MOHRI*, Seiji MORI*, Tatsushi SUZUKI*, Nobuyuki TAKAHASHI*, Yoshihisa TANAKA* and Seiichiro YAMAZAKI*

Fusion Research and Development Center
Tokai Research Establishment, JAERI
(Received November, 1982)

Tritium breeding blanket is incorporated in the INTOR design based on economic and tritium availability considerations. In Phase IIA, critical issues on 'Tritium', which were identified during the Phase I Workshop, were investigated. Main objectives of Phase IIA are to develop a tritium breeding blanket and to evaluate tritium containment.

Data base assesments of tritium containment were made. The design of the tritium breeding blanket was also revised.

Keywords: INTOR, Tritium, Blanket, Permeation, Contaimination Tritium System, Li_2O

+1 Division of Nuclear Fuel Research, Tokai Research Establishment, JAERI.

+2 Division of Radioisotope Production, JAERI.

+3 Division of Health Physics, Tokai Research Establishment, JAERI.

* Kawasaki Heavy Ind., Ltd.

INTOR フェーズⅡAワークショップ検討報告書
第 Ⅷ 章 ： トリチウムおよびブランケット

日本原子力研究所東海研究所核融合研究開発推進センター

成瀬 雄二・平岡 徹・田中吉左右・松田 祐二・吉田 浩
奥野 健二・小西 哲之・苫米地 顕・渡辺 斉[+1]・高橋 正[+1]
倉沢 利昌[+1]・野田 健治[+1]・竹下 英文[+1]・勝田 博司[+1]・工藤 博司[+2]
吉田 芳和[+3]・国分 守信[+3]・片桐 浩[+3]・安達 潤一[*]・青田 利一[*]
平田 慎吾[*]・小林 武司[*]・黒田 敏公[*]・三角 昌弘[*]・毛利 憲介[*]
森 清治[*]・鈴木 達志[*]・高橋 伸行[*]・田中 義久[*]・山崎誠一郎[*]

（1982年11月1日受理）

国際トカマク炉（INTOR）では，トリチウムの有効利用および経済性の観点からトリチウム増殖ブランケットを設置するように計画されている。フェーズⅡAの主な目的は，フェーズⅠの概念設計で明らかとなった“トリチウム”に関する重要項目の検討を深め，トリチウム格納に関する評価検討を行い，トリチウム増殖ブランケットの設計を進展させることである。

本報告書は，トリチウム格納に関するデータベースの評価結果およびより現実的な増殖ブランケットの検討結果をまとめたものである。

+1 燃料工学部
+2 アイソトープ事業部製造部
+3 保健物理部
* 川崎重工業㈱

CONTENTS

Page

目　　次

VIII TRITIUM AND BLANKET

1. Introduction

Tritium breeding blanket is incorporated in the INTOR design based on economic and tritium availability considerations. In Phase II A, critical issues on 'Tritium', which were identified during the Phase I Workshop, were investigated. Main objectives of Phase II A are to develop a tritium breeding blanket and to evaluate tritium containment. The reference blanket concept is based on solid breeder which offers the advantages of engineering design simplicity and relatively low stored chemical energy. From the viewpoints of continuous extraction of generated tritium, there exist various uncertainties in design parameters. It is indispensable to develop a tritium breeding blanket concept which is less sensitive to the uncertainties. Accumulation of basic data and revision of a tritium breeding blanket were done on the critical issues mentioned below and the future R&D items were identified.

a Tritium Permeation into Primary Coolant

- Evaluate models and experimental data for tritium permeation
- Estimate tritium permeation rates into water coolants of first wall and divertor/limiter plates
- Determine the maximum permissible concentration of tritium in water coolant
- Compare methods for tritium separation from water coolant
- Calculate tritium inventory in first wall and divertor/limiter plates

b Tritium Contamination of Reactor Environment

- Identify 'routine and normal' and accidental sources of tritium contamination in the reactor environment
- Confirm a strategy for building air circulation
- Evaluate plausibility of personnel access strategy
- Calculate tritium dose to persons in key locations in reactor building

c Tritium Breeding Blanket

- Completion of data base for the reference solid breeder material (Li_2O)
  - thermophysical properties
  - operation temperature range
  - data/model required in evaluation of tritium extraction and inventory
  - compatibility with structural material
  - improvement of effective thermal conductivety of breeder
- Revision of tritium breeding blanket design

2. Tritium permeation into coolant

2.1 Tritium permeation rates

2.1.1 Theoretical models and calculations

(a) Estimation of Tritium Permeation into Coolant

(1) Introduction

The INTOR first wall and divertor plate are exposed to large flux densities of energetic neutral/charged tritium. Energetic tritium particles penetrate first wall and divertor plate, in which they are scattered by the lattice atoms and lose energy by interaction with the electron and the lattice atoms. Once sufficiently slowed down, they move to the plasma region and to the coolant region in a diffusive fassion. Returning rate to the plasma region plays an important role with regard to determining the permeation rate into the coolant. This returning rate appears to be limited by diffusion process and/or surface recombination rates.

In this section, the implanted tritium release rate into the coolant is evaluated by using the diffusion and recombination models.

(2) Analytical condition

Main analytical condition are as follows:

a) First wall

i)	Tritium particle flux	3.1×10^{-4} Ncc-T_2/cm^{2}sec
ii)	Tritium particle energy	200 eV
iii)	Permeation depth in first wall	30 Å
iv)	Bombardment area of tritium particle flux	
	(Inboard)	114 m^2
	(Outboard)	266 m^2

v) Temperature distribution

(Outboard)

	Temperature (°C)											
(Plasma)	300	280	260	240	220	200	180	160	140	120	100 (Coolant)	100
	1.67	2.15	1.79	1.67	1.44	1.20	1.08	0.96	0.84	0.60		1.50
	Thickness (mm)											

(Inboard)

	Temperature (°C)											
(Plasma)	360	340	320	300	280	260	220	180	140	120	100 (Coolant)	100
	2.3	2.0	1.7	1.5	1.3	1.2	2.0	2.0	1.3	0.3		1.5
	Thickness (mm)											

b) Divertor

i) Tritium particle flux 1.5×10^{-2} Ncc-T_2/cm^{2}sec

ii) Tritium particle energy 400 eV

iii) Penetration depth in tungsten 40 Å

iv) Surface area 160 m^2

v) Temperature distribution

	Temperature (°C)									
(Plasma)	270	240 (W)	220	210	200 (Cu)	180	(Coolant)	120 (Cu)	100 (SS)	(End wall)
	1.4	1.0	0.6	0.9	2.1	0.8		6.0	9.0	
	Thickness (mm)									

(3) Calculation Model

a) Diffusion Model

Energetic tritium particle penetrates into the metal by the order of 10 Angstrom. Once sufficiently slowed down at its projected range, it moves to the plasma region and also to the coolant region in a diffusive fashion. The flow of implanted tritium particles is depicted in Fig. VIII-2-1. Returning rates from the surface to the plasma region are assumed to be limited by diffusion process.

Therefore, a steady state mass balances in the metal are:

$$J = J_1 + J_2 \qquad \text{(Total mass balance)} \qquad \text{(VIII-2-1)}$$

$$J_1 = D_1 \cdot (C_2 - C_1)/X_1 \qquad \text{(Diffusion flux to the plasma side)} \qquad \text{(VIII-2-2)}$$

$$J_2 = D_2 \cdot (C_2 - C_3)/X_2 \qquad \text{(Diffusion flux to the coolant)} \qquad \text{(VIII-2-3)}$$

$$C_1 = S \cdot P^{\frac{1}{2}} \qquad \text{(Tritium concentration at the surface)} \qquad \text{(VIII-2-4)}$$

where

J : Tritium bombardment flux (Ncc-T_2/sec cm^2)

J_1,J_2: Diffusion flux to the plasma and coolant side (Ncc-T_2/sec cm^2)

C_1 : Tritium concentration at the surface of plasma side (Ncc-T_2/cc-metal)

C_2 : Tritium concentration at the penetration depth (Ncc-T_2/cc-metal)

C_3 : Tritium concentration at the surface of the coolant side (Ncc-T_2/cc-metal)

D_1 : Diffusion coefficient at the penetration depth (cm^2/sec)

D_2 : Diffusion coefficient of plate (cm^2/sec)

P_1 : Partial pressure of tritium in the vacuum vessel (Torr)

X_1 : Penetration depth (cm)

X_2 : Thickness of first wall or divertor plate (cm)

S : Solubility coefficient (Ncc-T_2/cc-metal $Torr^{\frac{1}{2}}$)

Table VIII-2-1 shows the diffusion coefficients and tritium solubility coefficients.

b) Recombination Model

Returning rate governed by the recombination process is proportional to the square of the tritium concentration directly below the surface.

Therefore, a steady state mass balances are:

$$J = J_1 + J_2 \qquad \text{(VIII-2-5)}$$

$$J_1 = Kr\ (C_1)^2 \qquad \text{(VIII-2-6)}$$

$$J_2 = D_2 C_1 / X_2 \qquad \text{(VIII-2-7)}$$

where

Kr : T_2 molecular recombination rate constant

Knowledge about the value of the recombination rate constant Kr is presently uncertain. The data of the recombination rate constant are summarized in Fig. VIII-2-2.

(4) Results and Discussion

The distribution of tritium concentration in outboard and inboard first wall are shown in Fig. VIII-2-3 and Fig. VIII-2-4, respectively. The tritium concentration calculated from recombination model is higher than that from diffusion model. It seems from this results that recombination rather than diffusion is the rate limiting process for desorption of tritium from injected surface. However, the near surface tritium concentration obtained from recombination model is strongly affected by the surface condition, such as cleanliness, roughness, etc.

The distribution of tritium concentration in divertor plate is shown in Fig. VIII-2-5. For lack of data of recombination rate constant Kr on tungstem, the comparison between diffusion and recombination model can not be shown here. According to the diffusion model, tritium concentration in divertor plate is larger than that in first wall.

Table VIII-2-2 shows the tritium permeation rate into the coolant. As it can be seen from the results of the diffusion model, the permeation rate through the divertor plate is remarkably as large as 620 Ci/day.

Table VIII-2-1 Tritium solubility and diffusion coefficient

Stainless steel Solubility coefficient [1-5] ---- $6.78 \times 10^{-2} \exp(-1094.7 / T)$ STP cc-T_2/cc-steel $torr^{\frac{1}{2}}$ Diffusion coefficient [5,6] ---- $9.4 \times 10^{-3} \exp(-6873.8 / T)$ cm^2/sec
Tungsten Solubility coefficient [7] ---- $4.81 \times 10^{-6} \exp(-11123 / T)$ STP cc-T_2/cc-metal $torr^{\frac{1}{2}}$ Diffusion coefficient [7] ---- $2.37 \times 10^{-3} \exp(-4529 / T)$ cm^2/sec
Copper Diffusion coefficient [8] ---- $1.32 \times 10^{-2} \exp(-5687 / T)$ cm^2/sec

Table VIII-2-2 Tritium Permeation Rates into the Coolant

		Tritium permeation rate(Ci/day)		
		Diffusion model	Recombination model	
			USA data	EC data
first wall	outboard ($266\ m^2$)	1.6	34.	152.
	inboard ($144\ m^2$)	0.33	13.5	-
divertor plate ($160\ m^2$)		620.	(lack of data Kr)	
blanket ($2100\ m^2$)		0.7		

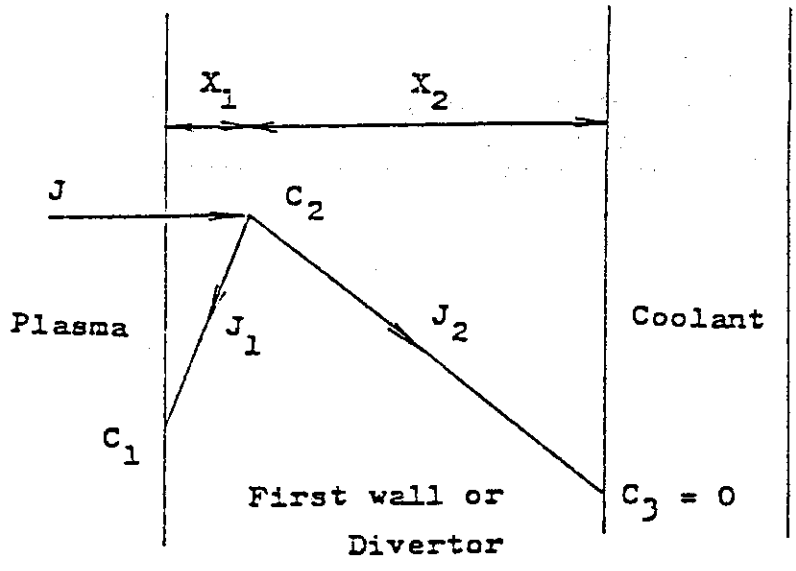

Fig. VIII-2-1 Schematic Flow of Implanted Tritium Particles

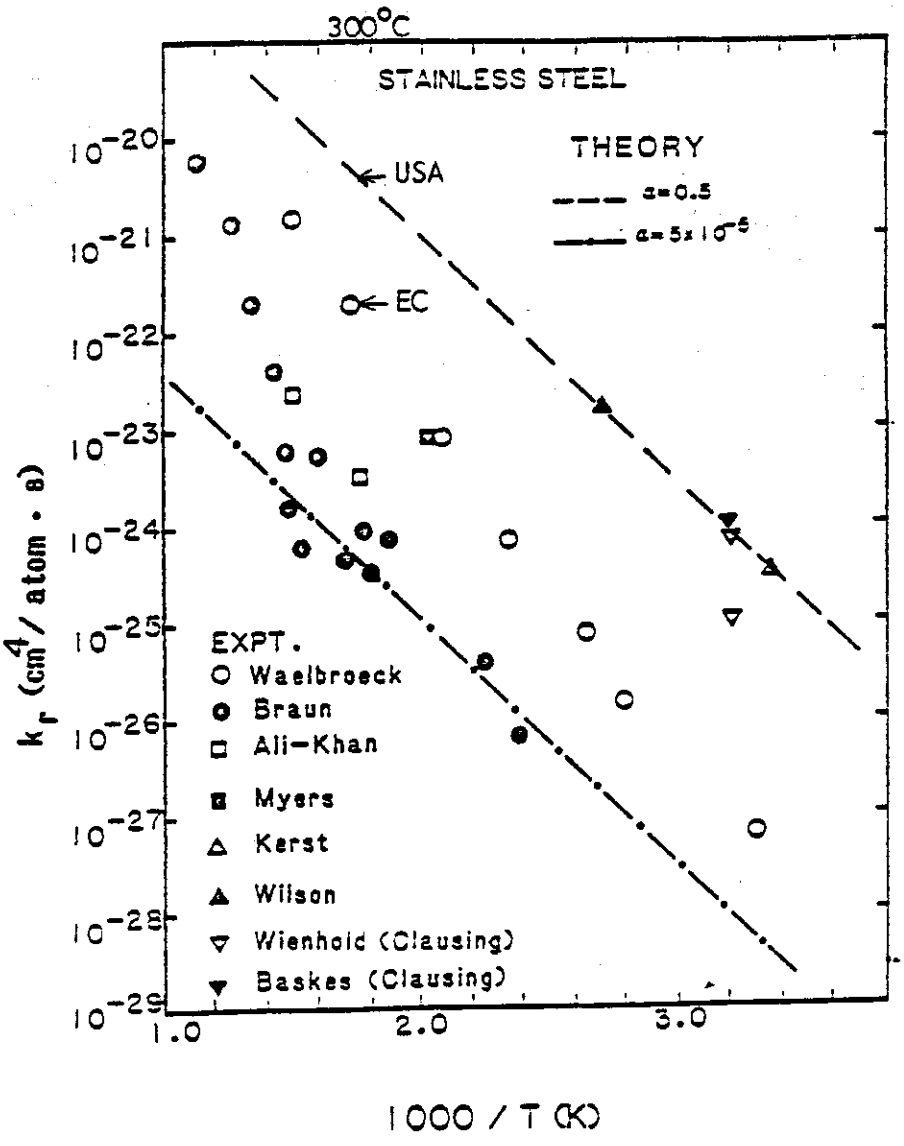

Fig. VIII-2-2 Recombination Rate Constant(K_r) on Stainless Steel [9]

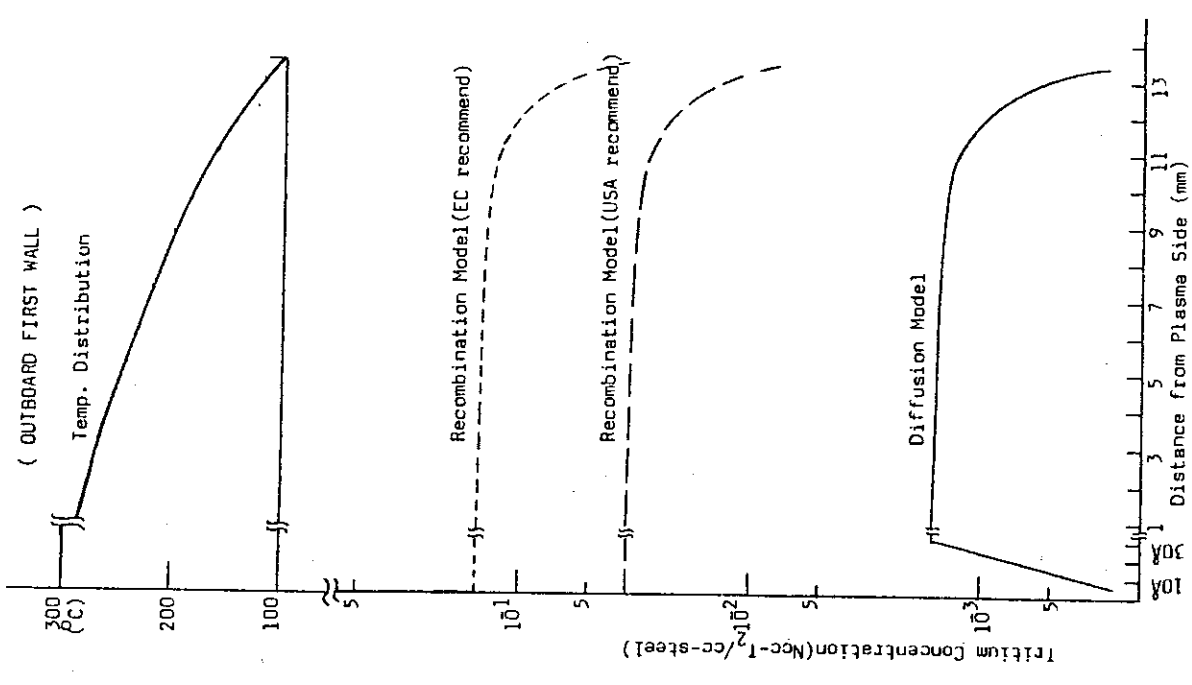

Fig. VIII-2-3 Tritium concentration in outboard first wall

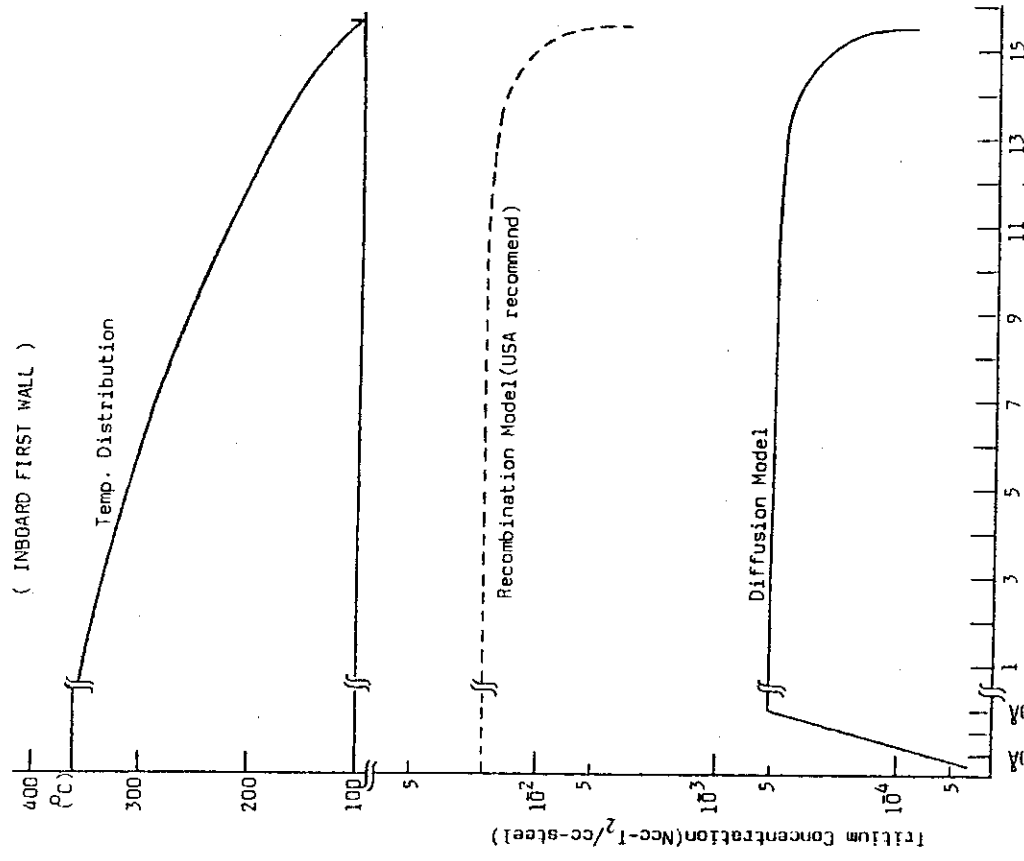

Fig. VIII-2-4 Tritium concentration in inboard first wall

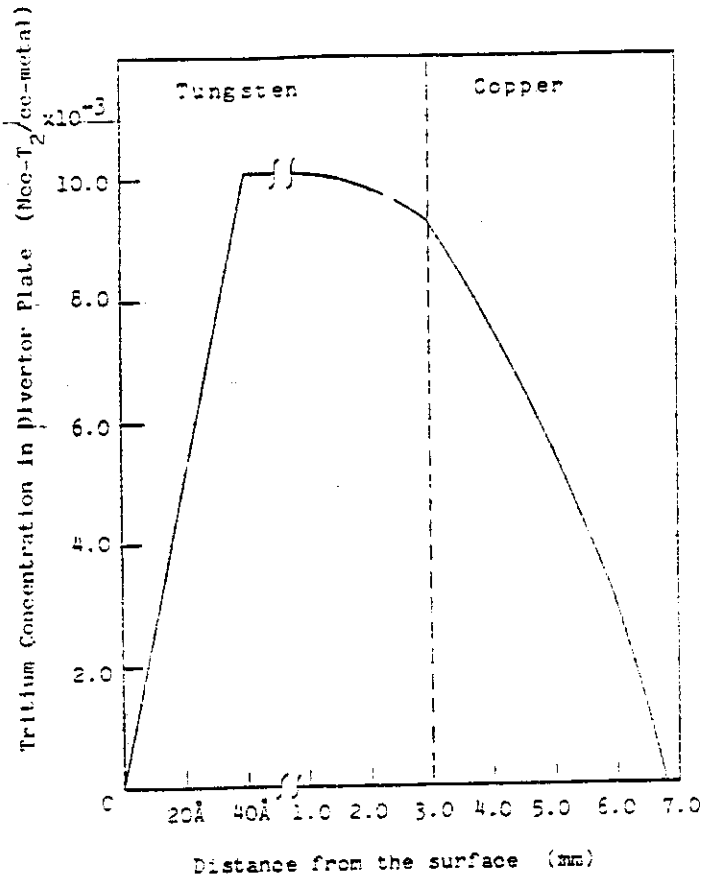

Fig. VIII-2-5 Tritium concentration in divertor plate

2.1.2 Experimental results

(a) Experimental Studies of Deuterium Permeation under Ion Bombardment

Energetic tritium particles implanted into the INTOR first wall are mostly reemitted into the plasma side, and partly permeated into the coolant side. However, it is suggested that the permeation rate into the coolant side may be considerably influenced by the radiation damages.

Recently, Tanabe et al.[10] have measured the permeation rate of deuterium implanted into the type 316 stainelss steel with energy of 20 KeV, and has found the effects of radiation damages produced near the projected range of implanted deuteron. Preliminary results of these works are summarized below;

Detailed procedure for the measurement has been described elsewhere[10]. Deuterons produced in an RF ion source are accelerated to 20 keV and injected to a specimen. The maximum flux of the deuteron beam is 9×10^{18} $D^4/m^2.S$. For the measurement of the permeation rate, deuterium which comes out to the other of the injected surface of the specimen is analyzed by a QMS. Two kinds of the measurement for the permeation rate are made in most case. One, which is hereafter called "injection", is the measurement of change of permeation rate immediately after the beam-on. The other, which is called "evolution", is the monitor of change of permeation rate shortly after the beam-off.

Fig. VIII-2-6 showed the change of permeation rate for 316 SS with two successive runs. When the beam was turned on, the permeation rate

increased up to a maximum value in a few minutes (injection curve) by the following gradual decrease. When turned off the beam, the permeation rate rapidly decreased (evolution curve). After sufficiently low permeation rate was achieved, the second run was successively performed. Although similar injection and evolution curves were obtained, the maximum value at the second run was smaller than that of the first run. Such depression of the maximum permeation rate with following runs was observed in all measurements.

It showed continuous decrease of the permeation rate for extended irradiation in Fig. VIII-2-7. Similar behaviour was also observed for a nickel specimen as shown in Fig. VIII-2-8. However, the decrease of the permeation rate through a nickel specimen was more pronounced than 316 SS.

The diffusion coefficient and the maximum permeation rate of deuterium for 316 SS were shown in Fig. VIII-2-9. These diffusion coefficients was obtained from the injection and evolution curves according to a simple diffusion model. The logarithms of diffusion coefficients determined from the evolution curve were linear with reciprocal temperature, and the diffusion coefficients from injection to virgin surface were in good agreement with those given by gaseous charging methods shown in a broken line. The valves of diffusion coefficient obtained from the injection curve were slightly smaller than those from the evolution curve at higher than 400°C.

Decreasing phenomenon in the permeation rate has never been observed in the usual permeation studies with gaseous charging methods.

Since the permeation rate was represented as the product of the diffusion coefficient of the bulk and the surface concentration near the projected range, the decrease in the permeation rate could be attributed to the decrease in diffusion coefficient and/or in surface concentration. Under the bombardment of energetic deuterons various types of defects such as vacancies, dislocations, interstitials and so on were produced near the projected range (~ 0.1 μm), and they were inferred to contribute to the decrease in permeation rate in two ways. The first was the decrease of surface concentration due to the increase of reemission rate of implanted deuterium from the injected side. With increasing fluence, vacancies produced by irradiation at near surface region would lead to the formation of micro pores or cracks which initiated channeling effect at or near surface. The second was trapping of deuterium by defects which had diffused into the deeper region than the projected range.

An effort to improve a diffusion model so as to take the effect of radiation damage is now being made.

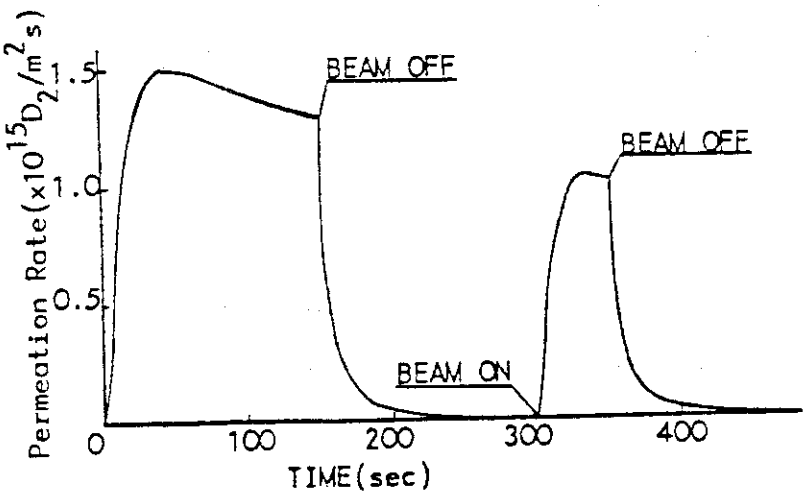

Fig. VIII-2-6 Change of permeation rate when beam bombardment was started and stopped for 316 SS of 0.05 mm thick at 440°C

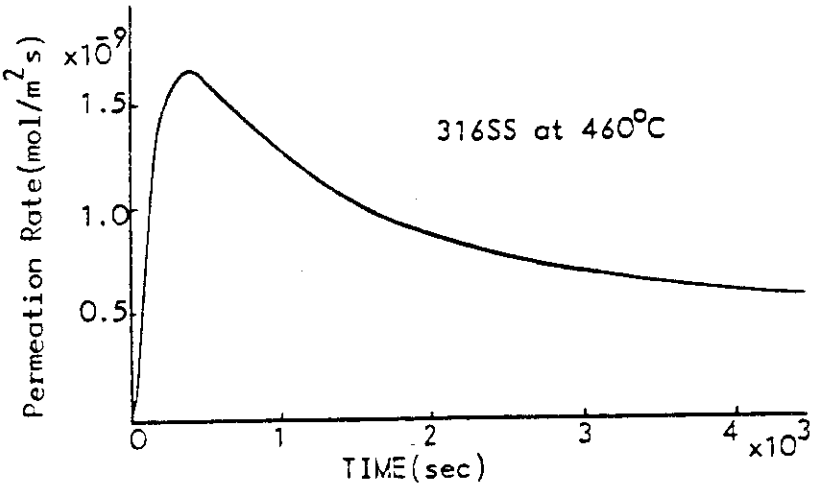

Fig. VIII-2-7 Change of deuterium permeation rate with time for 316 SS of 0.1 mm thick at 460°C

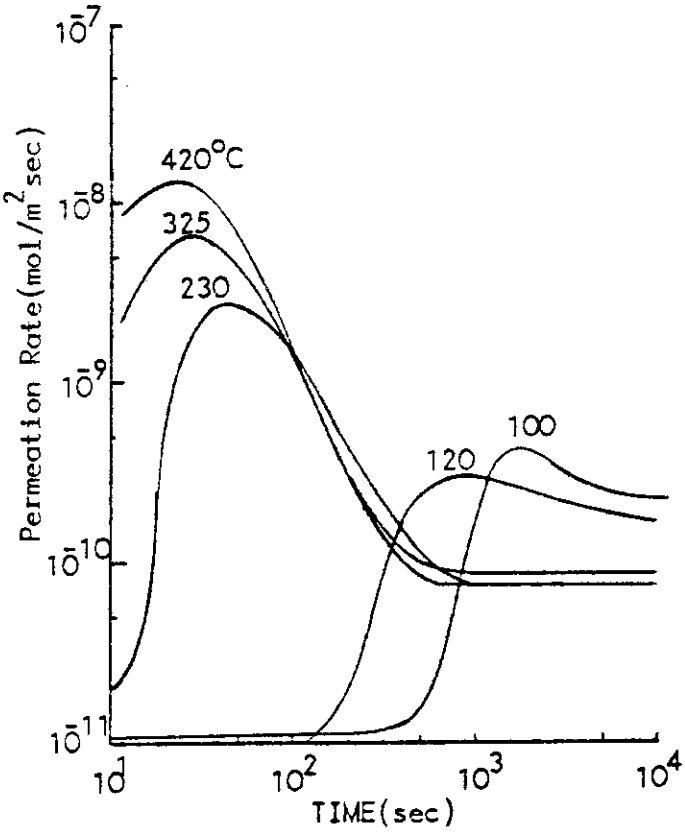

Fig. VIII-2-8 Change of permeation rate with time for Ni of 0.1 mm thick

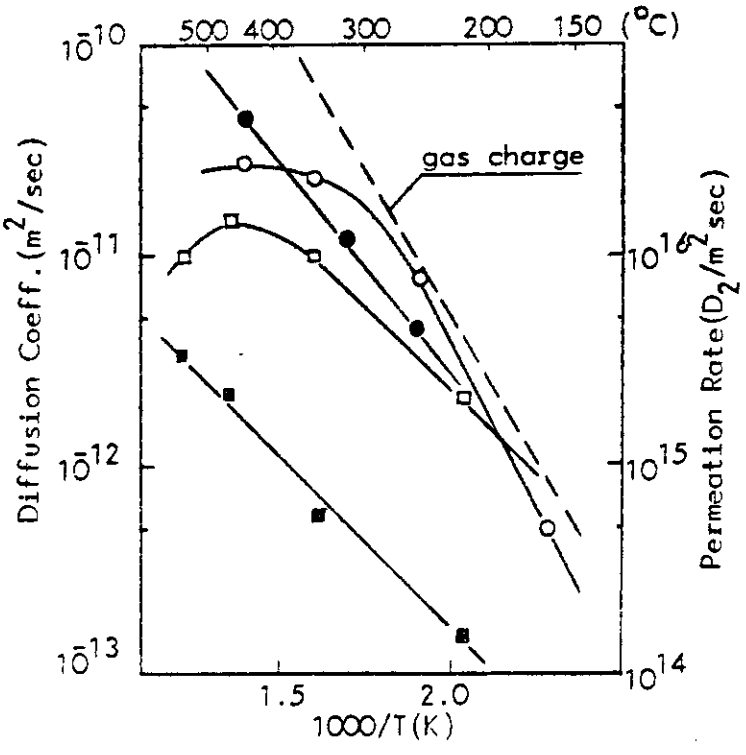

Fig. VIII-2-9 ○ and □ obtained from increasing curve for sample of 0.05 and 0.1 mm thick, respectively, and ● from decreasing curve for sample of 0.1 mm.

2.1.3 Calculational resuls

Calculational resuls of tritium permeation rate into coolant are shown in 2.1.1.

2.1.4 Permeation barrier

(a) Integrity of Oxide Film Layer as Tritium Permeatio Barriers

(1) Introduction

The permeation of tritium through the first wall and divertor plate is an essential problem to be clarified for the design of primary cooling system. Perhaps the most economical barrier to tritium permeation through these metal would be an oxide film layer coated on coolant side. Recent studies of tritium permeation into the coolant environment indicate that naturally-formed oxide layers can afford to reserve the permeation resistance. However, there is some risk for making extrapolation of these results because the integrity of oxide layer is not known during operation.

Preliminary study[11] of the oxide film integrity has been carried out under the condition of very low oxidation potential. The barrier effectiveness of oxide film layer has also been studied with the different surface-treated specimens.

(2) Experimental

The permeation time-lag method has been used to determine the permeabilities of hydrogen and deuterium for type 304 stainless steel at the temperature range of 812 ∿ 1,190 K, and the pressure range of 10^{-3} ∿ 10^{-1} MPa.

The total amount of H_2 gas permeating (Q) through the membrane of area (A) and thickness (Δx) in time (t) was given by following equation:

$$Q = \frac{DC_oA}{\Delta x} \quad t - \frac{(\Delta x)^2}{6D} \qquad \text{(VIII-2-8)}$$

where D was diffusion coefficient and C_o was the concentration of hydrogen at the inlet surface of the specimen corresponding to the inlet hydrogen pressure P_o. Equation (VIII-2-8) was derived from a solution of the membrane - diffusion problem, where hydrogen concentration C_1 at the outlet surface was zero. The time-lag (t_o) determined by extrapolation of steady state portion of the pressure-time curve was related to D by:

$$t_o = (\Delta x)^2/6D \qquad \text{(VIII-2-9)}$$

The specimens used in the experiment had an area of 1.77×10^{-4} m^2 and two kinds of thickness of 1×10^{-4} and 3×10^{-4} m.

(3) Results and Discussion

The compositions of the specimens used for the measurement were shown in Table VIII-2-3. The oxide film on the specimens were mainly composed of iron and chromium oxides, and a little amount of manganese and silicon oxides. In reducing atmosphere such as H_2 gas, iron oxide could be easily converted to metallic iron. Therefore, in the stainless steel-hydrogen system the characteristics of the chromium, manganese and silicon oxides at the surface were important in evaluating the hydrogen transport phenomena. Fig. VIII-2-10 showed the hydrogen-reduction equilibrium corresponding to the equation of

$$Cr_2O_3 + 3H_2 = 2Cr + 3H_2O \qquad \text{(VIII-2-10)}$$

$$MnO + H_2 = Mn + H_2O \qquad \text{(VIII-2-11)}$$

$$SiO_2 + 2H_2 = Si + 2H_2O \qquad \text{(VIII-2-12)}$$

The upper region of each curve were the oxide stable regions and the lower were the metal.

The permeabilities in increasing and in successively decreasing temperatures for type 304 stainless steel with oxide films measured at about 0.1 MPa (1 atm) of hydrogen pressure were shown in Fig.VIII-2-11. The time variations of the permeability at several temperature were depicted in Fig.VIII-2-12. At the temperature of 986 K variation of the permeability with time was not observed.

This results have indicated that oxide film layer were stable even under condition where the oxidation potential was very low. However, the permeability increased with time at the temperature higher than 1,050 K were shown in Fig. VIII-2-12. This increase of the permeability could be recognized as a result of reduction of the oxide film (mainly Cr_2O_3) by H_2 gas charge. Owing to Fig. VIII-2-10 water concentration in the H_2 gas was estimated to be about 20 ppm by volume as mentioned above. Therefore, manganese and silicon oxides in the oxide film of the specimen were considered to be unreduced by the H_2 gas at 1,190 K.

Since the oxidation potential of water in primary cooling system is higher than that in this experiment, it may be possible with the use of a water coolant to sustain the oxide film barrier.

Table VIII-2-3 Compositions of specimens(type 304 stainless steel) used for measurement

Thickness (mm)	Alloy components (%)						
	Ni	Cr	Mn	Si	P	S	C
0.1	9.2	19.1	1.13	0.42	<0.04	<0.03	<0.08
0.3	9.3	19.6	1.01	0.44	<0.04	<0.03	<0.08

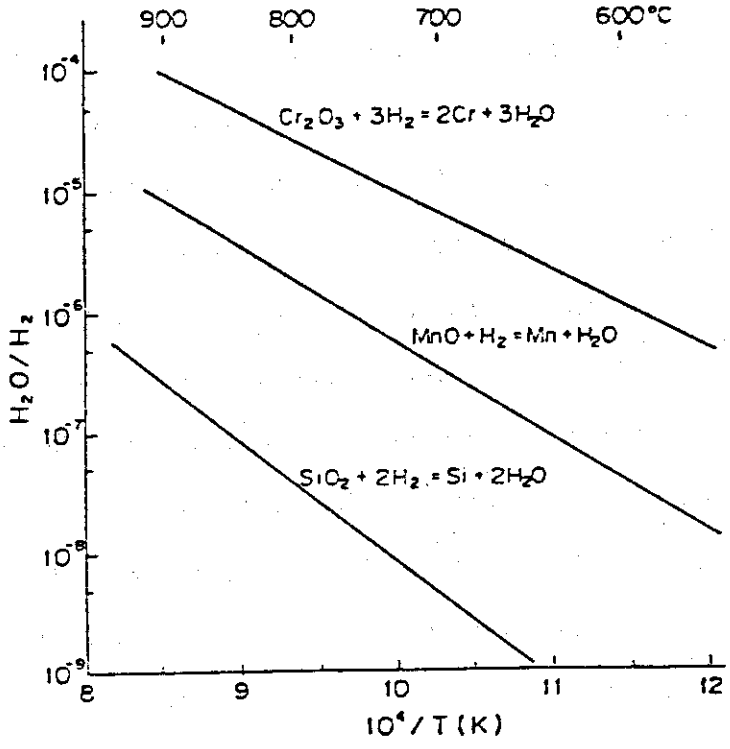

Fig. VIII-2-10 Hydrogen-reduction equilibriums for Cr_2O_3, MnO, and SiO_2 by H_2 gas

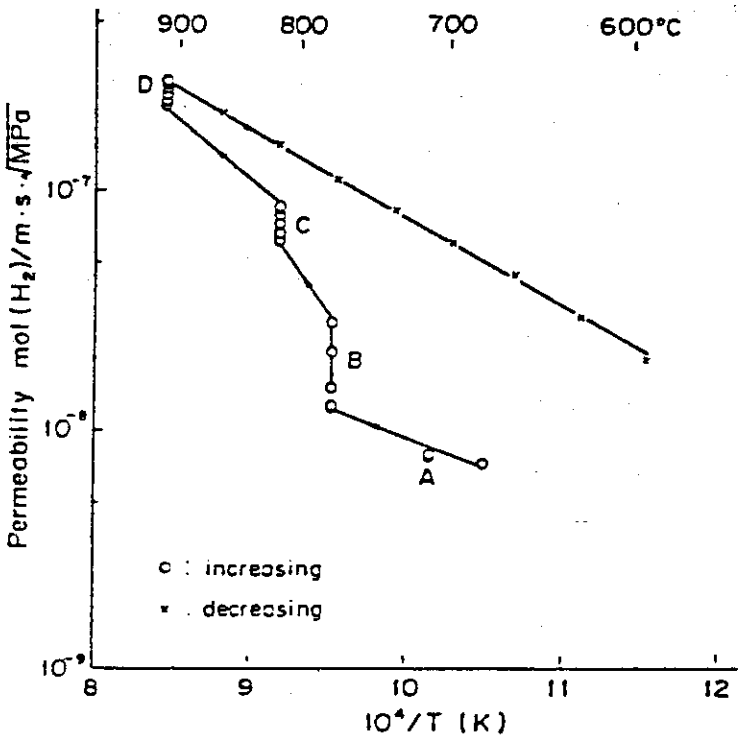

Fig. VIII-2-11 Temperature variation of hydrogen permeation for type 304 stainless steel with oxide film

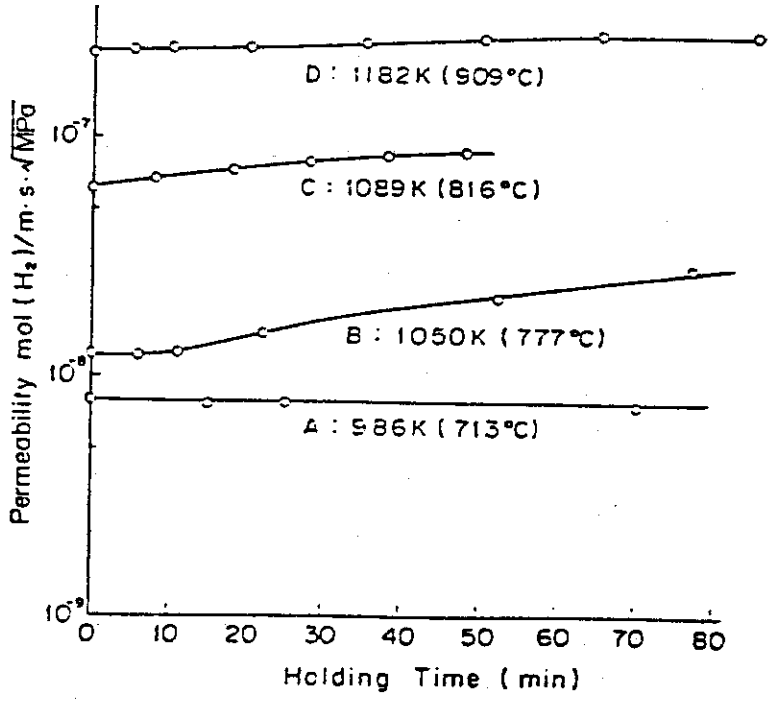

Fig.VIII-2-12 Time variation of hydrogen permeability for type 304 stainless steel with oxide film at several temperature

(b) Coating and vacuum gap as tritium permeation barrier

Tritium permeation rate through the divertor plate is remarkably large. Perhaps the most economical barrier to tritium permeation would be to allow oxide film layer on the coolant side. This oxide film layer seems to reduce the permeation rate by a factor of two or three. The integrity of oxide film layer, however, is uncertain under the non-equilibrium condition.

Additional permeation barrier to reduce the permeation rate by several orders of magnitude is discussed here.

a) Non-metallic coating

The diffusion coefficients for non-metallics are many orders of magnitude lower than the diffusion coefficients for the divertor construction materials (W, Cu). Fig. VIII-2-13 shows the diffusion coefficients of non-metallics compared with the divertor construction materials.

This results suggests that non-metallics would be effective tritium barriers if a suitable method of deposition can be devised and coating integrity can be maintained during actual operation. This concept is shown schematically in Fig. VIII-2-14.

Effectiveness of tritium diffusion barriers is given by:

$$\text{Decreasing factor} = \frac{\frac{X_1}{D_1}}{\left(\frac{X_1}{D_1}\right) + \left(\frac{X_2}{D_2}\right)} \qquad \text{(VIII-2-13)}$$

where

D_1, D_2 : Diffusion coefficients in substrate and coating, respectively

X_1, X_2 : Thickness of substrate and coating, respectively.

Table VIII-2-4 shows the decreasing factor of typical case.

b) Vacuum gap between tungsten and copper

The concept of vacuum gap is shown schematically in Fig. VIII-2-15. Vacuum gap between tungsten and copper is provided to the implanted tritium sink. Implanted tritium flux can not be directly diffused into the divertor coolant. Therfore, tritium permeation rate depends on the tritium concentration in copper related to the partial pressure within vacuum gap.

Table VIII-2-5 shows the decreasing factor in this case.

Table VIII-2-4 Effectiveness of Non-Metallic Coatings as Implanted Tritium Permeation Barriers

$$\text{Decreasing factor} = \frac{\left(\frac{X_1}{D_1}\right)}{\left(\frac{X_1}{D_1}\right) + \left(\frac{X_2}{D_2}\right)}$$

where , X_1 = 0.68 cm (tritium path length through divertor plate)

D_1 = 1.12×10^{-7} cm^2/sec (equivalent diffusion coefficient in divertor plate)

for T = 220 ^{o}C at coating material and X_2(thickness of coating) = 0.01 cm ,

Coatings	Decreasing Factor
Al_2O_3	10^{-12}
Si-doped PyC	10^{-18}
LTI PyC	10^{-11}

Table VIII-2-5 Effectiveness of Vacuum Gap as Implanted Tritium Permeation Barriers

$$\text{Decreasing factor} = \frac{R_1}{R_2} = \frac{\text{(Implanted permeation rates into the coolant)}}{\text{(Permeation rate related to the partial pressure near copper surface)}}$$

where , R_1 = 620 Ci/day

for K	(permeation coefficient in Cu , at 220°C)	$\doteq 5 \times 10^{-12}$	Ncc/s/cm/torr$^{\frac{1}{2}}$
L	(thickness)	= 0.38	cm
S	(surface area)	= 160	m^2
P	(partial pressure near Cu surface)	$= 1 \times 10^{-3}$	torr

Decreasing factor $\doteq 2 \times 10^{-4}$

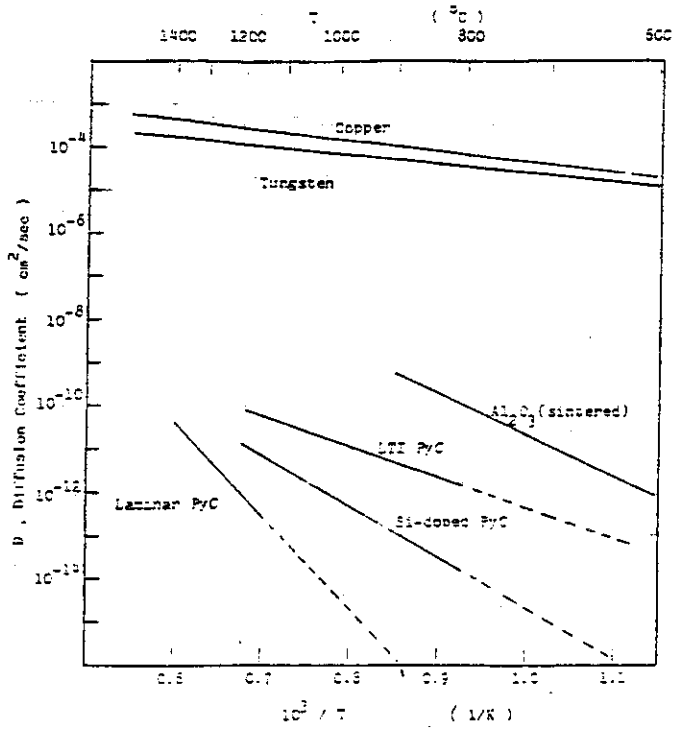

Fig. VIII-2-13 Comparison of tritium diffusion coefficient in non-metallics and divertor materials [12,13]

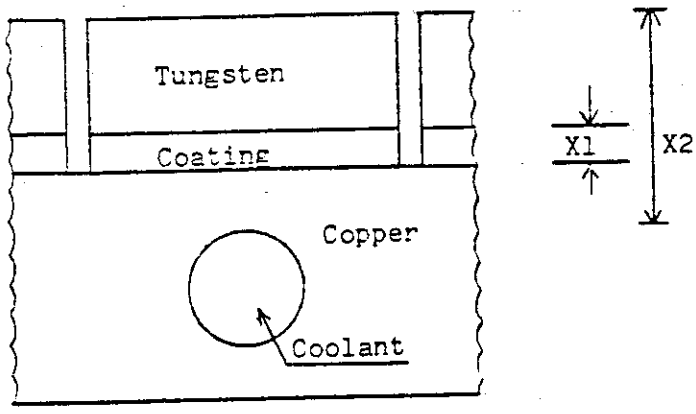

Fig. VIII-2-14 Concept of Non-Metallic Coating as Implanted Tritium Permeation Barriers

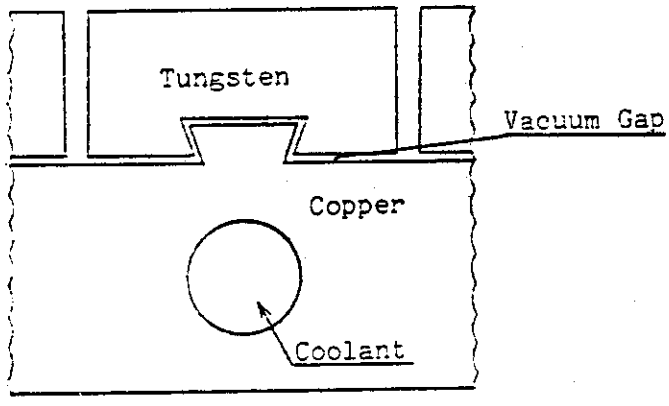

Fig. VIII-2-15 Concept of Vacuum Gap as Implanted Tritium Permeation Barriers

2.1.5 Gas releases during dwell time

(a) Evaluation of Tritium Releases during Maintenance (out gassing)

(1) Introduction

During the plant operation, tritium dissolves into the components placed in the plasma vacuum vessel. This dissolved tritium concentration depends on tritium partial pressure near the component and energetic charged/neutral tritium flux. This dissolved tritium is the source of tritium release to the reactor room during the repair and maintenance work. The evaluation of tritium release is carried out here. In addition, the methods of reducing the tritium releases into the reactor room are discussed.

(2) Design Conditions

a) Components in the plasma vacuum vessel

Components placed in plasma vacuum vessel are classified into three groups. The surface area, material and temperature distribution (during the reactor operation) of components are shown in Table VIII-2-6.

b) Tritium partial pressure and energetic tritium flux during the reactor operation

Tritium partial pressure near the components and the energetic tritium flux are shown in Table VIII-2-7.

c) Tritium partial pressure diring the maintenance —— 0 (10^{-8} Torr)

d) Temperature in plasma vacuum vessel during the maintenance —— 50°C

e) Solubility and diffusion coefficient —— (See 2.1.1)

(3) Analytical Methods

a) Tritium solubility

i) Dependence on tritium partial pressure

It can be assumed that tritium solubility in the components during the reactor operation is always maintained constant on the surface of the components. Therefore, tritium solubility near surface (S_0) is given by

$$S_0 = S_1 \cdot \sqrt{P} \qquad \text{(VIII-2-14)}$$

where

S_1: solubility coefficient

P : T_2 partial pressure

On the other hand, the distribution of tritium solubility in the components is derived with Fick's second law of diffusion described below

$$\frac{ds}{dt} = D\frac{d^2S}{dx2} \qquad \text{(VIII-2-15)}$$

where

S : solubility

D : diffusion coefficient

t : reactor operating period

x : distance from the surface of component.

And the initial and boundary conditions are as follows:

at $t = 0$, $x = 0$, $S = 0$

at $x = 0$, independent of t, $s = S_0$

Under these conditions, eq (VIII-2-15) is integrated as

$$S(x,t) = S_0\left[1-\frac{2}{\sqrt{\pi}}\int_0^{\frac{x}{2\sqrt{Dt}}} e^{-y^2}\,dy\right] \qquad \text{(VIII-2-16)}$$

ii) Dependence on energetic tritium flux

Energetic particle may penetrate into the wall and diffuse back to the surface or diffuse into the coolant. The implanted tritium inventory is evaluated by using the diffusion model.(see 2.2.1 : Estimation of Tritium Permeation into Coolant)

b) Tritium release during maintenance

Consider a slab of thickness l, in which tritium remains at uniform solubility S_0. If the tritium concentration on the surface is maintained at zero, the tritium concentration in the components is derived as a function of time with Fick's second law of diffusion described below

$$\frac{dS}{dt} = D\frac{d^2S}{dx^2} \qquad \text{(VIII-2-17)}$$

and with initial and boundary conditions

at $t = 0$, $S = S_0$ (initial)

at $x = 0$, $x = l$, $S = 0$ (boundary)

Then integrating eq (VIII-2-17). The solution is obtained as

$$S = S_0\frac{4}{\pi}\left[e^{-\frac{\pi^2 Dt}{l^2}}\sin\frac{\pi x}{l} + \frac{1}{3}e^{-\frac{(3\pi)^2 Dt}{l^2}}\sin\frac{3\pi x}{l} + \cdots\right] \qquad \text{(VIII-2-18)}$$

(4) Results and Discussion

a) Tritium solubility during the reactor operation

The starting point for the analysis of tritium release problem during the maintenance will be the tritium solubility in the component during the reactor operation.

The first wall (group (I)) is made of stainless steel. The maximum temperature of outboard and inboard is 300°C and 360°C, respectively. Tritium solubility in the first wall is affected by the energetic tritium particles and tritium partial pressure near the first wall. The distributions of tritium concentration in outboard and inboard are shown in Fig. VIII-2-16 and Fig. VIII-2-17, respectively. The implanted tritium solubilities in outboard and inboard are about 40 times and 10 times larger than those related to the partial pressure, respectively. Components of group (III) are made of stainless steel and their maximum temperature are 120°C. The components are placed in tritium gas of 1.5×10^{-5} Torr. As a function of the reactor operating time, Fig. VIII-2-18 shows the distribution of tritium solubility in group (II). The solubility in internal region rises with the operating time because of lower diffusion coefficient.

The divertor plate (group (III)) is also exposed to large flux of energetic tritium particles. The distribution of tritium solubility related to the tritium particle flux and tritium partial pressure is shown in Fig. VIII-2-19. Since the tritium particle flux is very large, the tritium solubility at the projected depth is much higher value than that related to the partial pressure.

b) Tritium release during the maintenance

The dissolved tritium in the near surface layers is released to the reactor room through the access ports when the plasma vaccum vessel is opened for maintenance. The dissolved tritium moves to plasma vacuum vessel in a diffusive fashion.

As a function of time after opening the plasma vaccum vessel, the tritium distribution in stainless steel and in tungsten are shown in Fig. VIII-2-20 and Fig. VIII-2-21, respectively.

Table VIII-2-8 shows the total tritium release from the surface of components by diffusion. The total amount of tritium released into the plasma vaccum vessel during the reactor maintenance of 4, 8 and 24 hours are about 270 Ci, 390 Ci and 660 Ci, respectively. The greater part of this released tritium depends on the energetic tritium particles which are implanted into the first wall and the divertor plate during the reactor operation.

However, the release of tritium can be decreased by baking the structure material prior to the maintenance. As a function of bakeout temperature and baking time, the tritium distributions in stainless steel and in tungsten are shown in Fig.VIII-2-22 and Fig.VIII-2-23, respectively. The residual tritium within the first 10^{-3} cm of stainless steel and within the first 3×10^{-2} cm of tungsten are assumed to be the source of tritium releases during the maintenance.

After a 24-hour bakeout at 150°C, the tritium solubility in stainless steel decreases by a factor of 10 at a depth of 10^{-3} cm.

In order to decrease the residual tritium in tungsten to a tolerable low level, tungsten should be baked at higher temperature. After a 48-hour at 500°C, tritium solubility in tungsten decreases by a factor of 60 at a depth of 3×10^{-2} cm.

The tritium releases into the reactor room can be more decreased by adopting the compartment system which subdivides the atmosphere of the reactor room into several separated parts. Tritium released into the compartment is removed by using the Effluent Air Detritiation System (ADS).

Table VIII-2-6 Design Conditions of Components in the Plasma Vacuum Vessel

	surface area	material	temperature
(i) Group (I)			
a) inboard (grooved)	560 m^2	s.s.	360-300°C---35% 300-240°C---25% 240-180°C---22% below 180°C 18%
b) outboard (grooved)	1040 m^2	s.s.	300-260°C---36% 260-200°C---30% 200-140°C---28% below 140°C 6%
(ii) Group (II)			
a) end wall of first wall	490 m^2	s.s.	120 °C
b) front wall of blanket	490 m^2	s.s.	120 °C
c) side wall of blanket	790 m^2	s.s.	120 °C
d) end wall of blanket	490 m^2	s.s.	120 °C
e) header for cooling pannel	60 m^2	s.s.	120 °C
f) piping system	290 m^2	s.s.	120 °C
g) ring flange	630 m^2	s.s.	120 °C
h) vacuum vassel wall	1360 m^2	s.s.	120 °C
i) support frame	650 m^2	s.s.	120 °C
(iii) Group (III)			
a) divertors	160 m^3	W(armor)	max. 270°C

Table VIII-2-7 Design Conditions of Tritium Sources

(i) Group (I) (inboard and outboard first wall)	
i) tritium bombardment flux	: 3.1 x 10^{-4} cc-T_2/cm^2/sec (1.7×10^{20} atom/m^2/sec)
ii) tritium particle energy	: 200 eV
iii) penetration depth in first wall	: 30 Å
iv) partial pressure	: 2 x 10^{-5} torr-T_2
(ii) Group (II) (vacuum vessel wall, etc.)	
i) partial pressure	: 1.5 x 10^{-5} torr-T_2
(iii) Group (III) (divertor plate)	
i) tritium bombardment flux	: 1.49 x 10^{-2} cc-T_2/cm^2/sec (8×10^{21} atom/m^2/sec)
ii) tritium particle energy	: 400 eV
iii) penetration depth in tungsten	: 40 Å
iv) partial pressure	: 1 x 10^{-3} torr-T_2

Table VIII-2-8 Total Tritium Releases during Maintenance

Time / Components		during 4 hrs maintenance	during 8 hrs maintenance	during 24 hrs maintenance
Group(I)	Inboard	0.65 Ci (0.19)	0.91 Ci (0.27)	1.6 Ci (0.45)
	Outboard	3.5 (0.31)	4.9 (0.44)	8.8 (0.77)
Group(II)		0.69 (0.69)	0.95 (0.95)	1.7 (1.7)
Group(III)		263 (4.8×10^{-12})	380 (7.0×10^{-12})	644 (1.2×10^{-11})
Total		269 (1.2)	387 (1.7)	656 (2.9)

( ) dependent on only partial pressure

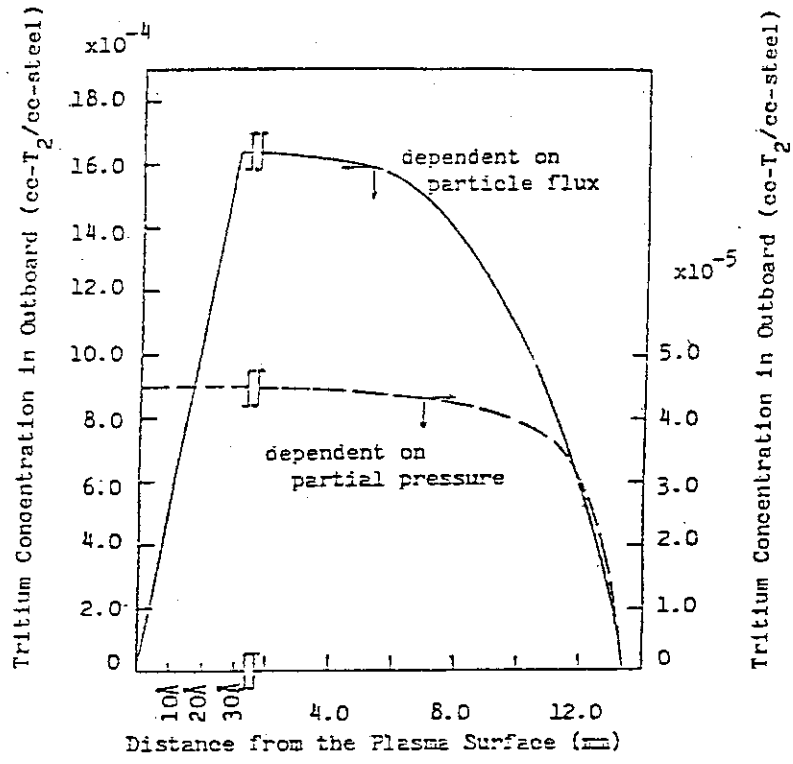

Fig. VIII-2-16 Tritium Concentration in Outboard First Wall

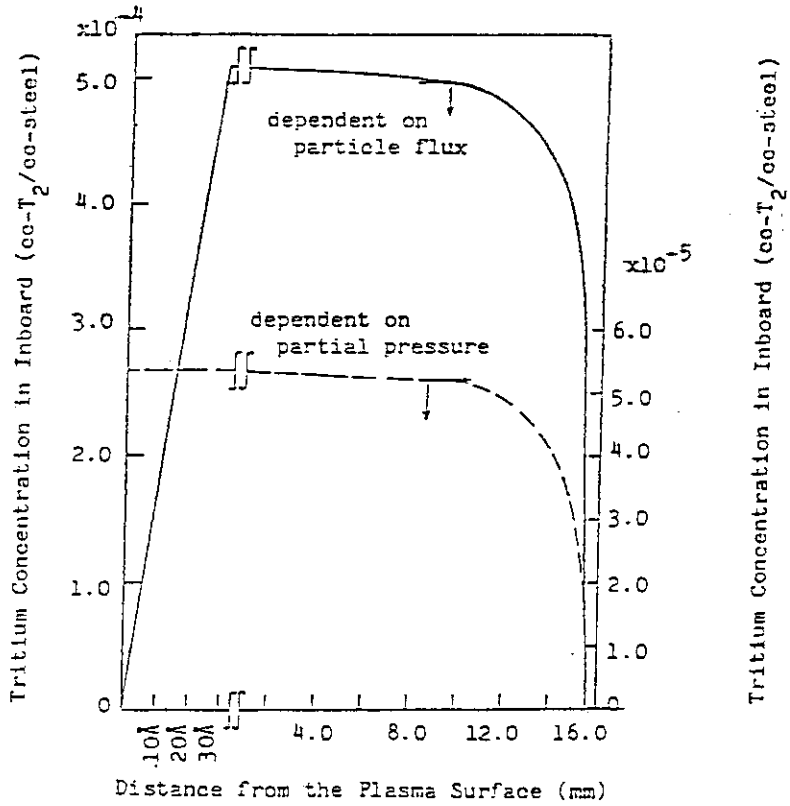

Fig. VIII-2-17 Tritium Concentration in Inboard First Wall

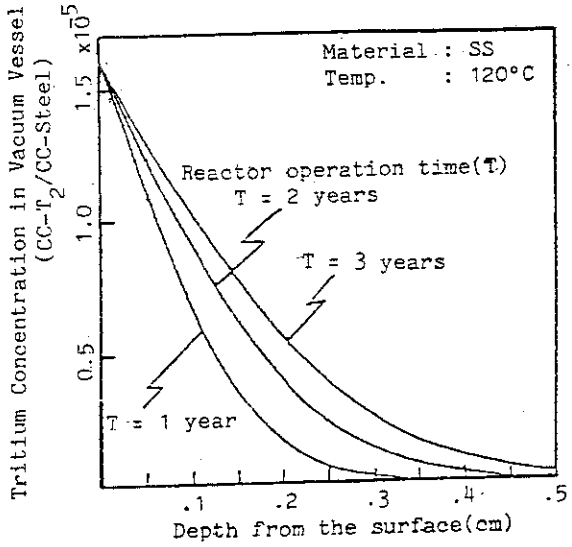

Fig. VIII-2-18 The Distribution of Tritium Concentration in Group(II)

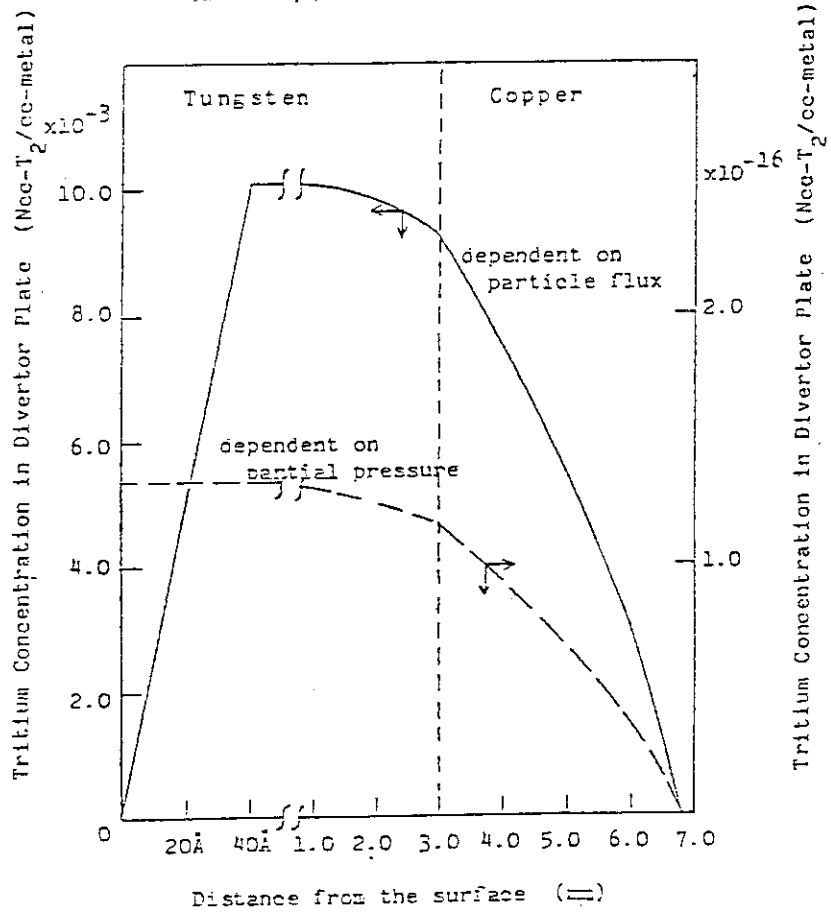

Fig. VIII-2-19 The Distribution of Tritium Concentration in Divertor Plate

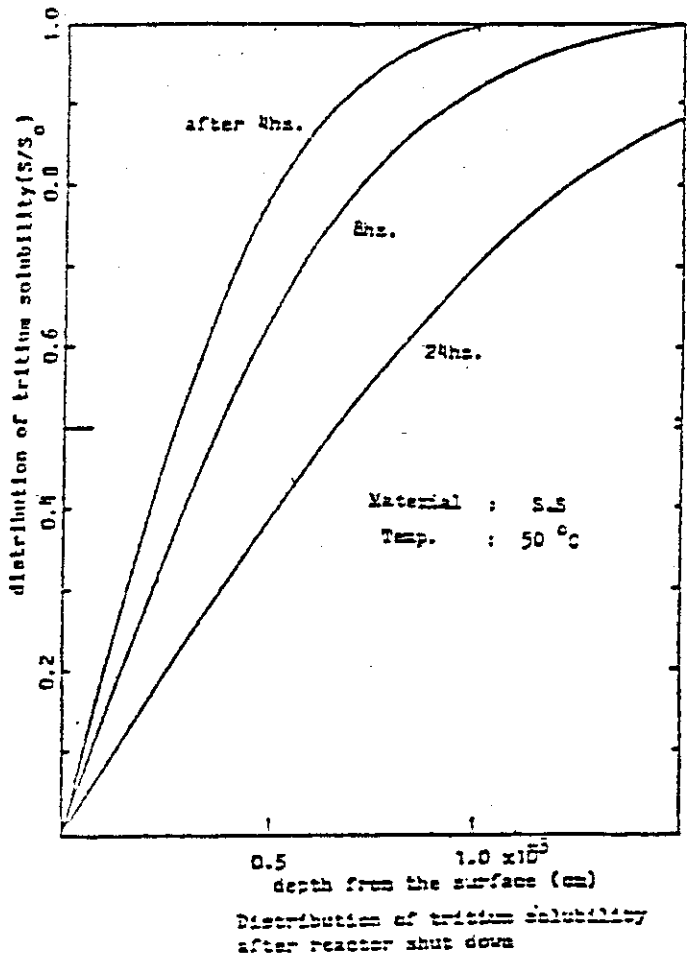

Fig. VIII-2-20 The Distribution of Tritium in Stainless Steel (during maintenance)

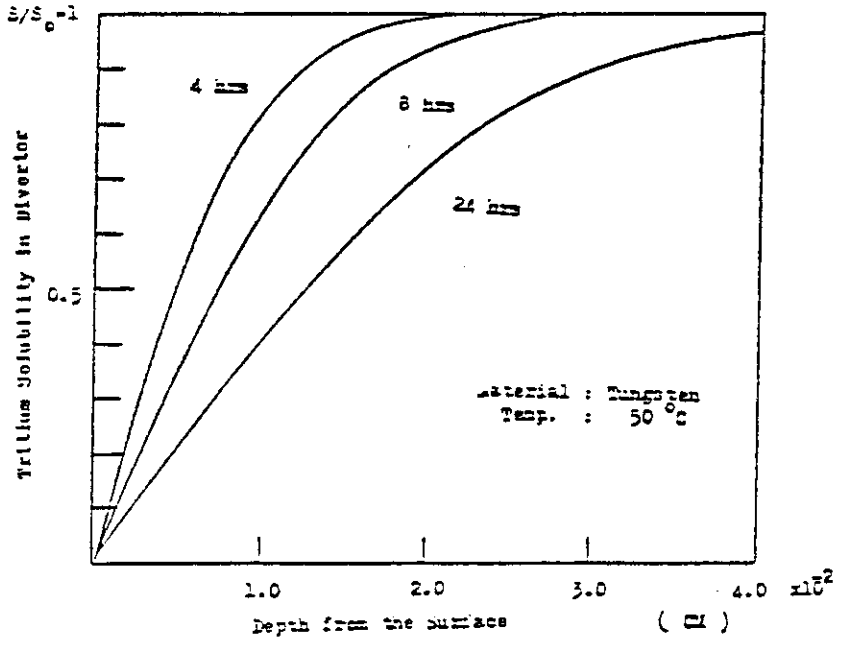

Fig. VIII-2-21 The Distribution of Tritium in Tungsten (during maintenance)

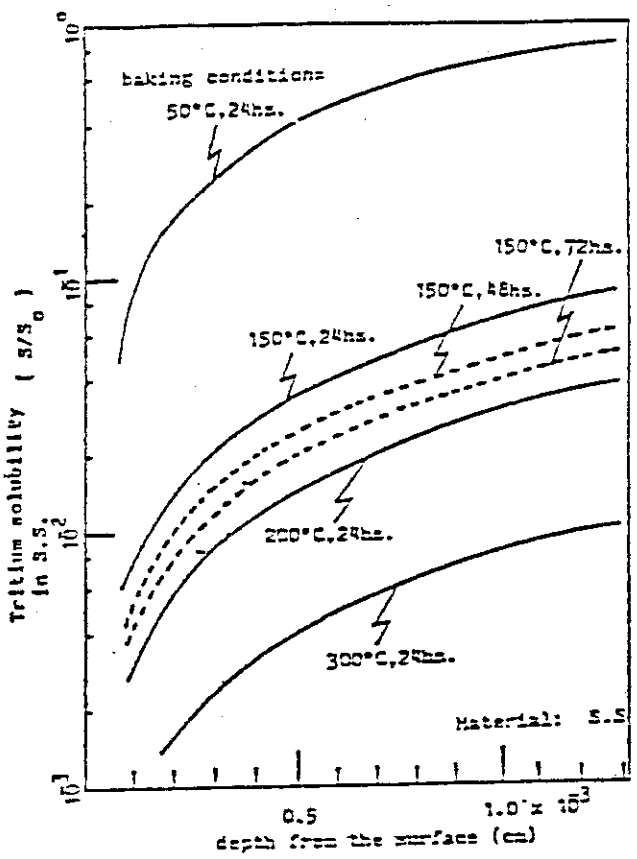

Fig. VIII-2-22 The Distribution of Tritium in Stainless Steel (baking effect)

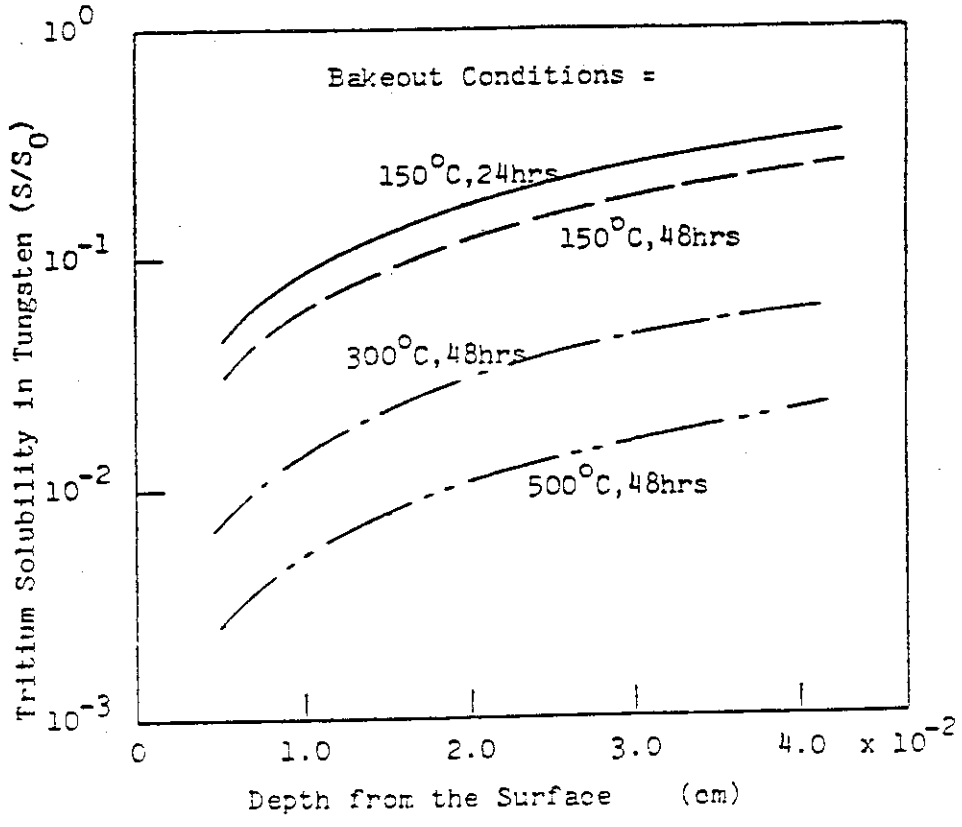

Fig. VIII-2-23 The Distribution of Tritium in Tungsten (baking effect)

2.1.6 Radiation effects

(a) Radiation-Enhanced Diffusion of Hydrogen in Stainless Steel

Radiation-enhanced tritium diffusion in the first wall and divertor has been identified as a serious problem because these materials are exposed to high radiation flux. However, the knowledge of this area is limited.

Recently, an experimental study of hydrogen diffusion in stainless steel under X-ray irradiation field has been presented by Ikeya et al.[14]. Although these works are in preliminary stage, the results are summarized below to call attention to this problem.

The hydrogen charging into type 304 stainless steel of ∿100 μm thickness was made by the cathodic charging method in a solution of 0.5 M H_2SO_4 at a current density of 30 mA/cm^2. The hydrogen-charged specimens were immersed in liquid glycerine and were exposed to X-rays from a Mo target X-ray tube operated at 45 kV and 15 mA. In order to estimate the amount of exhaled hydrogen, the volume of evolved hydrogen bubbles was measured by using a glass micro-cylinder. The exposure rate on the specimen was detected to be 30 ±5 rad/s with TLD.

Fig. VIII-2-24 shows the exhalation rate of hydrogen gas out of stainless steel as a function of the time after 30 min of hydrogen charging. The exhalation rates under X-ray irradiation and without irradiation decreased gradually with the time. They mentioned that exhalation rate at 10 min was enhanced from 4 x 10^{-6} cm^3/cm^3·s to 6 x 10^{-6} cm^3/cm^2·s by X-ray irradiation.

The radiation heating might also play a role to enhance the migration of hydrogen. The specimen was also irradiated by X-rays at liquid nitrogen temperature 77 K, at which hydrogen was not mobile without irradiation. The X-ray induced-migration of hydrogen was also observed at 77 K. From this result, they concluded that the X-ray induced migration of hydrogen was not due to the local heating [15].

The dose rate of $\sim 10^5$ rad/s in INTOR first wall is several orders of magnitude higher than that in the present experiments. The effects of irradiation on tritium diffusion in the first wall may become more severe problem. Further investigations are necessary including additional radiation effects.

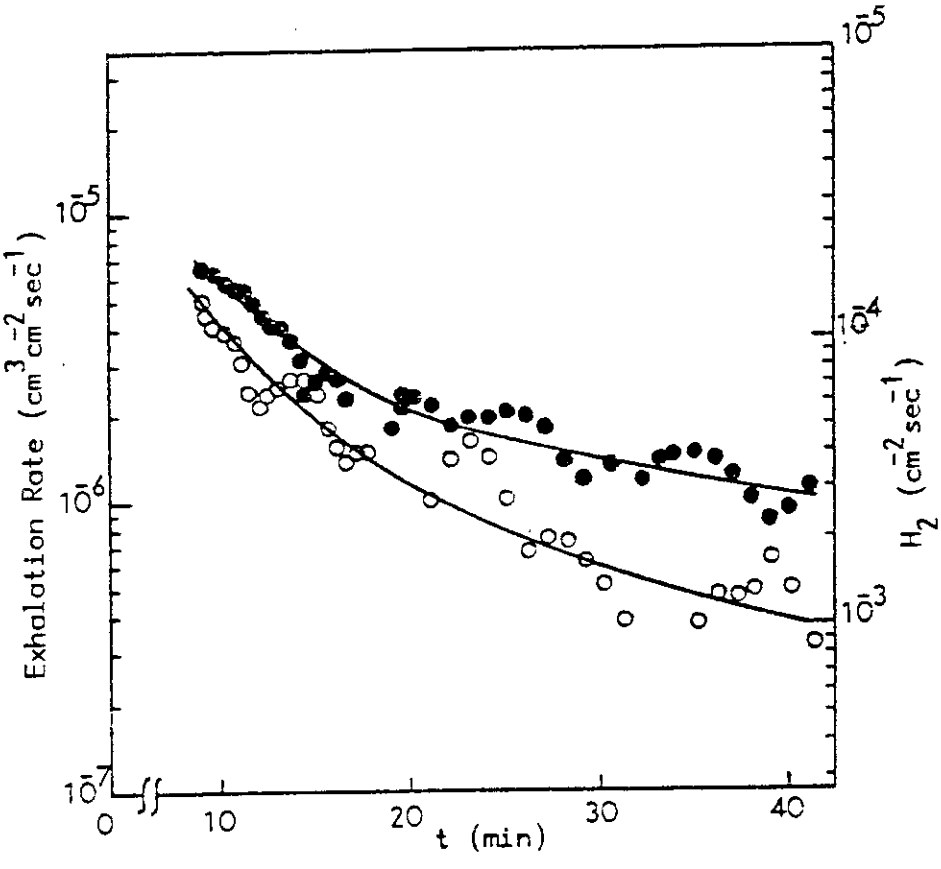

Fig. VIII-2-24

The exhalation rate of hydrogen gas out of stainless steel 304 in liquid glycerine under X-ray irradiation(●) and without irradiation(○) as a function of time after the cathodic hydrogen hydrogen charging in 30 min.

2.1.7 Conclusion

From the theoretical and experimental studies of tritium permeation rates into coolant, the following conclusions are pointed out;

i) The estimated tritium permeation rates through the first wall using the diffusion and recombination model are about 2 Ci/day and 50 Ci/day, respectively.

iii) The rate limiting process for desorption of the implanted tritium in the first wall seems to be the surface recombination rather than the diffusion in the projected region. Since the recombination rate constant is strongly affected by the surface conditions, further work are needed.

iii) The estimated tritium permeation rate through the divertor plate using the diffusion model is remarkably as large as 620. Ci/day.

iV) Experimental studies of deuterium permeation under ion bombardment show that various types of defects are produced near the projected range, and they are inferred to contribute to the decrease in permeation rate.

V) The experimental studies of the oxide film integrity and its effectiveness as permeation barrier have been carried out. These results have indicated that oxide film layer is stable even under the conditions of very low oxidation potential and relatively high temperature(986 K). Since the oxidation potential of water in primary coolant is higher than that in this experiment, it seems that naturally-formed oxide layers on coolant side can act effectively to reduce the tritium permeation rate.

Vi) In order to reduce the permeation rate by several orders of magnitude, there is a possibility to use the non-metallic coating and vacuum gap methods.

Vii) The total amount of tritium released into the plasma vacuum vessel during the reactor maintenance of 24 hours is about 660. Ci. The greater part of this released tritium is the energetic tritium particles which are implanted

into the divertor plate during the reactor operation. The tritium release, however, can be decreased by baking the divertor plate prior to the maintenance. Tritium release rate decreases by a factor of about 60 after 48-hour bakeout at 500 °C.

2.2 Tritium processing of the primary coolant

2.2.1 Methods of water detritiation

(a) Design Study of Primary Coolant Tritium Processing System

(1) Introduction

In order to maintain the tritium levels in the primary coolant at low level, there is a possibility to install a tritiated water processing unit in the Primary Cooling System. Various isotopic separation processes have been discussed for tritium processing method.

Water distillation process is a fundamentally simple technique employing simple equipments to perform a separation of diverse constituents and utilizing the differences in boiling point and volatility of isotopes. The technical feasibility of this process is well-established with a high assurance of success.

According to the recent economic-consideration[16], furthermore water distillation process appears to be more economical than chemical exchange process.

In this section, therefore, water distillation process is selected as a Primary Coolant Tritium Processing System in INTOR, and system design has been carried out.

(2) System Design Conditions

The features and design bases of a Primary Coolant Tritium Processing System are as follows:

i) Tritium release rate from the Primary Cooling System to the environment is to be less than 1 Ci/day during the normal operation.

ii) Tritium permeation rate into the primary coolant is assumed to be 620 Ci/day (see 2.1.1)

iii) Coolant leakage rate is assumed to be 1%/year of coolant hold up referred to the typical pressurized water reactor (PWR).

iv) The coolant is by-passed from the main coolant stream and treated by a Primary Coolant Processing System.

v) The tritium-depleted water is designed to be returned to the Primary Cooling System. While, the tritium-enriched water is sent to the Tritiated Liquid Waste Storage System.

vi) Water distillation process is adopted for the processing method because of its high reliability, simplicity, and low capital and running costs.

vii) Modern efficient packing material (ordered packing)[17,18] is used to reduce the HETP and pressure drop per theoretical plate. This will help not only to shorten the overall column height, but also to reduce the maximum pressure in column.

The design parameters are summarized in Table VIII-2-9.

(3) System Description

Fig. VIII-2-25 shows the flow diagram of Primary Coolant Tritium Processing System. The characteristics of the system are described below in terms of the major parts of the system.

i) pH Control Tank

In order to inhibit the corrosion of structural and packing materials, pH control tank is installed to adjust the pH value of feeding coolant stream.

This control tank must be provided also to assure smooth operation and to minimize the dynamic interaction between the Primary Cooling System and the Primary Coolant Tritium Processing System.

ii) Vaporizer

Impurities in feed coolant are the cause of trouble when they are introduced into the water distillation unit. Vaporizer, therefore, is designed to evaporate the coolant for removing the impurities as high boiling point residues.

iii) Water Distillation Unit

Water distillation unit consists of two fractional distillation towers with packing material. Each of distillation towers is 10 m in packed height and 2.5 m in inner diameter. Condenser and cold trap are installed at the top of the first tower, and a reboiler is installed at the bottom of the second tower. Structure configuration of the second distillation tower is shown in Fig. VIII-2-26.

The feed vapor stream with a flow rate of 10 tons/day encounters a liquid down flow at the about half height of the first tower. The column above the feed entry is a tritium stripping section because of its lower volatility, whereas the column below the feed entry is a tritium enriching section.

The vapor flowing out from the top of the first tower is condensed. Major part of the condensed stream is fed to the top of the first tower as a liquid down flow, and a part (9.9 tons/day) of it is returned to the Primary Cooling System. While, the tritium-enriched water from the bottom of the second tower is sent to the Tritiated Liquid Waste Storage System with a flow rate of 0.1 tons/day.

Fig.VIII-2-27 shows concentration profiles in this distillation column. It is seen from the figure that the steady state tritium concentrations at the top and the bottom plate are 6.2 Ci/m^3 and 5.58×10^3 Ci/m^3, respectively.

(4) Conclusions

From the design studies of the Primary Coolant Processing System, the following conclusions are pointed out.

i) To maintain the tritium release rate from the Primary Cooling System to the environment less than 1 Ci/day, the primary coolant must be treated at a flow rate of more than 10 tons/day. It is also found that anticipated tritium concentration in primary coolant is less than 62 Ci/m^3 assuming a tritium permeation rate of 620 Ci/day.

ii) Using the water distillation tower of the total packed height of 20 m, the feed stream (62 Ci/m^3) can be separately recovered as the tritium-depleted water (6.2 Ci/m^3) and the tritium-enriched water (5.58×10^3 Ci/m^3).

iii) The water distillation tower can be designed to be a reasonable size, which is to be about 2.5 m in diameter based on a processing flow rate of 10 tons/day.

Table VIII-2-9 Design parameters of Primary Coolant Processing System

Items	Design parameters
1) Primary Cooling System	
a) Tritium permeation into system	620. Ci/day
b) Tritium leakage rate from system	< 1. Ci/day
c) Coolant leakage rate	1. %/year
d) Processing rate	10. m^3/day
f) Tritium concentration of coolant	62. Ci/m^3
2) Primary Coolant Tritium Processing System	
a) Processing method	water distillation (under vacuum)
b) Packing column	ordered packing
c) Feed coolant to tower	
Feed rate	10. m^3/day
Tritium concentration	62. Ci/m^3
PH	6-7
d) Top product	
Production rate	9.9 m^3/day
Tritium concentration	6.2 Ci/m^3
e) Bottom production	
Production rate	0.1 m^3/day
Tritium concentration	5.58×10^3 Ci/m^3
f) Number of distillation towers	2
g) Diameter of distillation tower	2.5 m
h) Height of packed section	20. m (10.m/tower)
i) Average temp. in column	53. °C
j) Reflux ratio	22.
k) Theoretical number of stages	190 (95/tower)
l) H.E.T.P	10.5 cm
m) Hold up at reboiler	1.0 ton
n) Hold up at condenser	1.5 ton

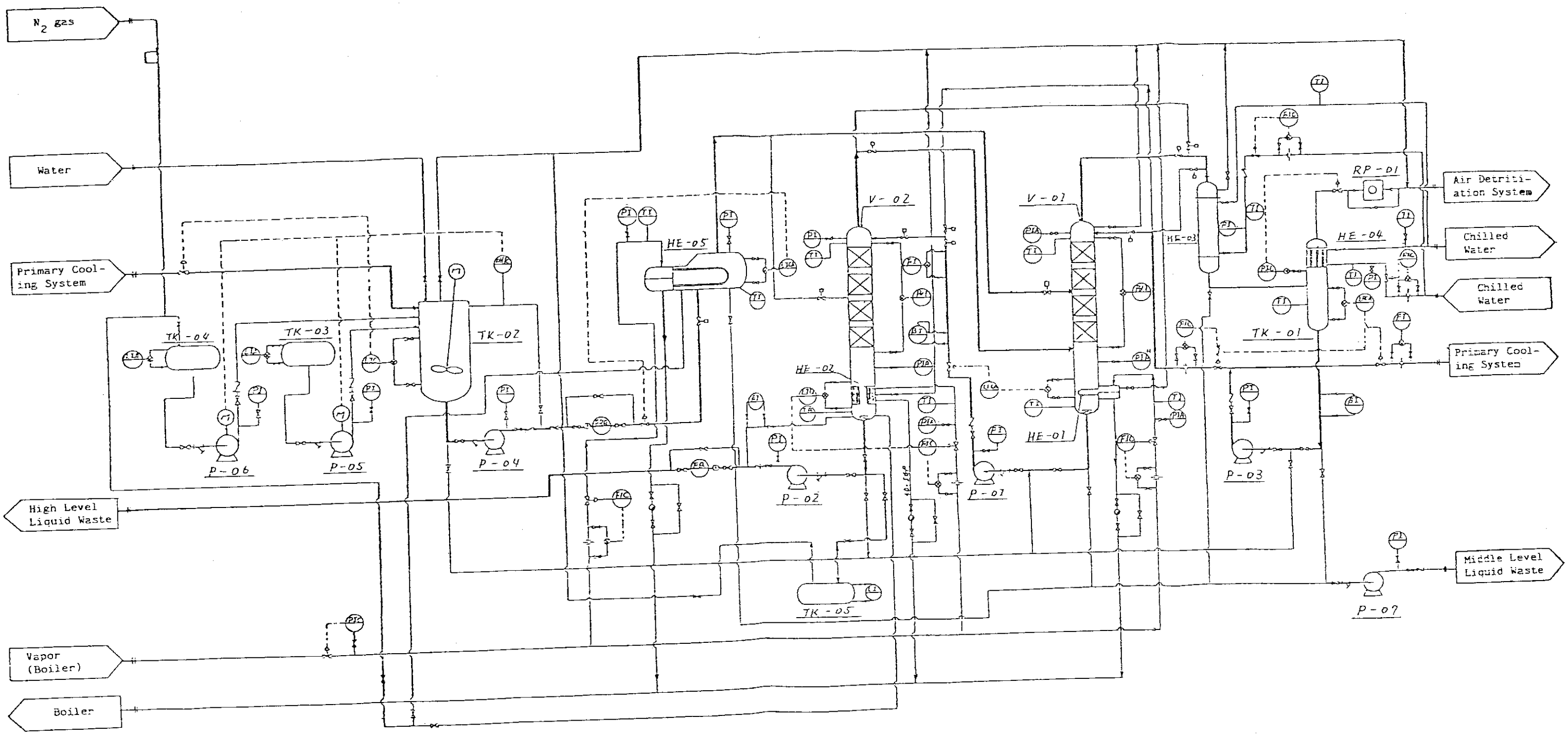

V-01	Distillation Tower(1st)	HE-04	Cold Trap	TK-01	Condensate Tank
V-02	Distillation Tower(2nd)	HE-05	Vaporizer	TK-02	PH Control Tank
HE-01	Reboiler(auxiliary)	RP-01	Vacuum Pump	TK-03	Acid Tank
HE-02	Reboiler(main)	P-01 ~ P-07	Transfer Pump	TK-04	Alkali Tank
HE-03	Condenser			TK-05	Concentration Tank

Fig. VIII-2-25 Flow Diagram of the Primary Coolant Tritium Processing System

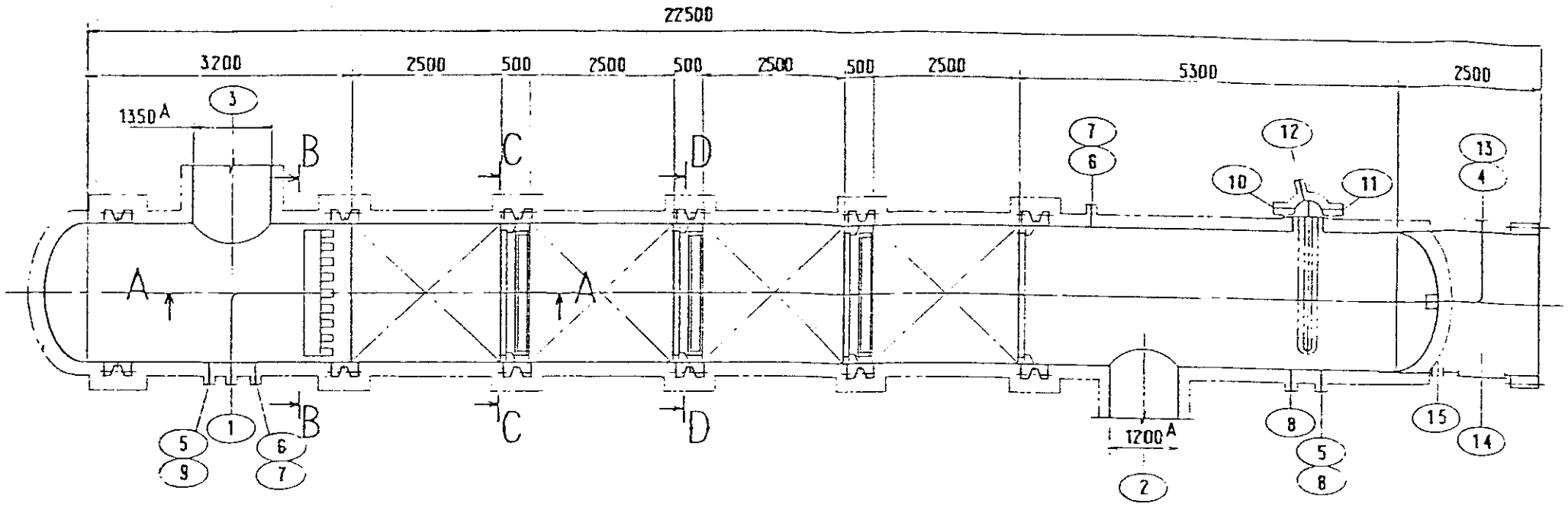

NO	NAME OF NOZZLE
1	LIQ. INLET
2	GAS INLET
3	GAS OUTLET
4	LIQ. OUTLET
5	TI CONN.
6	PI CONN.
7	PdI CONN.
8	LICA CONN.
9	VENT
10	STEAM INLET
11	CONDENSATE
12	VENT
13	PIPE WAY
14	ACCESS HOLE
15	SKIRT VENT

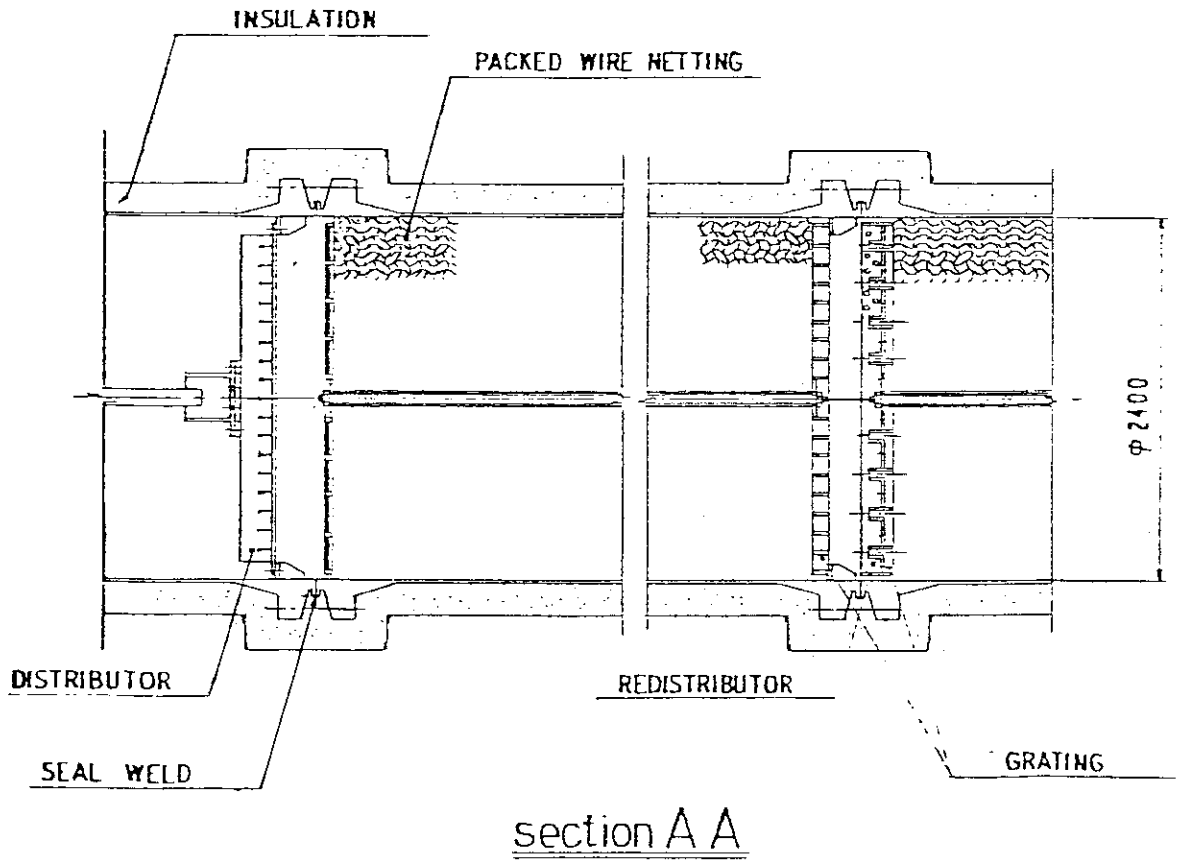

section A A

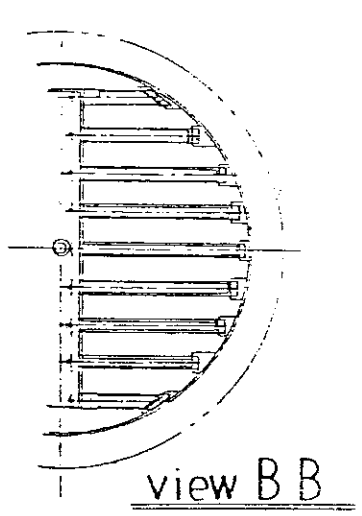

view B B

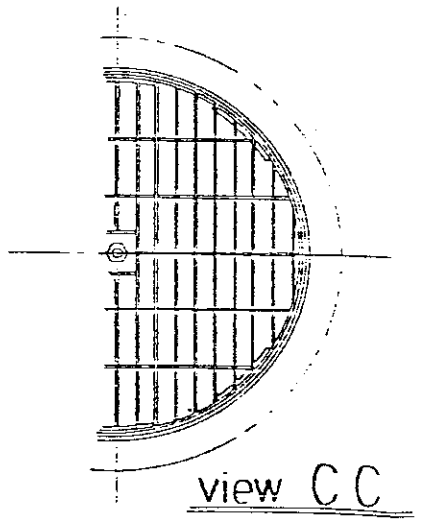

view C C

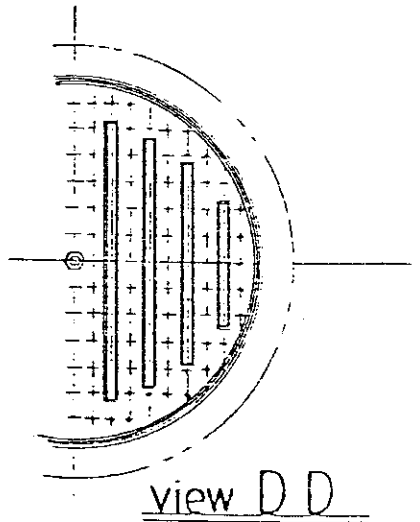

view D D

Fig. VIII-2-26 Structure Configuration of the Second Distillation Tower

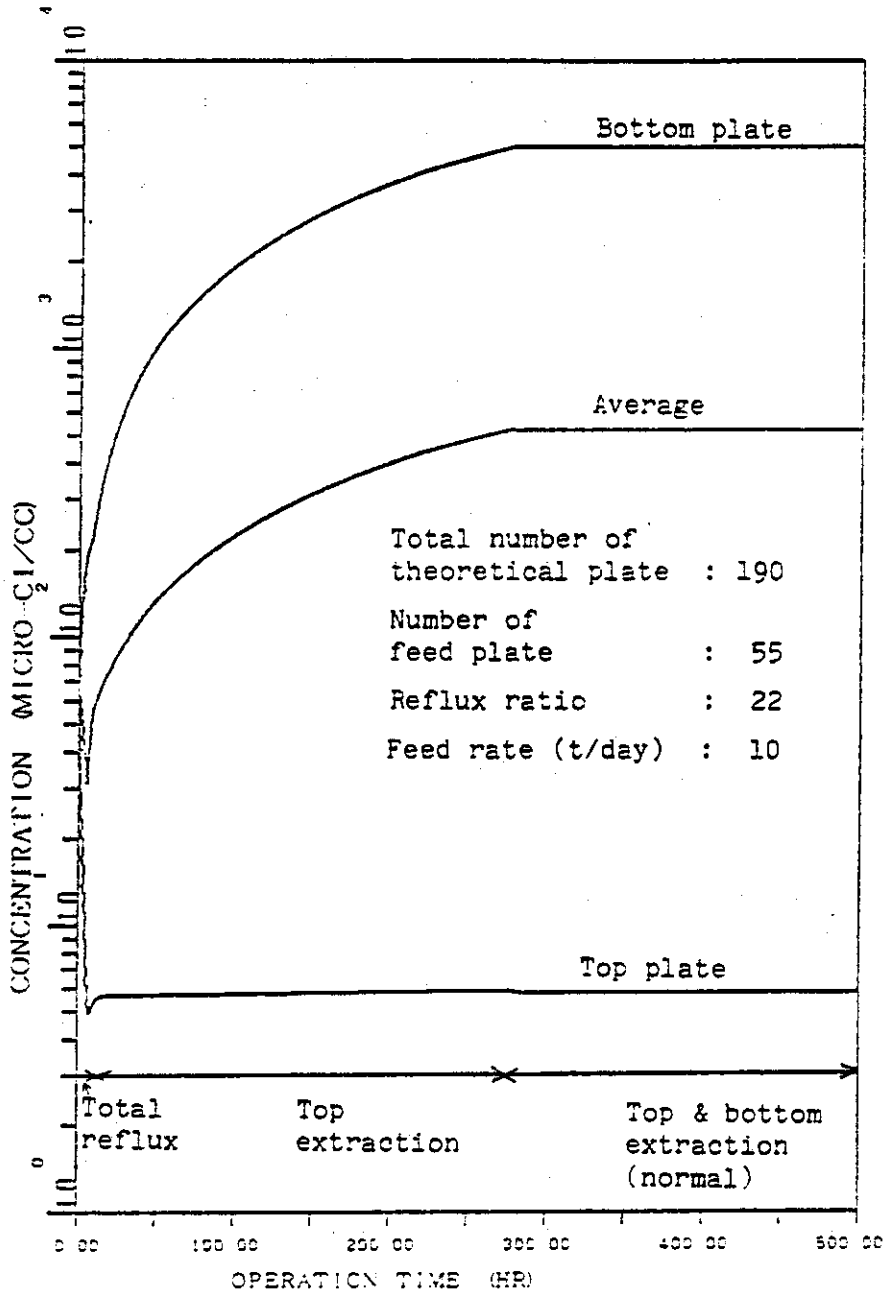

Fig. VIII-2-27 Tritium Concentration Profiles in Distillation Column

2.2.2 Cost and process comparison

(a) Comparison of Coolant Tritium Processing System

There are many candidate tritium processing methods for the coolant. The comparison of these methods is performed and tabulated in Table VIII-2-10.

Water distillation method has the following advantages;

i) Process is well-established for a large-scale heavy water production, already.

ii) Process is a simple technique with a high assurance of success.

iii) No critical materials are required for construction.

iV) No catalyst is required for operation.

v) Tritium leakage from process is relatively small because the conversion of coolant to diffusive gaseous-tritium is not required and process is operated under the vacuum condition.

Table VIII-2-10 Comparison of Tritium Processing Method

	Dual Temperature Exchange	Cryogenic Hydrogen Distillation	H_2-H_2O Exchange	NH_3-H_2 Exchange	Electrolysis	Water Distillation
Separation Factor	F	F	G	G	E	P
Processing Cost	E	G	E	E	P	F
Safety(leakage)	F	F	F	F	F	Best
Safety(Accessibility)	P	F	G	F	G	E
Maintainability	F	F	G	G	G	G
Operationability	F	F	F	F	G	G
Reliability	G	F	G	F	E	E
Capacity	G	F	G	G	P	P

E=Excellent, G=Good, F=Fair, P=Poor

2.2.3 Tritium concentration on water

(a) Tritium Processing in Coolant

(1) Introduction

Tritium can be released into the coolant from the plasma through the first wall and divertor plate. Tritium permeation into the first wall and divertor plate coolant is caused by both the energetic tritium particles and the tritium partial pressure.

In order to determine the controlled tritium concentration in coolant, there are following parameters to be considered,

i) tritium permeation rate into coolant,
ii) tritium release rate to the environment in normal condition,
iii) tritium release rate to the environment in abnormal condition,
iv) tritium inventory in coolant,
v) hold up of coolant,
vi) leakage rate of coolant, and
vii) characteristics of tritium processing system.

In this section, the effects of these parameters on the tritium concentration in coolant are evaluated in normal condition.

(2) Tritium concentration in primary coolant

Tritium can be lost from the primary coolant to the environment by leakage and permeation. Tritium release rate to the environment may be the product of the coolant leakage rate and the tritium concentration in coolant.

To minimize tritium release to the environment from the primary coolant, the tritium processing system of suitable capacity should be equipped to maintain the tritium concentration in coolant below the controlled value.

Coolant leakage rate is estimated to be about 1%/year of coolant hold up by the analogy of heavy water fission reactor. And coolant hold up of Primary Cooling System is estimated to be 500 m^3. Coolant leakage rate is therefore assumed to be about 0.014 m^3/day.

The relationship between tritium permeation rate into the primary coolant and the tritium concentration is analized.

a) Analytical method

When the tritium processing system is not installed, tritium concentration in the primary coolant is expressed as below.

$$\frac{d(HC)}{dt} = R - (\lambda H + \ell)C \qquad \text{(VIII-2-19)}$$

where

H : Hold up of primary coolant (m^3)
C : Tritium concentration in coolant (Ci/m^3)
R : Tritium permeation rate (Ci/day)
ℓ : Leakage rate of coolant (m^3/day)
t : Operating time (day)
λ : Decay constant of tritium (1/day)

When the tritium processing system is installed to treat tritiated water, tritium concentration in primary coolant is expressed as below.

$$\frac{d(HC)}{dt} = R + D\xi C - FC - (\lambda H + \ell)C \qquad \text{(VIII-2-20)}$$

where

D : Top product flow rate (m^3/day)
F : Feed rate (m^3/day)
ξ : Tritium concentration ratio of top product to feed (-)

b) Without tritium processing system

Assuming that there is no tritium in primary coolant at the start up of the reactor (at t=0, C=0), eq.(VIII-2-19) can be easily solved. The dependence of tritium concentration in primary coolant on the tritium permeation rate is shown in Fig. VIII-2-28 on condition that the coolant hold up is 500 m^3 and the coolant leakage rate is 0.014 m^3/day.

The relationship between tritium permeation rate and the tritium concentration at the end of plant life of 15 years (5475 days) is shown in Fig. VIII-2-29 taking coolant leakage rate as a parameter.

It is seen from Fig. VIII-2-30 that if the tritium permeation rate is 620 Ci/day, tritium release rate to the environment exceeds 1 Ci/day after 60 days from the start up and 10 Ci/day after 620 days.

If the tritium permeation rate is 620 Ci/day and the coolant leakage rate is 0.014 m^3/day, tritium concentration in coolant amounts to 4.3×10^3 Ci/m^3 and the trtium release rate to the environment amounts to 59 Ci/day at the end of plant life. And in order that the tritium release rate to the environment is maintained less than 1 Ci/day during the plant life of 15 years without tritium processing system, tritium permeation rate into the divertor coolant should be lowered below 10.5 Ci/day.

c) With tritium processing system

Tritium processing system separates the feed stream into the two stream. One is the top product of low tritium concentration and high flow rate. And the other is the bottom product of high tritium concentration and low flow rate. Tritium concentration reduction ratio of top product to feed is an important factor to design the tritium processing system. The primary coolant is by-passed from the main stream and treated by the tritium processing system in a recirculation mode. Therefore, it is not necessary to reduce the tritium concentration with high reduction ratio. In this calculation, this ratio is set to be 0.1.

In the case the operation of tritium processing system starts when the tritium leakage rate to the surroundings comes up to 1 Ci/day, tritium concentration in the primary coolant is shown in Fig.VIII-2-30. On the other hand, in the case the operation of tritium processing system starts at the same time as that of reactor, tritium concentration in the coolant is shown in Fig. VIII-2-31.

If the feed rate to the tritium processing system is set to be 9.33 m^3/day, tritium concentration in coolant can be maintained to 73 Ci/m^3 and tritium release rate to the environment can be reduced to 1 Ci/day.

It is seen from eq. (VIII-2-20) that feed rate to the tritium processing system affects the steady state tritium concentration in the coolant because $D\xi$ and $\lambda H + \ell$ may be neglected compared with F. The relationship between feed rate and the tritium release rate is shown in Fig.VIII-2-32 taking tritium permeation rate as a parameter. If the tritium release rate to the environment should be lowered below 10 Ci/day on condition that the tritium permeation rate is 620 Ci/day, primary coolant has to be treated with the feed rate of larger than 0.84 m^3/day at the steady state.

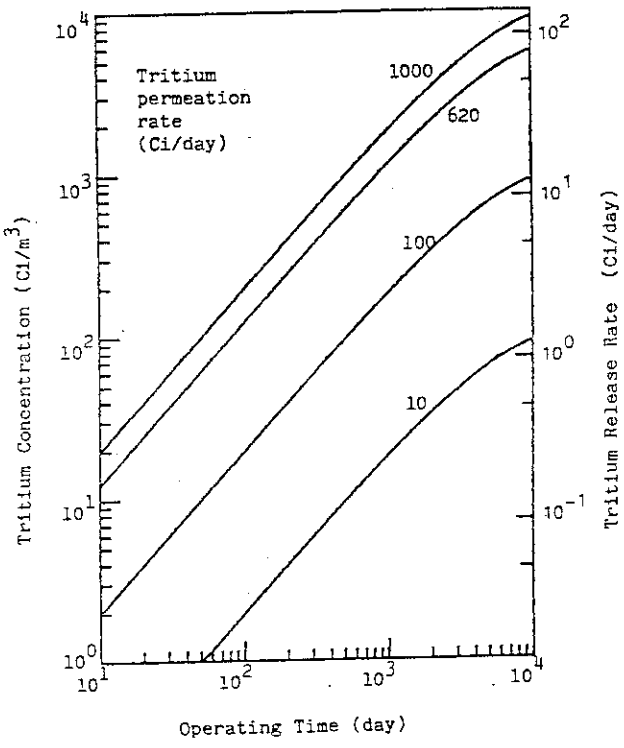

Fig. VIII-2-28

Increase of Tritium Concentration without Tritium Processing System

Coolant hold up ; 500 m^3

Coolant leakage rate ; 1 %-hold up/year

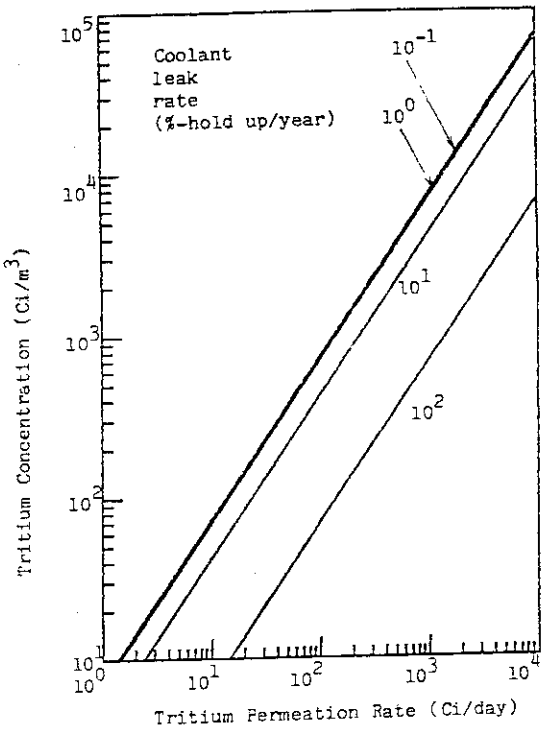

Fig. VIII-2-29

Tritium Concentration at the End of Plant Life (15 yr)

Coolant hold up ; 500 m^3

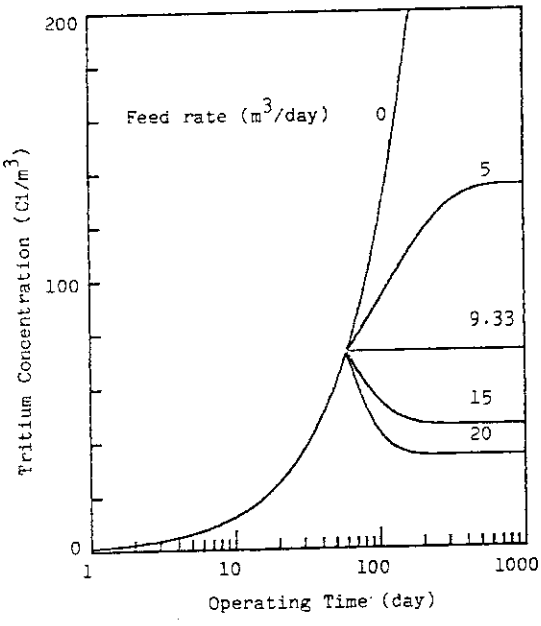

Fig. VIII-2-30 Tritium Concentration in Coolant with Tritium Processing System

Tritium processing system starts when tritium release rate to the surroundings comes up to 1 Ci/day.

Coolant hold up ; 500 m^3

Coolant leakage rate ; 1 %-hold up/year

Tritium permeation rate; 620 Ci/day

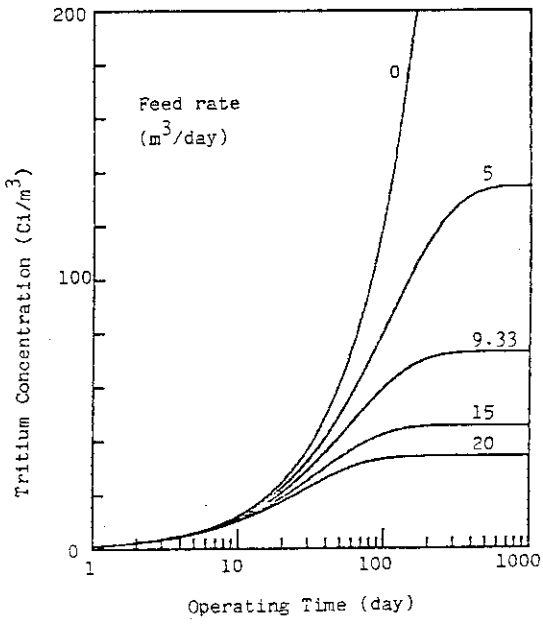

Fig. VIII-2-31 Tritium Concentration in Coolant with Tritium Processing System

Tritium processing system starts simultaneously with reactor.

Coolant hold up ; 500 m^3

Coolant leakage rate ; 1 %-hold up/year

Tritium permeation rate; 620 Ci/day

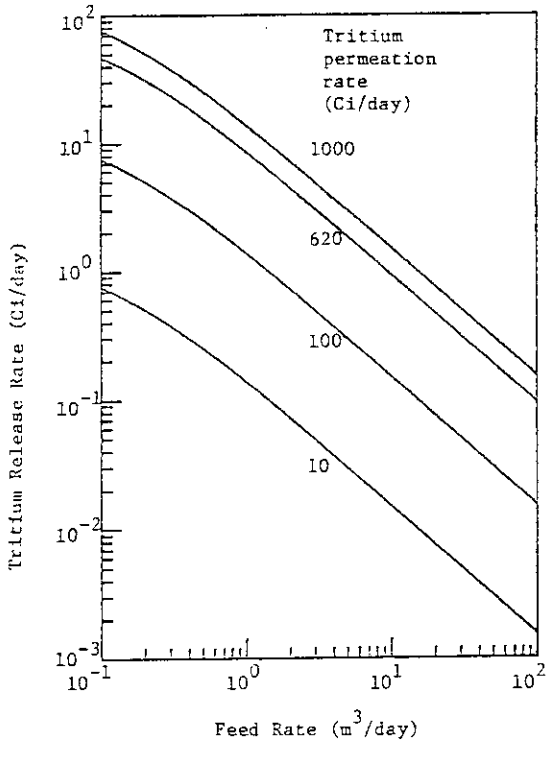

Fig. VIII-2-32 Dependence of Feed Rate on the Tritium Permeation Rate and the Tritium Release Rate

2.3 Conclusions and recommendations

The following conclusions and recommendations are based on the informations given in this section;

i) The estimated tritium permeation rates through the first wall using the diffusion and recombination models are about 2 Ci/day and 50 Ci/day, respectively.

ii) The rate limiting process for desorption of the implanted tritium in the first wall seems to be the surface recombination rather than the diffusion in the projected region. Since the recombination rate constant is strongly affected by the surface conditions, further work are needed.

iii) The estimated tritium permeation rate through the divertor plate using the diffusion model is remarkably as large as 620. Ci/day.

iV) From i) and iii) above, total tritium permeation rate into primary coolant is at the level of about 1,000 Ci/day.

V) Since the main source of tritium leakage into the reactor room during normal operation is tritiated-water coolant leakage from primary coolant, the tritium levels in primary coolant must be kept at low level. The most practical method to keep the acceptable tritium level in coolant is to install the tritium processing unit in Primary Cooling system.

Vi) It is recommended that the Tritium Processing System utilizing the water distillation method should be investigated in more detail.

Vii) It is recommended that tritium release rate from the Primary Cooling System should be kept to be less than 1.0 Ci/day. The amount of this tritium release rate to the environment through the stack may be allowed.

To keep this tritium release rate on condition of coolant leakage

of 1 %/year of coolant hold up, the primayr coolant must be treated at a flow rate of more than 10 tons/day. It is also found that anticipated tritium concentration in primary coolant is less than 62 Ci/m^3 assuming a tritium permeation rate of 620 Ci/day.

Viii) The total amount of tritium released into the plasma vacuum vessel during the reactor maintenance of 24 hours is about 660 Ci. The greater part of this released tritium is the energetic tritium particles which are implanted into the divertor plate during the reactor operation. The tritium release, however, can be decreased by baking the divertor plate prior to the maintenance. Tritium release rate decreases by a factor of about 60 after 48-hour bakeout at 500 °C. It is recommended that the baking method of the contaminated parts in vacuum vessel should be investigated in detail to prevent the tritium contamination of reactor room during the maintenance.

3. Tritium contamination of reactor environment

3.1 Sources of tritium contamination

(a) Tritium inventory in tritium system

The tritium system consists of Fuel Gas Circuration System (FCS), Breeding Blanket Tritium Recovery System (BRS), Tritium Storage System (TSS), etc. These systems are designed to minimize the tritium inventory to be as low as technically possible.

Careful estimations of tritium inventory are carried out here.

Table VIII-3-1 summarizes the tritium inventory for FCS. Table VIII-3-2 summarizes the tritium inventory for BRS. Table VIII-3-3 shows total tritium inventory in tritium system. As it can be seen, most of tritium inventory is contained in the Tritium Storage System (TSS). Howevew, the tritium in the TSS is located in a high integrity structure which is hermetically sealed. The tritium inventory in tritium system except the TSS is estimated to be 360g.

Table VIII-3-1 Tritium Inventory for FCS

System		Tritium Inventory	Remarks
FCS	Cryogenic Pumping Unit	117 g	six pumps
	Purification Units I , II	8 g	nine permeators
	Isotope Separation Unit	93 g	four distillation collumns
	Fuel Gas Adjustment Unit	23 g	
	Miscellaneous	25 g	
Total		266 g	

Table VIII-3-2 Tritium Inventory for BRS

Unit	Inventory	Remarks
Sweep Gas Recirculation Unit	33 g	four MS dryers
MS Dryer Regeneration Unit		
Electrolysis Unit	39 g	
Miscellaneous	15 g	
Total	87 g	

Table VIII-3-3 Tritium Inventories of Major Systems

	System	Inventory	Form	Remarks
(i)	Plasma Vacuum Vessel	0.08 g	Gas	
(ii)	Fuel Gas Circulation System (FCS)			
	Cryogenic Pumpig Unit	120 g	Gas	24 g/cryopump
	Other Units	150 g	Gas	Isotope Seperation unit ; 24 g
(iii)	Breeding Blanket Tritium Recovery System (BRS)	87 g	Oxide	Electrolysis Cell Unit ; 39 g
(iv)	Primary Cooling System (PCS)	3.2 g	Oxide	assumed the tritium permeation rate to be 620 Ci per day and the tritiated water processing rate to be 2.0 % of water inventory per day
(v)	Tritium Storage System	2300 g	UT_3	

(b) Pathways of Tritium Releases

Pathways of tritium releases are function not only of the reactor design, but also of the operating philosophy.

The expected pathways of tritium released to the environment from main tritium system are summarized as follows;

(1) Pathways of Tritium Release during Normal Operation

The major pathways of tritium release are as follows;

i) Leakage and permeation from the plasma vacuum vessel

- Leakage and permeation into the reactor room
- Permeation into the primary cooling system (blanket and divertor cooling system)

ii) Leakage from the tritium systems

Tritium Systems consist of Fuel Gas Circulation System (FCS), Breeding Blanket Tritium Recovery System (BRS), Tritium Waste Treatment System (WTS), and Tritium Removal System (TRS), Primary Cooling System (PCS), etc.

These primary systems are contained in secondary containments (glove box, hood, etc.) or in containment room.

Main leakage from the primary system is as follows;

- Loss from fluid system connections.
- Loss from valves, blowers, pumps, etc.
- Permeation
- Losses of tritiated water from the primary cooling system
- Losses associated with handling and disposal of tritium contaminated waste, etc.

The secondary containment system contains potential tritium releases resulting from mechanical equipment failures or operation errors, thereby protecting the environment and operating personnel.

The secondary containment atmosphere is maintained at a slight negative pressure and is continuously cleaned by the TRS.

The schematic pathway of tritium releases during normal operation is shown in Fig. VIII-3-1.

(2) Pathways of Tritium Releases at an Accident

In the case of the failure of the primary and secondary containments, tritium is released into the terminally containment.

In the event of an accident, the following steps are taken;

i) Each containment room is connected to the Emergency Air Cleaning System (ECS).

ii) Air supply and exhaust duct damper of normal ventilation system are closed.

iii) The ECS is actuated and operated until reducing the activity level of the contaminated room to the acceptable level.

iv) The contaminated room is always maintained at sub-atmospheric (about 1 inch of water negative) so as to prevent outleakage.

v) During the ECS operation, a part of the ECS flow air to balance infiltration air is exhausted to the Effluent Air Detritiation System (ADS).
The remainder is recirculated to the contaminated room.

Fig. VIII-3-2 shows schematic pathways of tritium releases at an accident.

(3) Pathways of Tritium Releases during Maintenance

The main maintenance is as follows;

- repair and maintenance of reactor
- repair and maintenance of divertor
- repair and maintenance of blanket, etc.

When the plasma vaccum vessel is opened for above maintenance, the dissolved tritium is released into the reactor room through the access ports.

To reduce the tritium releases to the environment two possible concepts can be considered. These pathways of tritium releases are shown in Fig. VIII-3-3.

These concepts are as follows;

(Concept A)

i) The structure materials in the plasma vacuum vessel is sufficiently baked out before the maintenance.

(Concept B)

i) The reactor room is divided into the several compartment.

ii) Tritium released into the compartment is removed by using the Effluent Air Detritiation System (ADS).

Notation

FCS	Fuel Gas Circulation System
BRS	Breeding Blanket Tritium Recovery System
PCS	Primary Cooling System
FRS	Fuel Receiver System
TSS	Tritium Storage System
WTS	Tritium Waste Treatment System
LES	Tritiated Liquid Waste Enrichment System
LPS	Tritiated Liquid Waste Packaging System
ERS	Effluent Tritium Removal System
SPS	Tritiated Solid Waste Packaging System
OPS	Tritiated Oil Packaging System
RPS	Radioactive Solid Waste Packaging System
WSS	Waste Storage System
LSS	Tritiated Liquid Waste Storage System
SSS	Tritiated Solid Waste Storage System
CSS	Tritiated Contaminated Component Storage System
RSS	Radioactive Solid Waste Storage System
TRS	Tritium Removal System
GPS	Inert Gas Purification System
ADS	Effluent Air Detritiation System
ECS	Emergency Air Cleaning System
DRS	Dryer Regeneration System

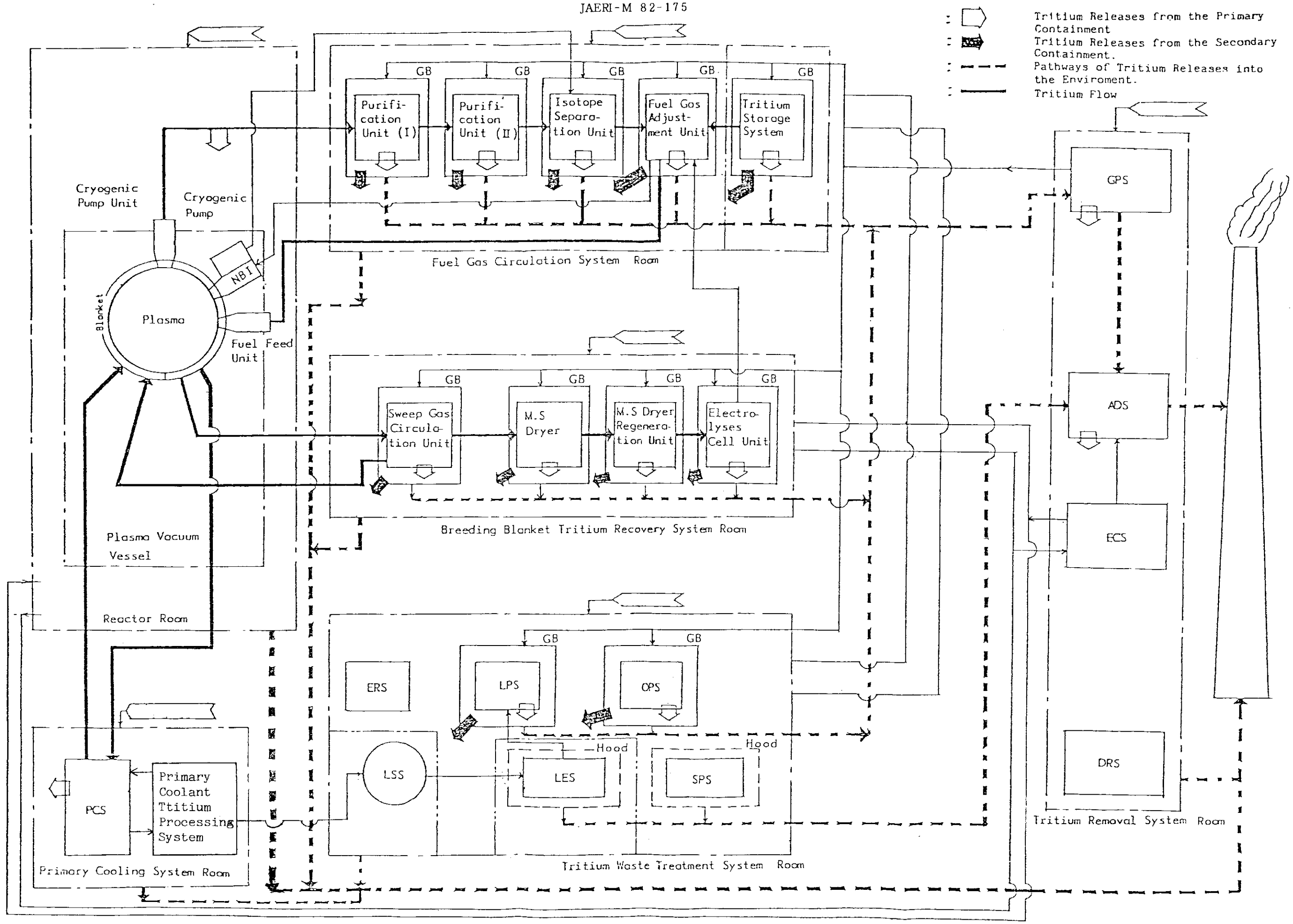

Fig.VIII-3-1 Schematic Pathway of Tritium Releases during Normal Operation

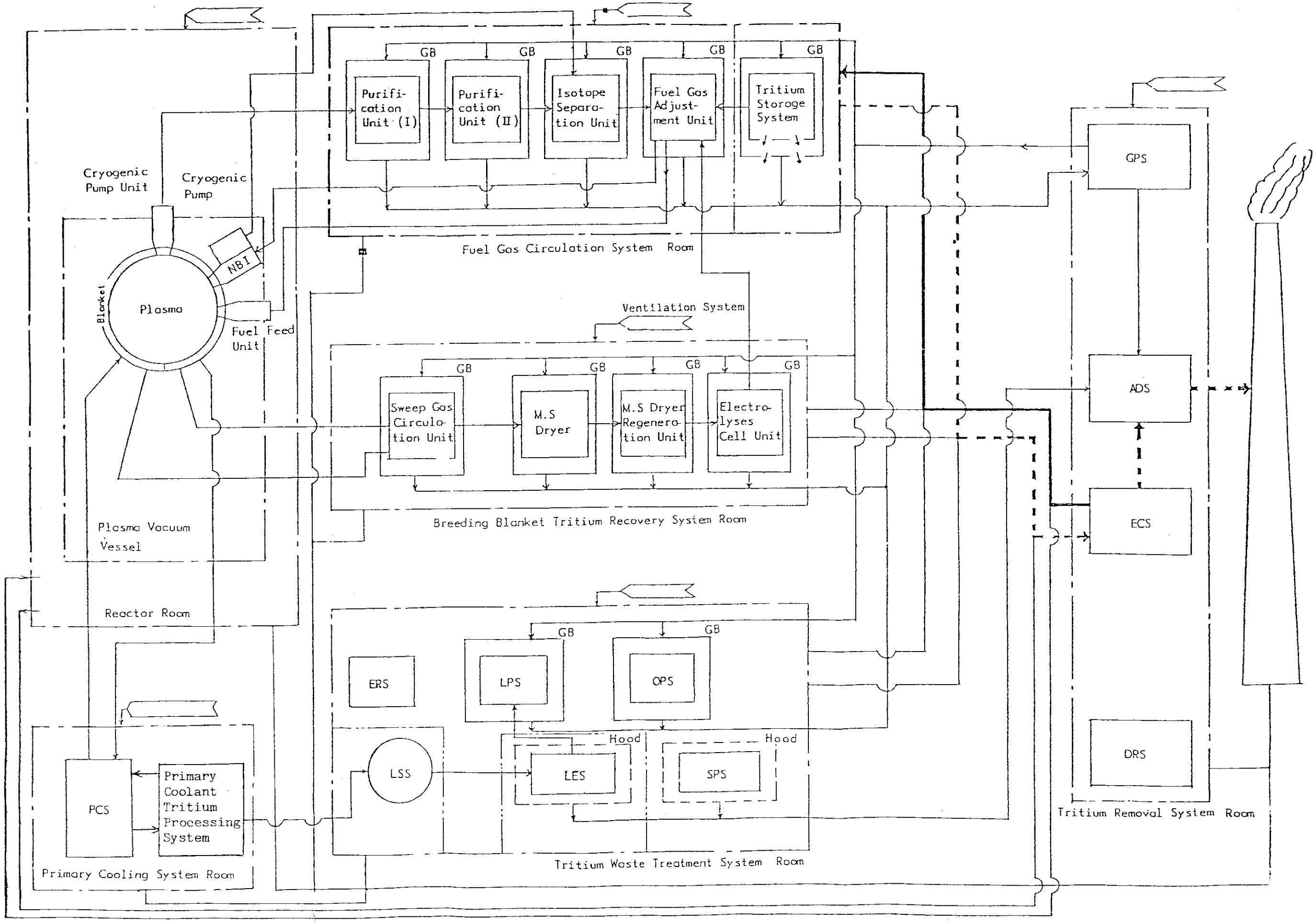

Fig. VIII-3-2 Schematic Pathway of Tritium Releases at an Accident

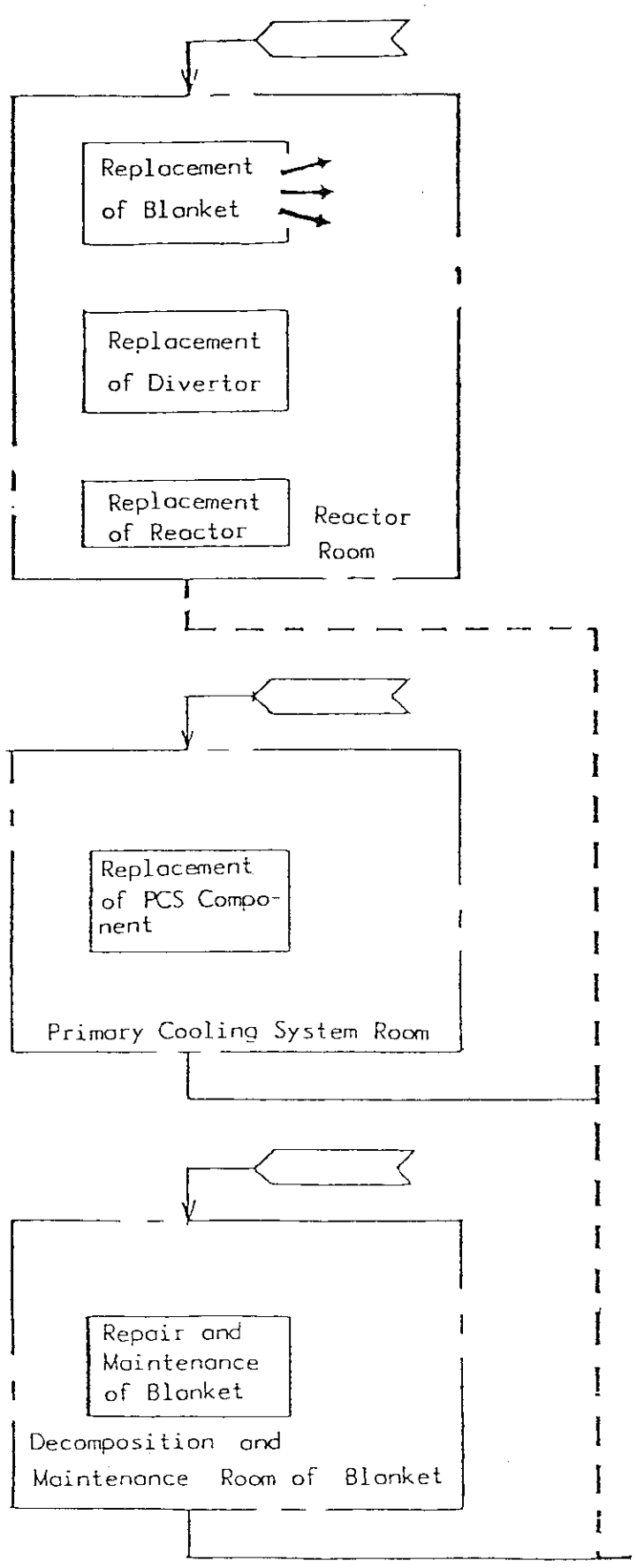

(Concept A)

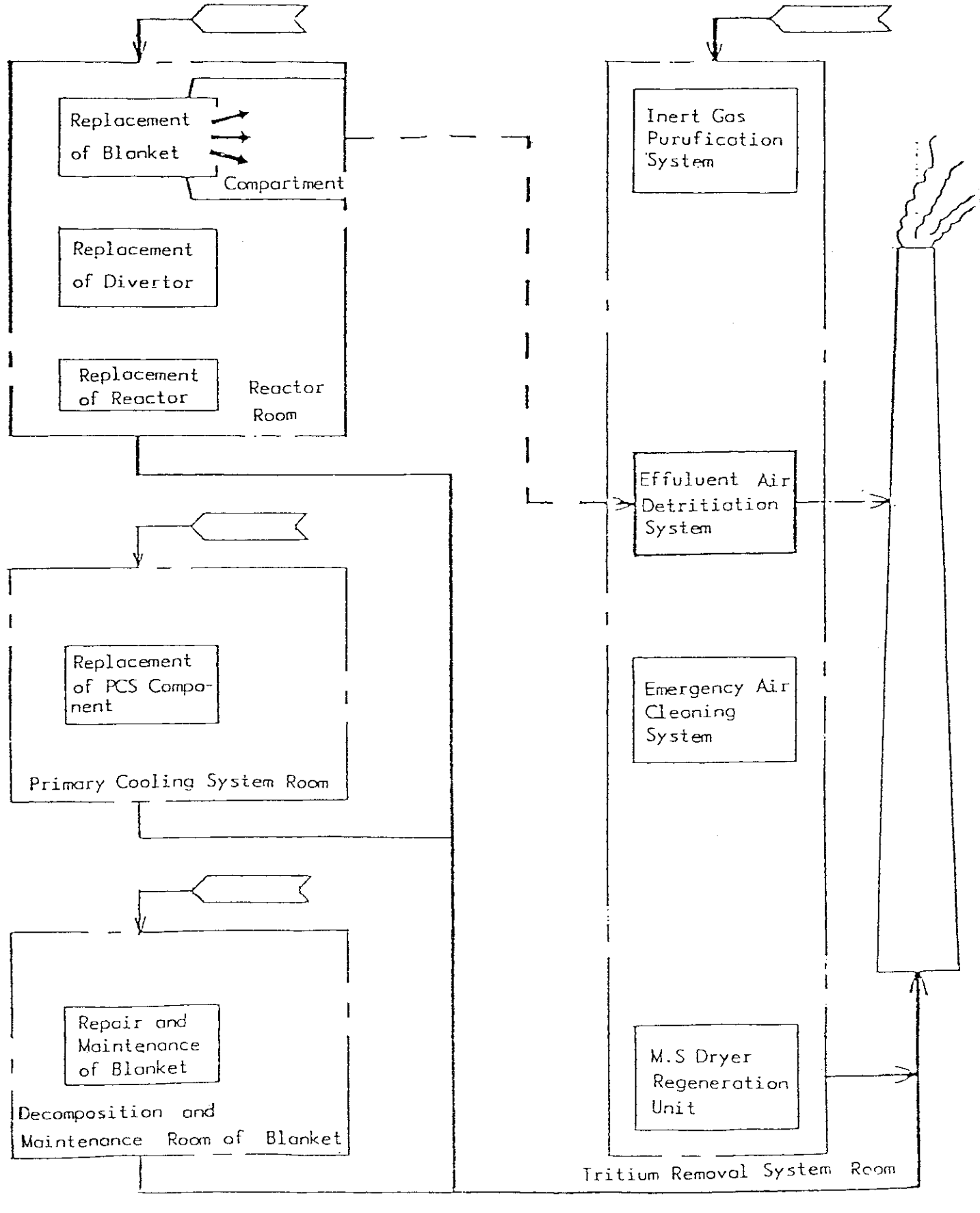

(Concept B)

Fig.VIII-3-3 Schematic Pathway of Tritium Releases during Maintenance

3.2 Tritium concentration levels on air

(a) Evaluation of Tritium Releases under Normal Operational Conditions

(1) Introduction

Among tritium systems, especially, fuel gas circulation system (FCS) and breeding blanket tritium recovery system (BRS) may treat tritium of great quantities. FCS and BRS are contained in gloveboxes (BBs) of secondary containments. In this section, tritium leak rates out of components of both FCS and BRS are evaluated, and then tritium permeation rates through gloves of GBs to the environment are evaluated.

(2) Analytical Model

Analytical model is shown below.

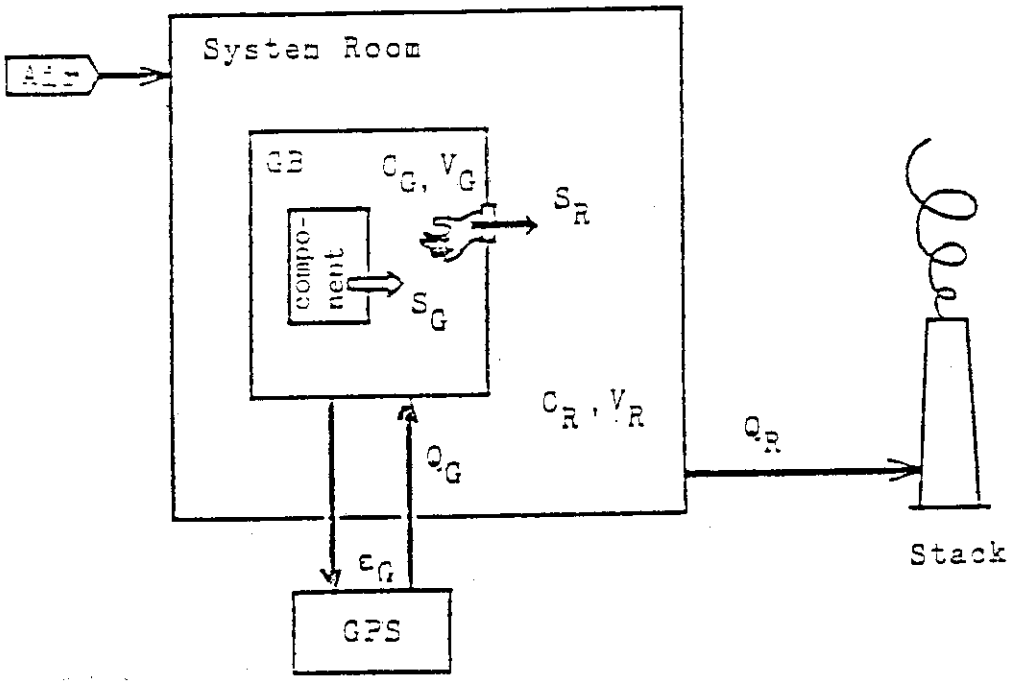

Notation

C (Ci/m^3) ; Tritium Concentration

V (m^3) ; Volume

Q (m^3/hr) ; Flow Rate

S (Ci/hr) ; Tritium Release Rate

ε (-) ; Tritium Removal Efficiency

(subscript)

G ; Glovebox

R ; System Room

(3) Analytical Conditions

a) Tritium Leak rate through component

Gas leak rate of single component is estimated to be 1.0×10^{-5} Acc/sec conservatively. Tritium concentration in a component is taken as that in normal operation. Tritium leak rate through a component is derived as a product of gas leak rate and tritium concentration.

b) Chemical form of tritium species in glovebox

Chemical form of tritium species in GB is estimated conservatively as follows;

FCS, $90\%T_2 + 10\%T_2O$,

BRS, $100\%T_2O$.

c) Tritium release rate through glovebox

Because GB is controlled at a slightly negative pressure, all the tritium release from GB into room is assumed to be in the mechanism of permeation through glove.

d) Parameters of glove

Parameters of glove are described as follows;

material ; Butyl Rubber

thickness ; 0.5 mm

surface area ; 1.0 m^2 per pair

e) Tritium permeation rate through glove

T_2O and T_2 permeation rate through glove are assumed to be equal to that of HTO and HT, respectively. Hence adopting Wittenberg's [19] data of tritium permeation through rubber films, tritium permeation rates per unit surface (λ) are derived as follows with subscript T_2 and T_2O;

$$\lambda T_2 = 4.2 \times 10^{-5} \ Ci/m^2 \cdot hr \cdot (Ci/m^3),$$

$$\lambda T_2O = 6.5 \times 10^{-4} \ Ci/m^2 \cdot hr \cdot (Ci/m^3).$$

f) Layout of glovebox in system room

As described in section 5, FCS and BRS are installed in five GB blocks in FCS room and in four GB blocks in GRS room, respectively.

g) Number of uncovered glove ports

Number of uncovered glove ports per GB block under normal operational conditions is assumed to be twenty - ten pairs of glove ports - except two GB blocks. These GB blocks are fuel gas receiver unit GB block of FCS and electrolysis cell one of BRS. Number of uncovered glove ports of fuel gas receiver unit is sixteen - eight pairs and that of electrolysis cell unit is eight - four pairs. These limitations are come from total number of glove ports.

h) Treatment of tritium in GB atmosphere

GB atmosphere is recirculated by Inert Gas Purification System (GPS) of Tritium Removal System (TRS). GPS is assumed to have a capacity of GB atmosphere change of ten times per hour and tritium removal efficiency (ε_G) of 0.99.

i) Ventilation of system room

System room is ventilated in a once-through mode at a room atmosphere change of six times per hour. Feed air is taken from outside of building.

(4) Fundamental Equation

$$V \frac{dC_G}{Gdt} = \dot{S}_G - \varepsilon_G Q_G C \qquad \text{(VIII-3-1)}$$

$$V \frac{dC_R}{Rdt} = S_R - Q_R C_R \qquad \text{(VIII-3-2)}$$

Assuming steady state, equations to be evaluated are as follows;

$$C_G = \frac{S_Q}{\varepsilon_G Q_G} \qquad \text{(VIII-3-3)}$$

$$C_R = \frac{S_R}{Q_R} \qquad \text{(VIII-3-4)}$$

where

$$S_R = C_G \qquad \text{(VIII-3-5)}$$

(5) Analytical Results

Analytical results are summarized in Table VIII-3-4. Tritium release rate into the system room is evaluated as follows;

FCS room ; 5.8×10^{-4} Ci/day,

BRS room ; 4.3×10^{-3} Ci/day.

And tritium concentration in the system room is evaluated as follows;

FCS room ; 1.4×10^{-9} Ci/m^3,

BRS room ; 2.0×10^{-8} Ci/m^3.

Tritium concentrations in both FCS and BRS room can be kept below the permissible level under normal operational conditions. The reason of high tritium concentration in electrolysis cell unit GB block is that tritium in it exists in T_2O form of high permeability through glove.

Table VIII-3-4 Tritium Concentration in System Room and Tritium Release Rate to Environment

		Tritium Concentration in Component	Number of Component	Leak Rate of Component	Total Leak Rate of Components in GB	Tritium Leak Rate	Volume of GB	GB Atmosphere Change Cycle	GB Recirculation Flow Rate	Tritium Concentration in GB	Tritium Permeation Rate from GB	Volume of System Room	System Room Atmosphere Change Cycle	System Room Recirculation Flow Rate	Tritium Concentration in System Room	Tritium Release Rate to Environment	Remarks
		Ci/m^3	n	Acc/sec	Acc/sec	Ci/hr	m^3	1/hr	m^3/hr	Ci/m^3	Ci/hr	m^3	1/hr	m^3/hr	Ci/m^3	Ci/day	
Fuel Gas Circulation System	Fuel Gas Reciever Unit	1.3×10^{6}	2	1.0×10^{-5}	2.0×10^{-5}	9.3×10^{-2}	2.7	10	27	3.4×10^{-3}	2.8×10^{-6}						No of Glove Ports - 16
	Purification Unit (I)	1.3×10^{6}	4	1.0×10^{-5}	5.0×10^{-5}	0.19	5.4	10	54	3.4×10^{-3}	3.5×10^{-6}						
	Purification Unit (II)	1.3×10^{6}	30	1.0×10^{-5}	3.0×10^{-4}	1.4	24.3	10	243	5.7×10^{-3}	5.9×10^{-6}	2.8×10^{3}	6	1.7×10^{4}	1.4×10^{-9}	5.8×10^{-4}	
	Isotope Separation Unit	1.3×10^{6}	14	1.0×10^{-5}	1.4×10^{-9}	0.65	17.1	10	171	3.8×10^{-3}	3.9×10^{-6}						
	D-T Gas Adjusting Unit	1.3×10^{6}	9	1.0×10^{-5}	9.0×10^{-5}	0.42	5.4	10	54	7.7×10^{-3}	7.9×10^{-6}						
Breeding Blanket Tritium Recovery System	Sweep Gas Recirculation Unit	1.4×10^{2}	5	1.0×10^{-5}	5.0×10^{-5}	2.4×10^{-5}	13.5	10	135	3.1×10^{-7}	2.0×10^{-9}						
	MS Dryer	1.6×10^{5}	4	1.0×10^{-5}	4.0×10^{-5}	2.3×10^{-2}	8.1	10	81	2.9×10^{-4}	1.9×10^{-6}						
	MS Dryer Regeneration Unit	1.6×10^{5}	4	1.0×10^{-5}	4.0×10^{-5}	2.3×10^{-2}	13.5	10	135	1.7×10^{-4}	1.1×10^{-6}	1.5×10^{3}	6	9.1×10^{3}	2.0×10^{-8}	4.3×10^{-3}	
	Electrolysis Cell Unit	2.3×10^{6}	11	1.0×10^{-5}	1.1×10^{-4}	0.92	1.35	10	13.5	6.8×10^{-2}	1.8×10^{-4}						No of Glove Ports - 8

(b) Handling Experiences of Tritium Water with Operations of a Heavy Water Reactor

A 165 MWe heavy water reactor, FUGEN, has been operated since 1978. A brief description of operational experiences of D_2O system of the reactor is given below.

The reactor has a D_2O system, containing 140 m^3 of D_2O, at 70°C circulating 1320 m^3/h for heat removal of 32.5 MWt. The concentration of tritium in the water is 2 Ci/l at present and is showly increasing with time of reactor operation. It is expected to approach to about 17 Ci/l after 30 years of operation.

Experiences so far obtained through operation of the reactor have indicated that tritium concentration in the air of the reactor containment having a volume of 45000 m^3 is of the order of 10^{-8} μCi/cc at normal operation so that no special suits are required for operational personel.

Care to restrict the tritium concentration in the air has been taken whenever a maintenance work to disassenble parts of the D_2O system are to be carried out. The past experience indicate that the concentration of tritium in the air in the vicinity of the place where such a maintenance work is done can be maintained at around 10^{-6} μCi/cc.

3.3 Air detritiation system and cost

(a) Sensitivity Analysis of Emergency Air Cleaning System

(1) Introduction

Multiple-barrier containment concept is adopted for confining tritium in fusion reactor. Reactor room is used as the final barrier for the tritium release to the environment in the event of abnormal tritium spill. Emergency Air Cleaning system (ECS) based on the processing by catalytic oxidization and followed by adsorption is provided to satisfactorily confine tritium in the room and to cleanup the room atmosphere below the permissible tritium concentration. Since the free volume of reactor room is huge, the order of 10^5 m^3, ECS is considered to be a system having enormous capacity.

There are a number of factors affected to the capacity of ECS. In this section, by picking up major factors concerning capacity of ECS, sensitivity analysis with regard to these parameters is carried out and practical capacity of ECS is evaluated.

(2) Evaluation of ECS Capacity Required to Reactor Room Cleanup

A parametric study is carried out to evaluate the tritium cleanup characteristics by means of computer code, which is modeled after TSOAK-M1 [20] and incorporated phenomenon: The reduction of ECS detritiation efficiency occurs by lowering of humidity in reactor room atmosphere. The following variables affect with ECS capacity: (i) the amount of tritium released; (ii) the volume of reactor room; (iii) the flow rate of ECS; (iv) the total surface area of reactor room; (v) the infiltration rate into the reactor room; (vi) the rate of formation of HTO and HT from T_2; (vii) the rate of adsorption/desorption at the surface of reactor room; and (ix) the rate of isotopic swamping at the inlet of adsorber in ECS. And assessment of ECS capacity is consequently made to evaluate the sensitivity of ECS cost to these parameters.

a) Tritium Cleanup Characteristics

It is assumed here that the air in reactor room of volume V is circulated through ECS of detritiation efficiency of ε at a volumetric flow rate of Q. Neglecting tritium soaking, tritium concentration (N) in reactor room with time (t) is approximately given by

$$V\frac{dN}{dt} = -\varepsilon QN \qquad \text{(VIII-3-6)}$$

Assuming that the detritiation efficiency of ECS is nearly unity, the flow rate of ECS (Q_T) required to reduce the initial tritium activity level (N_i) to the final one (N_f) in time τ is obtained from eq. (VIII-3-6).

$$Q_T = \frac{V}{\varepsilon\tau}\ln(N_i/N_f) \qquad \text{(VIII-3-7)}$$

The required flow rate of ECS for the following scenario is estimated to be 8.8×10^4 m^3/hr as an ideal case without tritium soaking using eq.(VIII-3-7): ECS cleans up the reactor room of 1.5×10^5 m^3 below the activity level of 5×10^{-6} Ci/m^3 within 24 hours in the event of accidental tritium spill of 10^2 g.

Numerical simulation of tritium cleanup operation is carried out using computer code modelled after TSOAK-M1 which takes tritium soaking into account. The values of parameters selected for the base case are summarized in Table VIII-3-5. The calculated results are plotted in Fig. VIII-3-4 and Fig. VIII-3-5. Residual tritium species concentrations (for T_2, HTO, HT and total tritium activity level) and ideal response neglecting tritium soaking are shown in Fig. VIII-3-4 as a function of time. Amount of soaked tritium and level of soaking effect (the difference of residual tritium in reactor room occurs whether

presense of tritium soaking, or not) are shown in Fig.VIII-3-5 together with the residual tritium concentration. As shown in Fig.VIII-3-4, tailing of residual tritium concentration after ten hours operation of ECS is ascribed to the slow desorption of initially adsorbed HTO since the residual tritium species in the reactor room is dominant of HTO after ten hours of operation. The adsorbed tritium as HTO amounts to be about 2×10^4 Ci at the maximum when it operates five hours. This adsorbed tritium becomes the relatively high level tritium source when the residual tritium concentration in reactor room becomes low.

b) Parametric Study of ECS Capacity

To assess the impact of factors on the capacity of ECS, parametric study of ECS capacity is carried out by varying selected base case parameters in Table VIII-3-5.

Fig.VIII-3-6 shows the effect of ECS flow rate and amount of tritium released on the tritium concentration after 24 hours of ECS operation. As seen in Fig.VIII-3-4, when the ECS of 1×10^5 m^3/hr is provided, this capacity is obtained from eq. (VIII-3-7) for 10^2 g release, ECS can cope with only the 10^0 g tritium release to cleanup atmosphere below the level of 5×10^{-6} Ci/m^3 in a day.

Fig.VIII-3-7 shows the effect of ECS flow rate and cleanup time on the tritium concentration after 24 hours of ECS operation. Cleanup time has minor effect on the flow rate of ECS. This result is ascribed to the tailing of the residual tritium concentration arising in these hours.

The dependence of required flow rate of ECS on the amount of tritium released and on the cleanup time is shown in Fig.VIII-3-8. Required flow rate of ECS proportionally increases by approximately the root of the amount of tritium released.

When the cleanup time increases from 24 to 48 hours, required flow rate decreases by 26%, and when the cleanup time decreases from 24 to 12 hours, it increases by 16%.

The formation of HTO and HT from T_2 in reactor room environment follows by a simple pseudo-second-order process. The rate of reaction of T_2 with H_2O to form HTO and HT is assumed to be independent on humidity herein. Reported values for the rate constant of formation of HTO and HT vary widely from 10^{-6} to 10^{4} $m^3/Ci/hr$[21]. The effect of this rate constant and flow rate of ECS operation is shown in Fig.Ⅷ-3-9. And Fig.Ⅷ-3-10 shows the dependence of required flow rate of ECS on this rate constant. If this rate constant is less than 10^{-4} $m^3/Ci/hr$, the required flow rate of ECS is almost equal to that for the ideal case (obtained by eq.(Ⅷ-3-7)),as seen in Fig.Ⅷ-3-10. And if the reaction rate constant is more than 10^{1} $m^3/Ci/hr$, the required flow rate of ECS amounts to be about as thirty-fold as that for the ideal case. Thus it is advantageous to design reactor room to minimize the rate of formation of HTO though the tritium soaking is affected by a number of factors.

Soaking of tritium, that is the adsorption and subsequent desorption of HTO, is treated according to TSOAK-M1 . The rate of HTO adsorption is taken to be proportional to the HTO concentration in reactor room and the rate of HTO desorption is taken to be proportional to the amount of soaked tritium (as HTO). There are a few data on the rate of adsorption/desorption of HTO. According to bench-scale -air -detritiation test conducted at ANL, both the adsorption rate and desorption rate are reported to be around 1×10^{-1} m/hr in cyclic detritiation. In once through flushing mode, however, both rates derease by the order of one or two.

The effect of adsorption/desorption rate on the required flow rate of ECS is shown in Fig.Ⅷ-3-11. If the adsorption rate is less than 10^{-4} m/hr, the required flow rate of ECS is almost

equal to that for the ideal case as in Fig.VIII-3-11. And if the desorption rate is around 10^{-1} m/hr, required flow rate increases by a factor of 2.6 as the one order increase of adsorption rate takes place. Although it is advantageous to minimize surface adsorption and desorption for the purpose of minimizing ECS capacity, reactor room surface of low desorption rate becomes the permanent tritium source for long days. It is therefore preferable to design reactor room of minimum surface adsorption but reasonable desorption rate.

Fig.VIII-3-12 shows the effect of total surface area in a given volume on the residual tritium concentration. It is seen in Fig.VIII-3-12, that this effect is minimal.

Fig.VIII-3-13 shows the effect of volume of reactor room on the required ECS flow rate. In this calculation, both the ratio of surface area to the reactor volume and relative infiltration rate are kept constant. It is seen from Fig.VIII-3-13 if the reactor room is divided into ten compartments, the required flow rate of ECS in the event of 10^{2} g tritium release in a compartment reduces by a factor of 2.

The effect of the design target level of tritium activity level in the reactor room on the required flow rate of ECS is shown in Fig.VIII-3-14. If this level is 5×10^{-7} Ci/m^3, required flow rate of ECS is 38-fold to that for the ideal case. And if the level is 5×10^{-5} Ci/m^3, required flow rate of ECS is 9-fold to that of the ideal case. It is explained that activity level is highly influenced by tailing effect.

In the absence of isotopic swamping, since process efficiency of ECS begins to reduce from nearly unity because of lowering of atmospheric humidity by water adsorption of ECS, and dominant residual tritium species is HTO as seen in Fig.VIII-3-4, cleanup operation can not be performed as expected.

In these calculations, when the humidity at the inlet of adsorber of ECS lowers down to 10^{2} ppm, water swamping unit

is assumed to be actuated to maintain inlet humidity of adsorber up to 10^2 ppm.

The effect of isotopic swamping rate and infiltration rate into the reactor room on the required flow rate of ECS are shown in Fig.VIII-3-15. It is seen in Fig.VIII-3-15 that in the absence of water swamping and in the infiltration of 0.1%-V/day case, required flow rate of ECS increase five-fold than that in the presense of swamping. But it is preferable to adopt the swamping rate of 10 ppm to minimize the amount of liquid waste recovered at adsorber.

(3) Conclusion

a) In the event of accidental tritium spill of 10^2 g, ECS of 8.8×10^4 m^3/hr is to be provided to cleanup reactor room of 1.5×10^5 m^3 below activity level of 5×10^{-6} Ci/m^3 in 24 hours not taking account of tritium soaking. When taking account of tritium soaking with medium values reported, required flow rate of ECS increases by a factor of 19 (to 1.7×10^6 m^3/hr).

b) The effect of cleanup time on required flow rate of ECS is relatively less.

c) Required flow rate of ECS is proportional to approximately the root of amount of tritium released.

d) Reactor room has to be designed to minimize rate of HTO formation.

e) It is preferable to design reactor room having the rate for minimum surface adsorption but reasonable desorption.

f) Even if the reactor room is divided into ten compartments, required flow rate of ECS is only reduced by a factor of two than the base case.

g) If the design target level of tritium activity level is low, requried flow rate of ECS is apt to be affected by a soaking effect.

h) It is preferable to adopt water swamping unit to achieve high detritiation efficiency in the case of low humidity in reactor room.

i) Further experimental study on the tritium soaking in reactor room is to be performed.

Table VIII-3-5 Parameters for the Base Case

Parameter	Symbol	Unit	Value	Remarks
Volume of reactor room	V	m^3	1.5×10^5	
Species of released tritium			T_2	
Amount of released tritium	S	g	1.0×10^2	
Volumetric flow rate of ECS	Q	m^3/hr	1.0×10^5	
Total area os reactor room surface	A	m^2	5.0×10^4	
Infiltration rate	L	m^3/hr	6.25	0.1%-V/day
Efficiency of oxidizing reactor	ε_1		0.999	
Efficiency of adsorber	ε_2		minimum 0.99	H_2O swmping
Reaction constant of HTO formation	C	$m^3/Ci/hr$	1.0×10^0	
Adsorption rate constant	E	m/hr	1.0×10^{-1}	
Desorption rate constant	F	m/hr	1.0×10^{-1}	

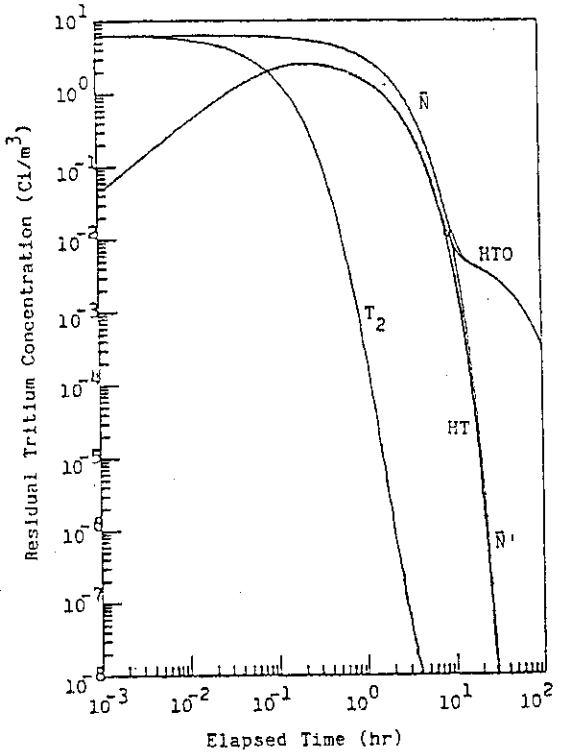

N̄ : total residual tritium concentration taking tritium soaking into account

N̄': total residual tritium concentration not taking tritium soaking into account

Fig.VIII-3-4 Residual tritium concentration

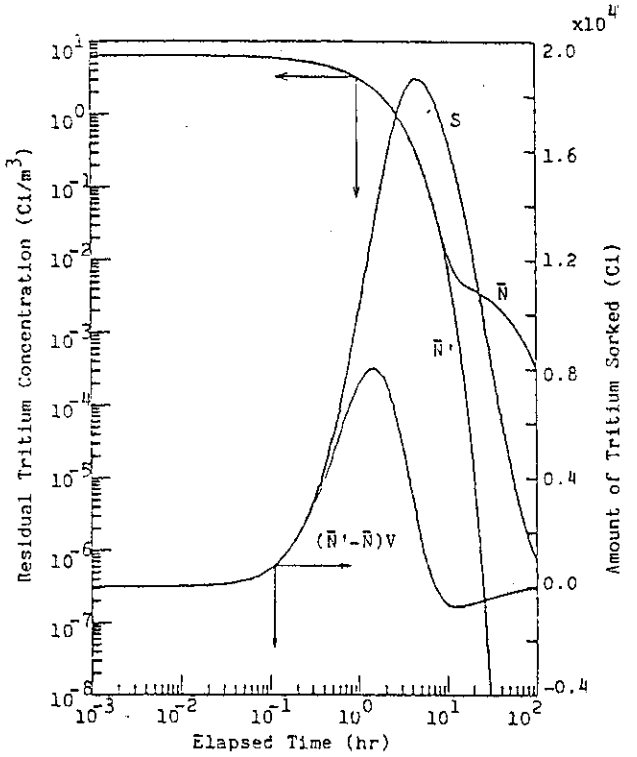

N̄ : total residual tritium concentration taking tritium soaking into account

N̄': total residual tritium concentration not taking tritium soaking into account

Fig.VIII-3-5 Amount of tritium sorked

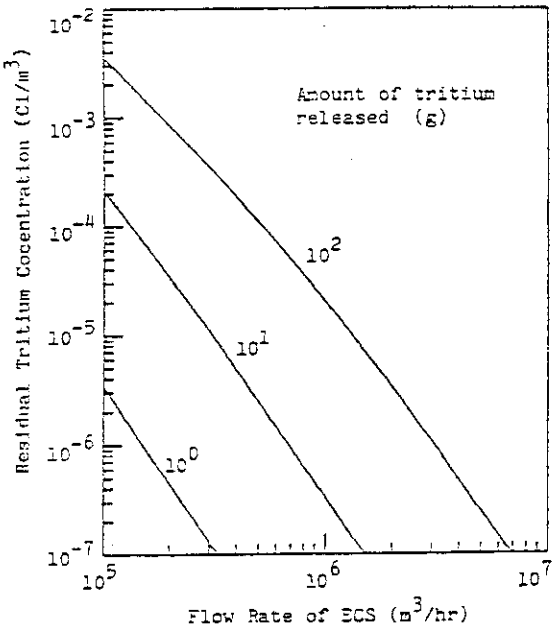

Fig.VIII-3-6 Dependence of residual tritium concentration on ECS flow rate and amount of tritium released

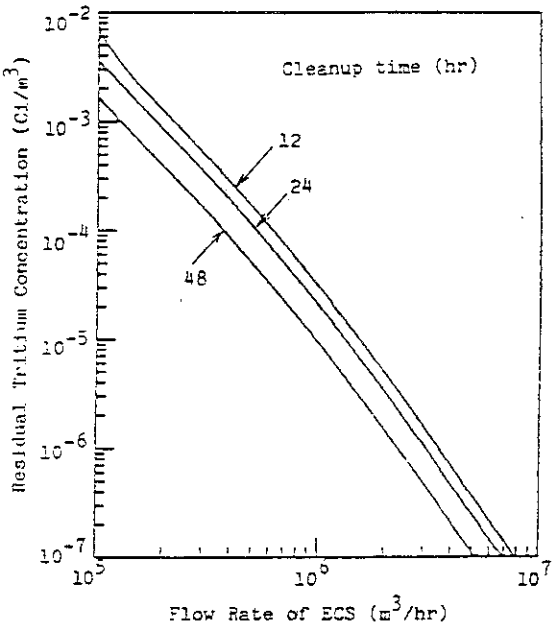

Fig.VIII-3-7 Dependence of residual tritium concentration on ECS flow rate and cleanup time

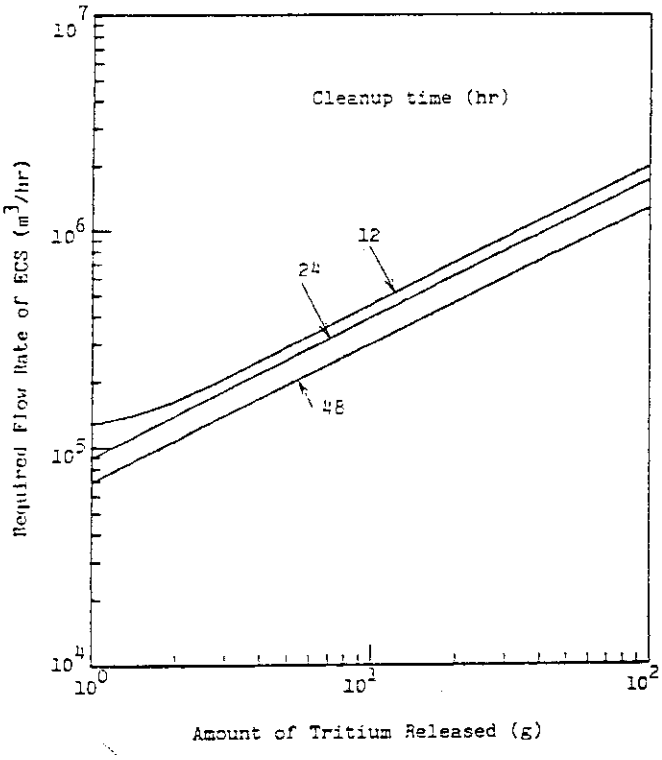

Fig.VIII-3-8 Dependence of required flow rate of ECS on amount of tritium released and cleanup time

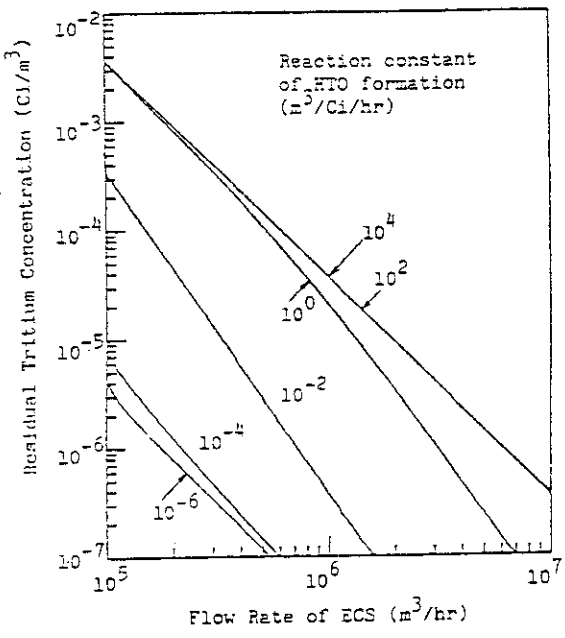

Fig.VIII-3-9

Dependence of residual tritium concentration on ECS flow rate and reaction constant of HTO formation

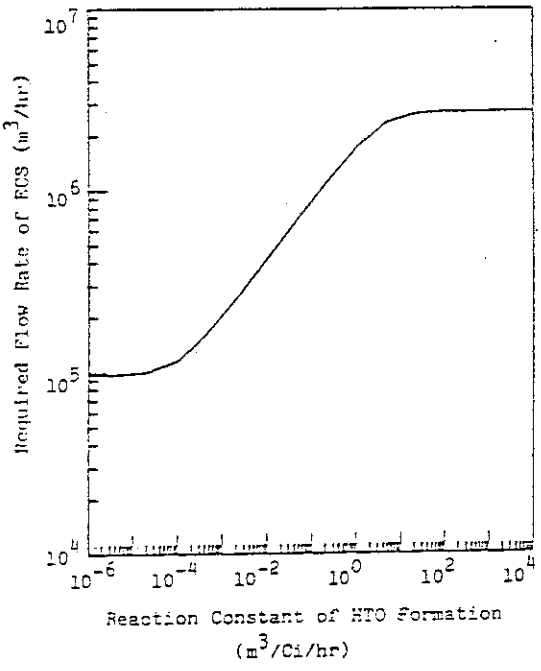

Fig.VIII-3-10

Dependence of required flow rate of ECS on reaction rate constant of HTO formation

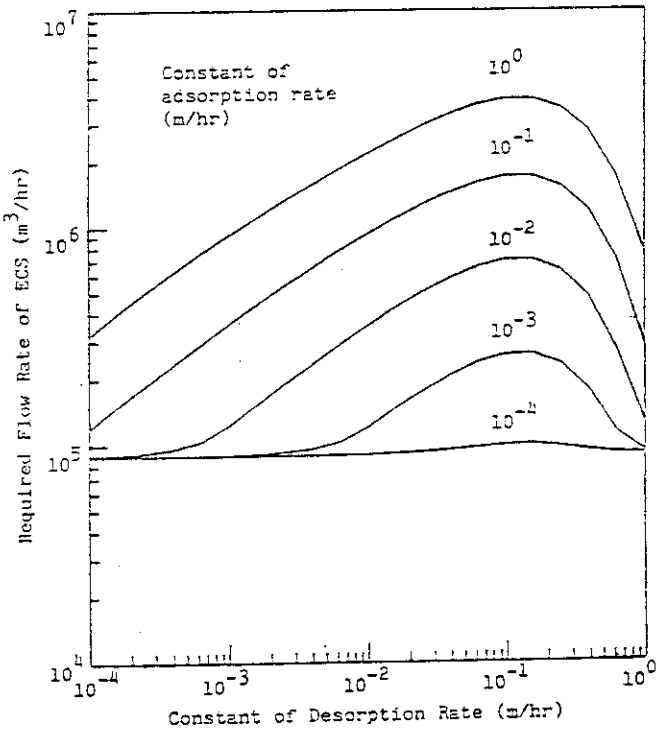

Fig.VIII-3-11

Dependence of required flow rate of ECS on constant of desorption rate and constant of adsorption rate

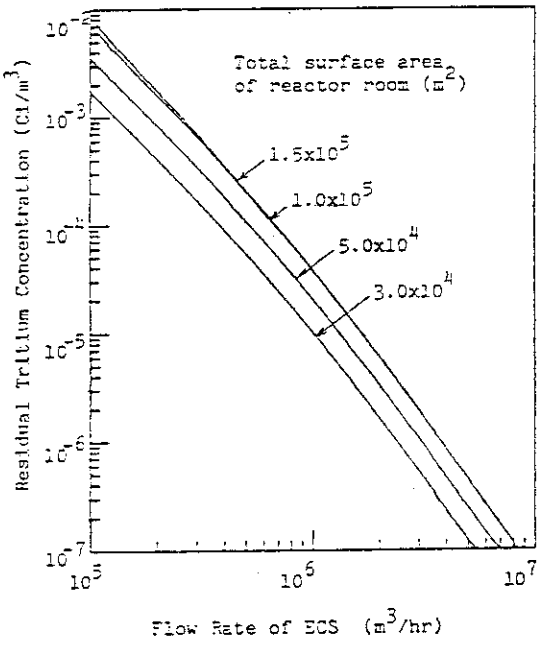

Fig.VIII-3-12

Dependence of residual tritium concentration on ECS flow rate and total surface area of reactor room

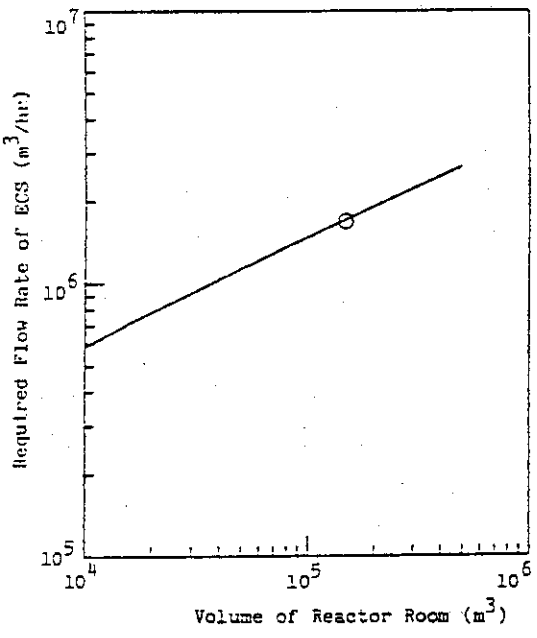

Fig.VIII-3-13

Dependence of required flow rate of ECS on volume of reactor room

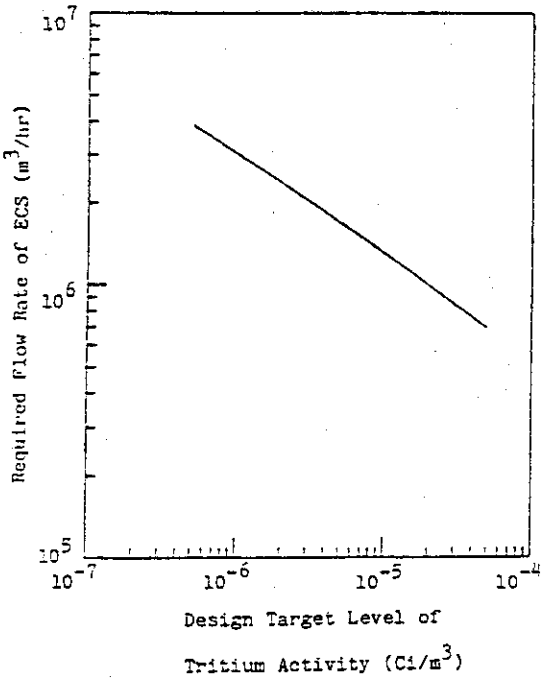

Fig.VIII-3-14

Dependence of required flow rate of ECS on design target level of tritium activity

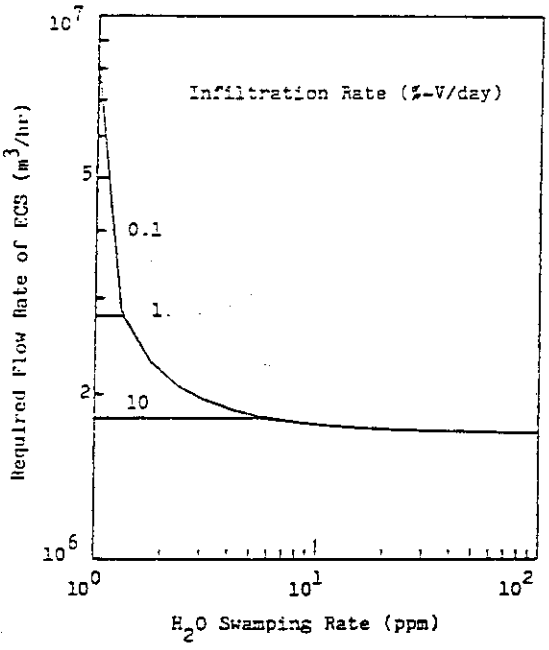

Fig.VIII-3-15 Dependence of required flow rate of ECS on H_2O swamping rate and infiltration rate into reactor room

3.4 Personnel access

(a) Worker Productivity in Tritium Contaminated Environment

When a large amount of accidental tritium is released into the reactor hall, a impractically large-capacity Emergency Air Cleanup System (ECS) is required to reduce the tritium contamination level below MPC for access of unprotected personnel to the reactor hall 24h after reactor shut-down. In the case of a practical (i.e. smaller) capacity ECS, some tritium protection measure (e.g. tritium protection suit) must be taken to permit personnel access under high-level tritium concentration. However, the wearing tritium protection suit significantly affects worker productivity.

The productivity reduction factor for nuclear facility decommissionig is presented here, in the following description[22].

$$M1 = F1 \cdot F2 \cdot F3 \cdot F4$$

where, F1, factor resulting from wearing anti-contamination suits =1.15
F2, factor resulting from wearing respirators =1.50
F3, factor resulting from contamination control =1.20
F4, factor from untimely crew change =1.0

From the above-mentioned description, the productivity reduction factor M1 is calculated to be 2.07 That is to say, the productivity will decrease by 50 percents approximately.

4. Tritium breeding blanket

4.1 Solid breeder

4.1.1 New data on solid breeder

(a) Fabrication and Inspection of Sintered Li_2O Pellets

(1) Introduction

A great amount of sintered lithium oxide pellets is required for blanket material of a fusion reactor.

To develop the mass production technique of the sintered pellets, an elementary work on the fabrication and the inspection of the sintered pellets were performed.

Three types of cylindrical pellets, which have low, medium and high density, were fabricated by die-pressing and sintering. Ceramic-grade Li_2O powder of high purity was used as the material. Die-pressed compacts were sintered in vacuum atmosphere at several temperatures. In the fabrication processes, Li_2O was handled in inert gas atmosphere and/or vacuum atmosphere.

(2) Fabrication processes of pellets

The fabrication processes used in the present work was as follows.

i) Agglomeration with mortar (particle size distribution after this treatment is shown in Fig. VIII-4-1

ii) Die-pressing (4 ton/cm^2)

iii) Dimension and weight measurement

iv) Sealing of pressed compact (green pellet) in furnace core tube (Pt-crucible was used)

v) Sintering in vacuum ($< 5 \times 10^{-5}$ Torr)

vi) Inspection

The temperature and sintering time were varied for each type of pellets.

type L ; 1000°C x 2 hr

type M ; 1100°C x 2 hr

type H ; 1200°C x 2 hr

Fractured surface microstructure of the green pellet and sintered pellets were obsereved with SEM (Fig.VIII-4-2)

(3) Material

Ceramic-grade Li_2O powder (particle size; -4") produced by CERAC/PURE inc. was used as raw material. Nominal purity of the powder was as follows.

(i) Specific analysis and X-ray analysis

LiOH	;	1.58% (Trace by X-ray)
Free C	;	0.01
Li_2CO_3	;	0.5% (None observed by X-ray)
Sulfur	;	0.005 max.
Li	;	Natural lithium isotopes

(ii) Spectrographic analysis

Al	0.005%	Fe	0.001%
Ca	0.005-0.05	Mg	0.001
Cu	0.001	Na	0.05-0.1
Ni	not detected	Pb	not detected
Si	0.001	Ag	not detected
Co	0.01	K	0.01
Mo	0.01	Mn	0.01
Sn	0.01	Ti	0.01

(4) Character of pellets

(i) Dimension and bulk density

Dimension and bulk density of the random samples (four pellets in each type) were measured. Following table summarizes the results of the measurements.

Type	Dimension (mm)		Bulk density (%T.D.)
	diameter	length	
H	4.86-4.95	4.89-5.30	87.7-91.3
M	5.05-5.09	5.36-5.55	82.3-83.2
L	5.27-5.37	5.00-5.92	73.2-78.1

(ii) Porosity

Porosity of the sintered pellet of a random sample in each type was measured by following liquid immersiom method. Each sample was evacuated to 1 x 10^{-2}Torr for 1 hr after measuring weight by precise balance in air atmosphere, and then immersed in fluid paraffin for 10 minutes while evacuation by vacuum pump was continued. Fluid paraffin was suitable liquid because of its low viscosity (41.9-44 centi-stokes) and non-reactivity with Li_2O.

Weighing and calculation after immersion were done by the conventional method. Following table shows the results of the measurements.

Type	Apparent density* (%T.D.)	Porosity (%)	
		open	closed
H	88.3	1.0	10.7
M	83.6	3.4	13.0
L	76.5	7.6	15.9

* immersion density

(iii) Specific surface area

Specific surface area of random samples (three pellets in each type) was measured by BET method with krypton adsobate. The adsorption measurement was performed at liquid N_2 temperature (77K). Following table shows the results of the measurement.

Type	Surface area (m^2/g-Li_2O)
H	0.38
M	0.57
L	1.3

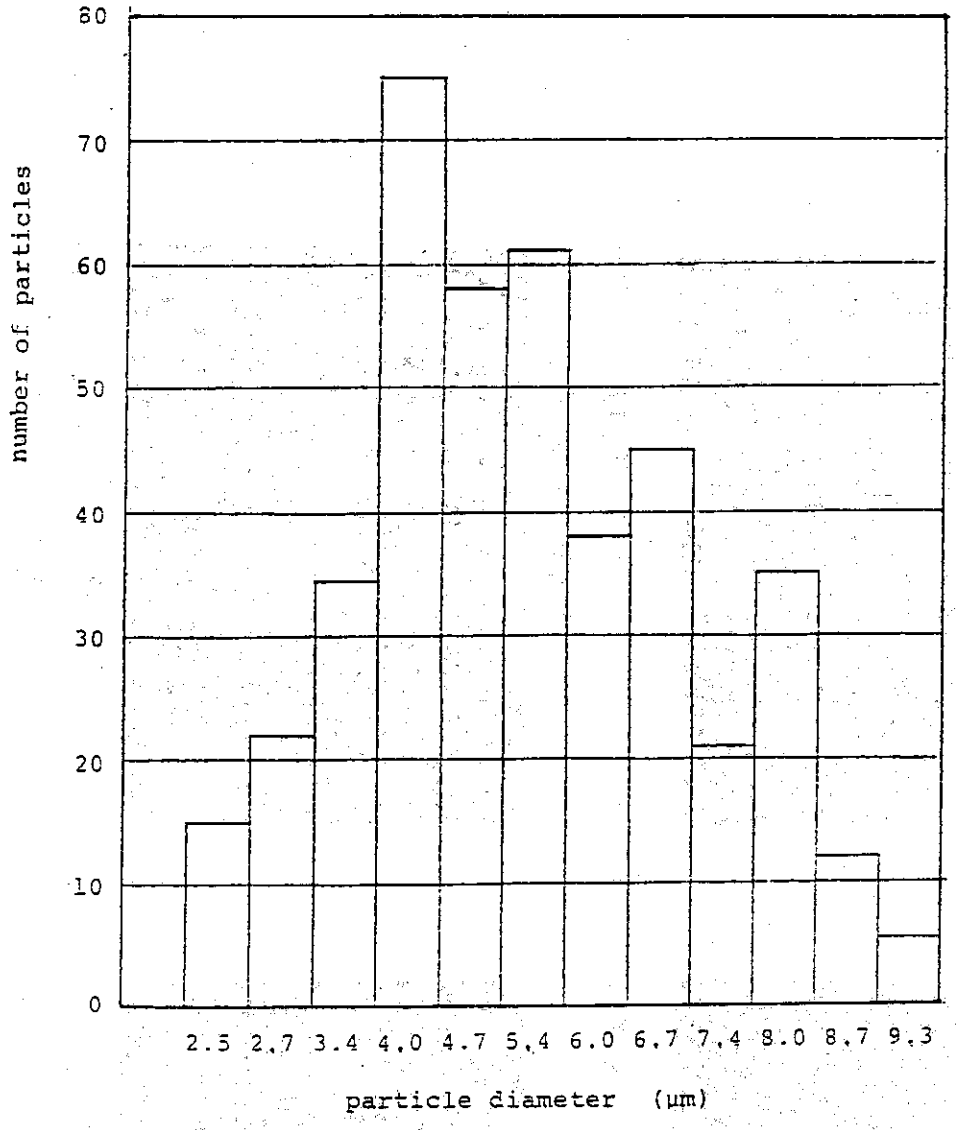

Fig.VIII-4-1 Particle size distribution of Li_2O powder after agglomeration with mortar

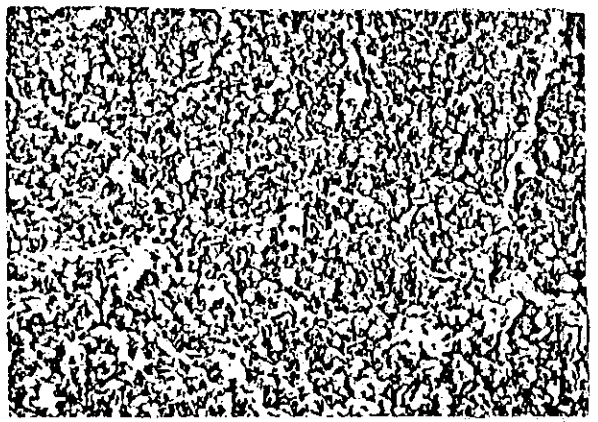

67 % T.D x 280
Green Pellet

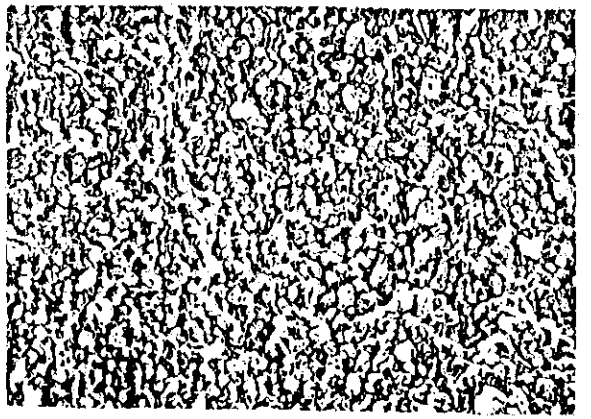

75 % T.D x 280
1000°C × 2hr

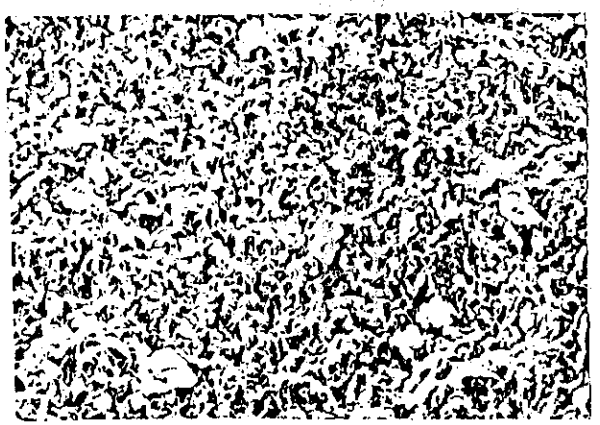

85 % T.D x 280
1100°C×2hr

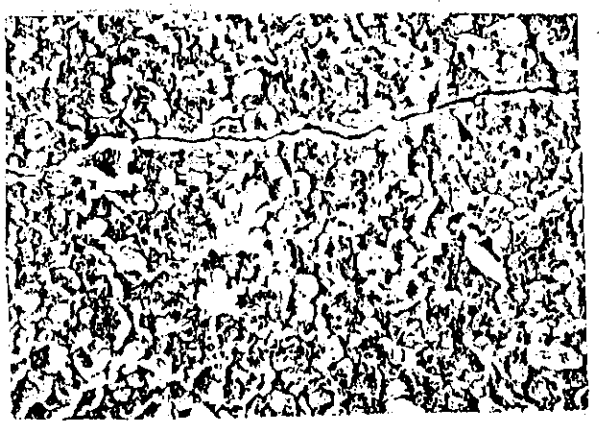

90 % T.D x 280
1200°C×2hr

Fig.VIII-4-2 Microstructure of Li_2O pellets

(b) Solubility and Diffusivity of Hydrogen in Li_2O Pellet

In order to understand the mechanism of tritium release process and to evaluate tritium inventory in the Li_2O blanket of fusion reactor, thermodynamical studies of hydrogen behaviors in Li_2O are very important. In the present work, solubility and diffusivity of hydrogen as well as reactivity in the system were measured by thermodynamical method such as equilibrium-quenching and hot-extraction method.

(1) Experimental

(i) Reactivity in Li_2O - hydrogen system

In order to examine chemical reactivity between Li_2O pellet (M type) and hydrogen gas, analytical measurement of extracted gas from the pellet equilibrated with deuterium gas at about 970K was done with quadrupole mass spectrometer.

In the experiment, D_2O species could not be observed. From this result, it was thought that hydrogen gas would not react with Li_2O pellet in the temperature. This fact would be supported by the thermodynamical data in Li_2O - hydrogen system.

(ii) Hydrogen solubility in Li_2O

Pressure variation of dissolved amount of hydrogen in Li_2O is shown in Fig.VIII-4-3. The temperature, at which the pellet was equilibrated to the hydrogen or deuterium atmosphere for half a day or 3 days as maximum, was maintained at 823K. It was confirmed that enough equilibration at that temperature was attained during half a day equilibration. This result is also supported from the hydrogen diffusion data obtained by the present study. In the hot-extraction process, the pellet was heated to 963K for more than 2 hours. If solubility is given by $S = S_0 e^{-Q/RT} \cdot P^{\alpha}$, α took the value of about 0.5(Sieverts' law) as seen in Fig.VIII-4-3. This result implies atomic and/or ionic hydrogen rather than molecular hydrogen dissolved in the pellet. The isotope relation for solubility between protium and deuterium (S_H/S_D) in the Li_2O pellet was seemed to be not much different from that observed in metals such as a stainless steel[11]. The activation energy of solubility for protium and deuterium in the Li_2O pellets was 16kJ/mol and 19kJ/mol, respectively. Hydrogen solubility in ceramics of Al_2O_3 [23] and SiC[24] and in the metals of platinum[25] and molybdenum[26] is shown in Fig.VIII-4-4 comparing with the earlier data of Li_2O. It is interesting to note that the hydrogen solubility in these ceramics is larger than that in metals of platinum and molybdenum.

(iii) Hydrogen diffusivity in Li_2O

Diffusion coefficient for hydrogen and deuterium in Li_2O is shown in an Arrhenius plot in Fig. 2.4. The activation energy is 34kJ/mol and 40kJ/mol for protium and deuterium respectively. The activation energy of the diffusion coefficient by Guggi et al.[27] 28.7kJ/mol in the temperature range of 773K to 973K, is close to our result. The tritium diffusion coefficient obtained by Kudo and Okuno[28] in the temperature range of 580K to 700K is higher than our results by about two orders of magnitude and its activation energy is 104kJ/mol.

It will be worth while studying the hydrogen diffusion mechanism to compare the hydrogen diffusion coefficient with the self diffusion coefficients of lithium and oxygen in Li_2O. The hydrogen diffusion coefficient determined in our experiment is about 3 orders of magnitude lower than the self diffusion coefficient of Li, however, it is about

one order of magnitude higher than that of oxygen in Li_2O in the temperature range below 1073K as shown in Fig.VIII-4-5. From these results, hydrogen is thought to diffuse independently from Li and O in Li_2O.

(The detailed description is found in Reference [A1].)

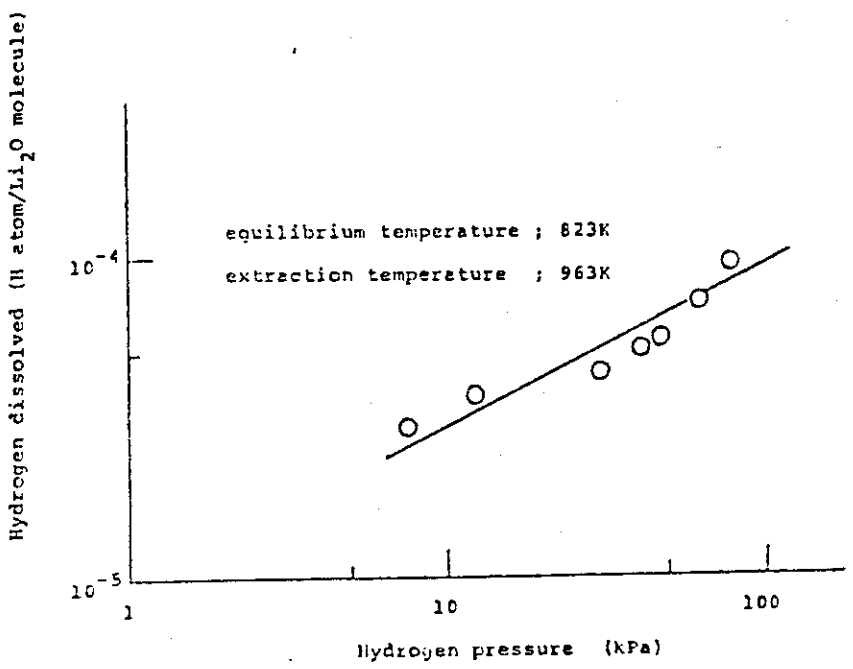

Fig.VIII-4-3 Pressure variation of amount of dissolved hydrogen in Li_2O pellet.

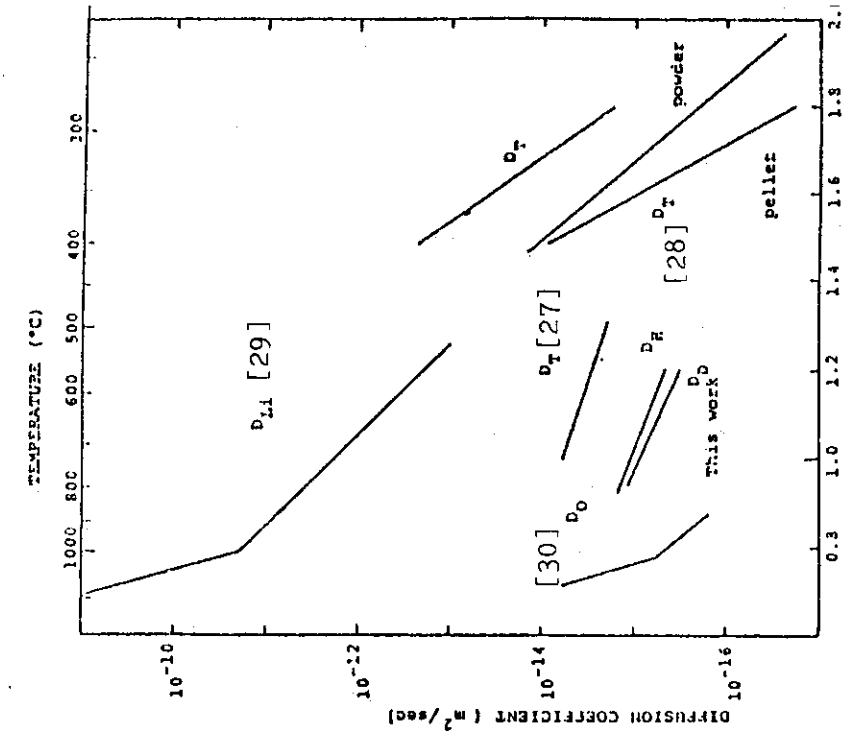

Fig.VIII-4-5 Diffusion coefficient for Li, O and hydrogen in Li_2O.

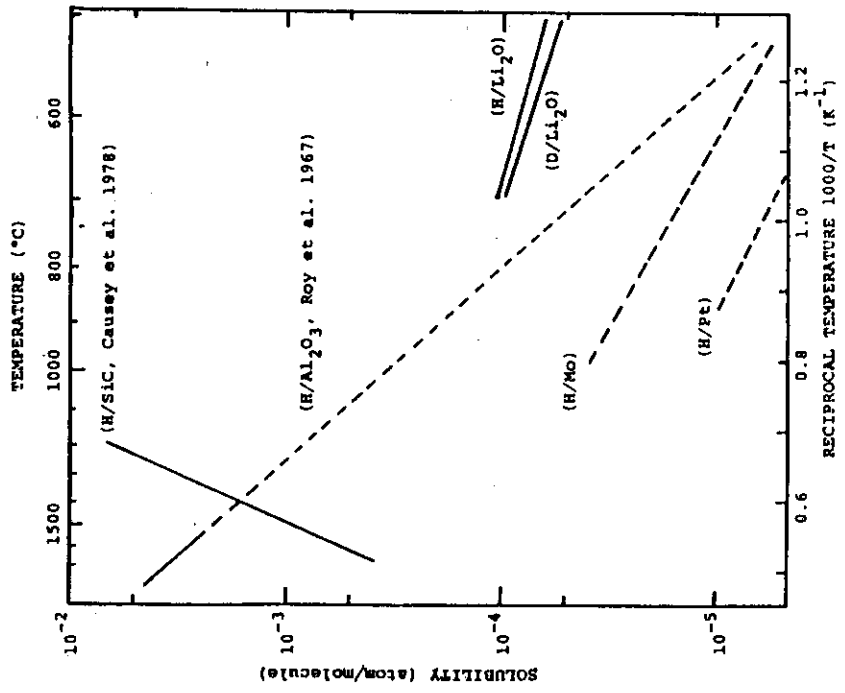

Fig.VIII-4-4 Hydrogen solubility in ceramics and metals.

(c) Effect of Temperature on Sintering and Grain Growth of Li_2O

The kinetics of sintering depends upon a number of factors including selection of starting material. Takahashi et al.[31] studied the sintering behavior of Li_2O using Cerac Li_2O powder. They gave the results for shrinkage as a function of temperature, as shown in Fig.VIII-4-6. By extrapolating their data to lower temperatures, it is seen that the sintering of Li_2O starts at temperatures of 850 ~ 900 °C.

The grain growth of Li_2O was also reported by the same authors[32]. In this case, Li_2CO_3 was used as a starting material. Their data are plotted in Fig.VIII-4-7. As seen from this figure, the grain growth becomes appreciable above 1,160 °C.

Although the starting materials were different between the two studies cited above, it may be concluded that the grain growth begins to occur at higher temperatures by 200 ∿ 300°C than the sintering does.

References

1) T. Takahashi and T. Kikuchi, JAERI-M 7518 (1978)

2) T. Takahashi and S. Nasu, Annual Meeting of the Atomic Energy Society of Japan, Tokyo (1981)

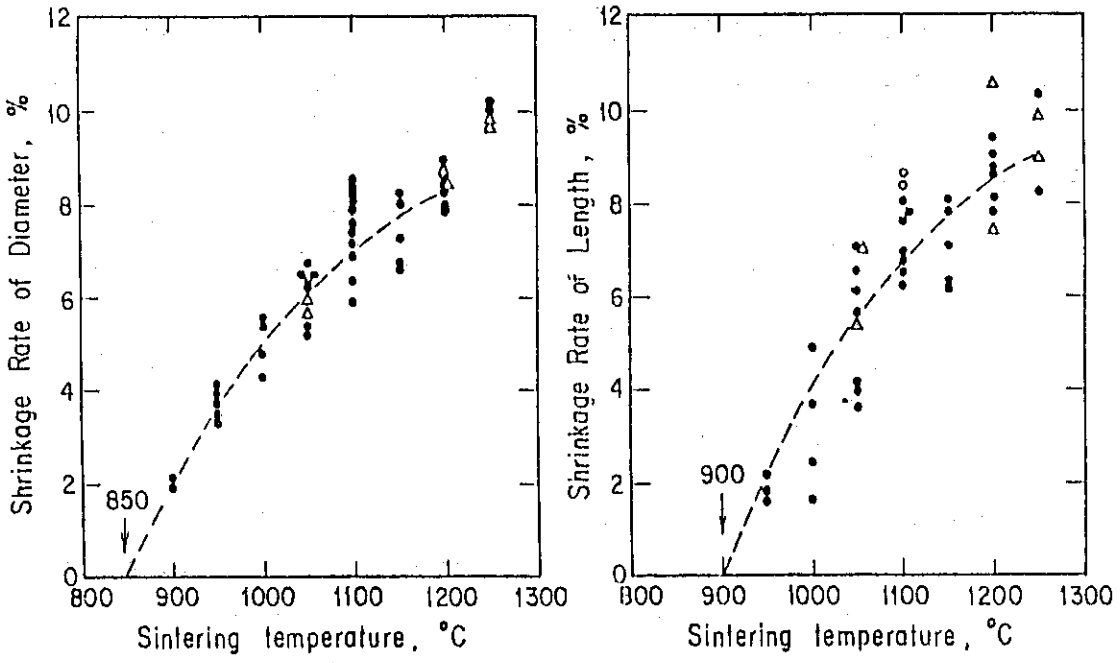

Fig.VIII-4-6. The effect of sintering temperature on the shrinkage of diameter and length of Li_2O. sintering time : 4 h

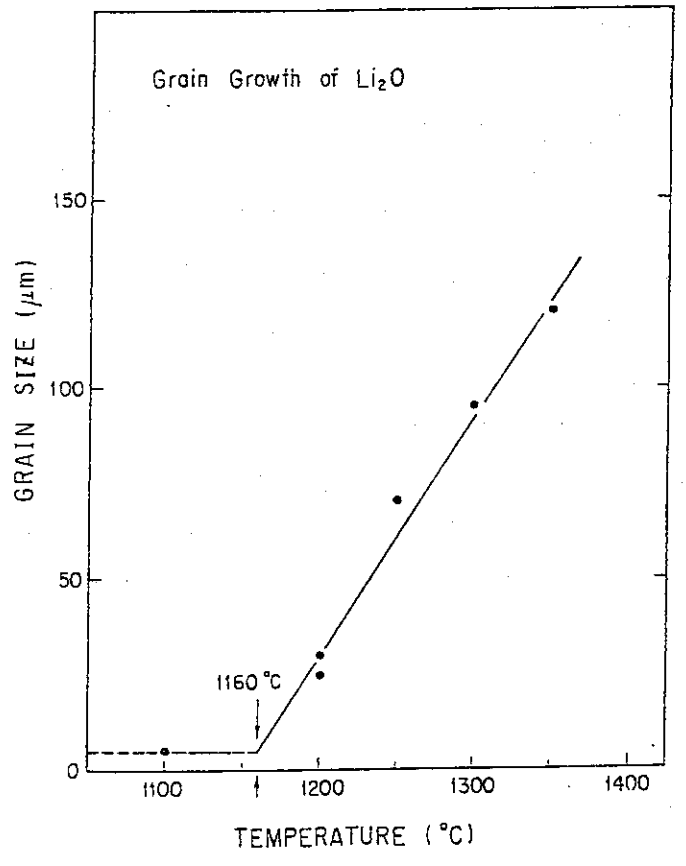

Fig.VIII-4-7 GRAIN GROWTH OF Li_2O

(d) Reaction of Li_2O with Moisture in He Atmosphere

It is important to clarify the effect of moisture in He purge gas on the chemical stability of Li_2O, as Li_2O is very hygroscopic. It is pointed out, recently, that the amount of vaporization of Li_2O in He atmosphere containing moisture is not negligibly small for design of tritium producing blanket[9]. The weight change of Li_2O powder at high temperatures has been measured using a thermobalance in the flowing He gas containing various amounts of moisture.

The procedure of Li_2O sample preparation and outline of the experimental apparatus is shown in Table VIII-4-1 and Fig.VIII-4-8,respectively.

Fig.VIII-4-9 shows the weight change of Li_2O specimen in the case of 12 vpm moisture in He. The maximum of weight gain appears at 400°C and then the weight of specimen decreases rapidly. These rapid weight changes causes the increase and decrease of moisture content in the flowing He gas. From these results, it is deduced that on heating LiOH phase in Li_2O powder decomposes to Li_2O and water above 400°C, and in reverse on cooling Li_2O phase and water vapor synthesize LiOH below 325°C.

Fig.VIII-4-10 shows the partial pressures of water vapor above LiOH and Li_2O as the present work (A). In addition, the equilibrium pressures of water vapor above LiOH and Li_2O which have been measured by an effusion method using Knudsen cell, are shown as the present work (B). These values of our present work (A) are lower than ones of Gregory et al.[33].

The apparent vapor pressure of Li_2O, which is calculated by trnspiration method, are shown in Table VIII-4-2. Since our experiment does not satisfy the condition keeping the satulated vapor pressure around specimen, the rate of vaporization loss seems to be larger than that of Tetenbaum[9].

Vaporized substances from Li_2O powder were observed to be mostly deposited on the surface of nickel foil lapped inside a quartz tube,

and did not deposit on the cold parts of the quartz tube. Since the region of nickel foil is kept at high temperature enough to decompose LiOH, the precipitates of LiOH does not retain. There may be no problem that the vaporization of Li_2O under He atmosphere containing moisture affects the tritium inventory.

(The detailed description is found in Reference[A2].)

Table VIII-4-1 The procedure of sample preparation and setting

Sample Preparation

Li_2CO_3 (powder)* $\xrightarrow[670°C]{Vac.}$ Li_2O (powder) + CO_2 (g)↑

Experimental Procedure

Sampling & weighing in air.
⇓ (contaminated with H_2O & CO_2)
Sample setting in air.
⇓ (contaminated with H_2O & CO_2)
Li_2O powder $\xrightarrow[1000°C]{Pure\ He}$ Li_2O powder.
⇓ Specimen preheated in He atmosphere.
Measured by thermobalance.
(thermogravimetric method)

Heating rate, Cooling rate } 3.34 ± 0.02°C/min

* Li_2CO_3 powder (99.995% purity) as a starting material was purchased from CERAC / PURE , Inc.,

Table VIII-4-2 Apparent vapor pressure of Li_2O in He flow

Vppm H_2O in He	Apparent vapor pressure*, atm	
	1173K	1273K
12	3.0×10^{-5}	1.7×10^{-4}
30	4.7×10^{-5}	1.8×10^{-4}
113	1.8×10^{-4}	6.6×10^{-5} ** (115ppm. at 1268K)
290	3.2×10^{-4}	9.5×10^{-4}
420	3.7×10^{-5} **	1.0×10^{-4} ** (440ppm. at 1263K)

* Calculated using the transpiration equation

$$P = (w/u)(RT/M) \times 2$$

w : the rate of weight loss (g/min)
u : He flow rate (cm^3/min)
RT : 22.4×10^3 $cm^3 \cdot atm/mol$
M : molecular weight of Li_2O, 30 g/mol

** Values measured by M. Tetenbaum et al.

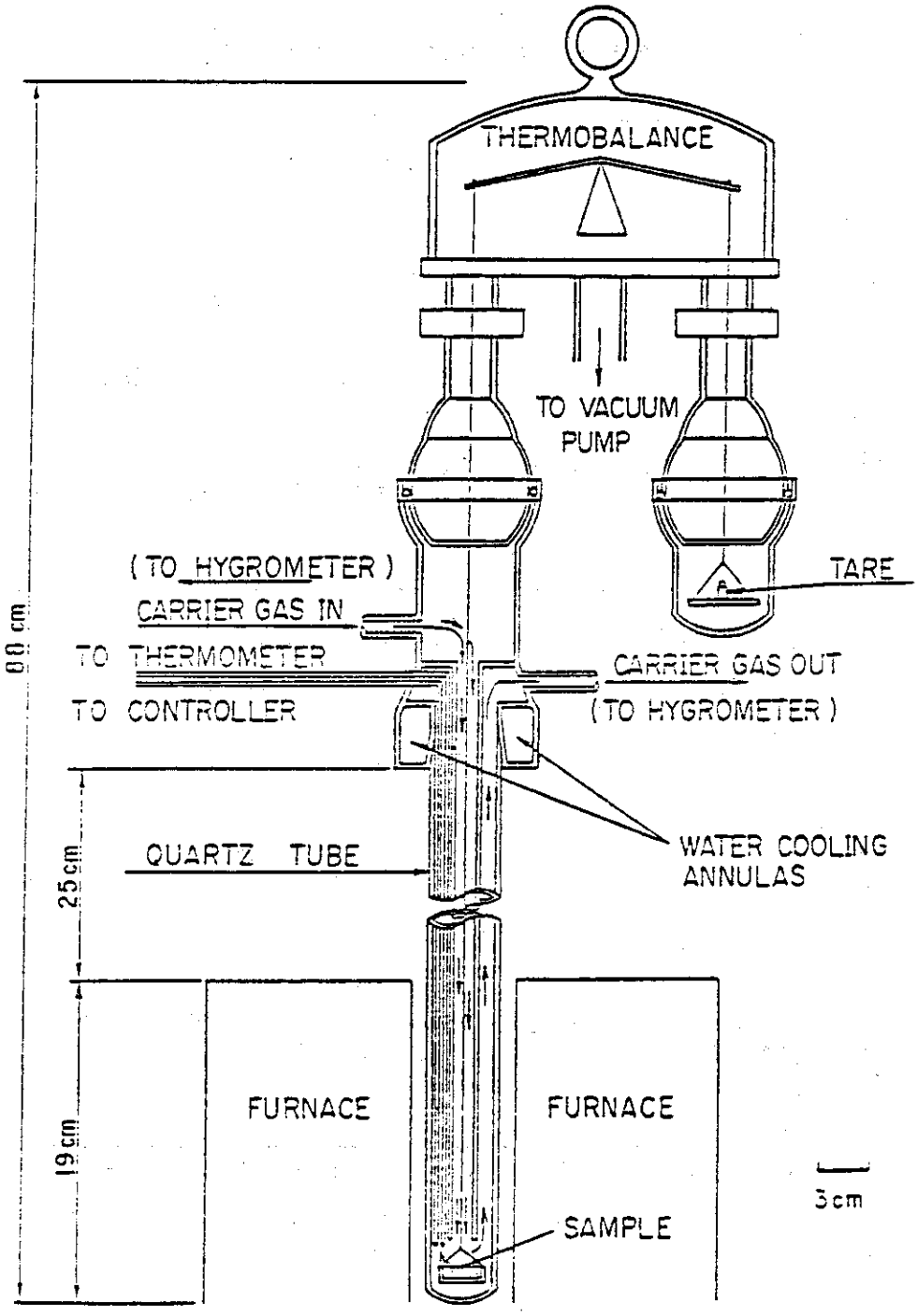

Fig. VIII-4-8 Outline of the apparatus measuring the weight change of Li_2O

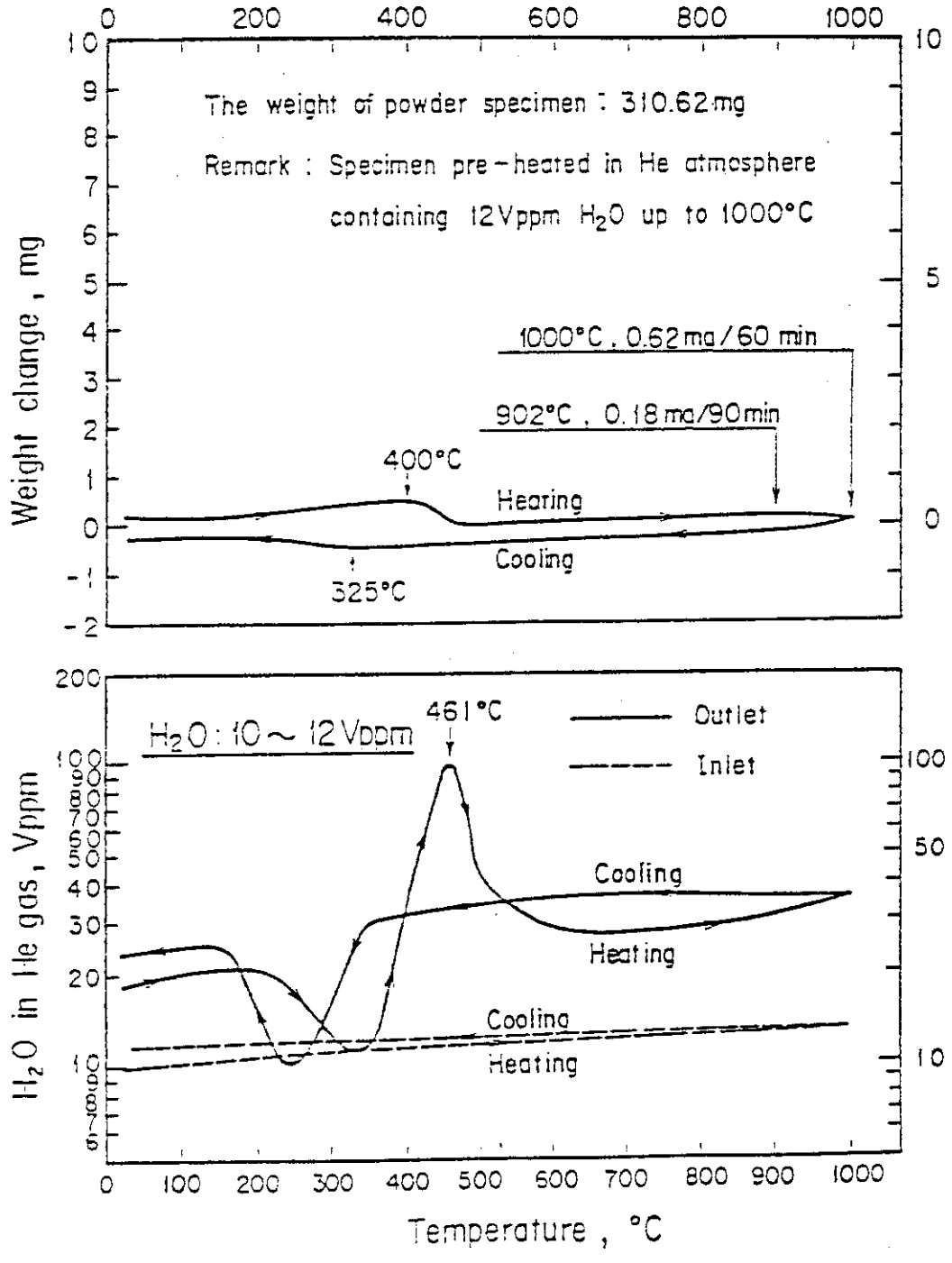

Fig.VIII-4-9 Weight change of specimen in He atmosphere containing 12 vppm H_2O

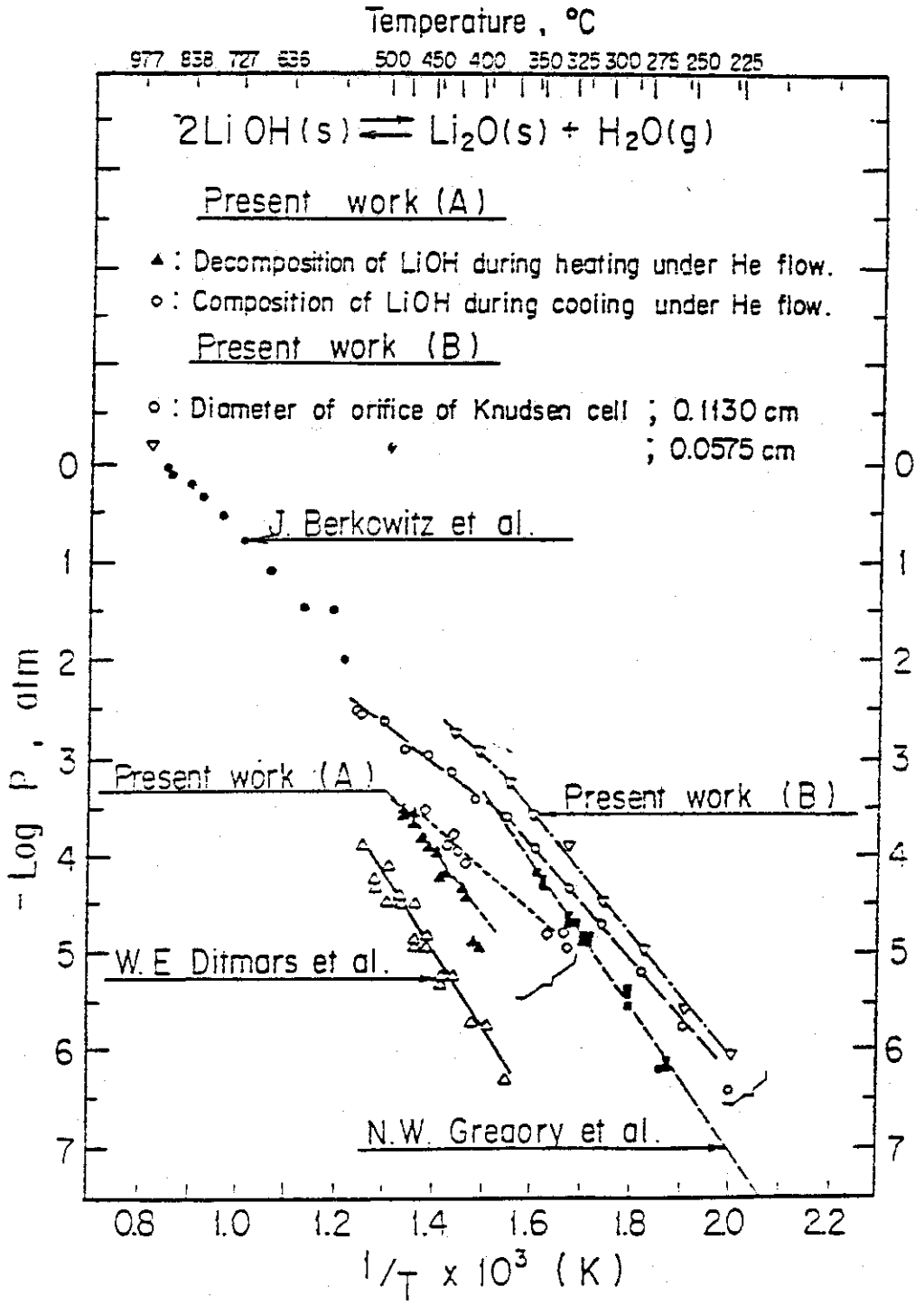

Fig.VIII-4-10 The equilibrium pressures of water vapor above LiOH and Li_2O

4.1.2 Radiation effects

(a) Rates of Tritium Release from Neutron-irradiated Sintered Li_2O Pellets

The tritium release behavior in various candidate materials irradiated with neutrons has been studied with emphasis laid on the behavior in Li_2O which was selected as the blanket material for experimental fusion reactors of the Japan Atomic Energy Research Institute (JAERI)[34] in the present work, the study has been extended to measure the tritium release rate for sintered Li_2O pellets irradiated with neutrons to the fluence of 5.4×10^{15} cm^{-2}.

(1) Experimental

Two kinds of the sintered Li_2O pellet (L Type) were subjected to the rate measurement after the neutron irradiation. One (OPEL-1) was the pellets as received from Mitsubishi Atomic Power Industries and the other (OPEL-2) was the same pellets but heat-treated under vacuum for 1 h at 770K and the for 2 h at 970K before the irradiation. The chemical forms of gaseous tritiated species released from neutron-irradiated pellets heated under vacuum were analyzed by means of radio-gas chromatography in the same manner described in the previous work[28]. The HTO(g) release rates were determined by measuring the amounts of HTO released under vacuum in the temperature range 570-720K.

Table VIII-4-3 lists the distribution of tritiated species released from neutron-irradiated Li_2O pellets heated stepwise up to 1070K under vacuum, together with that from Li_2O powders obtained in the previous work [28]. The HTO fraction from the preheated pellet (OPEL-2) was smaller than that from the OPEL-1 pellet. The HT fraction released from the pellets were larger than that from powders irradiated to the same neutron fluence. The predominant species was HTO. Hence the rate measurements have been focused on the HTO(g) release process in the present work.

Isothermal release curves fo HTO(g) were obtained for the OPEL-1 and OPEL-2 pellets. The HTO(g) release curves for OPEL-1 pellet were analyzed to be the first-order reaction, similar to the thermal decomposition reactions of LiOH(s), LiOD(s) and LiOT(s). The Arrhenius plot of the rate constants (k) is shown in Fig.VIII-4-11. The rate constants for the thermal decomposition reactions of LiOH(s) and LiOT(s) are also plotted in the figure. The apparent activation energy obtained for the OPEL-1 pellet agreed to that of the thermal decomposition reactions of LiOH and LiOT powders. The results revealed that the presence of LiOH played a fatal role in the HTO(g) release from the OPEL-1 pellet.

On the other hand, the HTO(g) release from the OPEL-2 pellet was found to proceed controlled by the diffusion of tritium in analogy with Li_2O powders. The Arrhenius plot of the diffusion coefficient for tritium produced in Li_2O is shown in Fig.VIII-4-12, comparing with that obtained for Li_2O powders and the data reported by Guggi et al.[27] and Vasiliev dt al.[35].

(2) Conclusion

The rate-determining step of HTO(g) release from sintered Li_2O pellet (76.5% TD) irradiated with neutrons was the diffusion of tritium in the grain, similar to the case of Li_2O powders. Alternatively, the grain size of pellets was revealed to given the overall tritium release rate. The diffusion coefficient determined for the Li_2O pellet with the average grain radius of about 5μm was $D = 59.6\exp(-36900/RT)\ cm^2s^{-1}$. It would be possible to use the present data for estimating the rate of HTO(g) release from Li_2O pellets with the density lower than 89%TD, since the tritium release behavior in the pellets (<89%TD) has been found to be identical to that in Li_2O powders.[36]

In addition, the results of this work indicated that the presence of LiOH in Li_2O pellets played important role in the course of tritium release.

(The detailed description is found in ref.[A3])

Table VIII-4-3 Distribution of tritiated species released from neutron irradiated sintered Li_2O pellets heated stepwise up to 1070K under vacuum.

Material	Neutron fluence cm^{-2}	Distribution (%)				
		HTO	HT	CH_3T	$C_2H_{2n-1}T$ (n=1,2,3)	Retention
Li_2O pellet[a]	5.4×10^{15}	97.8	1.4	0.6	0.01	0.2
Li_2O pellet[b]	5.4×10^{15}	95.4	3.5	0.5	0.03	0.6
Li_2O powder	5.4×10^{15}	99.1	0.4	0.1	0.2	0.2
LiOH powder	3.6×10^{16}	99.4	0.3	0.1	0.2	0.01

a) OPEL-1; as received.

b) OPEL-2; heated at 770 K for 1 h and at 970 K for 2 h under vacuum before irradiation.

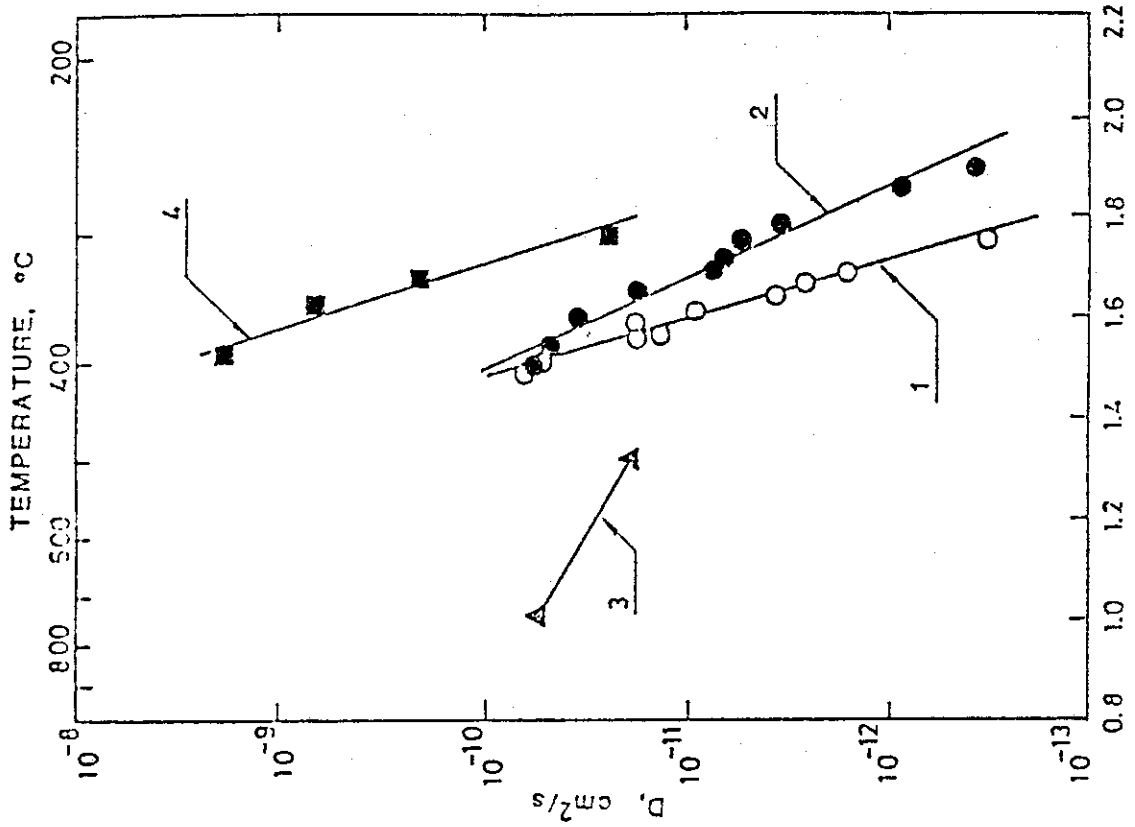

Fig.VIII-4-12 Arrhenius plots of the diffusion coefficient for tritium produced in (1)OPEL-2 pellet (this work) (2)Li_2O powder irradiated to 8.1×10^{16} cm^{-2} (ref.28) (3)Li_2O powder (ref.27) and (4)Li_2O powder (ref.35).

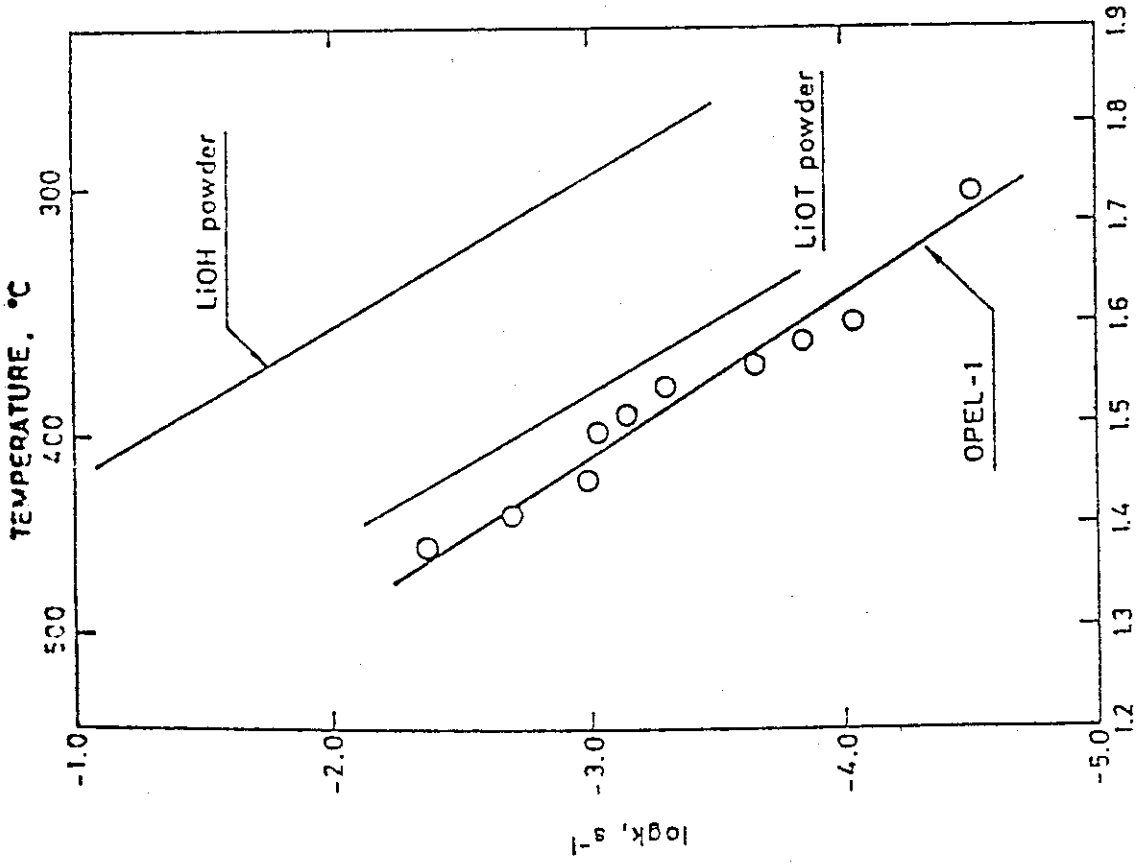

Fig.VIII-4-11 Arrhenius plots of the rate constant determined for OPEL-1 pellet, LiOH powder and LiOT powder.

(b) Irradiation Damage in Li_2O

(1) Introduction

Lithium oxide (Li_2O) is a prime candidate material of solid blanket breeding materials of fusion reactors[34,37]. In the blanket materials, irradiation damages will be enormously induced during operation of the reactors by the following radiations; 1) neutrons with kinetic energies up to 14.1 MeV, 2) tritons (2.7 MeV) and helium ions (2.1 MeV) produced by the $^{6}Li(n,\alpha)^{3}H$ reactions and 3) γ-rays. Such damages will aggregate to form voids and consequently swelling of Li_2O will occur. In addition, the damages have influence on tritium release from Li_2O through enhancement of tritium diffusion or trapping of tritium. In view of this, studies of the irradiation damages are very important for development of the fusion reactors.

The irradiation damages in Li_2O irradiated by fission reactors, a heavy-ion accelerator and a ^{60}Co γ-ray source have been investigated in order to obtain fundamental knowledge of the irradiation damages due to the $^{6}Li(n,\alpha)^{3}H$ reactions with thermal neutrons, high energetic neutrons and γ-rays, respectively[38 - 41]. In this report, the results obtained for such irradiation damages in Li_2O are briefly described.

(2) Experimental

Specimens used were single crystals grown from Li_2O powder with floating zone melting technique using an infrared imaging furnace[42].

The single crystals were cleaved on {111} planes to obtain rectangular specimens ($2\times2\times6$-8 mm^3) having the rotational axis as the direction of <110>. The thermal neutron flux and the fast neutron flux in JRR-4 and JRR-2 were as follows; the thermal neutron flux 3-4×10^{17} neutrons/m^2.s, the fast neutron flux 4-6×10^{16} neutrons/m^2.s in JRR-4, the thermal neutron flux 2.6×10^{17} neutrons/m^2.s, the fast neutron flux 1×10^{15} neutrons/m^2.s in JRR-2. In the reactors, the specimens were simultaneously irradiated by γ-rays as well as neutrons. The γ-ray dose rate in the reactors used was of the order of 1×10^{8} R/h. In order to study the effect of γ-ray irradiation on damage production, γ-ray irradiation was done at room temperature by the ^{60}Co γ-ray source at JAERI. The dose rate in this irradiation was about 5×10^{5} R/h. High energetic heavy ion irradiation was carried out in ultra high vacuum at an ambient temperature using an irradiation chamber attached to a 20 MeV tandem accelerator at JAERI. As projected ions, oxygen ions with energies of 100 MeV and 112 MeV were used to induce displacement damages without contamination due to injection of impurity ions. After the irradiation, irradiation damages induced in Li_2O were observed at room temperature by ESR (electron spin resonance) method. The ESR spectrometer used was JEOL JES-PE-3X.

(3) Results and Discussion

ESR spectra exhibiting hyperfine structure were observed from Li_2O single crystals irradiated to the order of 10^{20} to 10^{23} thermal neutrons/m^2. The hyperfine structure was found to be dependent on the crystal orientation in the applied magnetic field H of the ESR spectrometer. Typical examples of the spectra for the specimen irradiated to 4.5×10^{21} thermal neutrons/m^2 are shown in Fig.VIII-4-13 together with hyperfine line intensity ratios predicted

for F^+-centers (an oxygen vacancy trapping an electron) as shown schematically in Fig.VIII-4-14. Traces 1(a), 1(b) and 1(c) were obtained with the specimen oriented so that H was along directions of <100>, <110>, and <111>, respectively. The g-value of these spectra was determined to be 2.002± 0.001. The separation between peaks were in the range 9.2 to 9.5 G, and the individual line widths were in the range 4.6 to 4.8 G. Every observed spectrum has the hyperfine structure with more than 20 peaks and the resolution in the directions of <110> and <111> is poorer than that in the direction of <100>. In addition, the spectrum in the direction of<111> is slightly less resolved in comparison with that in the direction of <110>. Such spectra can be due to F^+-centers from agreement between characteristic features of the observed spectra and hyperfine line intensity ratios calculated for F^+-centers. On the following assumptions, the intensity ratios were calculated: 1) The nuclear Zeeman and nuclear quadrupole interaction energies can be neglected. 2) Only the hyperfine interaction with 8 Li nuclei in the first shell of the F^+-center is taken into account. 3) Although natural Li_2O contains about 92.6% ^7Li and 7.4% ^6Li, all Li nuclei in the first shell are assumed to be ^7Li nuclei with nuclear spin I=3/2 for simplicity. In case of a result calculated for the direction of <100> , 25 hyperfine lines are located at an interval of $a/g\mu_B$ G, where a is an isotropic term of hyperfine coupling constant, μ_B Bohr magneton. For the direction of <110>, 169 lines segregate into 25 groups separated at an interval of $a/g\mu_B$ G, and the separation of each line in each group is $2b/g\mu_B$ G, where b is an anisotropic term of hyperfine coupling constant. For the direction of <111> , 133 lines also segregate into 25 groups situated at an interval of $a/g\mu_B - 0.67b/g\mu_B$, and the separation of each line in each group is $2.67b/g\mu_B$. The hyperfine line intensity ratios of each case

are shown as histograms in Fig.VIII-4-13. As is seen in Fig.VIII-4-13, with respect to the resolution of the spectra and relative intensity ratios of hyperfine lines, the observed spectra are in good agreement with the calculated results. Thus, the observed spectra with the hyperfine structures can be attributed to F^+-centers.

The spectra due to the F^+-centers were not observed in the specimens irradiated up to 10^8 R by the ^{60}Co γ-ray source. This suggests that the photochemical process does not readily occur in Li_2O and that the spectra are due to tritons and helium ions produced by the $^6Li(n,\alpha)^3H$ reactions with thermal neutrons or fast neutrons. In an optical absorption study of irradiation damages in Li_2O irradiated by fission reactors (JRR-4, JRR-2), the formation of the damages was found to be predominantly due to tritons and helium ions produced by the $^6Li(n,\alpha)^3H$ reactions by comparing the spectrum obtained by irradiation of neutron cut off with Cd foils (only fast neutrons) with those obtained by irradiation without Cd foils (thermal and fast neutrons)[40]. Thus, F^+-centers in Li_2O irradiated by the fission reactors were predominantly attributed to the $^6Li(n,\alpha)^3H$ reactions and γ-ray irradiation does not contribute to formation of the F^+-centers.

The isochronal and isothermal annealing behavior of the F^+-centers were investigated. Fig.VIII-4-15 shows results of isochronal annealing experiments. For the specimens irradiated to 4.5×10^{21} and 1.7×10^{23} thermal neutrons/m^2, a complete disappearance of the F^+-centers at about 630 K followed after an initial decrease in the intensity at about 420 K and remarkable decrease between 520 and 600 K. On the other hand, for the specimens irradiated to 3.8×10^{20} thermal neutrons/m^2 a complete disappearance at 580 K followed after the considerable decrease at 420 K. The difference

of temperature initiating the recovery of the F^+-centers in neutron fluences seems to arise from the difference in the amount and distribution of the F^+-centers rather than that in the specimens used. Isothermal annealing experiments were carried out at 530, 580 and 630 K for the specimens irradiated to 4.1×10^{21} or 5.3×10^{21} thermal neutrons/m^2 and the results are shown in Fig.VIII-4-16. From the isothermal annealing curves, the activation energy for recovery of the F^+-centers was determined to be about 135 kJ/mol.

ESR spectra of Li_2O single crystals irradiated to 1×10^{16} ions/cm^2 by O^{+7} with energy of 112 MeV also had a hyperfine structure and was dependent upon the crystal orientation in the applied magnetic field H. As typical examples, the spectra in case that H was along the directions of <100>, <110> and <111> are shown in Fig.VIII-4-17. The characteristic features (g-value, line widths, etc.) and the angular dependence of the hyperfine structure agree with those of F^+-centers in neutron-irradiated Li_2O single crystals and the hyperfine line intensity ratios calculated for the F^+-centers. Thus, the spectra with the hyperfine structure of oxygen-ion irradiated Li_2O single crystals can be due to F^+-centers. Fig. VIII-4-18 shows examples of the spectra of Li_2O single crystals irradiated to 3×10^{16} ions/cm^2 by O^{+6} with energy of 100 MeV. In these spectra, an isotropic spectrum is observed to be superposed on a spectrum having the hyperfine structure, which is due to the F^+-centers from the shape and the angular dependence. The line width of the isotropic spectrum is very narrow and the spectrum is not depend on the orientation of the specimen. These suggest that the isotropic spectrum can be attributed to colloidal Li metal centers. Such isotropic spectra were observed in sinterd pellets and pressed powder of Li_2O irradiated to the order of 10^{23} thermal

neutrons/m^2 [39,43] while these spectra were not in Li_2O single crystals irradiated to the order of 10^{23} thermal neutrons/m^2. From the facts, grain boundaries of the sintered pellets and surfaces of the pressed powder were considered to play an important role in precipitation of the colloidal Li metal. In this light, it is interesting that the spectra due to colloidal Li metal centers were observed for Li_2O single crystals irradiated by O^{+6} ions with high energy.

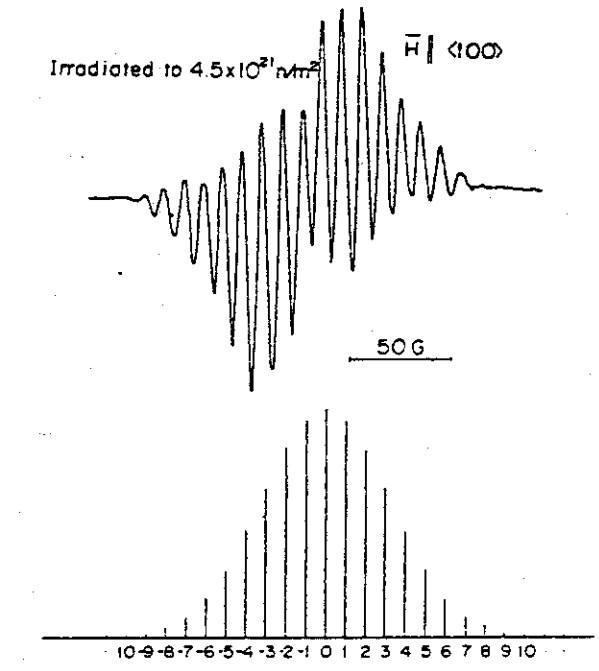

(a)

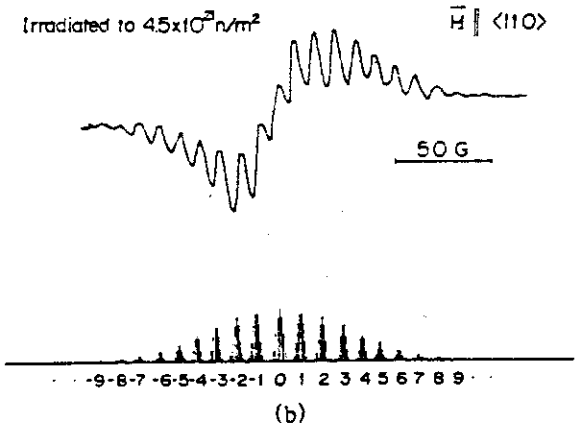

(b)

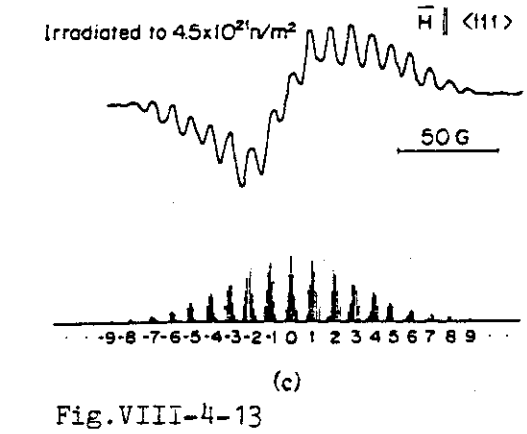

(c)

Fig.VIII-4-13

The ESR spectra of Li_2O single crystals irradiated to 4.5×10^{21} thermal neutrons/m^2 and hyperfine line intensity ratios predicted for the F^+-centers.

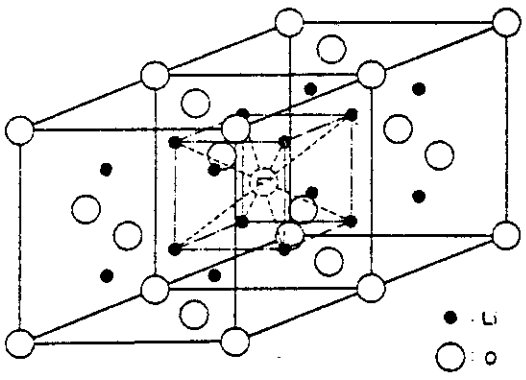

Fig.VIII-4-14
A schematic illustration of the F^+-centers in Li_2O.

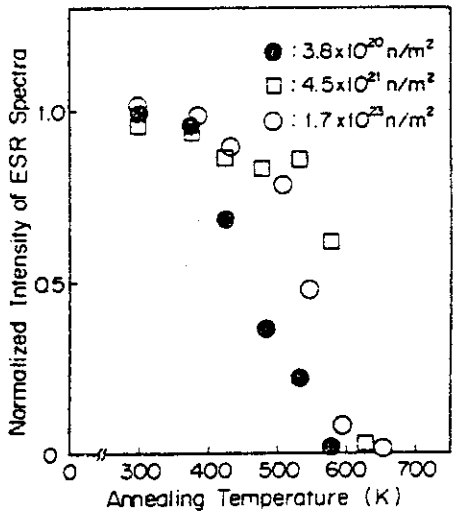

Fig.VIII-4-15
The behavior of the F^+-centers during isochronal annealing experiments.

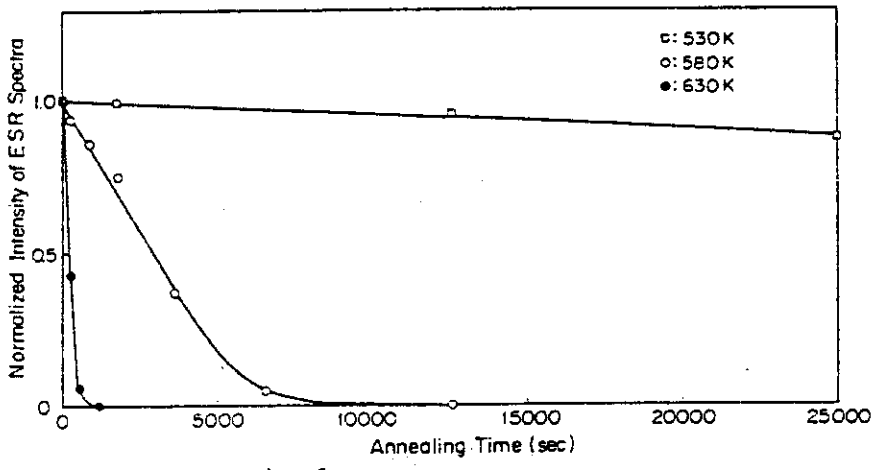

Fig.VIII-4-16
The behavior of the F^+-centers during isothermal annealing experiments for the specimens irradiated to the order of 10^{21} thermal neutrons $/m^2$.

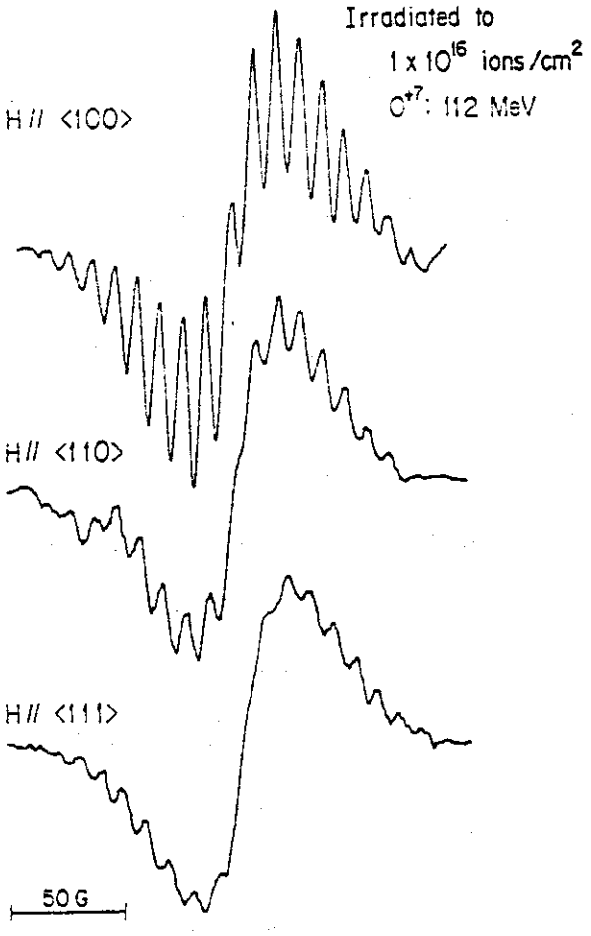

Fig.VIII-4-17
ESR spectra of Li_2O single crystals irradiated to 1×10^{16} ions/cm^2 by O^{+7} with energy of 112 MeV.

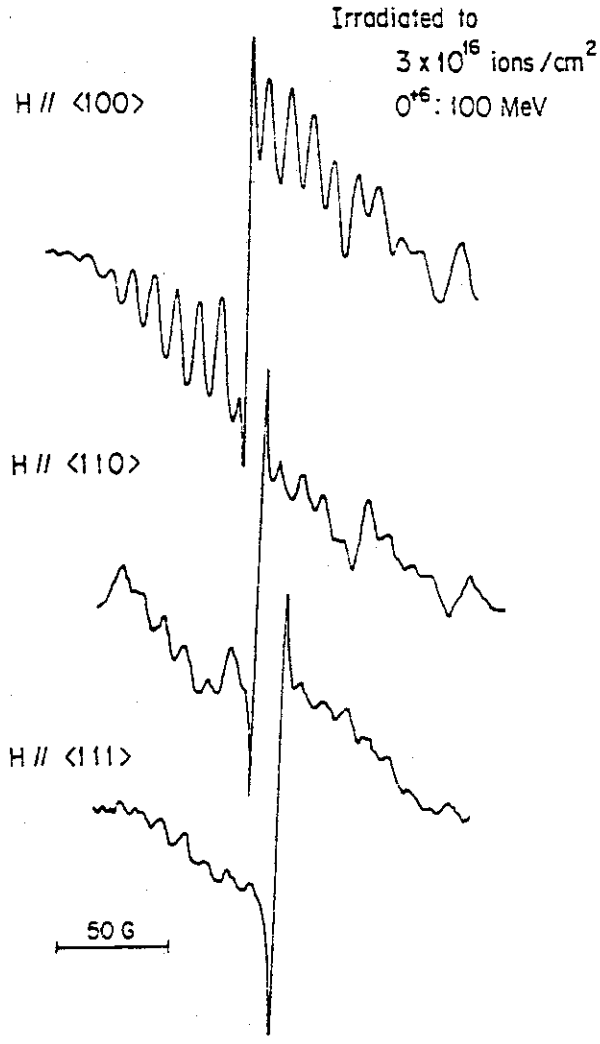

Fig.VIII-4-18
ESR spectra of Li_2O single crystals irradiated to 3×10^{16} ions/cm^2 by O^{+6} with energy of 100 MeV.

4.1.3 Tritium recovery requirement

(a) The Operational Temperature Range for Li_2O

- Thermochemical Studies -

(1) Introduction

Lithium Oxide (Li_2O), which has an advantage of high melting point, can be expected to be operated within the wide temperature range. However, the chemical stability of Li_2O breeder depends sensitively on temperature and moisture.

At high temperature, low-levels of water in the breeding blanket may rapidly react with Li_2O and lead to formation of gaseous lithium hydroxide (LiOT(g) and LiOH(g)). The rate of LiOH(g) formation is equivalent to that of Li_2O mass transfer. At low temperature, LiOT(s) formation becomes a severe problem because of unacceptable tritium inventory. Therefore, Li_2O breeder has to be designed within a reasonable temperature range.

In this section, reliable and precise thermodynamic studies have been carried out so as to understand the acceptable temperature range of Li_2O breeder.

(2) Partial Pressure of Water in Blanket

The sources of water vapor in blanket purge gas are as follows:

i) tritiated water (T_2O) released from Li_2O,

ii) leakage of water through pin holes of cooling tubes, and

iii) water vapor as impurity in the helium gas stream at the inlet of blanket.

The production rate of T_2O is evaluated to be 10.3 g-T_2O/hr in the conditions below.

- Fusion Power 620 MWth
- Burn time 100 sec
- Dwell time 40 sec
- Breeding ratio 1.0

Leak rate of H_2O in breeder is difficult to evaluate at present for lack of data.

Table VIII-4-4 summarizes the mesured leak rate of H_2O in steam generators of representative fission reactors[44]. Judging from Table VIII-4-4 ., the leak rate of H_2O in the INTOR blanket would be of the order of 10 g-H_2O/hr.

The partial pressure of water at the inlet of blanket is estimated to be less than 10^{-6} atm because molecular sieve dryers are equipped with breeding blanket tritium recovery system.

The partial pressure P_{HTO} of water in the purge gas stream can be calculated from the equation.

$$P_{HTO} = \left(\frac{L}{18} + \frac{10.3}{22} \right) \times \frac{22.4}{V \times 10^3} + Pin \qquad \text{(VIII-4-1)}$$

where

L : Leak rate of H_2O through pin holes (g-H_2O/hr)

V : Flow rate of helium purge stream (Nm^3/hr)

Pin : Partial pressure of water at the inlet of blanket ($<10^{-6}$ atm)

For example, in the case of L = 10 g-H_2O/hr, V = 200 Nm^3/hr and Pin = 10^{-6} atm, the partial pressure, P_{HTO}, calculated from eq. (VIII-4-1) is 1.15 x 10^{-4} atm.

Accordingly, the partial pressure of H_2O in blanket is considered to be of the order of 10^{-4} atm.

(3) $LiOH/Li_2O$ Phase Equilibria

Lithium oxide reacts exothermically with water vapor (T_2O, H_2O) to form lithium hydroxide (LiOT, LiOH).

$$Li_2O(s) + H_2O(g) \rightleftarrows 2LiOH\ (s \text{ or } \ell) \qquad (VIII\text{-}4\text{-}2)$$

$$Tm = 445°C$$

Calculated phase diagram is shown in Fig.VIII-4- 9 as a function of partial pressure P_{H_2O} of water and temperature. Consideration of this phase diagram is important for blanket design. The blanket must be operated in a regime where Li_2O (s) is stable.

The temperature of Li_2O in blanket is kept above 400°C in order to lower the tritium inventory. It is seen from Fig.VIII-4-19 that the partial pressure of water in blanket has to be maintained below 10^{-3} atm. Then, the leak rate of H_2O can be permitted as high as 1.5 x 10^2 g-H_2O/hr when the flow rate of purge stream is 200 Nm^3/hr. It is found from Table VIII-4-4 that the leak rate of H_2O in blanket can be possibly maintained below 1.5 x 10^2 g-H_2O/hr.

By the way, the partial pressure of T_2O in the bulk of purge gas flow is 5.2 x 10^{-5} atm when the flow rate is 200 Nm^3/hr.

For the equilibrium pressure of T_2O at 400°C (10^{-3} atm) is high enough as compared with that in the bulk (5.2×10^{-5} atm), $T_2O(g)$ decomposed from LiOT(s) could migrate into purge stream easily.

(4) Mass Transfer of Li_2O

a) Vaporization Behavior of Li_2O

The volatility of Li_2O is significant in the presence of water. With water vapor in the purge gas, LiOH(g) is assumed to be the primary gaseous spieces according to the following reaction:

$$Li_2O(s) + H_2O(g) \rightleftarrows 2LiOH(g) \qquad \text{(VIII-4-3)}$$

The equilibrium constant Kp(T) of this reaction is defined as:

$$Kp(T) = \frac{a[LiOH]^2}{a[Li_2O]\ a[H_2O]} = \frac{P_{LiOH}^{\ 2}}{P_{H_2O}} \qquad \text{(VIII-4-4)}$$

The equilibrium pressure P_{LiOH} of LiOH(g) is given as follows:

$$P_{LiOH} = (P_{H_2O} \cdot Kp(T))^{1/2} \qquad \text{(VIII-4-5)}$$

where, P_{H_2O} is given by eq. (VIII-4-1)

One can calculate the equilibrium pressure of LiOH(g) dependent on P_{H_2O}, using JANAF thermochemical data.

The dependence of $P_{LiOH(g)}$ on the temperature is shown in Fig. VIII-4-20.

On the other hand, in the absence of water, the predominant vapor spieces over Li_2O were observed to be Li(g) and Li_2O(g) by Kudo et al.[45] and Kimura et al.[46]. The partial pressures of Li(g) and Li_2O(g) derived from extrapolation of mass spectrometric measurements are included in Fig. VIII-4-20.

From Fig. VIII-4-20, it is clear that the equilibrium prssure of LiOH(g) dependent on partial pressure P_{HTO} of water is several orders of magnitude higher than that of Li(g) or Li_2O(g).

b) Weight Loss of Li_2O

The enhanced volatility of Li_2O in the presence of water causes weight loss of Li_2O.

The losing rate of Li_2O due to LiOH(g) transpiration can be evaluated by the following equation.

$$W = P_{LiOH} \times \frac{V \times 10^3}{22.4} \times \frac{1}{2} \times 29.88 \qquad \text{(VIII-4-6)}$$

where

W : Losing rate of Li_2O (g-Li_2O/hr)

P_{LiOH} : Equilibrium partial pressure of LiOH(g) given by eq. (VIII-4-5)

V : Flow rate of helium purge stream (Nm^3/hr)

One can calculate the total weight loss of Li_2O during 15 years' operation of the INTOR blanket taking account of the staged operation schedule proposed in Phase I.

The dependence of weight loss of Li_2O on the operational temperature of blanket is shown in Fig.VIII-4-20, on condition that the flow rate of purge stream is 200 Nm^3/hr. In the case that V is 200 Nm^3/hr, temperature is 900°C, and P_{H_2O} is 10^{-4} atm, the total weight loss due to LiOH(g) transpiration amounts to 126 Kg during 15 years' operation.

The relationship between temperature and weight loss of Li_2O is shown in Fig.VIII-4-21, on condition that flow rate V is 200 Nm^3/hr.

And the relationship between temperature and weight loss is shown in Fig.VIII-4-22, on condition that leak rate of H_2O is 10 g-H_2O/hr.

It is seen from Fig.VIII-4-21 or Fig.VIII-4-22, that in the case of V = 200 Nm^3/hr, L = 10 g-H_2O/hr, and T = 1,000°C, the total weight loss of Li_2O due to LiOH(g) transpiration is as much as that due to burn-up of ^6Li atoms (662 Kg/15 yrs) which is about 0.6 percent of the initial charge (110 ton).

The above considerations of maximum allowable temperature was made on the basis of Li_2O weight loss. Additional studies - such as controllability of Li_2O temperature and behaviour of sintering - must be conducted before deciding the operational temperature for Li_2O.

(5) Impacts of LiOT(g) Transpiration on Breeding Blanket Operation

LiOH(g) transpiration might cause the following problems;

i) increase of tritium inventory due to deposit of LiOT(s) on the low temperature structure materials such as cooling tubes,

ii) compatibility of LiOH(s) with materials,

iii) effect of LiOH(s) deposit on the temperature control,

iv) decrease of tritium breeding performance due to weight loss of Li_2O,

v) method to recover tritium from LiOT(s) deposit, and

vi) effect of LiOH(s) deposit on the purge gas stream (Plugging).

Among these problems the most severe problem would be item i). Condensation of LiOT(s) may lead to an increase of tritium inventory. So, preliminary theoretical study of LiOT(g) behaviour in blanket is carried out in the next section.

The other items ii) - vi) can not be considered to be severe under the condition of INTOR reference blanket.

Table VIII-4-4 Leak rate of H_2O in steam generator [44]

Reactor	Power	Leak rate of H_2O in steam generator
Peach Bottom (First core)	40MWth	4.5 g/hr
Fort st. Vrain	842MWth	18 g/hr

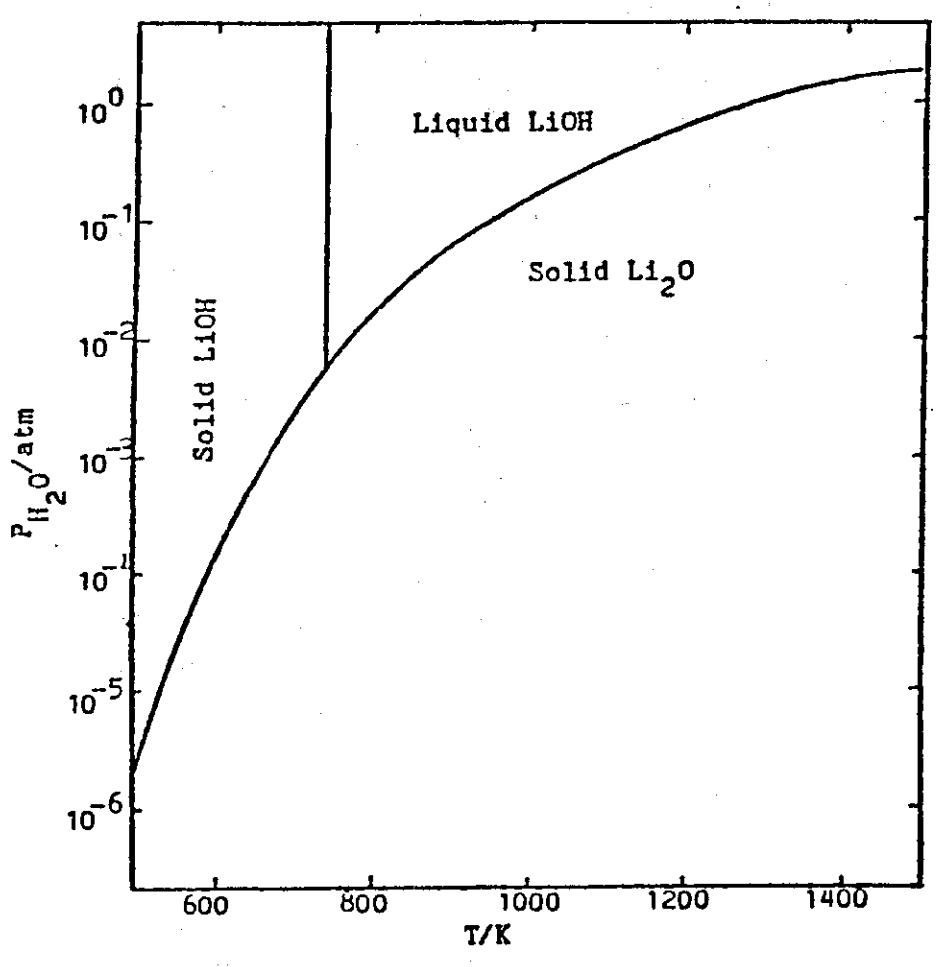

Fig.VIII-4-19 Li_2O/LiOH phase equiliblia as a function of P_{H_2O} and temperature

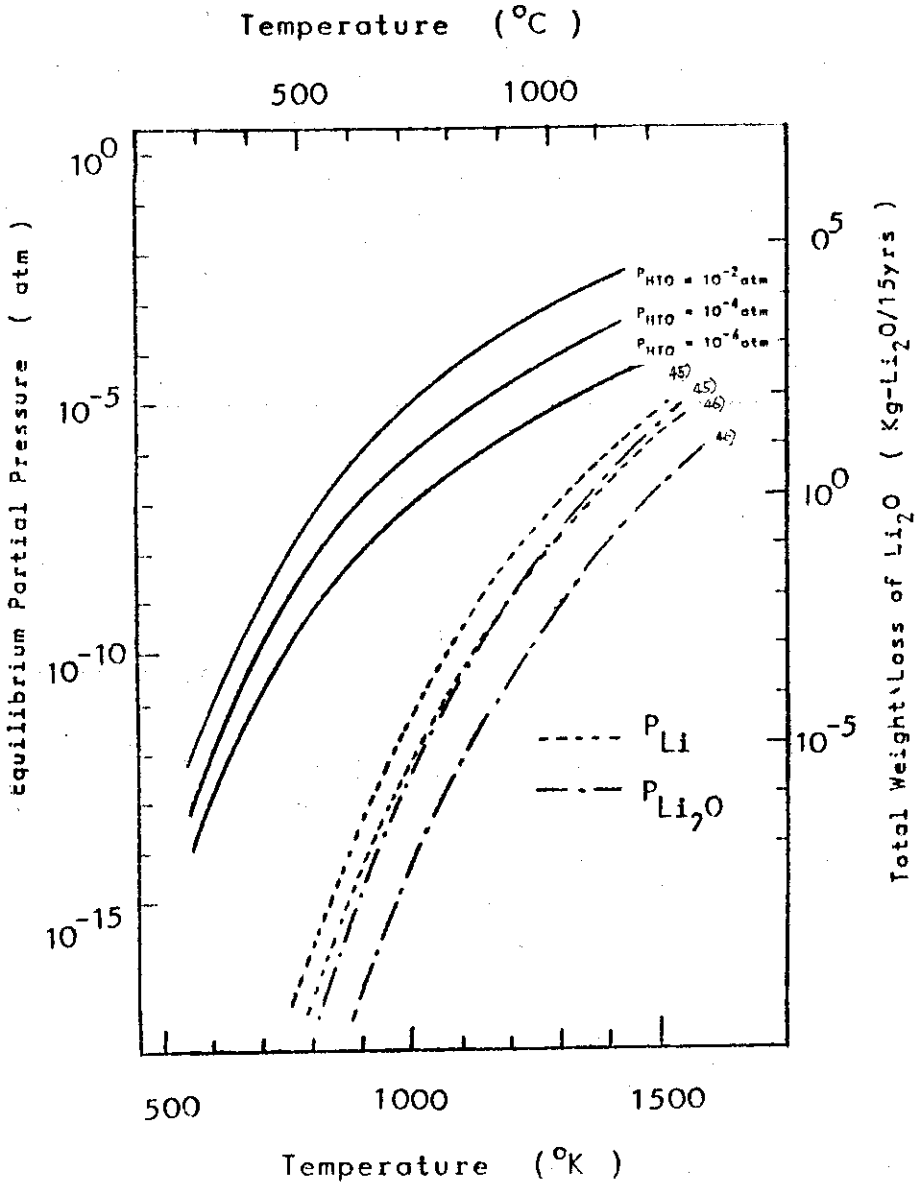

Fig.VIII-4-20 Equiliblium Partial Pressure of LiOH(g),Li(g), and Li_2O(g); and Total Weight Loss due to LiOH(g) Transpiration when V = 200 Nm^3/hr.

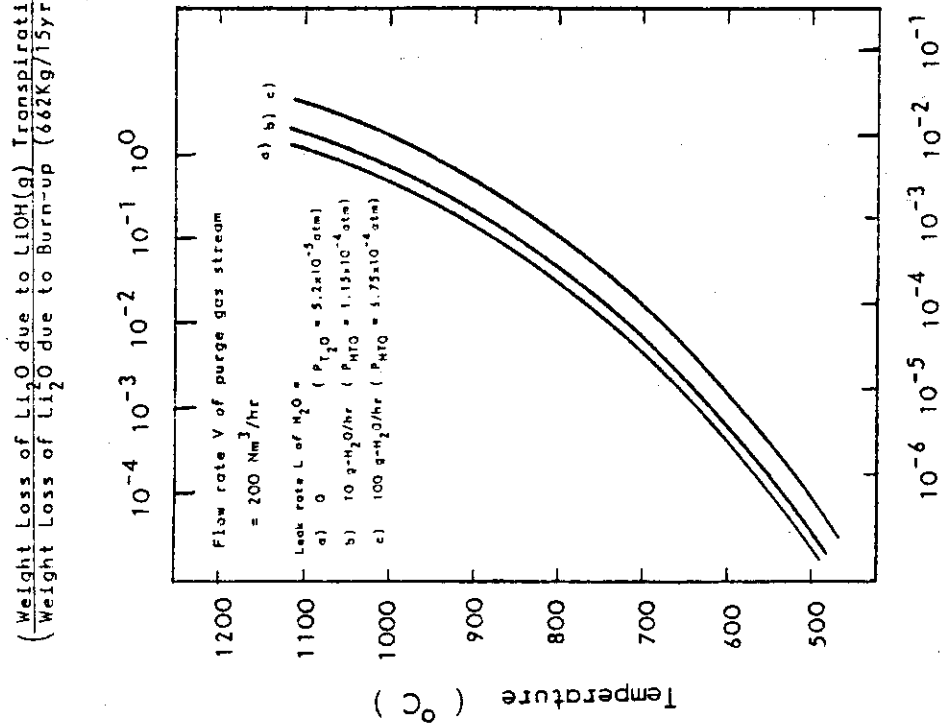

Fig.VIII-4-21 Relationship Between Weight Loss of Li_2O due to LiOH(g) Transpilation and Temperature.

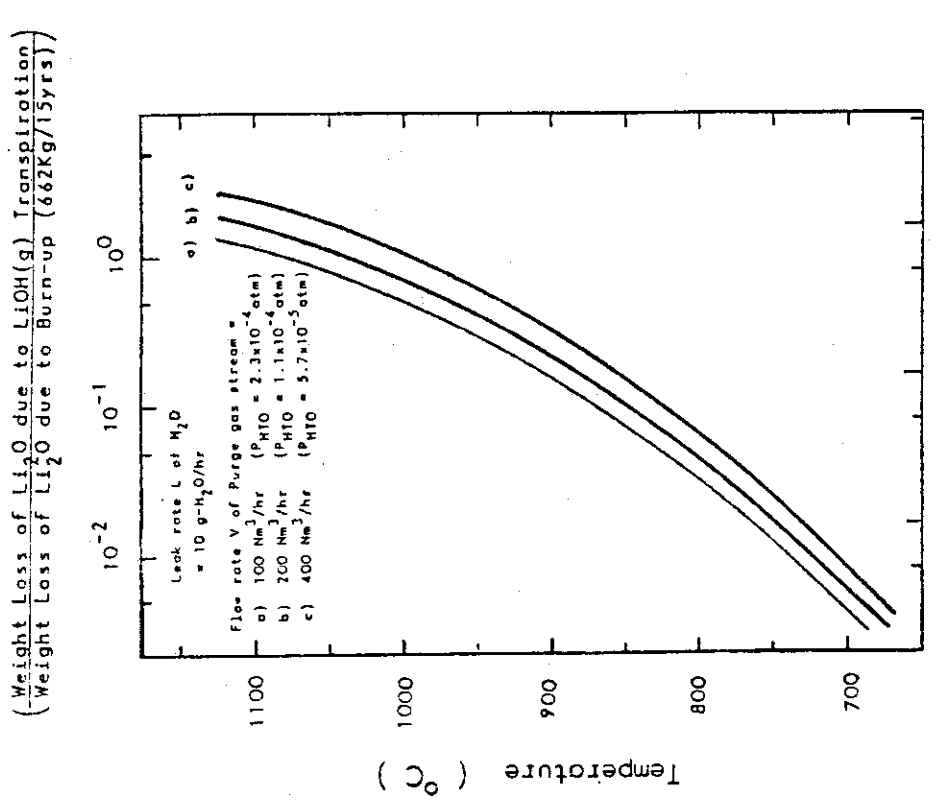

Fig.VIII-4-22 Relationship Between Weight Loss of Li_2O due to LiOH(g) Transpiration and Temperature.

(b) Kinetic Behaviour of LiOT(g) in Blanket

(1) Introduction

Wide operating temperature range of Li_2O breeder is required for simplification of the breeding blanket design and suitable margin for uncertainties of the predicted power density. At high temperature, however, water vapor in the purge gas reacts with Li_2O to form LiOH(g)/LiOT(g), which causes condensation of solid LiOH(s)/LiOT(s) at the low temperature zone and weight loss of breeder.

In the previous section the weight loss of Li_2O breeder by the purge gas stream was estimated as a function of breeder temperature and flow rate of purge gas. Those analyses show that the total weight loss of Li_2O due to LiOH(g)/LiOT(g) transpiration is negligible compared with the initial charged Li_2O ($\sim$ 110 tons) even if the Li_2O breeder was maintained at a temperature of 1,000°C.

On the other hand, there is a possibility of the condensation of LiOH(g)/LiOT(g) vapor in blanket. If the LiOH(g)/LiOT(g) vapor condenses on the structure materials kept at a temperature above 350°C, LiOT(s)/LiOH(s) successively decompose to Li_2O(s) and HTO(g) according to the LiOH/Li_2O phase diagram . Whereas, if the LiOH/LiOT vapor condenses on the materials at the low temperature below 350°C, precipitation of stable LiOT(s) causes to lead to an increase of tritium inventory.

In this section, therefore, the behaviour of LiOT(g) vapor in blanket is discussed using simple kinetic theory.

(2) Kinetics of LiOT(g) Molecules

The following kinetic pictures have to be considered to understand the behavior of LiOT(g) in blanket.

i) Average Molecular Velocity of LiOT(g)

From simple kinetic theory of gases at low density, the mean molecular velocity $\bar{V}$ of LiOT(g) molecules is given by

$$\bar{V} = \left(\frac{8kT}{\pi m}\right)^{1/2} \quad [\text{cm S}^{-1}] \qquad \text{(VIII-4-7)}$$

where, m : mass of a molecule [g]
k : Boltzmann constant [1.38×10^{-16} erg·K^{-1}]
T : temperature of gas [K]

ii) Collision Frequency of a LiOT(g) Molecule with He Atoms

The frequency Z_{He} of molecular collision of a LiOT(g) molecule with helium atoms is

$$Z_{He} = 2N_{He}\pi d^2\left(\frac{8kT}{\pi\mu}\right)^{1/2} \quad [\text{S}^{-1}] \qquad \text{(VIII-4-8)}$$

where, N_{He} : concentration of He atoms per unit volume of gas [atoms·cm^{-3}]
μ : reduced mass of LiOT and He [3.4 g]
d : collision diameter [cm]

The collision frequency of a LiOT(g) molecule with other LiOT(g) molecules is negligibly small compared with Z_{He}.

iii) Mean Free Path

The mean free path, the average distance traveled by a LiOT(g) molecule between successive collision, is given by

$$\lambda = \frac{\bar{V}}{Z_{He}} \quad [\text{cm}] \qquad \text{(VIII-4-9)}$$

iv) LiOT(g) Striking on Li_2O Breeder Surface

The frequency Z of molecular bombardment on stationary surface exposed to gas, per unit area, is

$$Z = \frac{1}{4} N_{LiOT} \bar{V} \qquad [cm^{-2} \cdot s^{-1}] \quad \text{(VIII-4-10)}$$

where, N_{LiOT} : concentration of LiOT(g) molecules per unit volume of gas $[cm^{-3}]$

The surface area of Li_2O pebbles per unit volume of breeder zone is about 42 cm^2/cm^3-breeder and the void fraction is about 0.3, because unit volume of breeder contains about 1,300 pebbles of 1 mm diameter. Consequently, the frequency Z_{Li_2O} of molecular collision of a LiOT(g) molecule with pebble is given by

$$Z_{Li_2O} = \frac{Z \times 42\ cm^2/cm^3\text{-breeder}}{N_{LiOT} \times 0.3\ cm^3\text{-gas}/cm^3\text{-breeder}} \qquad [s^{-1}] \quad \text{(VIII-4-11)}$$

The calculated results for $\bar{V}$, Z_{He}, λ, and Z_{Li_2O} are shown in Fig. VIII-4-23 - Fig. VIII-4-26 . In the calculation of Z_{He}, the collision diameter and the helium pressure are assumed to be about 2 Å and 1 atm, respectively. Moreover Z_{Li_2O} is calculated based on the equilibrium pressure of LiOT(g) under the typical blanket condition:

- T_2O pressure $\sim 10^{-5}$ atm
- Temperature 400 ~ 1,000°C

From these figures, it is understandable that the profiles of kinetic behaviour of LiOT(g) molecules in purge gas are as follows:

i) LiOT(g) molecules move at high speed. The average molecular speed is about 1,000 m/S.

ii) LiOT(g) molecules move randomly colliding mainly with neighboring He atoms. This collision frequency is nearly 10^{10} per one second.

iii) The mean free path of LiOT(g) molecule is about 10^3 Å.

iv) The LiOT(g) molecules also collide with the surface of Li_2O(s) pebbles. This collision frequency is about 10^5 per one second, which is much smaller than that with He atoms.

By the way, LiOT(g) molecules are transported both by convective flow of purge stream and by diffusive flow resulting from a concentration gradient. Though the diffusivity of LiOT(g) in He gas is not known, from reported diffusivities of other materials the diffusivity of LiOT(g) in He can be estimated to be about 1 cm^2/sec at room temperature. Considering the normal temperature dependence of diffusivity ($D \propto T^{1.8}$), the diffusivity of LiOT(g) at 1,000°C might be about 16 cm^2/sec.

The average distance traveled by diffusing LiOT(g) molecules is given by the mean square displacement.

$$\overline{X^2} = 2Dt \qquad \text{(VIII-4-12)}$$

where, D : diffusivity
t : time

This equation can be used to give a rapid estimate of the mean distance of diffusion. For example, the average distance traveled by a LiOT(g) molecule in one second is 1 ∿ 6 cm at the breeder temperature (400 ∿ 1,000°C).

(3) Conclusions

The following behaviours of LiOT(g) in blanket are clarified from the investigation described above.

i) LiOT(g) molecules move at random on the collision with He atoms and surface of Li_2O pebbles. The collision frequency of a LiOT(g) molecule with He atoms is much greater than that with Li_2O pebbles. And this collision frequency is considerably high to be nearly 10^{10}/sec at 400 ∿ 1,000°C.

For the above reasons, it is reasonable to consider that the temperature of LiOT(g) molecules is nearly equal to that of the neighboring He gas.

ii) LiOT(g) vapor formed at higher temperature breeder zone is transported to lower temperature breeder zone by convective and diffusive flows. The LiOT(g) molecules are to collide sufficiently with helium atoms and effectively condense as LiOT(s) during transportation through the pore matrix of the breeder particles. These effects show that the partial pressure of LiOT(g) reached lower temperature zone is fairly small compared with that at higher temperature zone.

Therefore, it is reasonable to consider that LiOT(g) vapor pressure in blanket is maintained by its equilibrium pressure based on He temperature and partial pressure of T_2O(g).

iii) The structure materials, such as coolant tubes and blanket vessels, are surrounded by the low temperature zone of breeder. And the equilibrium pressure of LiOT(g) over Li_2O(s) at low temperature, as calculated before , is quite low (∿10^{-11} atm, at 400°C). It seems fairly certain that the amount of LiOT(s) deposit on the surface of structure materials at low temperature is negligibly small.

iv) It is true that LiOT(g) molecules move at high speed (∿1,000 m/sec), but because of high collision frequency and short mean free path, its diffusivity is not large. As described above, the distance traveled by a LiOT(g) molecule in one second by diffusion would be 1 ∿ 6 cm. While, the velocity of helium purge gas flow is about 6 cm/sec. Therefore, it is unreasonable to consider that much greater quantities of Li_2O could be transported due to the high speed motion of LiOT(g) molecule than due to convective transport of LiOT(g) vapor.

v) If the low temperature breeder zone (∿400°C) is provided to the purge gas outlet where the equilibrium pressure of LiOT(g) is very low (∿10^{-11} atm, at 400°C), the quantities of LiOT transported out of the blanket can be reduced remarkably. For example, the total amount of LiOT(g) transported out of the blanket would be only 0.5 g during 15 yrs' operation in the case of He flow rate of 200 Nm^3/hr.

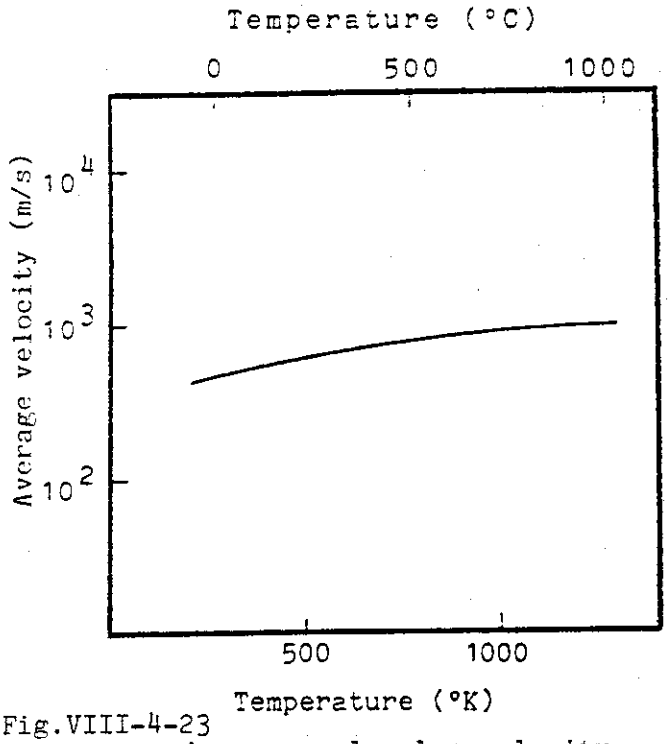

Fig.VIII-4-23 Average molecular velocity of LiOT(g).

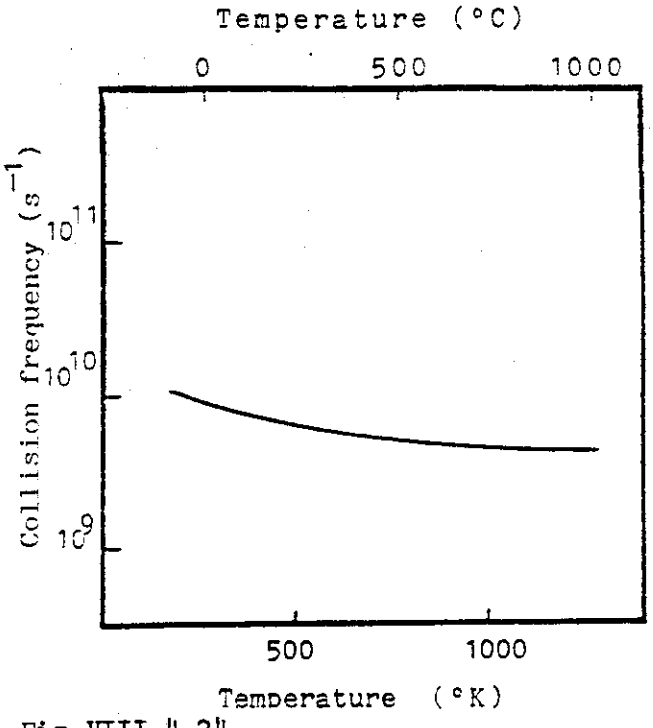

Fig.VIII-4-24 Collision frequency of a LiOT(g) molecule with He atoms.

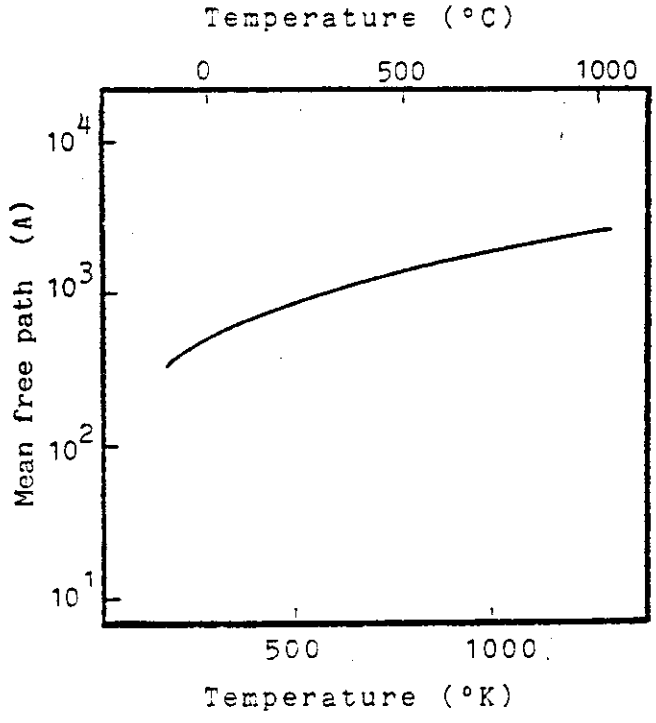

Fig.VIII-4-25 Mean free path of LiOT(g).

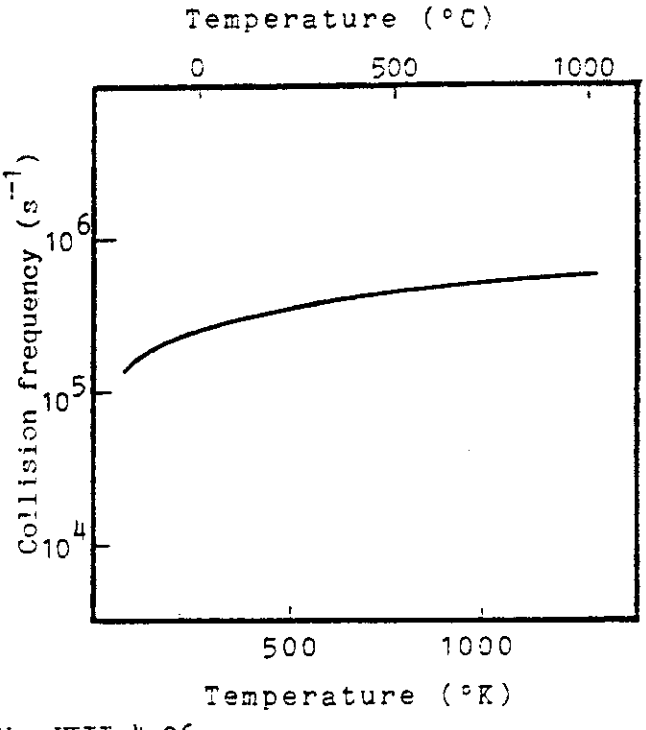

Fig.VIII-4-26 Collision frequency of a LiOT(g) molecule with Li_2O pebbles.

4.1.4 Blanket Design

(a) Feasibility Study of Tritium Breeding Blanket

(1) Introduction

a) Objectives

Objectives of the study are :

① neutronic investigation of blanket configuration to obtain high tritium breeding ratio

② to investigate blanket structure which is easy to control temperature of breeder material and is less sensitive to reactor operating conditions.

b) Scope

The study is grouped into three categories :

① A neutronic analysis was carried out for BOT/NM blanket which was proposed as Japanese design in phase 1 to define optimum neutronic parameters, considering structural feasibility of blanket.

② A neutronic analysis was carried out for INTOR reference (BOT/SM) blanket which is considered to be easy to control temperature of breeder material.

③ A parametric thermal analysis of breeder material was carried out to define design parameters (e.g. dimension of breeder zone and helium gap).

c) Method of Analysis

Neutronic analysis was performed using one dimensional transport (SN) code ANISN with infinite cylindrical model and S_8-P_3 approximation. Coupled 42-group neutron and 21-group gamma-ray cross section sets (GICX40) based on the ENDF/B-III and IV nuclear data files were used in the analysis.

Steady state temperature distribution in breeder zone was analyzed using equivalent one dimensional cylinder model.

(2) Tritium Breeding Performance

a) Parametric Study of Tritium Breeding Ratio (BOT/NM)

i) Geometrical Model (see Fig. VIII-4-27)

Geometrical model for ANISN is shown in Fig. VIII-4-28. The following assumptions are taken into consideration:

① Thickness of blanket front wall (i.e. first wall armor) is 4 mm which is the minimum thickness to withstand the inner pressure of 1 ata.

② First wall is cooling tube panel type. Corrugated panel type is also considered for comparison.

③ Lead (Pb) and beryllium (Be) are considered as neutron multiplier.

④ Breeder is lithium oxide (Li_2O) pebble (85% T.D.). Packing fraction of breeder pebbles in blanket vessel is 70%.

⑤ Water (H_2O) and/or helium (He) are considered as coolant.

⑥ There is no internal coolant in neutron multiplier zone when its thickness is not more than 5 cm.

⑦ Thickness of blanket is 50 cm.

In the model, each blanket subzone is homogeneously mixed.

ii) Results

Table VIII-4-5 summarizes the results of calculation, and Table VIII-4-6 shows the neutron balance of Cases A-1 and A-7.

① H_2O Coolant (Case A-1 ∿ Case A-14)

Fig.VIII-4-29 shows the dependence of tritium breeding ratio (TBR) upon lead multiplier thickness. The TBR is optimized at a lead multiplier thickness of ∿ 5 cm.

Fig.VIII-4-30 shows the dependence of TBR upon ^6Li enrichment. The TBR is optimized at 30% ^6Li enrichment when lead multiplier is 5 cm thickness.

The maximum TBR is 1.184 when 5 cm-thick lead multiplier and 30% enriched ^6Li are used (Case A-7). If first wall is replaced by corrugated panel, the TBR increases to 1.207 (Case A-11). If the thickness of first wall armor is increased from 4 mm to 10 mm, the TBR decreases to 1.130 (Case A-12). An increase of the stainless steel first wall armor thickness by 1 mm results in a TBR decrease of 9×10^{-3}.

② He/H_2O Coolant (Case B-1 ∿ Case B-10)

First wall and neutron multiplier are cooled by helium gas and partition wall and breeder zone are cooled by water (H_2O). Beryllium is used as neutron multiplier because of the high melting point (1,284°). Fig.VIII-4-31 shows the dependenee of TBR upon beryllium multiplier thickness. The TBR is optimized at a beryllium thickness of ∿ 5 cm.

Fig.VIII-4-32 shows the dependence of TBR upon ^6Li enrichment. The TBR is optimized at 30% ^6Li enrichment when beryllium multiplier is 5 cm thickness.

The maximum TBR is 1.348 when 5 cm-thick beryllium multiplier and 30% enriched ^6Li are used (Case B-7).

③ He Coolant (Case C-1 ∿ Case C-10)

Fig.VIII-4-33 shows the dependence of TBR upon blanket thickness when no neutron multiplier is used. Blanket thickness of 50 cm is not enough in this case, and TBR increases up to ∿ 100 cm.

Fig.VIII-4-34 shows the dependence of TBR upon beryllium multiplier thickness. The TBR is optimized at a beryllium thickness of ∿ 5 cm (blanket thickness 50 cm).

The maximum TBR is 1.362 when 5 cm-thick beryllium multiplier and 30% enriched ^6Li are used (Case C-7).

If the thickness of first wall armor is increased from 4 mm to 10 mm, the TBR decreases to 1.277 (Case C-8). An increase of the stainless steel first armor thickness by 1 mm results in a TBR decrease of 0.014.

iii) Improvement of Blanket for High TBR Performance

In the blanket described above, neutron multiplier is placed in a separate zone in front of breeder zone. From neutronic point of view, however, it is desirable that neutron multiplier and breeder are placed closely. Therefore tritium breeding performance will be improved if neutron multiplier and breeder are homogeneously mixed in the same zone. For example beryllium pebbles and lithium oxide pebbles are mixed and packed in blanket vessel.

Properties of candidate neutron multiplier materials are shown in Table VIII-4-7. The threshold energies for (n, 2n) reaction of beryllium and lead are 1.9 Mev and 6.8 Mev, respectively. Since neutrons generated by Pb (n, 2b) reaction have rather high energy, they can be further multiplied by Be (n, 2n) reaction. Therefore Pb-Be two-step multiplying system can be considered.

Inventory of breeder will be reduced if some percentage of breeder can be replaced by an effective solid moderator and/or multiplier such as graphite and beryllium.

The following four blanket arrangements were considered in the study :

① Pb-(Pb/Li_2O mixture) system (see Fig. VIII-4-35)

The first zone consists only of lead neutron multiplier and the second zone consists of lead and breeder followed by the third zone consisting only of breeder.

② Pb-(Be/Li_2O mixture) system (see Fig. VIII-4-36)

The first zone consists only of lead multiplier followed by the second zone consisting of beryllium and breeder.

③ Be/Li_2O mixture system

Blanket is filled with mixture of beryllium and lithium oxide pebbles.

④ Pb-(Be/Li_2O mixture) - (C/Li_2O mixture) system (see Fig. VIII-4-37)

In the blanket arrangement illustrated in Fig. VIII-4-36, rear part of Be/Li_2O mixture zone is replaced by graphite/Li_2O mixture.

Results of analysis for above four arrangements are summarized in Table VIII-4-8.

① Pb-(Pb/Li_2O mixture) system (He coolant)

Three cases with different ratios of lead and lithium oxide were analyzed (Case D-8, 9, 10). The maximum TBR is 1.398 when lead volume fraction is the largest. It is not practical to place lead and lithium oxide in the same zone because the melting point of lead is low (328°C).

② Pb-(Be/Li_2O mixture) system

Four cases with different ratios of beryllium and lithium oxide were analyzed (Case D-1 ~4) for He coolant. The maximum TBR is 1.515 when beryllium volume fraction is the largest (see Fig. VIII-4-38). When water is used as coolant (Case D-11, 12), the TBR is 1.292.

③ Be-Li_2O mixture system

Four cases with different ratios of beryllium and lithium oxide and with different coolants were analyzed (Case D-13, 14, 15, 16). The maximum TBR of water coolant case is 1.495, and that of helium coolant case is 1.592, when beryllium volume fraction is the largest.

④ Pb-(Be/Li_2O mixture) - (C/Li_2O mixture) system (He coolant)

Three cases with different ratios of graphite and lithium oxide were analyzed (Case D-5, 6, 7). The maximum TBR is 1.431 when no graphite is used.

Table VIII-4-9 shows the neutron balance of Cases D-1 and D-14.

iv) Discussions (BOT/KM type)

Blanket structure should be determined not only by breeding performance but also by structural complexity, fablicability, cost, coolant system, tritium inventory and safety. Fig.VIII-4-39 shows the relation between breeding performance and structural complexity and cost. One must pay the penalty of structural complexity or high cost in order to improve the breeding performance.

The following measures will be taken to increase TBR:

① to place neutron multiplier

② to enrich ^6Li

③ to replace H_2O with He or D_2O as coolant

It is better from neutronics viewpoint that neutron multiplier and breeder are placed in the same zone than that multiplier is placed in a separate zone.

Beryllium is very attractive material in neutronic and thermal properties. In this study the maximum TBR of 1.592 was obtained when beryllium and lithium oxide are homogeneously mixed and He is used as coolant. In case of H_2O coolant, the TBR is also large and 1.495. As thermal conductivity of beryllium is excellent, the effective thermal conductivity of breeder zone will be much improved if beryllium is mixed with lithium oxide. The problem to be examined is tritium solubility in beryllium.

Resource limitation and relatively high cost of beryllium are of main concern regarding the use of beryllium. As there is not large difference between the costs of beryllium and lithium oxide, the cost of blanket will not increase extremely even if some portion of lithium oxide is replaced with beryllium. Even when some portion of beryllium is replaced with graphite to reduce the quantity of beryllium, the TBR is rather high. Thus, the quantity of beryllium will be adjusted according to the required breeding ratio.

Accuracy of neutronics calculation and breeding blanket coverage should be also taken into consideration to determined blanket configuration. If uncertainty of 10% is expected in neutronics calculation, the breeding ratio should be greater than 0.67 to meet the INTOR

specification(>0.6). If the effective blanket coverage is 0.6, the local TBR of 1.12 is required.

High breeding performance may cause the safety problem relating the storage of surplus tritium. So the breeding performance should be discussed from the viewpoint of tritium fuel cycle including the construction of the other reactor.

b) Parmetric Study of Tritium Breeding Ratio (BOT/SM)

i) Blanket Structure

Fig. VIII-4-40 shows the blanket structure of BOT/SM type. The following items are assumed :

① First wall thickness is 7 mm.

② First wall structure is tube panel type.

③ Coolant is H_2O.

④ Moderator is graphite.

⑤ Breeder is Li_2O (30% ^6Li enrichment)

⑥ Neutron multiplier is lead or beryllium.

ii) Geometrical Model

The basic blanket configuration is shown below.

There are several modeling methods for breeder zones to be considered.

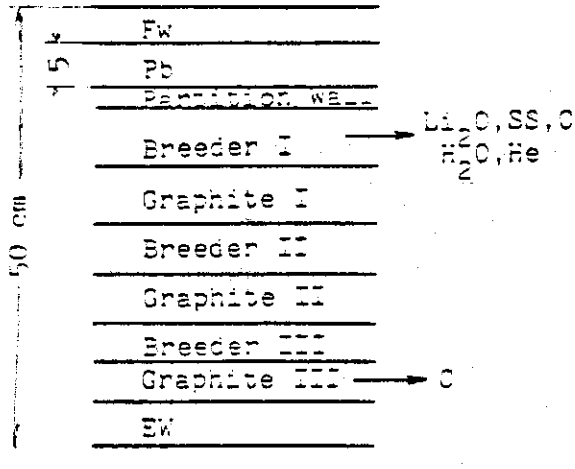

There are :

① Homogeneous A

Materials are homogeneously mixed in breeder zones according to the actual volume fractions (incl. Li_2O, SS, H_2O, C, He).

② Homogeneous B

Materials exclusive of C and He are homogeneously mixed (The sum of volume fractions for Li_2O, SS and H_2O is 1.0).

③ Heterogeneous C

The thickness of each material (SS, Li_2O, H_2O) is determined according to the volume fractions (see the figure below) of Homogeneous B model.

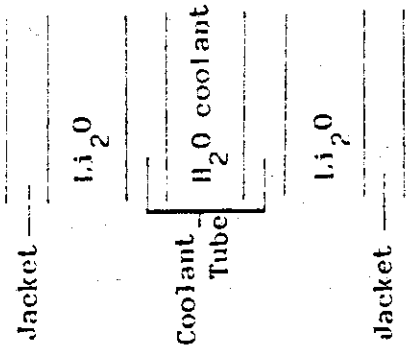

④ Heterogeneous D

The thickness of each material is the actual one. (see figure below)

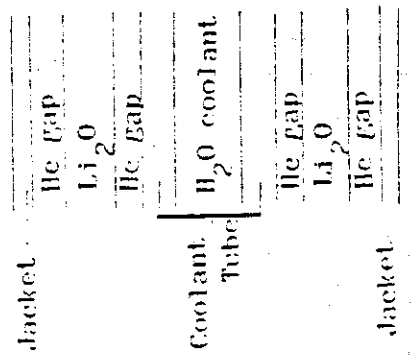

Calculational results for the four models are shown in Table VIII-4-10. In the calculations, the first wall thickness is assumed to be 4 mm in order to compare them with that of BOT/NM blanket. Discrepancy between four models is less than 10%. Homogeneous models do not represent heterogeneity of BOT/SM structure and heterogeneous models and homogeneous B model do not represent the actual volume of each material. The TBR of BOT/SM is about 10% lower than BOT/NM.

iii) Results

Results of parametric study for BOT/SM blanket are shown in Table VIII-4-11. Homogeneous B and Heterogeneous C models were used.

① Effect of Moderator in the First Breeder Zone

By comparing the results of Case E-1 and Case F-1 (which replaces graphite with void), it is better that there is no graphite in the first breeder zone.

② ^{6}Li Enrichment in the First Breeder Zone

Natural lithium is assumed in the first breeder zone of Case F-2. The TBR decreases compared to Case F-1 which uses 30% ^{6}Li enrichment.

③ Thickness of Moderator Zone

Four cases with different moderator arrangements (thickness of three moderator zones) were analyzed (Case G-1, 2, 3, 4). Among the four cases, arrangements with the thick second moderator zone (Case G-3) gives the highest TBR, but the differences are small.

④ Coolant in the First Wall

H_2O in the first wall is replaced by D_2O or He (Case H-1, 2). By comparing Case H-1 with Case G-3, and Case H-2 with Case I-2, TBR's increase by ∿ 13% and ∿ 16%, respectively.

⑤ Effect of ^6Li Enrichment (Model Homogeneous B)

Four cases with different ^6Li enrichments were analyzed (Case I-1, 2, 3, 4). The effect is not strong and the maximum variation of TBR is ∿ 8% relative to the natural lithium case.

The neutron flux distributions of Case I-2 are shown in Fig. VIII-4-41.

⑥ Effect of Moderator Selection

Three materials, graphite, water (H_2O), beryllium were examined as moderator material (Case I-2, J-1, 2)

TBR is the largest in the beryllium case and the worst in the water case. Beryllium is not so much moderator as neutron multiplier. (see Fig. VIII-4-49)

⑦ Effect of SS Jacket and Tube Thickness

Effect of jacket and tube thickness on TBR is examined (Case K-1, 2). Actual thicknesses of jacket and tube are 1 mm and 1.5 mm, respectively. In the calculational model of Case G-3, they are 2.7 mm and 1.1 mm. In the Case K-1, they are 1 mm and 1.1 mm, and in the Case K-2, 1 mm and 2 mm. The effect is not large and the variation of TBR is ∿ 2%.

⑧ Effect of Breeder and Moderator Zone Number

The number of breeder and moderator zone is doubled i.e. 6 breeder zones and 6 moderator zones (Case L-1) while total thickness is kept. The TBR is a little decreased compared to the 3 zone case.

⑨ Effect of First Wall Coating

1 mm coating zone (Be or C) is added in front of first wall (Case M-1, 2,). The TBR is a little increased in the case of beryllium and is a little decreased in the case of carbon compared to the Case G-3.

iv) Blanket for High TBR Performance

In the BOT/SM blanket, breeder tubes are placed in the graphite bed. In order to obtain high TBR, the graphite bed is replaced by lead or beryllium. The structure is shown in Fig. VIII-4-42.

① Calculational Model

The model for Pb-Be-C bed system is shown in Fig.VIII-4-43. In the breeder zone, materials are homogeneously mixed. Pb-Be bed system eliminates the graphite bed zone and replaces it with beryllium. Be bed system uses only beryllium.

② Results

Results of calculation are shown in TableVIII-4-12. The TBR is the largest (1.529) in Be bed system (Case N-3). If first wall is cooled by D_2O, the TBR increased to 1.561 (Case N-4). In the thick (13 mm) first wall case (N-5), the TBR is decreased from 1.486 (Case N-2) to 1.410.

v) Discussions (BOT/SM type)

① On the Calculational Models

Relation of breeder volume (zone thickness) and TBR of the four calculational models is shown as follows :

Model	Breeder zone thickness (cm)	TBR
Homo. A	8.24	1.015
Homo. B	15.86	1.108
Hetero C	15.94	1.088
Hetero D	11.8	1.067
BOT/NM	22.18*	1.184

* Actual thickness (37.6 cm) x Packing fraction (0.59)

The relation is illustrated in Fig. VIII-4-44. It seems that breeder volume and TBR have positive correlation. Therefore, only homogeneous A model and BOT/NM model which represent the actual breeder volume seems to give TBR values close to the actual values. Homogeneous B and Heterogeneous C represent the difference between homogeneous and heterogeneous models because they have almost the same breeder volume. Heterogeneous effect is -2% in this case. As for calculational model, further investigation should be based on multi-dimensional calculation.

② On the Blanket Structure

BOT/SM blanket has been developed for purpose of reducing tritium inventory (i.e. reducing breeder volume) and easier temperatute control. Tritium breeding performance, however, seems to be inferior to BOT/NM blanket. The following characteristics were observed ;

ⓐ Breeder (mixture of Li_2O and H_2O coolant) has comparable showing-down power to graphite.

ⓑ Thermal neutron fluxes for BOT/NM and BOT/SM are illustrated in Fig. VIII-4-45. BOT/SM is better because thermalized neutrons are absorbed in breeder on the spot.

ⓒ Fig. VIII-4-46 shows the energy group contribution to ^6Li (n, α) T reaction at various points of breeder for BOT/SM blanket. Thermal neutron contribution to TBR is about 6% in all. Thermal neutrons are absorbed at the surface of

breeder and intermediate neutron contribution is predominant inside the breeder.

ⓓ In BOT/SM blanket which has smaller volume of breeder, more neutrons go back toward the plasma, because absorption in breeder zone decreases (see Fig. VIII-4-47).

ⓔ BOT/SM blanket has larger structure volume fraction than BOT/NM.

ⓕ It is better that the first breeder zone eliminates moderator. Graphite is not so much a moderator as a reflector. Among the tree moderator zones, it is better that the second one is thick. (see Fig. VIII-4-48)

ⓖ When breeder and moderator zones are divided into smaller zones, structural volume fraction tends to increase and TBR decreases.

ⓗ TBR does not vary much because of thicknesses of jacket and coolant tube if they are reasonable thicknesses.

③ Blanket Structure for High TBR Performance

TBR increases remarkably by placing breeder tube in lead or beryllium moderator bed. Because thermal conductivities of lead and beryllium are excellent, the similar structure to BOT/SM is possible. Careful attention must be paid when lead is used because melting point is rather low.

④ Conclusions

ⓐ One dimensional calculation for BOT/SM has large (∿ 10%) uncertainty due to calculational model. Multi-dimensional calculation is required for further investigation.

ⓑ TBR of BOT/SM is lower than that of BOT/NM by ∿ 10%.

ⓒ The dependences of TBR upon arrangements of moderator, structure volume fraction, ^{6}Li enrichment are not very strong.

ⓓ The TBR of reference BOT/SM structure is around 1.0.

ⓔ TBR is remarkably improved by replacing graphite with lead or beryllium partially or wholly.

(3) Temperature Control of Breeder

In-situ recovery of tritium produced in blanket has to be attained for economy and safety of a fusion reactor. Therefore the temperature of breeder is necessary to be controlled in the acceptable range. The temperatures of breeder will be controlled by coolant tube arrangements and helium gap between coolant tube and breeder according to the nuclear heating rates. The conditions to be necessary for continuous extraction of produced tritium in breeder have a lot of uncertainty yet due to the lack of experimental data. Parametric studies of breeder temperature have been carried out to clarify the conditions to maintain the temperature of breeder within the acceptable range. And the sensitivity to several uncertain conditions of blanket design such as allowable temperature range, effective thermal conductivity of breeder and nuclear heating rates in breeder zone was estimated.

a) Analytical Conditions

1-D thermal analysis with the equivalent cylindrical model shown in Fig. VIII-4-50 has been carried out for evaluating the temperature distribution in breeder. The maximum allowable temperature of breeder, effective thermal conductivity of breeder are chosen as survey parameters in this study. These parameters are summarized in Table VIII-4-13. Other analytical conditions are shown in Table VIII-4-14. The following assumptions have been adopted in this analysis.

i) Nuclear heating rates in equivalent breeder cell region are constant and uniform.

ii) Outer surface of breeder is adiabatic.

iii) Axial heat conduction is neglected.

iv) Heat in breeder zone is transfered to coolant tube by conduction and radiation through helium gap.

b) Results and Discussions

The acceptable ranges for breeder temperature control are shown in Figs. VIII-4-51∼VIII-4-60. The relations of gap width and allowable equivalent outer radius of breeder for each allowable breeder temperature range and nuclear heating rates are indicated in Figs. VIII-4-51 and VIII-4-52. In Figs. VIII-4-53∼VIII-4-60, allowable equivalent outer radius of breeder for each temperature range is shown as the function of nuclear heating rates.

i) The Effect of Maximum Allowable Temperature

The acceptable ranges of equivalent outer radius of breeder for the case of 900°C and 700°C of the maximum allowable temperatures as examples are shown in Figs. VIII-4-51～VIII-4-60. As seen from these figures, it is naturally expected that the higher maximum allowable temperature allows the much wider acceptable range. Therefore the breeder that has higher maximum allowable temperature should be selected to design the tritium breeding blanket in consideration of a lot of uncertainties. And the more accurate maximum allowable temperature of breeder must be evaluated.

ii) The Effect of Thermal Conductivity of Breeder

The values of thermal conductivity of breeder used in this analysis are 2 W/mK and 3 W/mK. It is found from making a comparison between Fig.VIII-4-51 and Fig.VIII-4-52 that the higher thermal conductivity leads the wider acceptable range of blanket design. At INTOR Phase 1, 2 W/mK as the thermal conductivity of solid breeder is used for estimating rather conservatively considering its reduction due to irradiation and its temperature dependency. If higher conductivity can be adopted, the difficulty in blanket design will be reduced. And it is preferable to select the breeder which has high thermal conductivity.

iii) The Effect of Gap Width

The temperature control of breeder is possible with the practicable helium gap width as shown in Figs. VIII-4-51 and VIII-4-52.In the acceptable

range, the temperature difference in breeder reduces as the helium gap width increases and its increases as the width decreases. The temperature control with wider gap is relatively easier than with narrower gap. But, since the wide gap reduces the amount of breeder, it causes some penalty to the tritium breeding performance.

iv) Margin for the Change of Nuclear Heating Rates

The maximum and minimum allowable nuclear heating rates to control the breeder temperature in the acceptable range are evaluated for the designed equivalent outer radius of breeder R. The margin for the nuclear heating rates is defined as follows ;

$$\frac{\Delta q'''}{q'''}\ (\%) = \frac{q'''(R) - q'''_m(R)}{q'''(R)} \times 100$$

where $q'''(R)$: maximum allowable nuclear heating rates for R

$q'''_m(R)$: minimum allowable nuclear heating rates for R

The margins for the change of nuclear heating rates are shown in Figs.VIII-4-61 VIII-4-65. In Figs. VIII-4-61∼VIII-4-64, they are shown as the function of maximum allowable nuclear heating rates. The relation of maximum allowable temperature and the margin is shown in Fig. VIII-4-65 as example. In that case, the nuclear heating rate of breeder is 15 W/cc and the thermal conductivity of breeder is 3 W/mK. From these results, the margin is rather small when 0.5 mm of gap width is chosen. When the wider gap is chosen, the margin becomes from 40 to 50% for 700°C of maximum

allowable temperature and from 60 to 70% for 900°C of that. Higher thermal conductivity of breeder brings naturally a larger margin. Generally, to take the design with a large margin means that the optimum breeder geometry is not selected from the nuclear point of view. Therefore to take too large margin should be avoided in actual design.

v) Conclusions

From these discussions, following conclusions are pointed out

① As the thermal conductivity of breeder has a great influence on the acceptable range of blanket design and the margin for temperature control, it is preferable to select the breeder with high thermal conductivity. Lithium oxide, which has the highest thermal conductivity in all candidate solid breeding materials*, is the best material from the view point of temperature control.

The value of 2 W/mK was used as the thermal conductivity of a solid breeder in INTOR Phase 1 tentatively. It is necessary for the future blanket design to estimate the effective thermal conductivity more accurately, including the effects of helium gas in pore matrix, coolant tube wall, and breeder temperature distribution. (* Thermal conductivities[9,47] of lithium oxide and other candidate solid breeding materials are shown in Figs. VIII-4-66 and VIII-4-67.)

② Higher maximum allowable temperature leads larger acceptable range of blanket design and larger margin for temperature control. As the value of maximum allowable temperature has a lot of uncertainties yet, more studies are required.

It is indicated that lithium oxide has the widest operating temperature range in the candidate solid breeding materials.

③ The margin for the change of nuclear heating rates in temperature control is several tens of percents under the conditions assumed in this study. The margin becomes large when the allowable temperature range is large and the thermal conductivity of breeder high. Therefore lithium oxide is the most preferable solid breeding material from these viewpoints as discussed in ① and ② . But further investigations are required to design the realistic blanket. It should be evaluated whether the margin estimated in this study is sufficient or not when taking account of the consistency with neutronics performance, several uncertainties (such as the accuracy of nuclear heating rates estimation, power fluctuation, geometrical errors in fabrication, the accuracy of physical properties of materials etc.)

The constant and uniform nuclear heating rates in the equivalent breeder cell region are assumed in this analysis. The pulse heating effect on breeder temperature of actual operation mode must be considered for the future. The attenuation of heating rates in breeder and the variation in poloidal direction also have to be taken account.

⑪ The temperature control of breeder is possible with the practicable helium gap width. Under the assumptions adopted in this study, the wide gap brings the large margin for the change of nuclear heating rates and the low sensitivity for the variation of gap width. Although the wide gap is preferable from the viewpoint of thermal characteristics, the influence on the breeding performance of gap width have to be considered.

Table VIII-4-5 Results of TBR Parameter Analysis

(Tube in Shell Type Blanket, Case A-1 ~ Case C-10)

Case NO.	Coolant	Mult.*	Parameters: Mult.* Thickness (cm)	Parameters: ^{6}Li Enrich.** (%)	Parameters: First Wall Thickness*** (cm)	Parameters: Blanket Thickness (cm)	Remarks	Tritium Breeding Ratio: T_6	Tritium Breeding Ratio: T_7	Tritium Breeding Ratio: Total
A-1	H_2O	-	-	Natural	0.4 + 1.5	50		0.051	0.264	1.115
A-2	H_2O	Pb	3	Natural	0.4 + 1.5	50		0.952	0.164	1.116
A-3	H_2O	Pb	5	Natural	0.4 + 1.5	50		0.996	0.129	1.125
A-4	H_2O	Pb	10	Natural	0.4 + 1.5	50		0.970	0.072	1.042
A-6	H_2O	-	-	Natural	0.4 + 1.5	40	Inner Blanket	0.805	0.252	1.057
A-7	H_2O	Pb	5	30	0.4 + 1.5	50		1.007	0.097	1.104
A-8	H_2O	Pb	5	50	0.4 + 1.5	50		1.112	0.069	1.181
A-9	H_2O	Pb	5	90	0.4 + 1.5	50		1.136	0.014	1.150
A-10	H_2O	Pb	5	30	0.4 + 1.5	40	Inner Blanket	1.068	0.089	1.137
A-11	H_2O	Pb	5	30	0.4 + 1.3	50	Corrugated Panel First Wall	1.106	0.101	1.207
A-12	H_2O	Pb	5	30	1.0 + 1.5	50	Thick First Wall	1.043	0.087	1.130
A-13	H_2O	Pb	3	30	0.4 + 1.5	50		1.035	0.123	1.158
A-14	H_2O	Pb	10	30	0.4 + 1.5	50		1.066	0.054	1.120

* Neutron multiplier ** Enrichment *** Armor + Cooling part

**** First wall-Ho, Breeder-H_2O

Table VIII-4-5 (cont'd)

Case NO.	Parameters: Coolant	Mult.	Mult. Thickness (cm)	^{6}Li Enrich. (%)	First Wall Thickness (cm)	Blanket Thickness (cm)	Remarks	Tritium Breeding Ratio: T_6	T_7	Total
B-1	He/H_2O****	-	-	Natural	0.4 + 1.5	50		0.875	0.279	1.155
B-2	He/H_2O	Be	3	Natural	0.4 + 1.5	50		1.089	0.185	1.274
B-3	He/H_2O	Be	5	Natural	0.4 + 1.5	50		1.151	0.149	1.300
B-4	He/H_2O	Be	10	Natural	0.4 + 1.5	50		1.046	0.086	1.132
B-6	He/H_2O	-	-	Natural	0.4 + 1.5	40	Inner Blanket	0.824	0.262	1.090
B-7	He/H_2O	Be	5	30	0.4 + 1.5	50		1.236	0.112	1.348
B-8	He/H_2O	Be	5	50	0.4 + 1.5	50		1.258	0.079	1.337
B-9	He/H_2O	Be	5	90	0.4 + 1.5	50		1.277	0.016	1.292
B-10	He/H_2O	Be	5	30	0.4 + 1.5	40	Inner Blanket	1.199	0.103	1.302
C-1	He	-	-	Natural	0.4 + 1.5	40	Inner Blanket	0.735	0.283	1.018
C-2	He	-	-	Natural	0.4 + 1.5	50		0.806	0.298	1.104
C-3	He	-	-	Natural	0.4 + 1.5	60		0.852	0.306	1.158
C-4	He	-	-	Natural	0.4 + 1.5	90		0.899	0.311	1.210
C-5	He	-	-	30	0.4 + 1.5	50		0.905	0.223	1.128
C-6	He	Be	3	30	0.4 + 1.5	50		1.167	0.151	1.318

Table VIII-4-5 (cont'd)

Case NO.	Coolant	Mult.	Parameters: Mult. Thickness (cm)	Parameters: ^{6}Li Enrich. (%)	Parameters: First Wall Thickness (cm)	Parameters: Blanket Thickness (cm)	Remarks	Tritium Breeding Ratio: T_6	Tritium Breeding Ratio: T_7	Tritium Breeding Ratio: Total
C-7	He	Be	5	30	0.4 + 1.5	50		1.240	0.122	1.362
C-8	He	Be	5	30	1.0 + 1.5	50	Thick First Wall	1.169	0.108	1.277
C-9	He	Be	10	30	0.4 + 1.5	50		1.127	0.070	1.197
C-10	He	Be	15	30	0.4 + 1.5	50		0.879	0.039	0.918

Table VIII-4-6 Neutron Blance in TIS Blanket

Case A-7 { Pb 5 cm / H_2O / 30% ^6Li

	Gain	Balance	Absorption	Neutron Multiplication
DT neutron	+1.0	1.0		
1. FW armor	-0.030	0.970	0.053	0.023
2. FW cooling part	-0.054	0.916	0.096	0.042
3. Pb multiplier	+0.268	1.185	0.033	0.301
4. Partition wall	-0.016	1.169	0.020	0.004
5. Breeder zone	-1.129	0.040	1.152	0.024
6. End wall	-0.005	0.035	0.007	0.002
Leakage into shield	0.035	Total	1.361	0.396

Case A-1 { H_2O / natural Li

	Gain	Balance	Absorption	Neutron Multiplication
DT neutron	+1.0			
1. FW armor	-0.005	0.995	0.029	0.024
2. FW cooling part	+0.003	0.998	0.049	0.052
3. Breeder zone	-0.938	0.060	0.990	0.052
4. End wall	-0.012	0.048	0.013	0.001
Leakage into shield	0.048	Total	1.081	0.129

Table VIII-4-7 Properties of Candidate Neutron Multiplier Materials

Material	Be	BeO	Pb	PbO
Density, g/cm^3	1.85	2.96	11.34	9.53
Atom or molecules number density $n/cm^3 \times 10^{-24}$	0.1236	0.07127	0.03348	0.02571
σ(n,2n) at 14MeV, barns	0.5	0.5	2.2	2.2
Σ(n,2n) at 14MeV, cm^{-1}	0.0618	0.0256	0.0737	0.0565
Threshold energy for (n,2n) cross section, MeV	1.868	1.868	6.765	6.765
σ(n,γ) at 0.0253 eV barns	0.0095	0.0095	0.17	0.17
Melting point, °C	1278	2520	327.5	888
Thermal conductivity* at 25 °C, W/m-°K	201	216**	35.3	2.8

* At 25 °C

** Pure beryllium oxide, hot pressed

Table VIII-4-8 Results of High TBR Performance Blanket Analysis. (Case D-1 ~ Case D-16)

Case NO.	Blanket Configulation: Coolant	Mult.	Mixed Breeder Zone (Volume Fraction): Mult.	Li_2O	Breeder Zone: C	Li_2O	Remarks	Tritium Breeding Ratio: T_6	T_7	Total
D-1	He	Pb 5cm	Be 29%	30%	-	-	see Fig. 4-3-2	1.427	0.055	1.482
D-2	He	Pb 5cm	Be 40%	19%	-	-	"	1.481	0.034	1.515
D-3	He	Pb 5cm	Be 15%	44%	-	-	"	1.338	0.081	1.419
D-4	He	Pb 5cm	Be 49%	10%	-	-	"	1.497	0.018	1.515
D-5	He	Pb 5cm	Be 40%	19%	0%	59%	see Fig. 4-3-3	1.372	0.059	1.431
D-6	He	Pb 5cm	Be 40%	19%	29%	30%	"	1.334	0.035	1.369
D-7	He	Pb 5cm	Be 40%	19%	40%	19%	"	1.322	0.026	1.348
D-8	He	Pb 5cm	Pb 60%	15%	0%	59%	see Fig. 4-3-1	1.321	0.077	1.398
D-9	He	Pb 5cm	Pb 40%	35%	0%	59%	"	1.295	0.090	1.385
D-10	He	Pb 5cm	Pb 15%	60%	0%	59%	"	1.256	0.109	1.365
D-11	H_2O	Pb 5cm	Be 40%	19%	-	-	see Fig. 4-3-2	1.262	0.030	1.292

Table VIII-4-8 (Cont'd)

Case NO.	Blanket Configulation: Coolant	Mult.	Mixed Breeder Zone (Volume Fraction): Mult.	Li_2O	Breeder Zone: C	Li_2O	Remarks	Tritium Breeding Ratio: T_6	T_7	Total
D-12	H_2O	Pb 5cm	Be 30%	29%	-	-		1.232	0.046	1.278
D-13	H_2O	-	Be 50%	9%	-	-		1.466	0.029	1.495
D-14	H_2O	-	Be 40%	19%	-	-		1.390	0.061	1.451
D-15	He	-	Be 40%	19%	-	-		1.469	0.068	1.537
D-16	He	-	Be 50%	9%	-	-		1.560	0.032	1.592

Table VIII-4-9 Neutron Balance in High TBR Blanket

Case D-1 { Pb 5 cm / Be 40%, Li_2O 19% / H_2O

	Gain	Balance	Absorption	Neutron Multiplication
DT neutron	+1.0			
1. FW armor	-0.045	0.955	0.068	0.023
2. FW cooling part	-0.088	0.867	0.125	0.037
3. Pb multiplier	+0.255	1.122	0.045	0.300
4. Partition wall	-0.028	1.094	0.030	0.002
5. (Be,Li_2O) Mixed zone	-1.050	0.044	1.358	0.308
6. End wall	-0.022	0.022	0.021	——
Leakage into shield	0.022	Total	1.647	0.669

Case D-14 { Be 40%, Li_2O 19% / H_2O

	Gain	Balance	Absorption	Neutron Multiplication
DT neutron	+1.0			
1. FW armor	-0.011	0.989	0.035	0.024
2. FW cooling part	-0.010	0.978	0.060	0.050
3. (Be-Li_2O) Mixed zone	-0.932	0.047	1.548	0.616
4. End wall	-0.023	0.024	0.022	——
Leakage into shield	0.024	Total	1.665	0.689

Table VIII-4-10 Effect of Calculation Model on Tritium Breeding

Case NO.	Cal. Model	$^6Li(n,\alpha)T$	$^7Li(n,n'\alpha)T$	TBR	Remarks
E-1	Homo. A	0.981	0.034	1.015	FW 19mm (Cooling part 15mm, SS 4mm)
E-2	Homo. B	1.046	0.062	1.108	"
E-3	Hetero.C	1.026	0.062	1.088	"
E-4	Hetero.D	1.021	0.046	1.067	"
A-7	TIS Type Blanket	1.087	0.097	1.184	" Case A-7

Table VIII-4-11 Results of TBR Parameter Analysis

(BOf/SM Blanket, Case E-1 ~ Case M-2)

Case NO.	Cal.* Model	Parameters: Coolant	^{6}Li Enrichment (%)	Moderator	Mod.** Arrangement (cm) I	II	III	Remarks	Tritium Breeding Ratio: T_6	T_7	Total
E-1	Homo. A	H_2O	30	C	7.06	6.25	5.59	SS Armor 4mm	0.981	0.034	1.015
E-2	Homo. B	H_2O	30	C	"	"	"		1.046	0.062	1.108
E-3	Hetero. C	H_2O	30	C	"	"	"		1.026	0.062	1.088
E-4	Hetero. D	H_2O	30	C	"	"	"		1.021	0.046	1.067
F-1	Homo. A	H_2O	30	C	"	"	"	No Graph. in Bree. I	0.907	0.030	1.025
F-2	Homo. A	H_2O	30	C	"	"	"	No Graph. & Natural Li in Bree. I	0.934	0.043	0.977
G-1	Hetero. C	H_2O	30	C	10	0	0.9	SS Armor 7mm	1.006	0.052	1.058
G-2	Hetero. C	H_2O	30	C	12	6	0.9		1.004	0.050	1.054
G-3	Hetero. C	H_2O	30	C	3.31	10	5.59		1.014	0.064	1.078
G-4	Hetero. C	H_2O	30	C	4.4	4.5	10		1.004	0.064	1.070
H-1	Hetero. C	D_2O/H_2O	30	C	3.31	10	5.59		1.158	0.064	1.222
H-2	Homo. B	He/H_2O	30	C	7.06	6.25	5.59		1.192	0.061	1.253

* Calculational model ** Moderator arrangement

Table VIII-4-11 (cont'd)

Case NO.	Cal. Model	Parameters: Coolant	^6Li Enrichment (%)	Moderator	Mod. Arrangement (cm) I	II	III	Remarks	Tritium Breeding Ratio: T_6	T_7	Total
I-1	Homo. B	H_2O	Natural	C	7.06	6.25	5.59		0.935	0.078	1.013
I-2	Homo. B	H_2O	30	C	"	"	"		1.025	0.050	1.083
I-3	Homo. B	H_2O	60	C	"	"	"		1.062	0.033	1.095
I-4	Homo. B	H_2O	90	C	"	"	"		1.081	0.008	1.089
J-1	Homo. B	H_2O	30	H_2O	"	"	"		0.918	0.055	0.973
J-2	Homo. B	H_2O	30	Be	"	"	"		1.290	0.053	1.343
K-1	Hetero. C	H_2O	30	C	3.31	10	5.59	Jacket 0.1*, Cooling tube 0.11	1.032	0.072	1.104
K-2	Hetero. C	H_2O	30	C	"	"	"	Jacket 0.1*, Cooling tube 0.2	1.029	0.067	1.096
L-1	Homo. B	H_2O	30	C				6 Breeder Zones	1.019	0.048	1.067
M-1	Hetero. C	H_2O	30	C	3.31	10	5.59	Be Coating 0.1*	1.016	0.064	1.080
M-2	Hetero. C	H_2O	30	C	"	"	"	Graphite Coating 0.1*	1.008	0.064	1.072

Table VIII-4-12 Results of High TBR Performance Blanket Analysis
(BOT/SM Type Blanket, Case N-1 ～Case N-5)

Case NO.	Coolant	Parameters Arrangement (cm)	Remarks	Tritium Breeding Ratio T_6	T_7	Total
N-1	H_2O	Pb--Be--C bed 4.2 0.25 26.65	FW Armor 0.7 (cm)	1.257	0.049	1.306
N-2	H_2O	Pb--Be bed 4.2 34.9		1.439	0.047	1.486
N-3	H_2O	Be bed 39.1		1.477	0.052	1.529
N-4	D_2O/H_2O	Pb--Be bed 4.2 34.9		1.514	0.047	1.561
N-5	H_2O	Pb--Be bed 4.2 34.9	FW Armor Thick. 1.3	1.368	0.042	1.410

Table VIII-4-13 Survey Parameters

1) Allowable Temperature Range		
Minimum Allowable Temperature	400	°C
Maximum Allowable Temperature	700 - 1000	°C
2) Thermal Conductivity of Breeder	2 , 3	W/mK
3) Gap Width	0.5 - 2.0	mm
4) Nuclear Heating Rates of Breeder	0.5 - 30	W/cc

Table VIII-4-14 Analytical Conditions

1) Coolant	H_2O	
inlet pressure	1.5	MPa
inlet/outlet temperatures	60/100	°C
2) Coolant Tube	type 316 SS	
inner/outer diameters	10/13	mm
3) Gap	helium gas	
pressure	0.1	MPa
4) Emmisivity		
Breeder	0.3	
Coolant Tube	0.6	

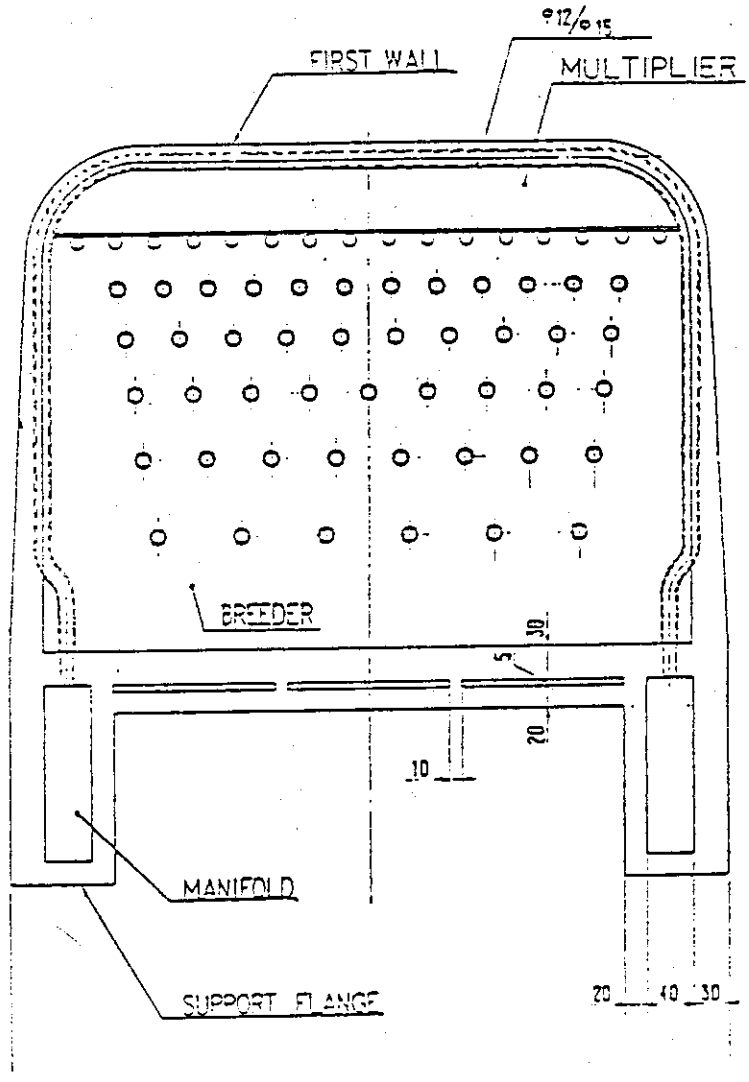

Fig. VIII-4-27 Tube in Shell Type Blanket

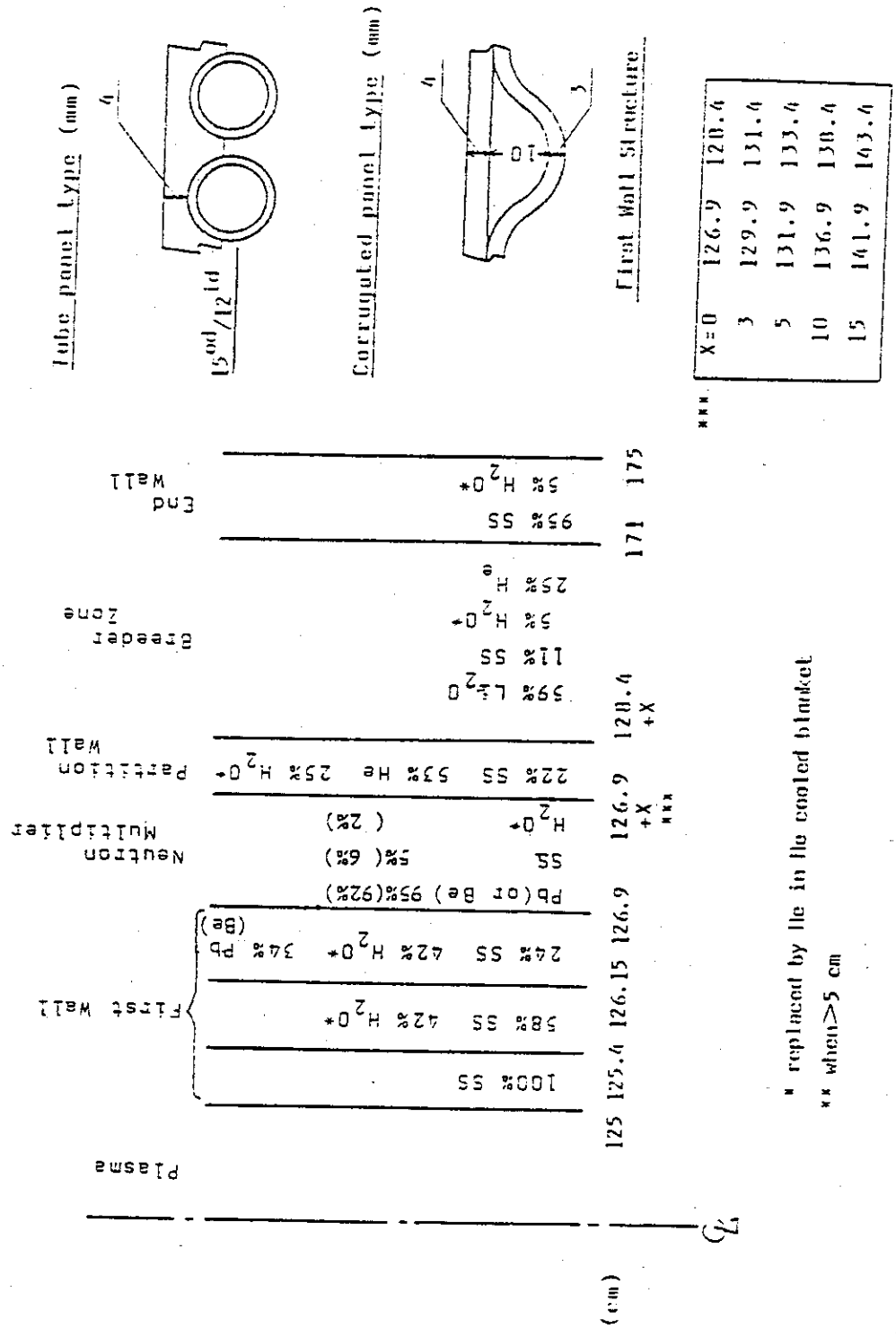

Fig. VIII-4-20 Geometrical Model for ANISN Calculation

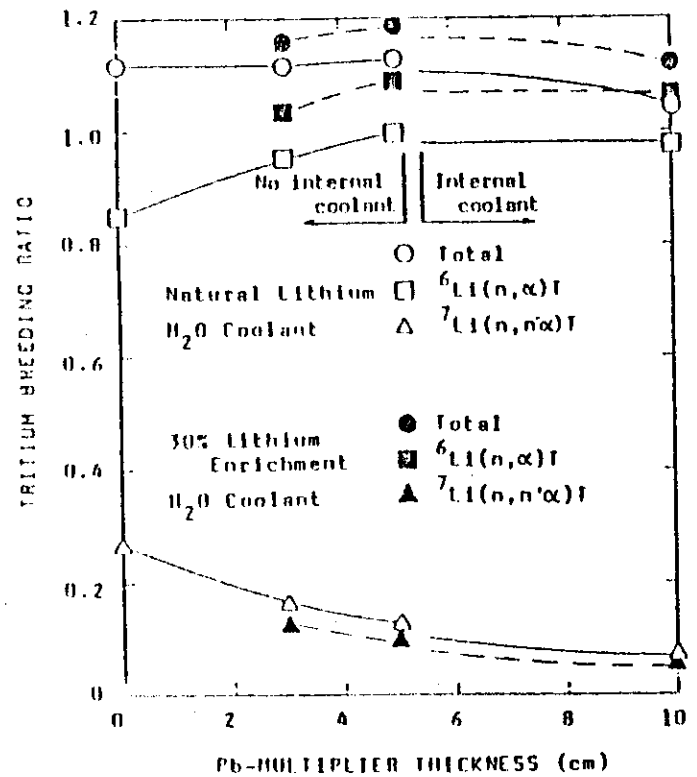

Fig. VIII-4-29 Effect of Pb Multiplier Thickness on Tritium Breeding

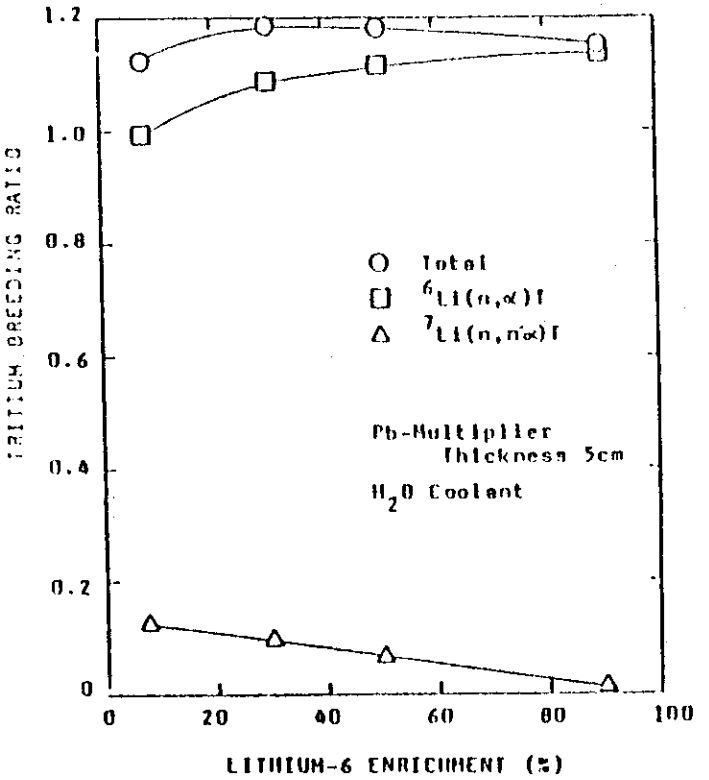

Fig. VIII-4-30 Effect of ^{6}Li Enrichment on Tritium Breeding

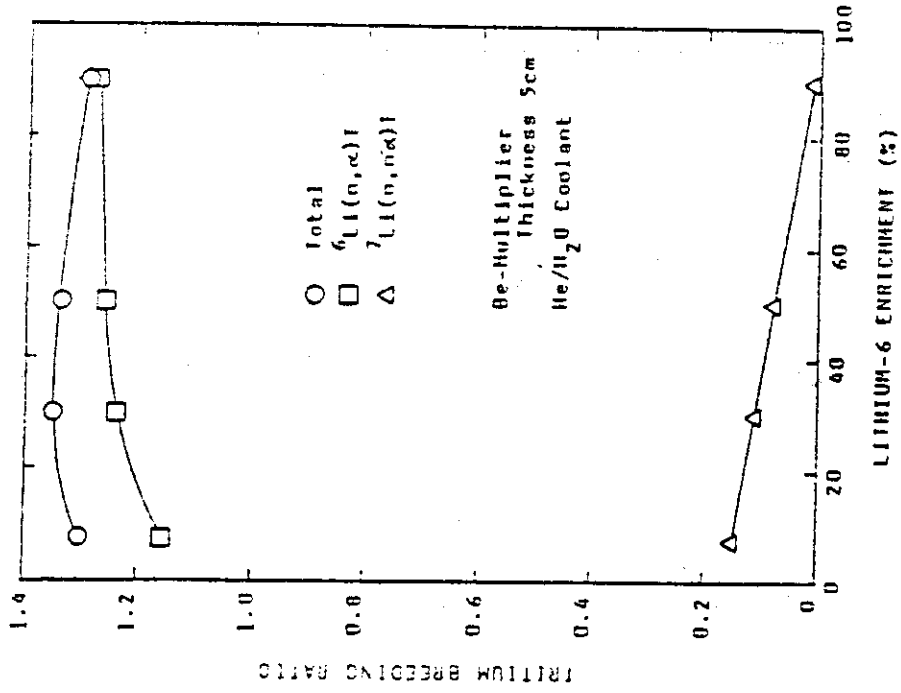

Fig. VIII-4-32 Effect of ^{6}Li Enrichment on Tritium Breeding

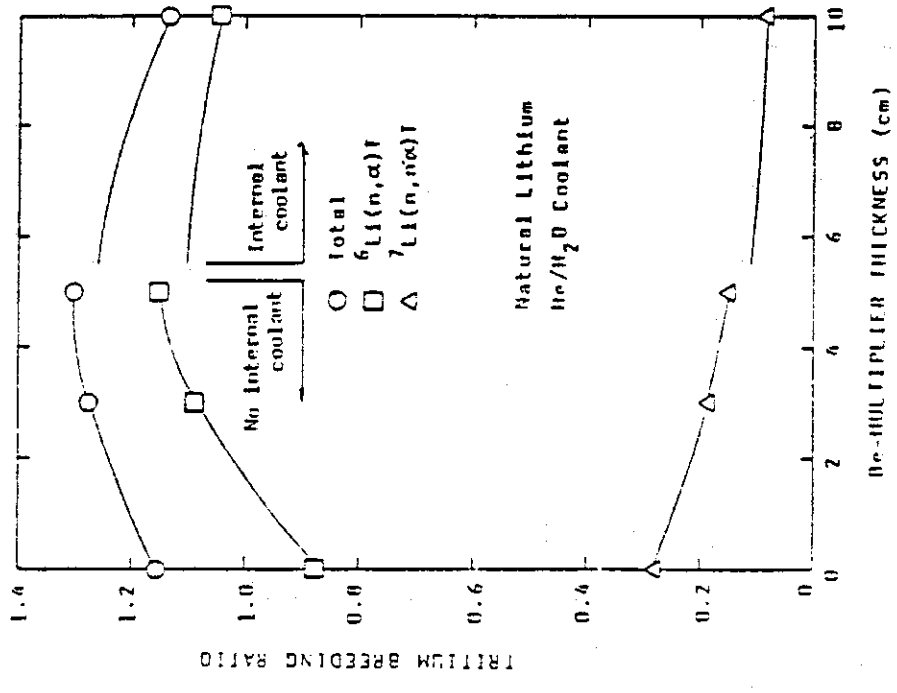

Fig. VIII-4-31 Effect of Be Multiplier Thickness on Tritium Breeding

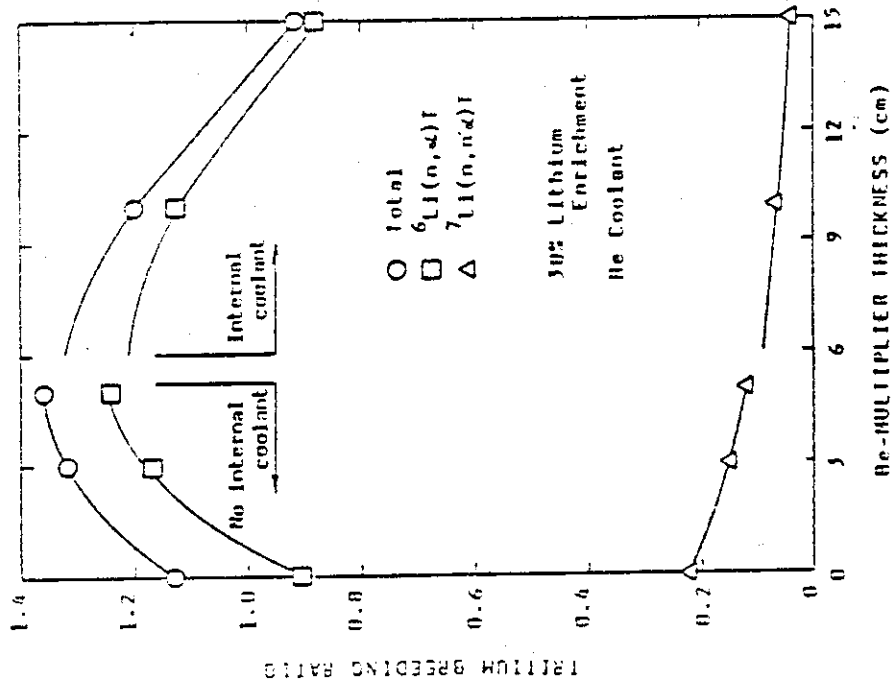

Fig. VIII-4-34 Effect of Be Multiplier Thickness on Tritium Breeding

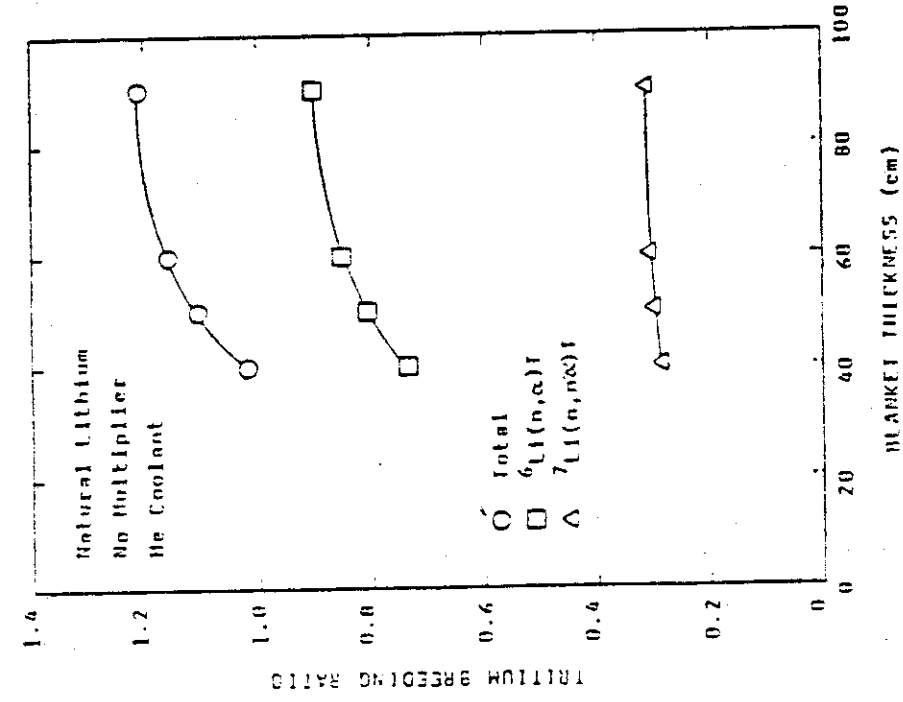

Fig. VIII-4-33 Effect of Blanket Thickness on Tritium Breeding

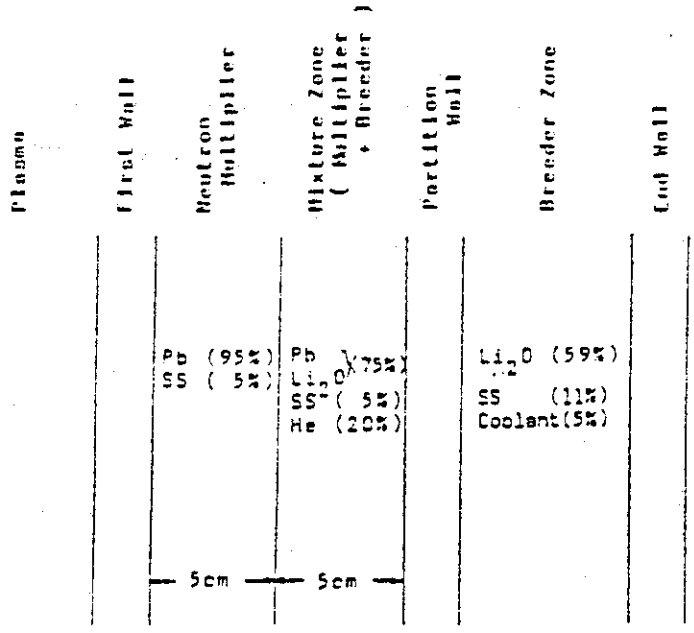

Fig. VIII-4-35 Blanket Concept of Pb-Li_2O Mixed Zone

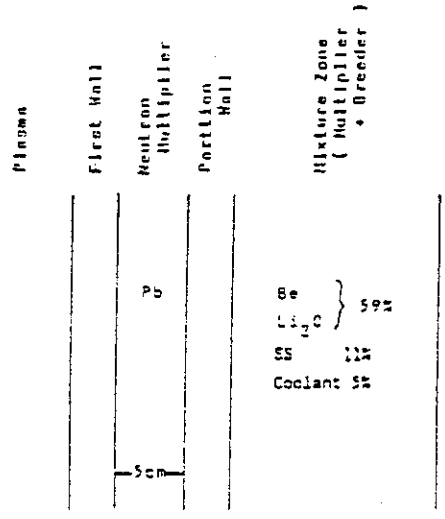

Fig. VIII-4-36 Blanket Concept of Be-Li_2O Mixed Zone

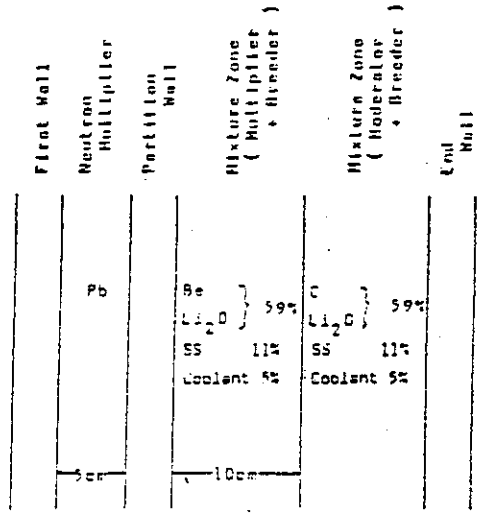

Fig. VIII-4-37 Blanket Concept of Be-C-Li_2 Mixed Zone

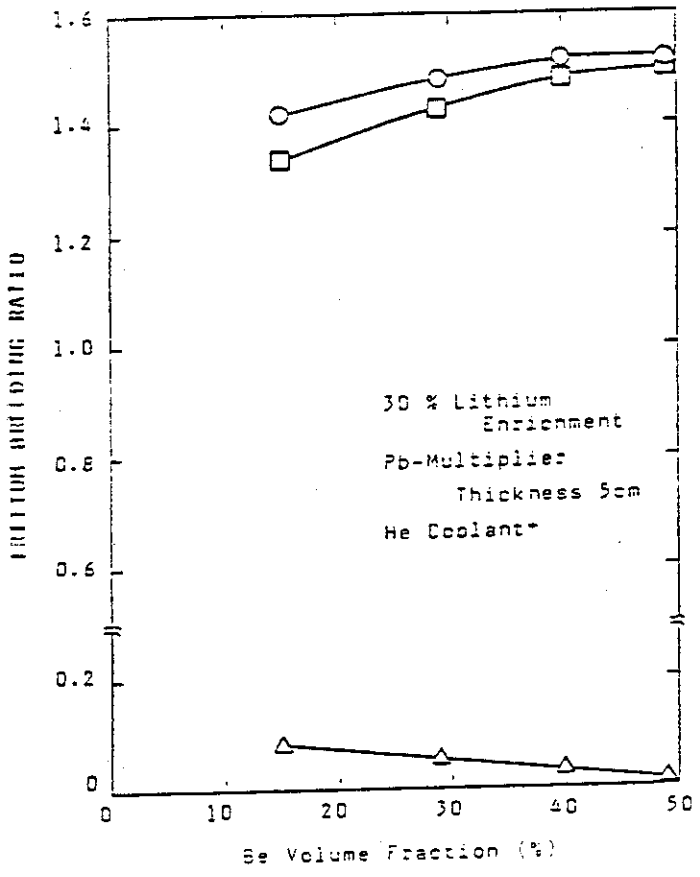

Fig. VIII-4-38 Effect of Be Volume Fraction on Tritium Breeding

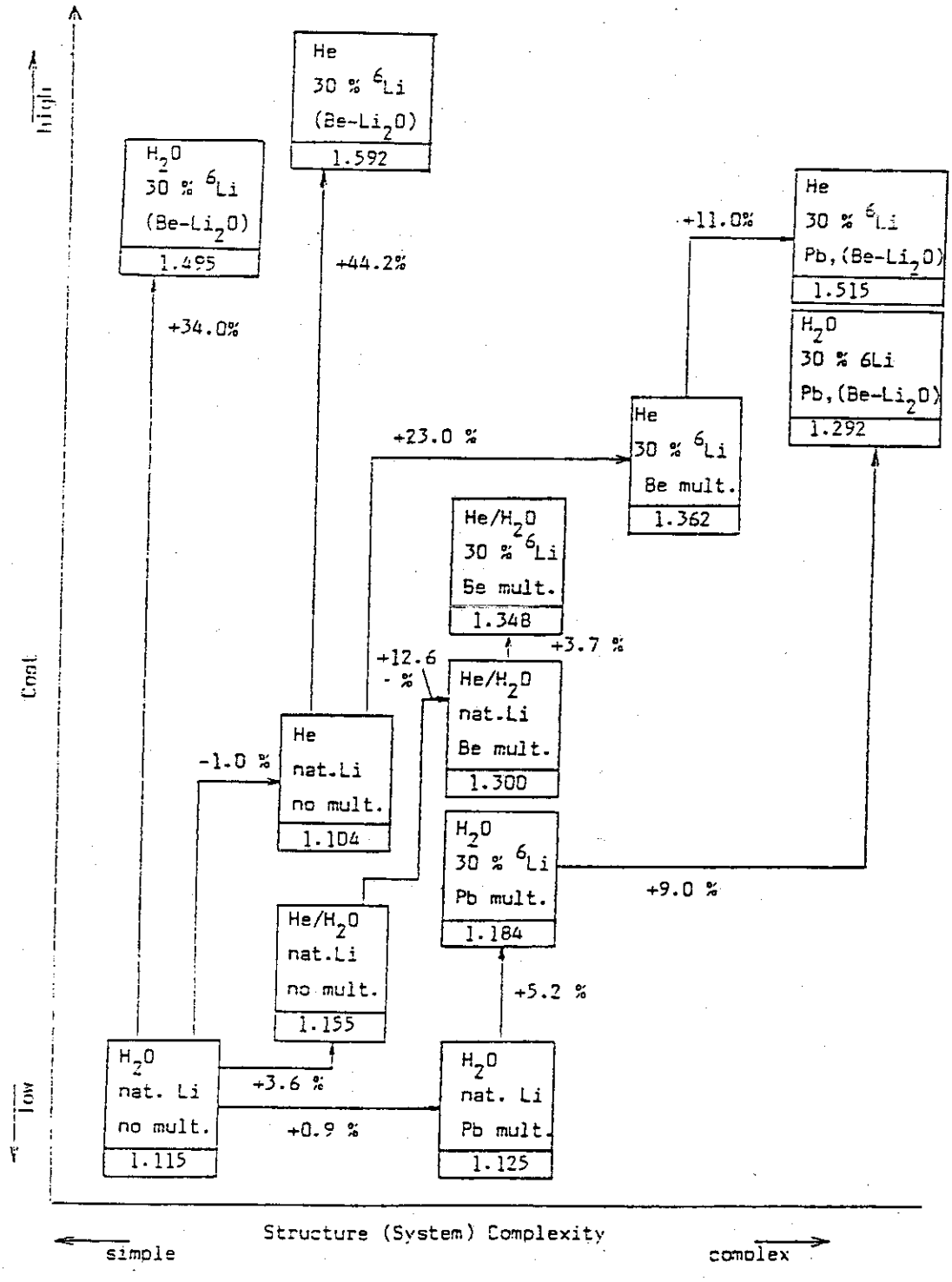

Fig. VIII-4-39 Relation of TBR Improvement with Structure Complexity and Cost

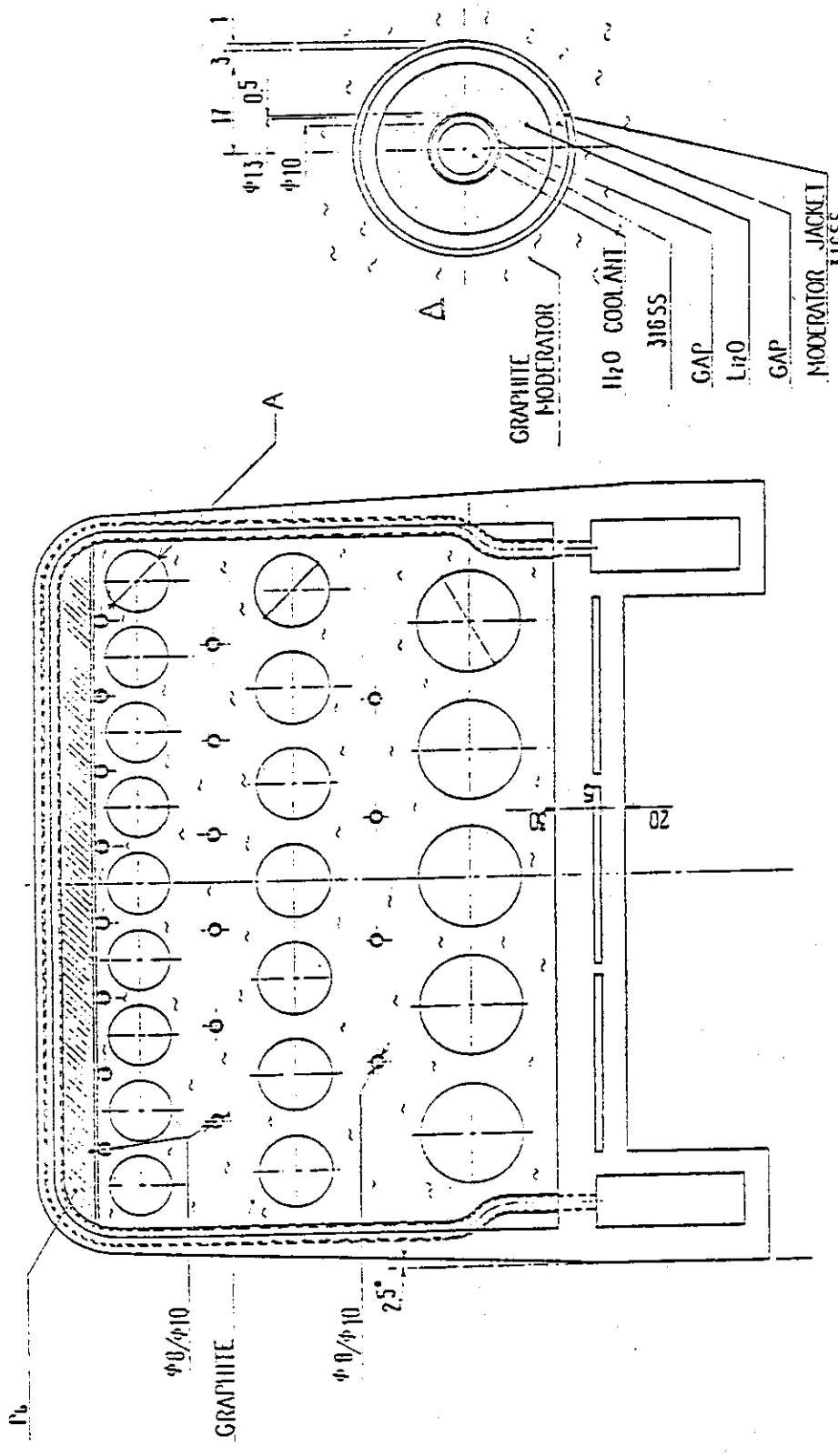

Fig. VIII-4-40 DOT/SN Blanket Structure

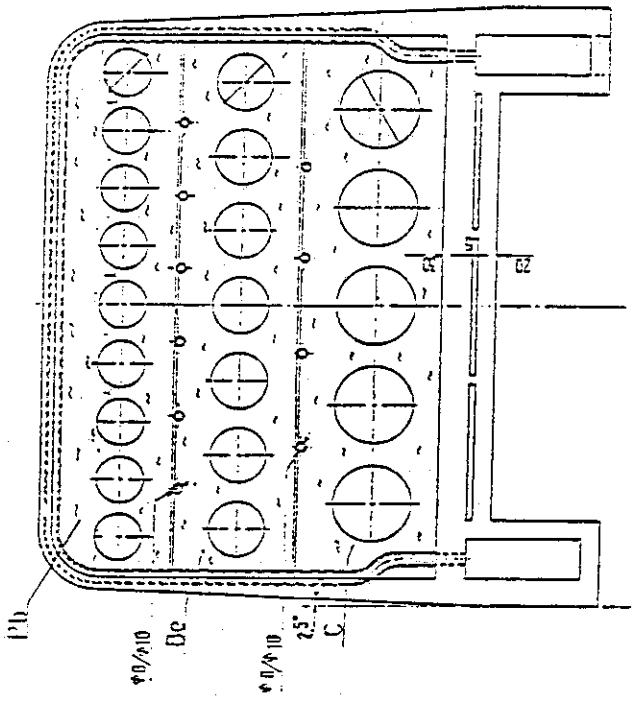

Fig. VIII-4-42 Blanket Concept of Pb-Bo-C System

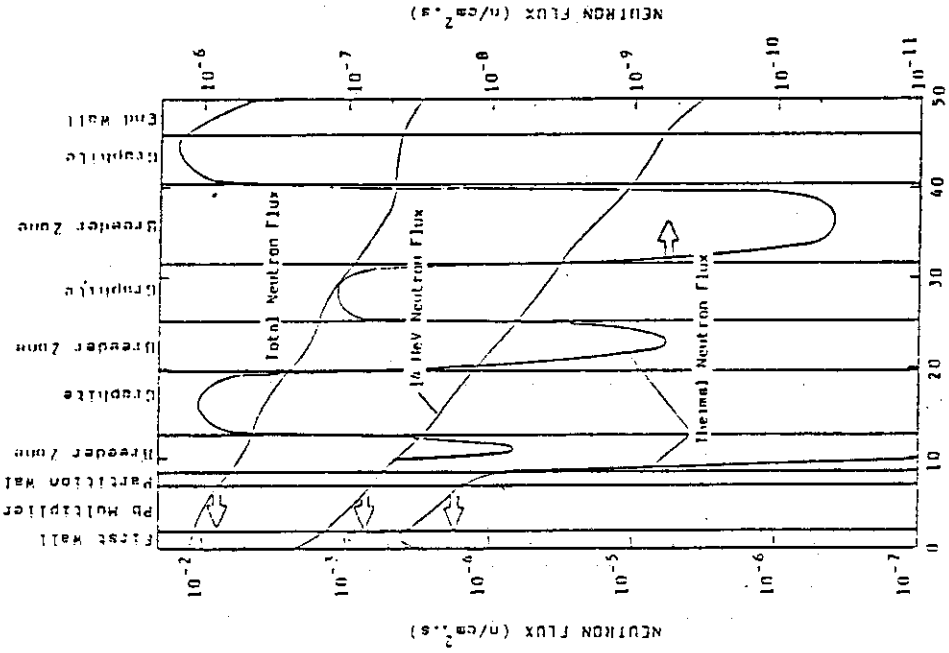

Fig. VIII-4-41 Neutron Flux Distribution in DOT/3M Blanket (Case I-2)

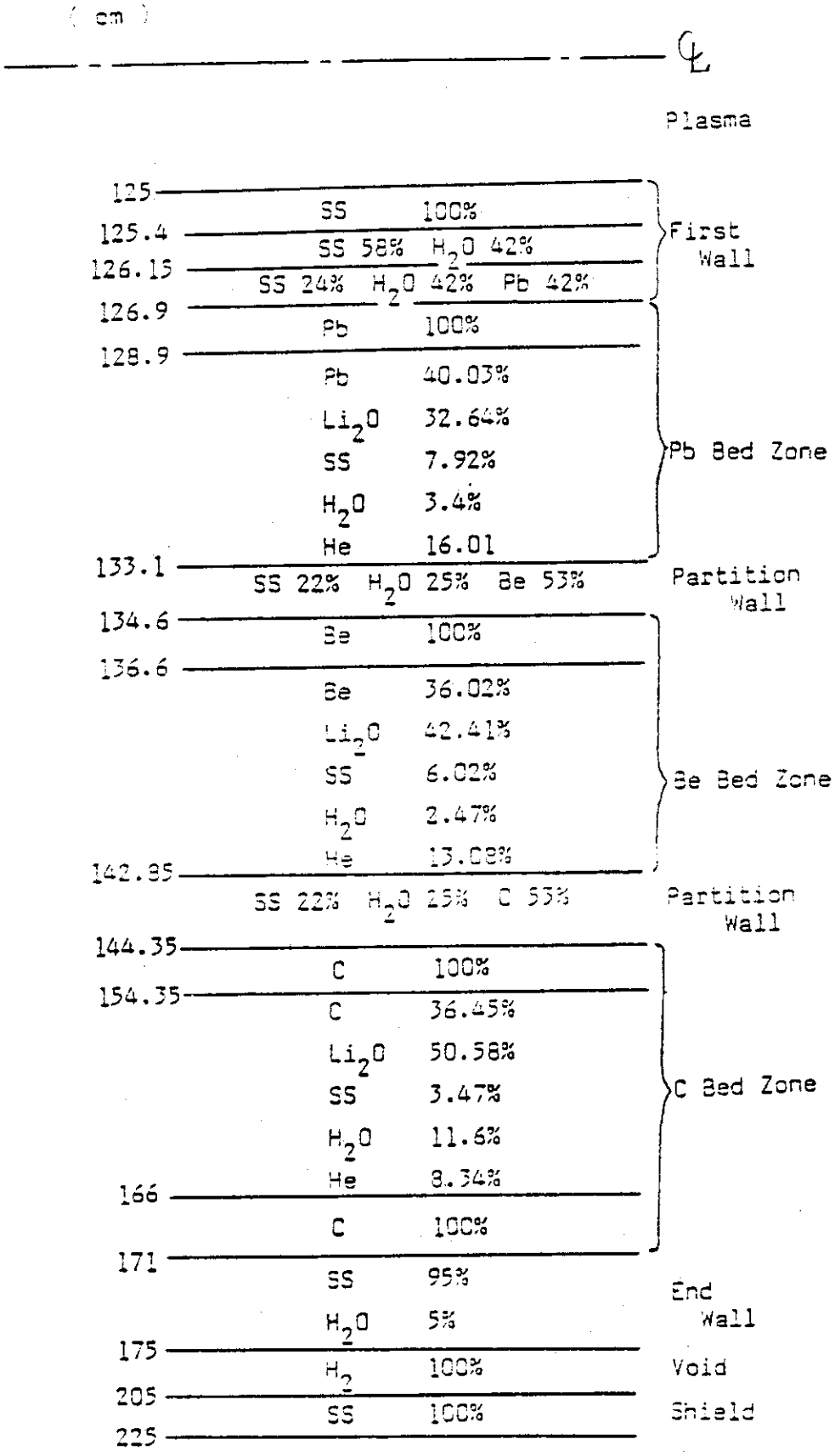

Fig.VIII-4-43 Geometrical Model for Pb-Be-C system

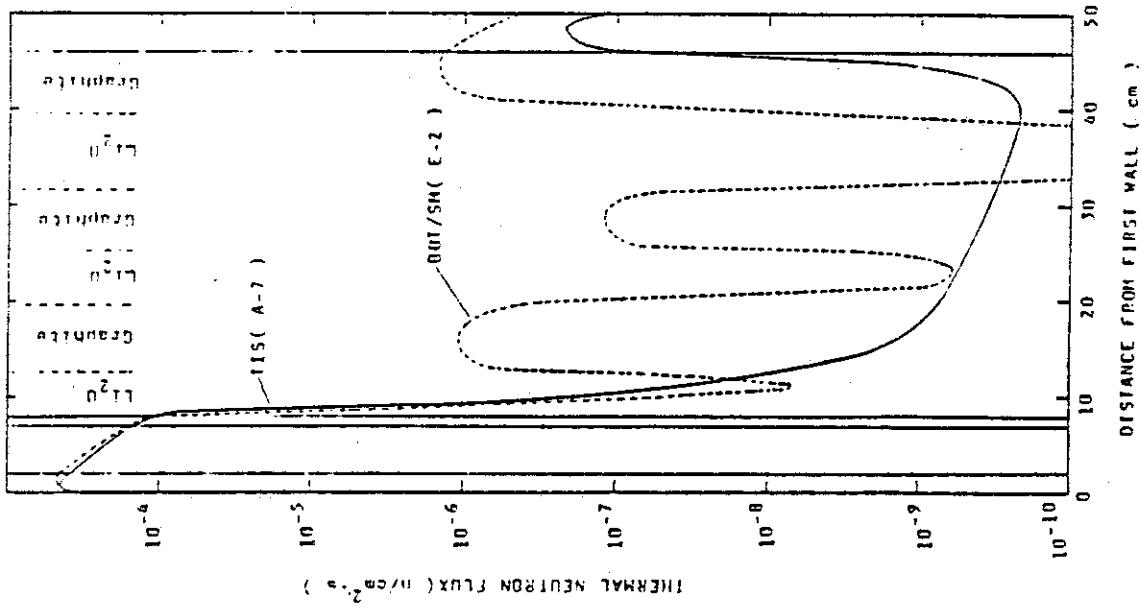

Fig. VIII-4-45 Thermal Neutron Flux Distribution in Blanket (Case A-7, E-2)

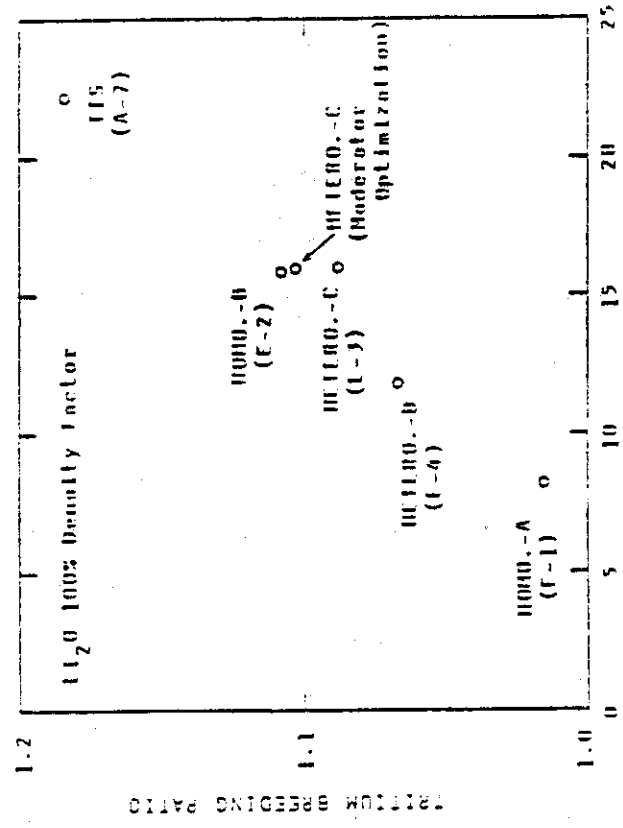

Fig. VIII-4-44 Effect of Breeder Volume on Tritium Breeding

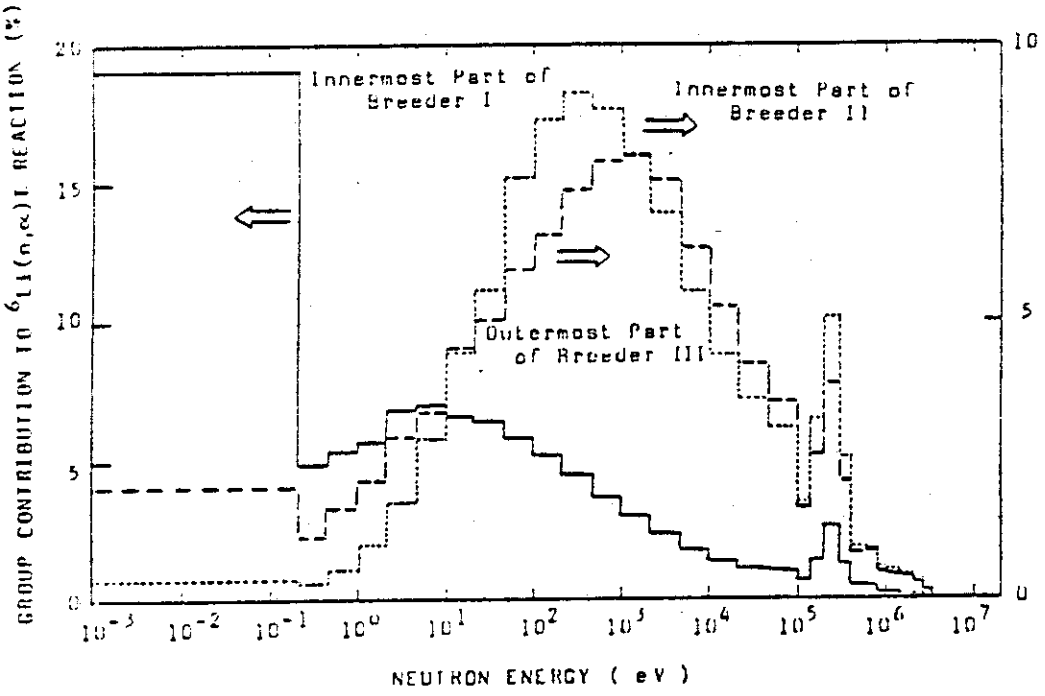

Fig. VIII-4-46 Energy Group Contributions to ^{6}Li(n,α)T Reaction

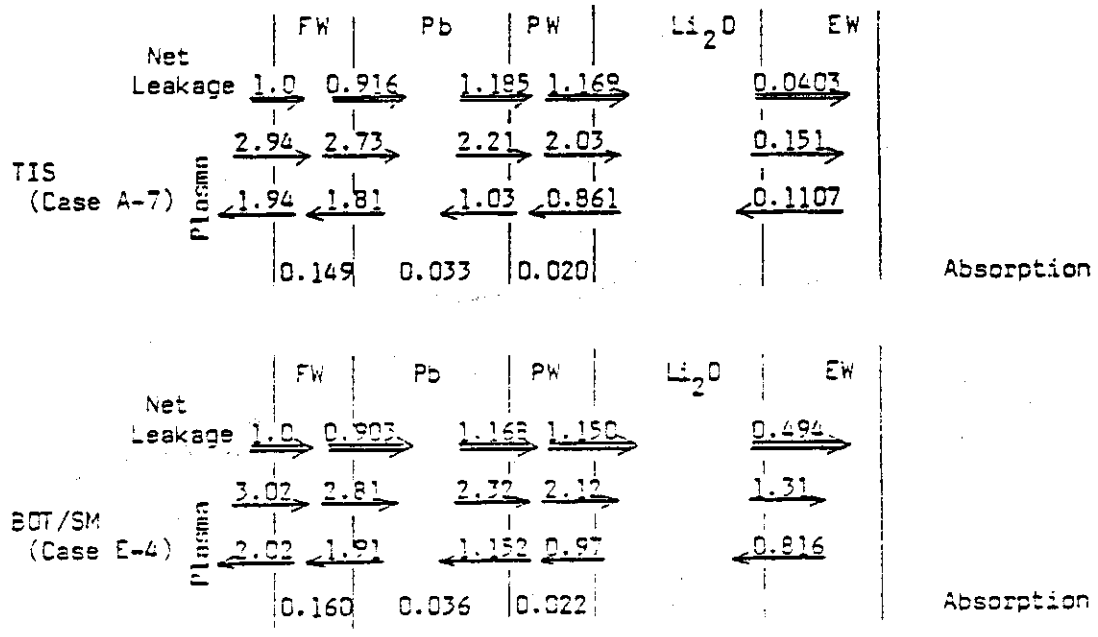

Fig. VIII-4-47 Neutron Current Crossing Each Zone Boundary

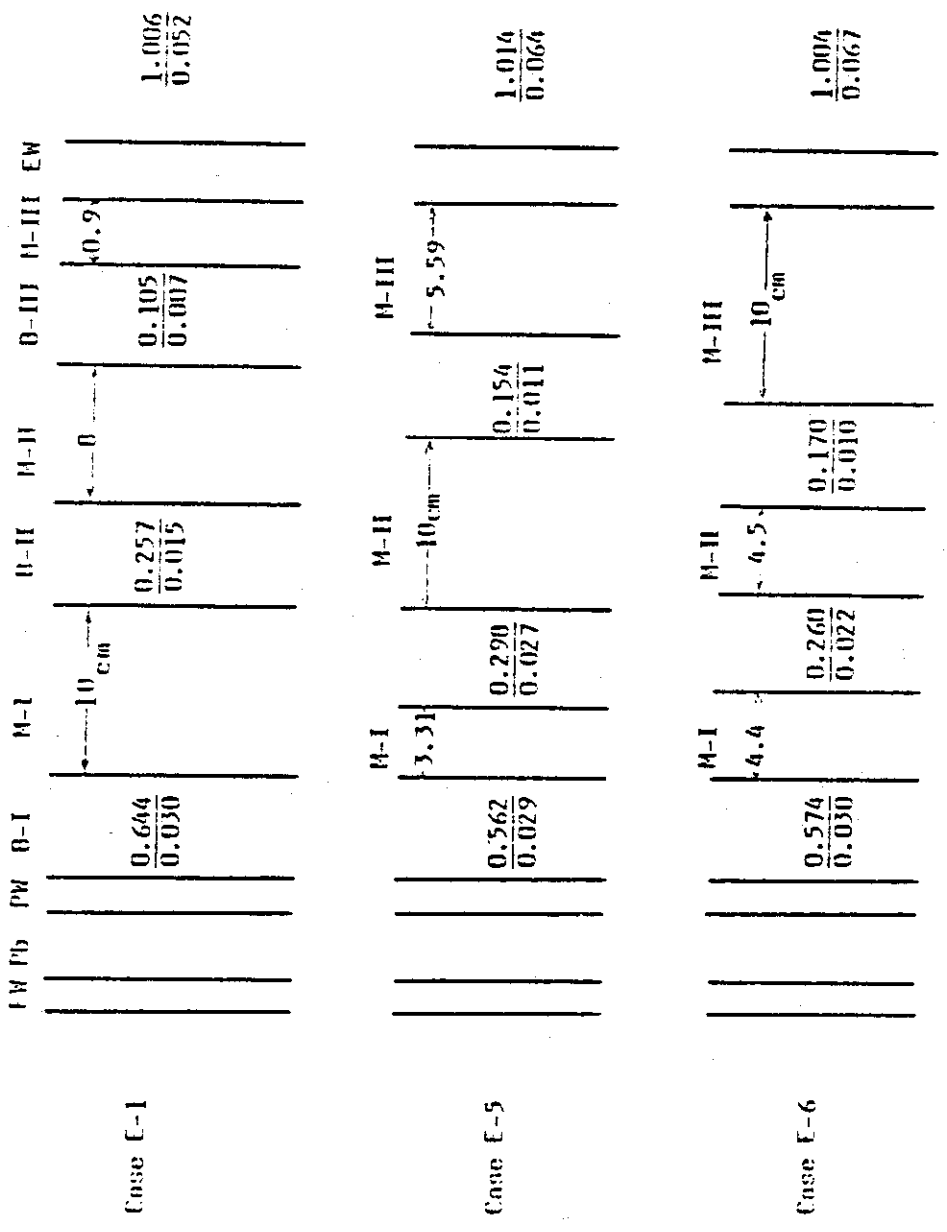

Fig. VIII-4-48 Effect of Moderator Arrangement on Tritium Breeding

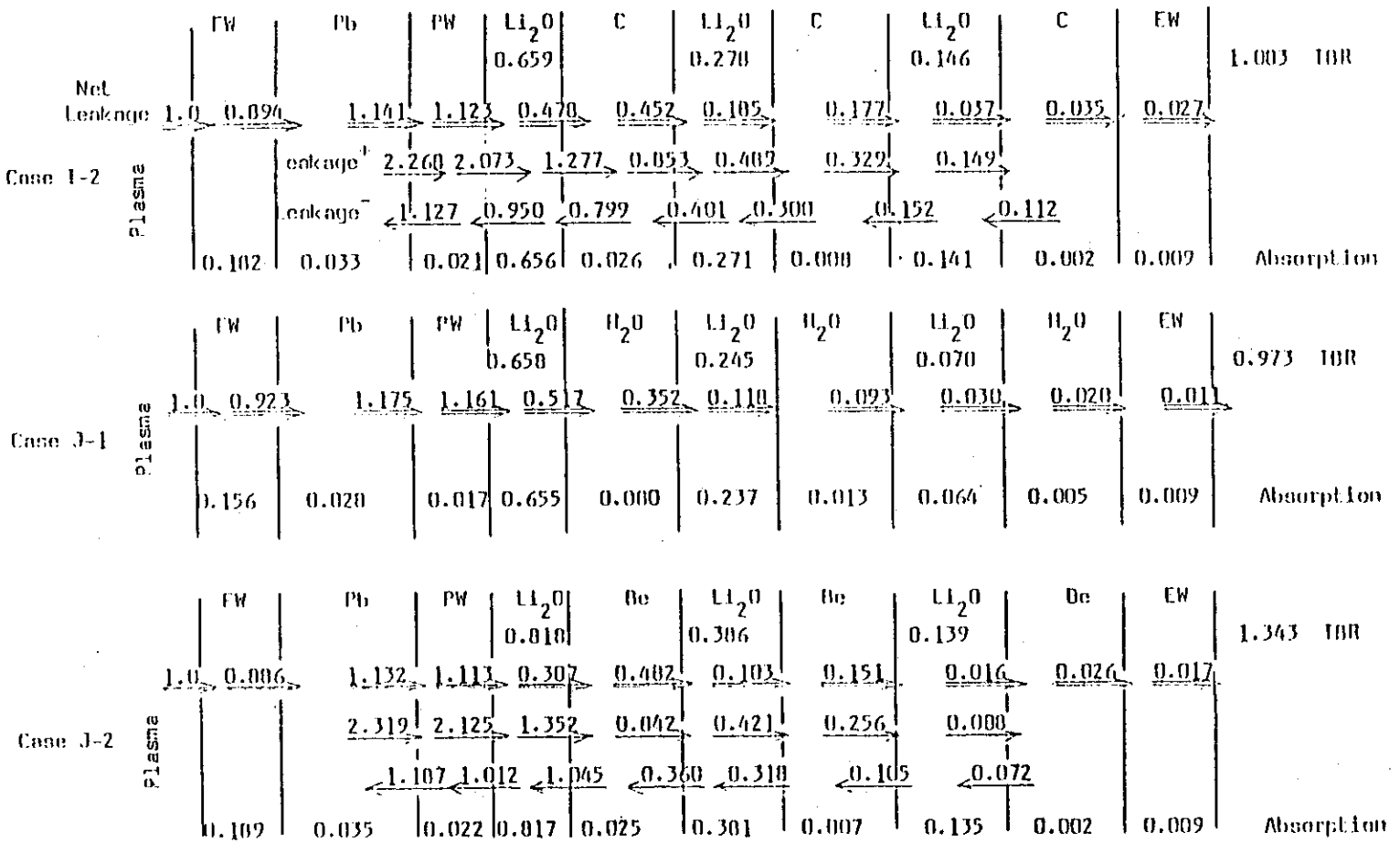

Fig.VIII-4-49 Number of Neutrons Crossing the Zone Boundaries
(Effect of Moderator Selection, 30% ^6Li, H_2O Coolant)

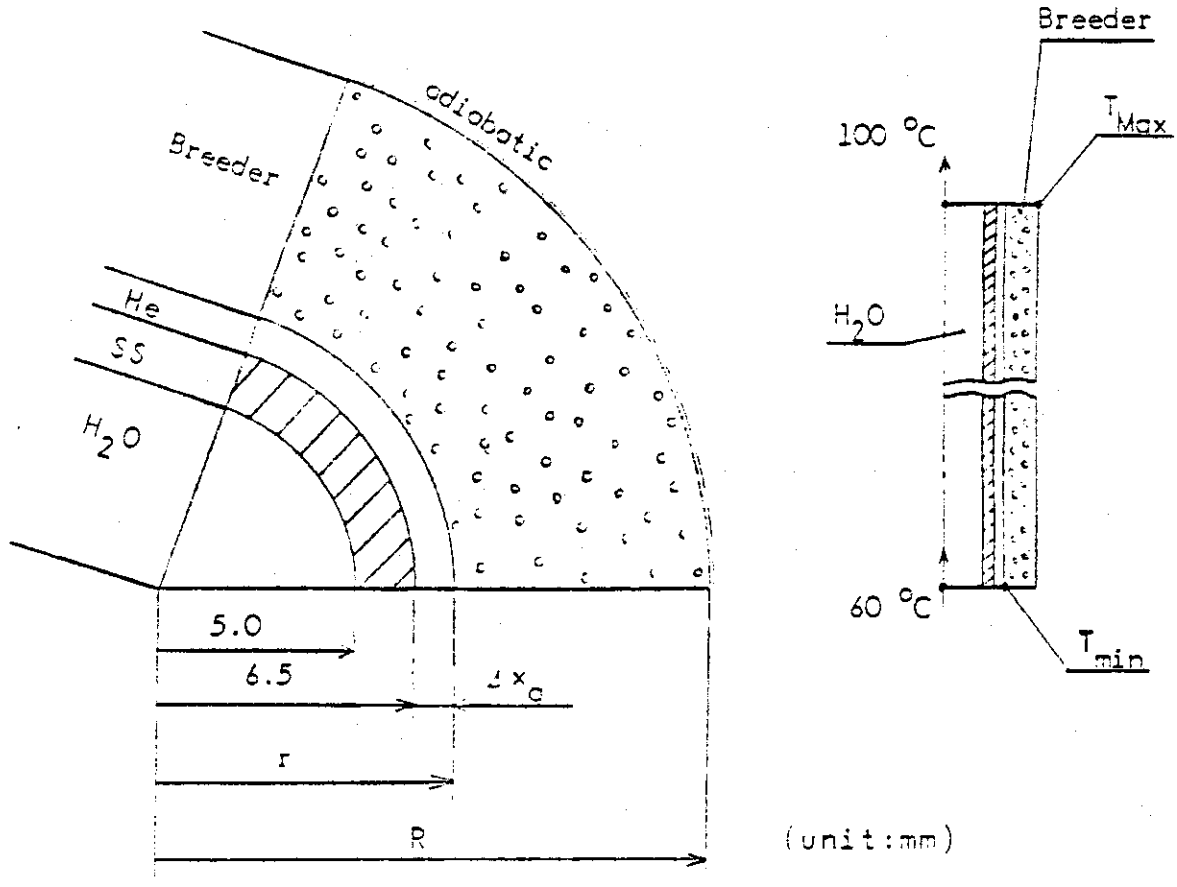

Δx_g : gap width

r : inner radius of breeder

R : equivalent outer radius of breeder

Fig. VIII-4-50 Analytical Model

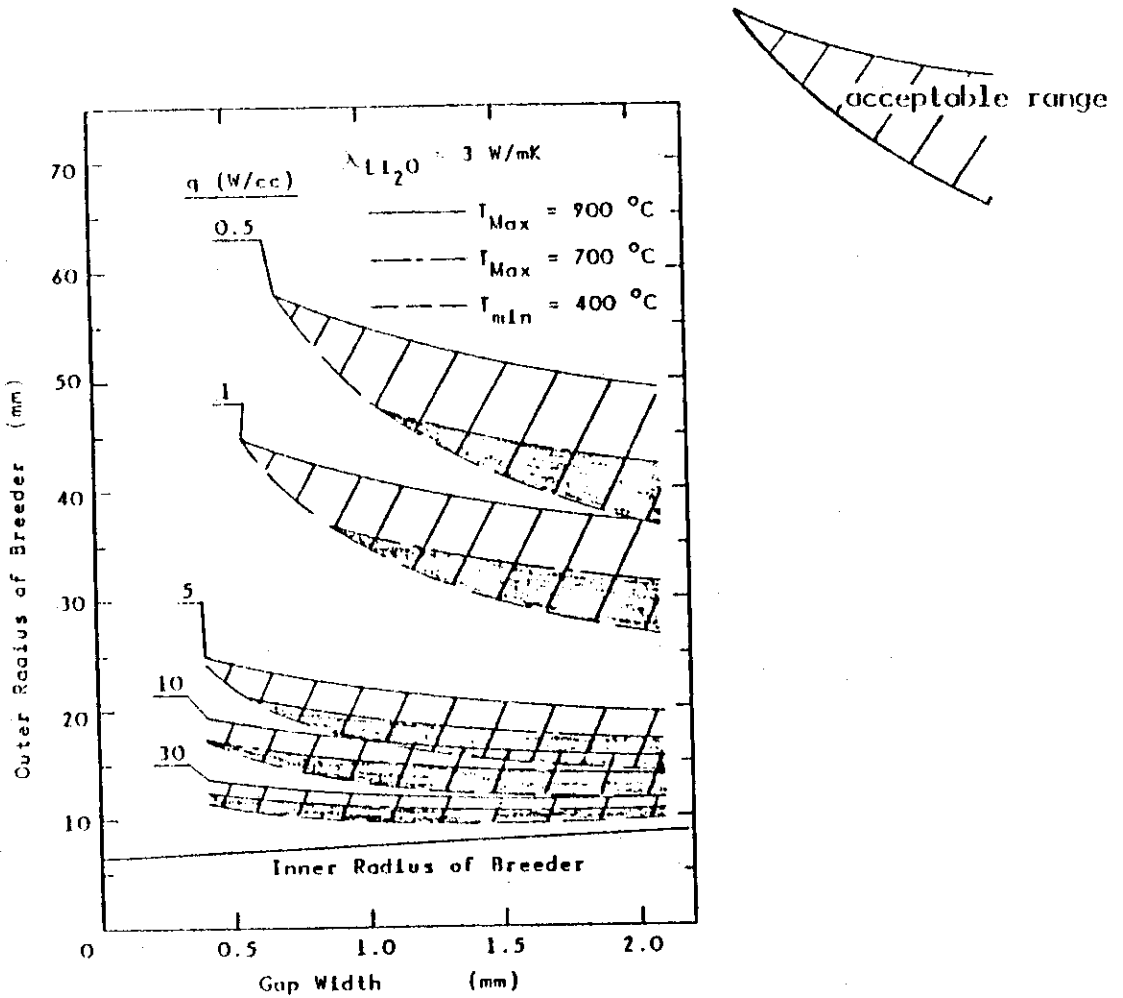

Fig. VIII-4-51 Acceptable Design Range of Blanket (1)

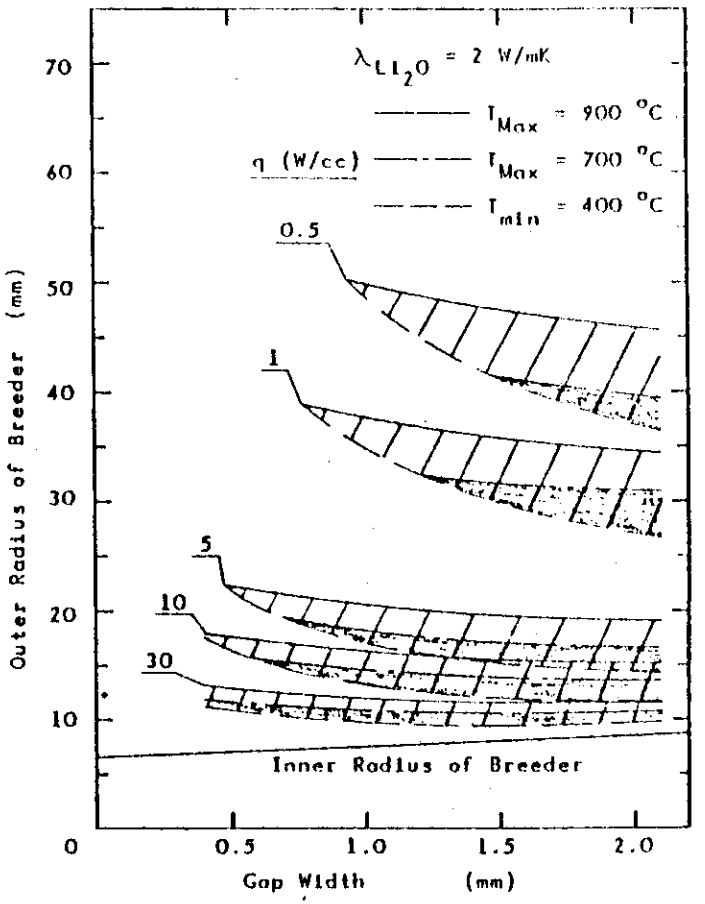

Fig. VIII-4-52 Acceptable Design Range of Blanket (2)

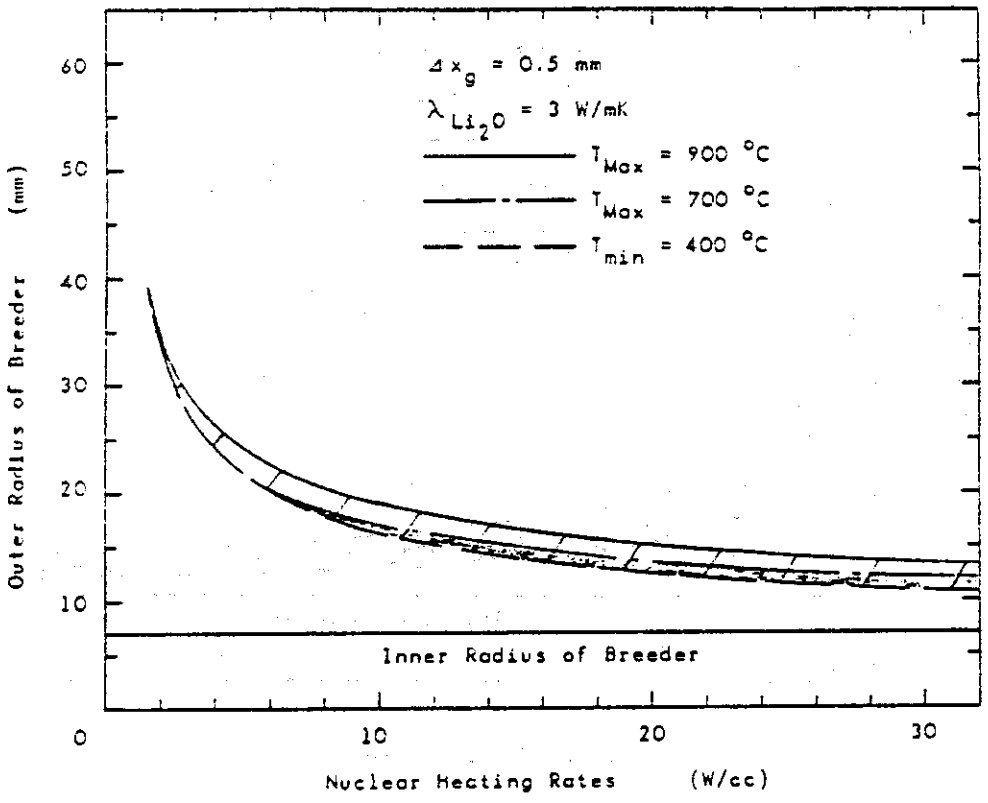

Fig. VIII-4-53 Acceptable Design Range of Blanket (3)

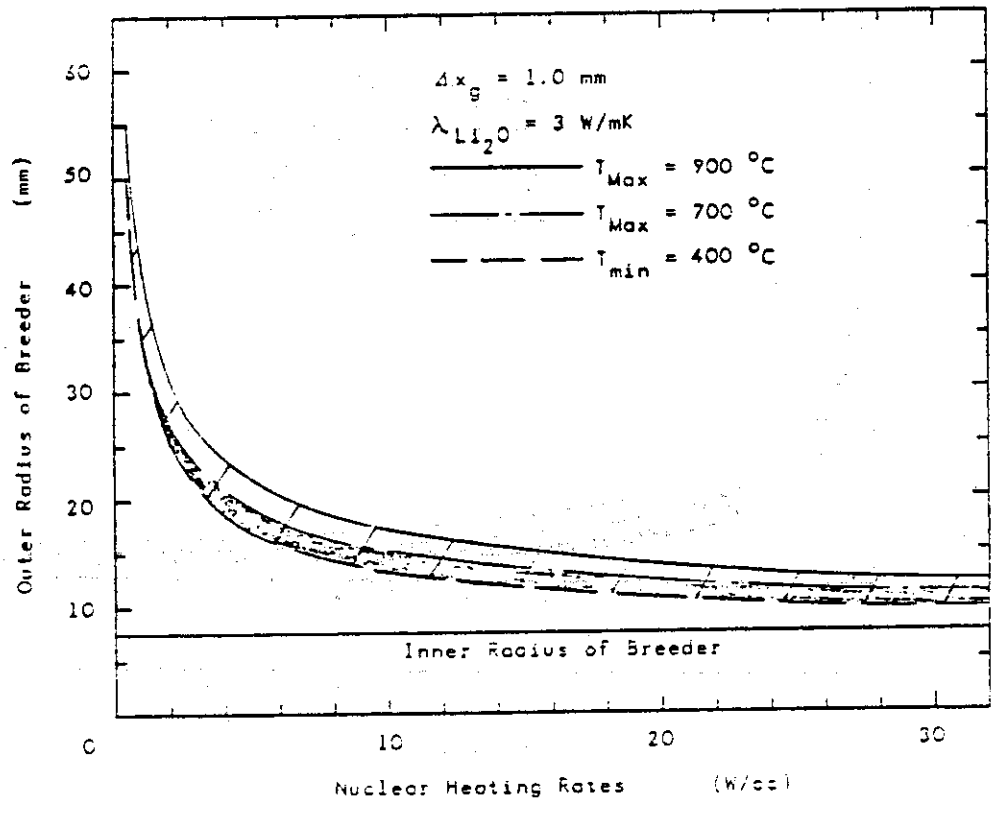

Fig. VIII-4-54 Acceptable Design Range of Blanket (4)

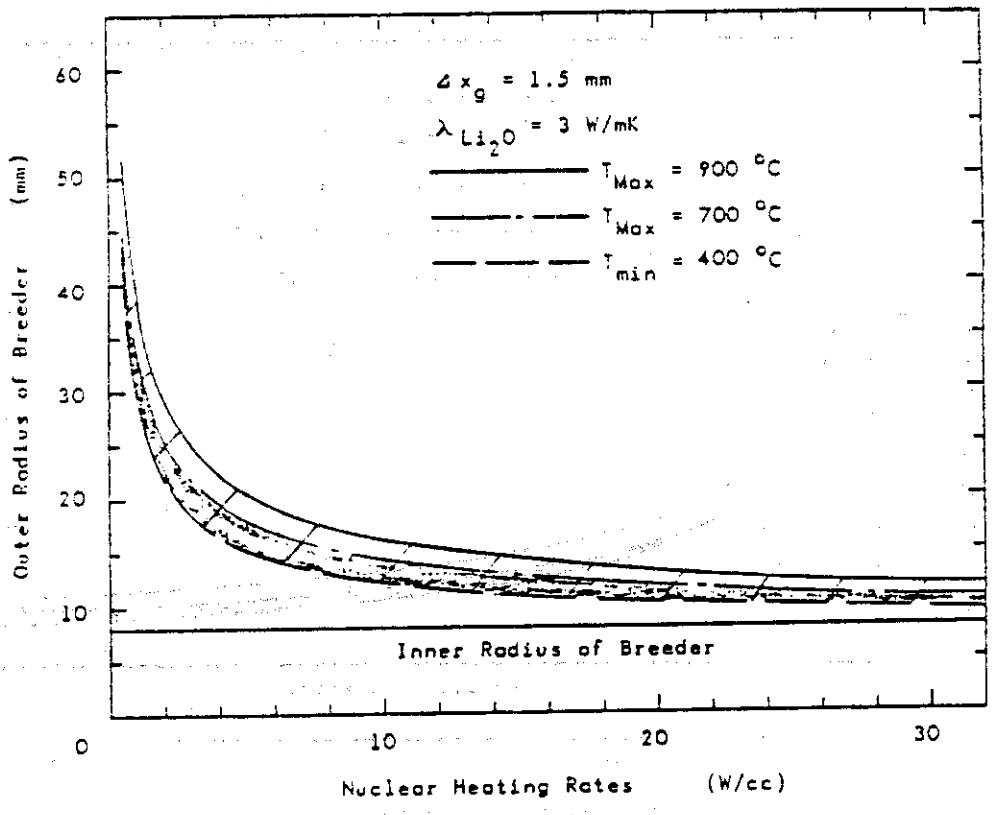

Fig. VIII-4-55 Acceptable Design Range of Blanket (5)

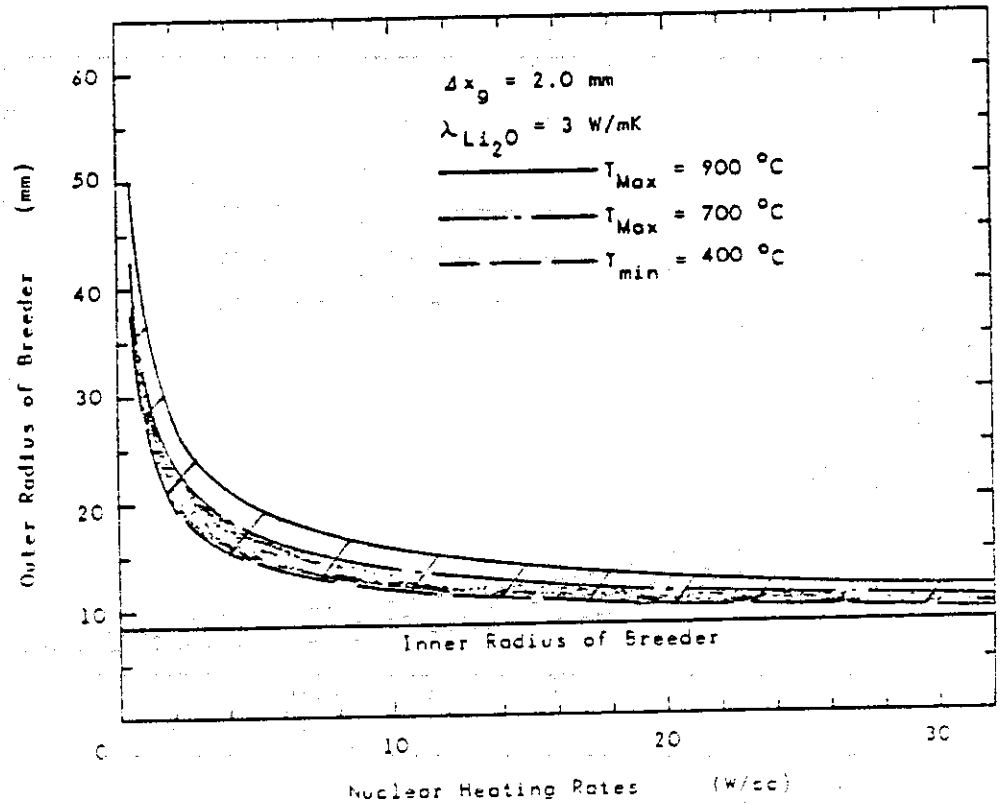

Fig. VIII-4-56 Acceptable Design Range of Blanket (6)

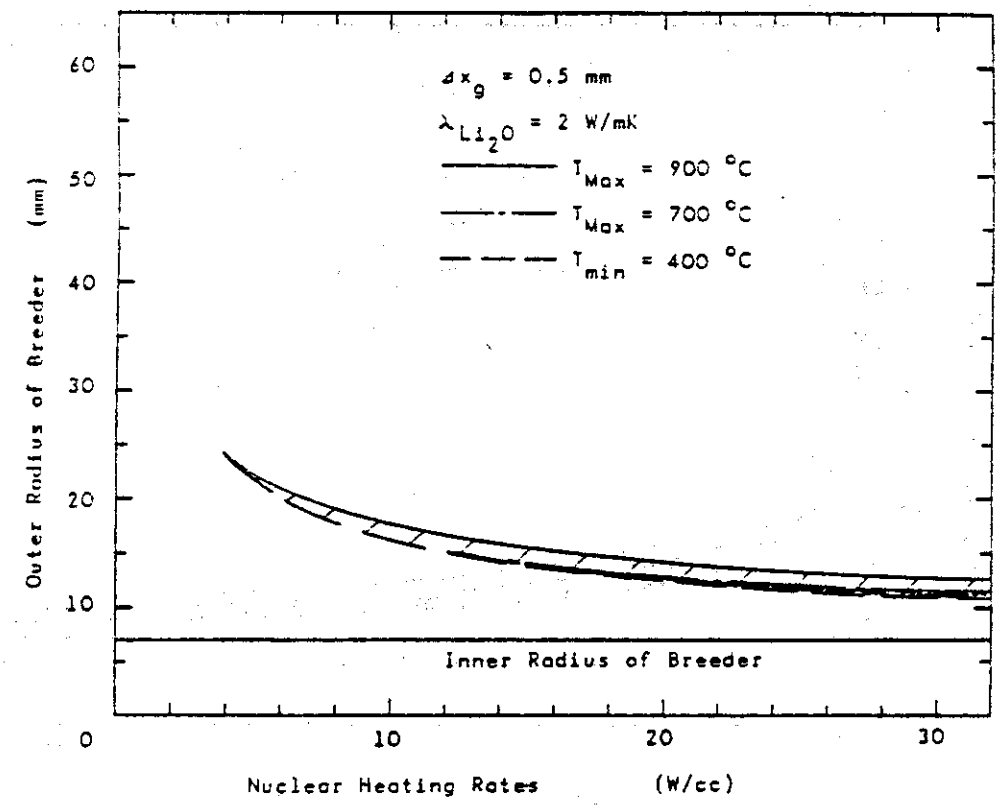

Fig. VIII-4-57 Acceptable Design Range of Blanket (7)

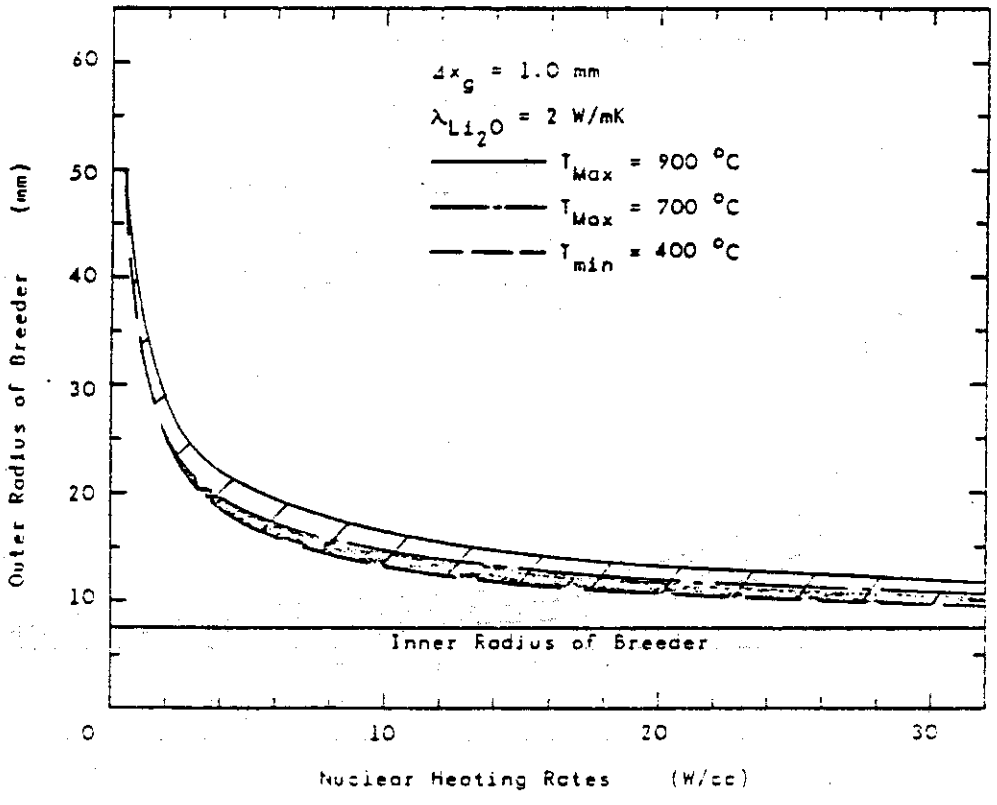

Fig. VIII-4-58 Acceptable Design Range of Blanket (8)

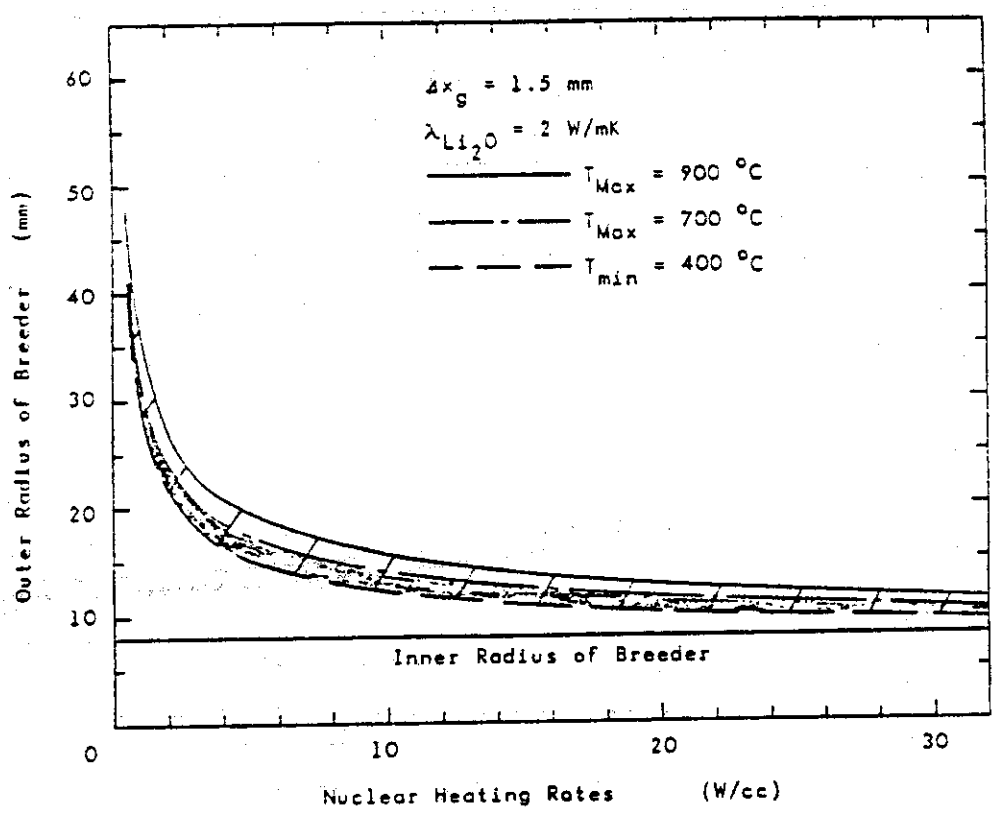

Fig. VIII-4-59 Acceptable Design Range of Blanket (9)

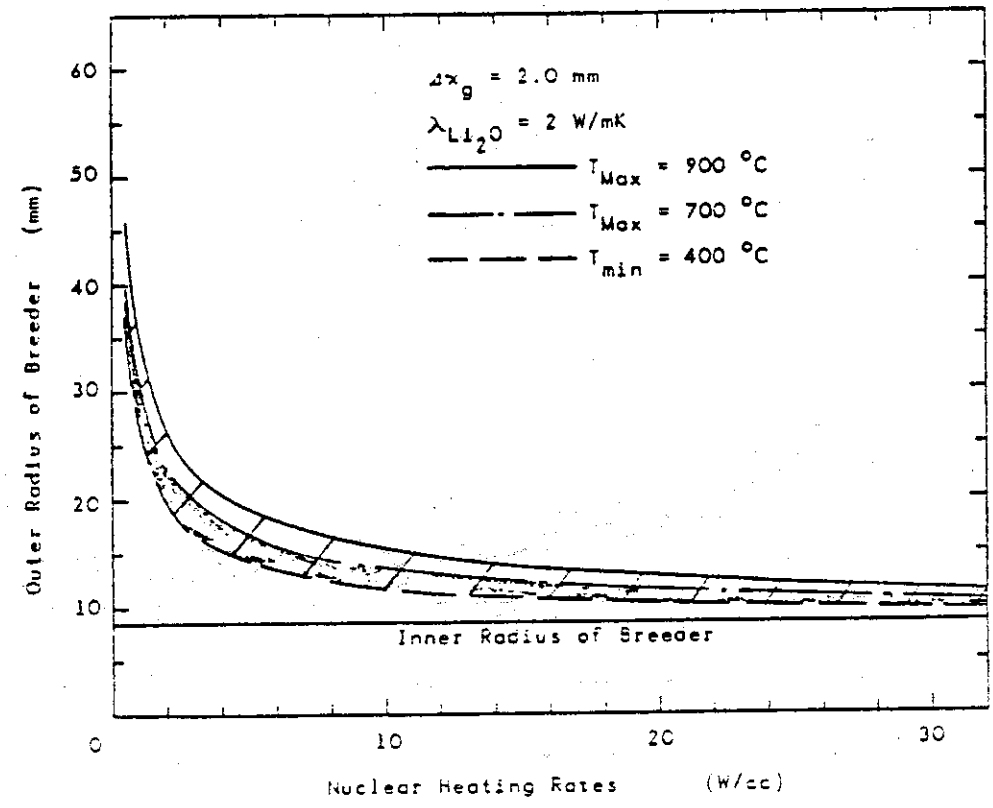

Fig. VIII-4-60 Acceptable Design Range of Blanket (10)

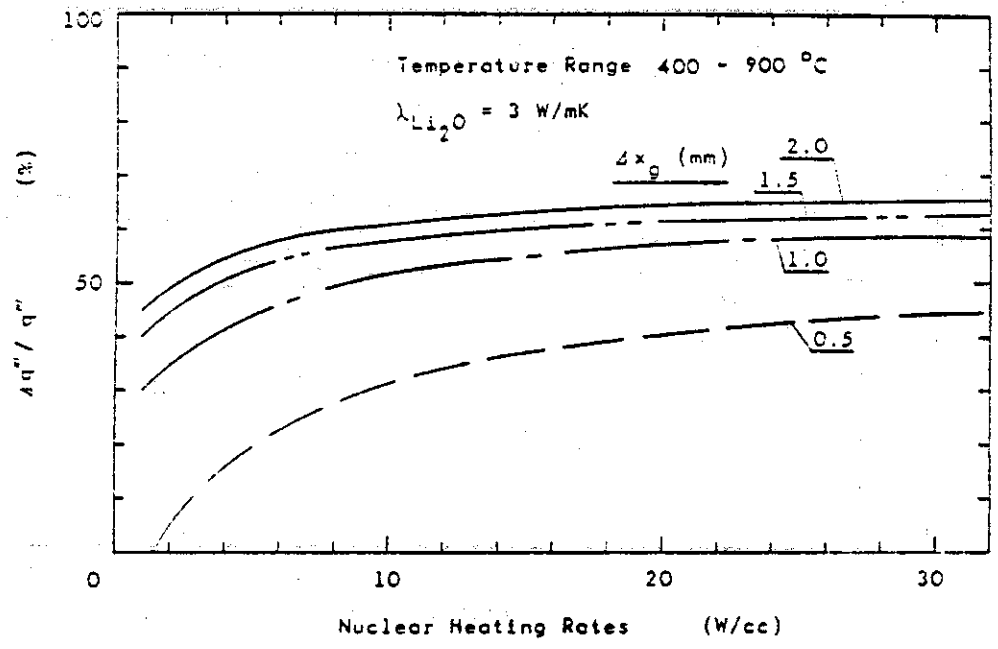

Fig. VIII-4-61 Margin for Nuclear Heating Rates in Breeder Region (1)

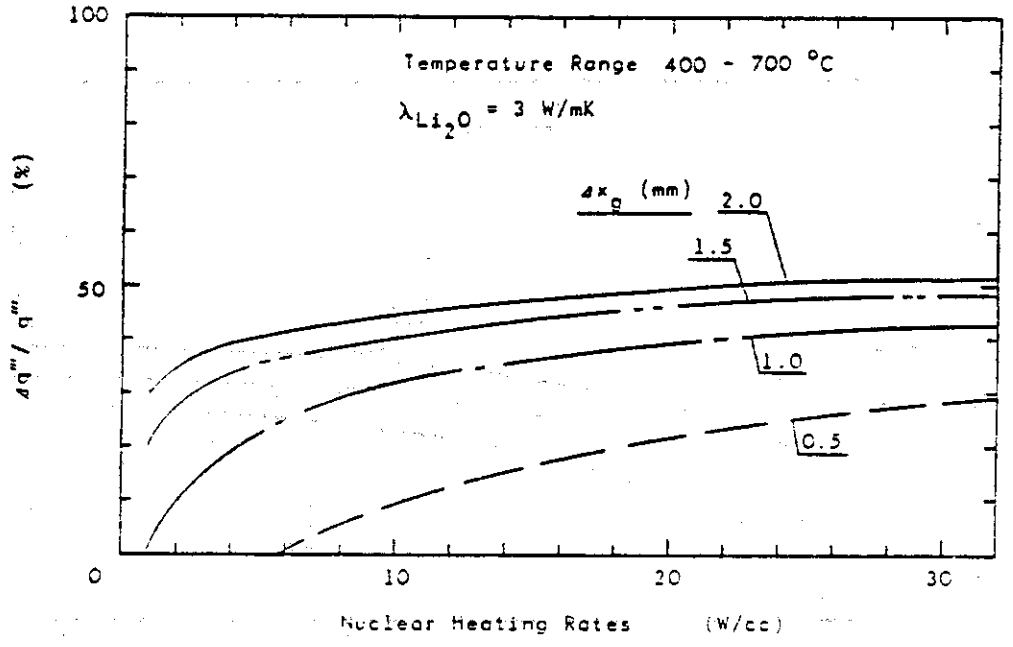

Fig. VIII-4-62 Margin for Nuclear Heating Rates in Breeder Region (2)

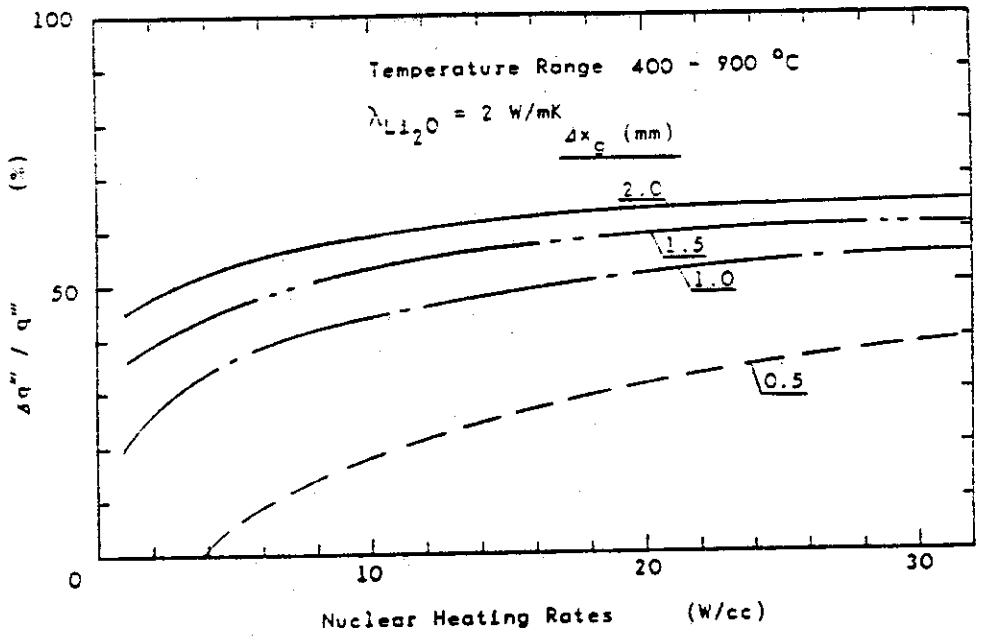

Fig. VIII-4-63 Margin for Nuclear Heating Rates in Breeder Region (3)

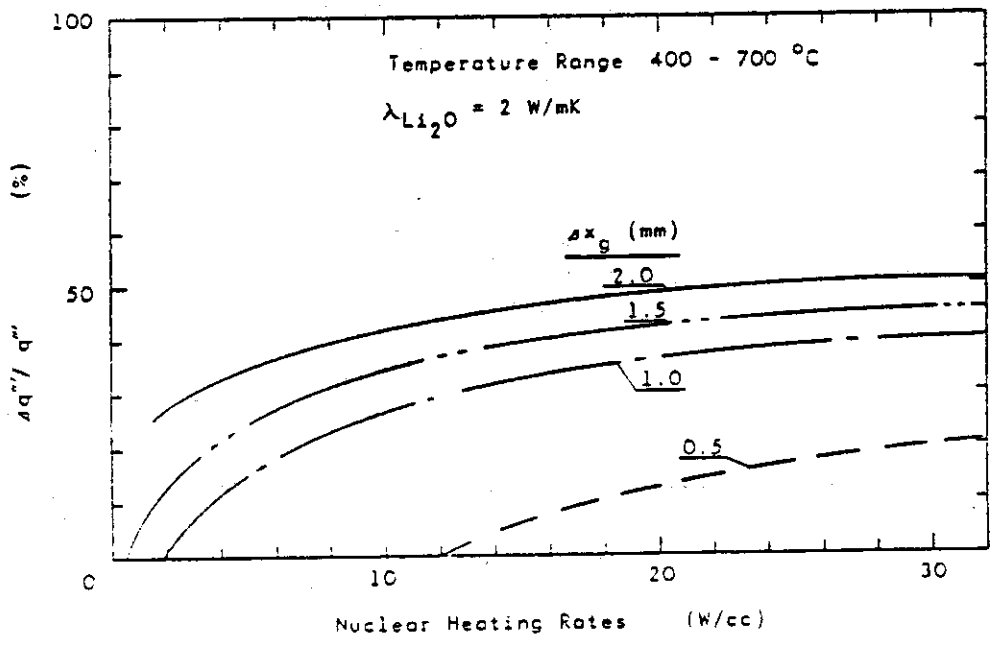

Fig. VIII-4-64 Margin for Nuclear Heating Rates in Breeder Region (4)

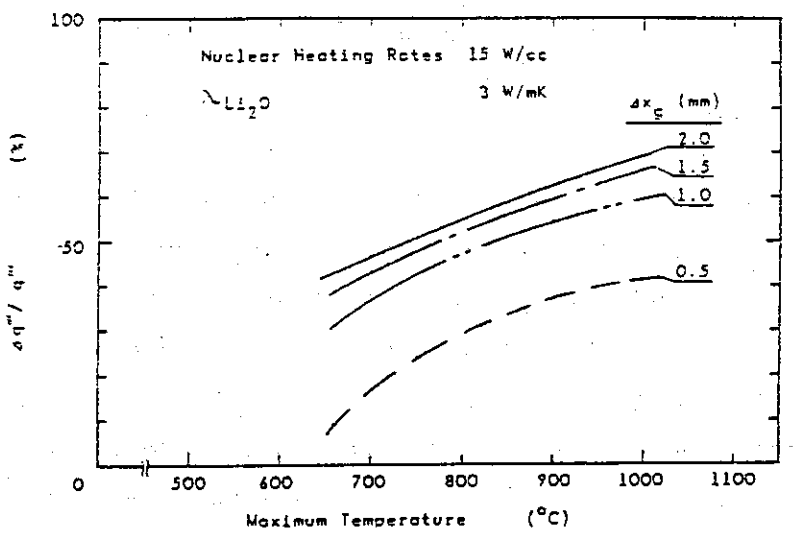

Fig. VIII-4-65 Margin for Nuclear Heating Rates in Breeder Region (5)

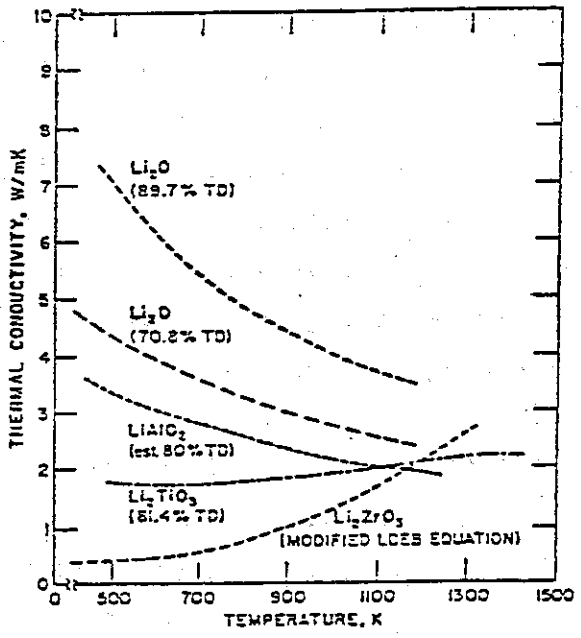

Fig. VIII-4-66 Thermal Conductivities of Li_2O and Other Candidate Solid Breeders[9]

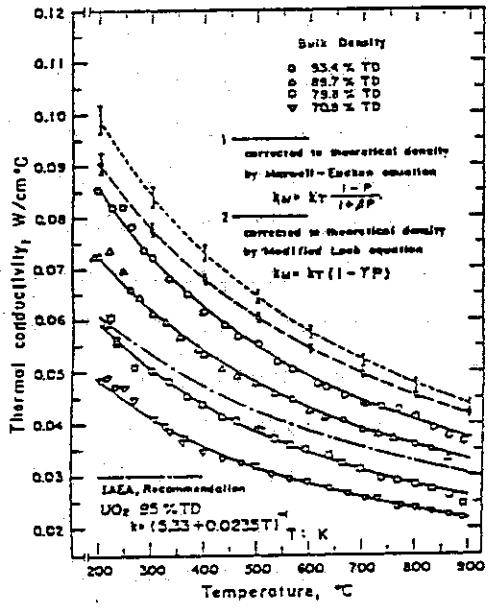

Fig. VIII-4-67 Temperature Dependency of Li_2O Thermal Conductivity[47]

4.1.5 Sensitivity to Power Variation

(a) Revision of the Tritium Breeding Blanket Design

(1) Objective

The design of the tritium breeding blanket which uses lithium Oxide (Li_2O) as the breeder was revised. The objective of the task is to investigate the conditions that permit the continuous in-situ recovery of tritium generated in the breeder, i.e., to clarify the range of power density variation which makes it possible to control the breeder temperature in the specified range, and to develop the blanket concept which is less sensitive to the power density variation anticipated in INTOR operation (including uncertainties of the predicted power density due to uncertainties of material properties and neutronics calculation).

(2) Permissible Range of Power Density Variation (PRPD)

Permissible Range of Power Density variation (PRPD) depends on the Nominal Values of the Design Parameters (NVDP), Limits of Temperature Range during reactor Operation (LTRO), fabrication errors, uncertainties of material properties, and concepts of temperature control (whether or not to adopt active control concept).

In the present design, the breeder temperature is controlled by properly arranging coolant tubes according to the predicted nuclear heating rate, and by providing the thermal resistance layers (gas gap) around the tubes.

To fix the NVDP close to the LTRO makes the PRPD narrow. On the contrary, to select the NVDP with a margin is the cause of the increase of structural complexity and deterioration of tritium breeding performance though it is possible to make the PRPD wider. Therefore, the NVDP should be determined considering the various uncertainties (fabrication errors, material property uncertainties, etc.) as well as the power density variation anticipated in INTOR operation.

The Permissible Range of Power Density variation (PRPD) in which temperature control is possible is divided into the following two categories:

① the PRPD which can be covered by selecting the NVDP, i.e., which is permitted without alteration of temperature control concept : $\Delta_{passive}$

② the PRPD which is permitted by alteration of temperature control concept, i.e., which is permitted by some method of active control : Δ_{active}

a) PRPD without Active Control (Δp)

It is needless to say that it is desirable to operate the blanket within the range of Δp.

Fig. VIII-4-68 shows the relation between the NVDP and the PRPD (Δp) when the predicted nuclear heating rate is normalized to unity. Permissible reduction rate of power density is determined by the lower limit of the LTRO, and permissible increase rate of power density is determined by the upper limit of the LTRO. As is evident from the figure, it is impossible to permit blanket operation within a factor of 2 or more variation of power density without taking some method of active control when the LTRO for Li_2O is 400°C ∿ 1,000°C.

As an example of practical design, if the range of 450°C ∿ 700°C or 450°C ∿ 800°C is selected as the NVDP for Li_2O, the PRPD (Δp) is 85% ∿ 130% of the predicted (nominal) power density or 85% ∿ 130% of it, respectively.

b) PRPD with Active Control (Δ_a)

For the blanket operation beyond the above-mentioned range of power density (Δp), some method of active control is required. One possible way to permit blanket operation in this

range without changing blanket structure (e.g. re-arrange of coolant tubes) is to regulate the thermal resistance of gas gap around the coolant tubes. There are some methods to regulate the thermal resistance of the gap: ① changing thermal properties of gas filled in the gap (replacing or mixing with the other gas), ② changing the mode of heat transfer of the gas (i.e. heat conduction in stagnant gas, heat convection by flow gas and free-molecule thermal conductivity in low pressure gas), ③ combinating ① and ②.

Fig. VIII-4-69 shows the PRPD when thermal resistance of the gap is ideally regulated. The following measures were considered for the blanket operation beyond the Δp:

i) To increase thermal resistance of the gap by varying the condition of helium in the gap, i.e., obstructing the flow of helium, which is the nominal condition of the gap in this case, and making the stagnant condition. In this case, if the NVDP is 450°C ∿ 700°C, the Δa would be 32% ∿ 75% of the nominal power density.

ii) To mix helium and another inert gas (e.g. argon, Ar) in proper ratio and pass it through the gap. In this case, it is possible to vary the thermal resistance of the gap continuously, as shown in Fig. VIII-4-70. Activation of argon and influence on the tritium recovery system, however, should be examined.

iii) To regulate the thermal conductivity of helium by reducing its pressure. Because the pressure must be reduced into the level of 10^{-2} torr, it would not be compatible with the concept of continuous tritium recovery.

(3) Sensitivity Analysis for Breeder Temperature

Sensitivity analysis was carried out on the effect of the packing structure and characteristic of Li_2O pebbles in the blanket vessel to the temperature distribution in the breeder. Temperature of breeder (Li_2O) is controlled by the coolant tube arrangement and the thermal resistance layers around the tubes. An example for the sensitivities of the maximum breeder temperature is shown below.

Sensitivity to Heating Rate	+4°C/%[a]
Sensitivity to Tube Arrangement	+40°C/mm[b]
Sensitivity to Effective Thermal Conductivity	
to Packing Fraction of Li_2O Pebbles	+8°C/%[c]
to Thermal Conductivity of Li_2O	+2°C/%[d]

Notes: These values are for the foremost part of the blanket.
a. Heating rate increase by 1% (i.e. 100 → 101%)
b. Pitch of tube increase by 1 mm (i.e. 25 → 26 mm)
c. Packing fraction decrease by 1% (i.e. 70 → 69%)
d. Thermal conductivity decrease by 1% (i.e. 100 → 99%)

(4) Revision of the Blanket Design

Being based on a principle of simple blanket structure, the present design is revised in order to permit the blanket operation in wider range of power density variation. The blanket structure is BOT/NM type and the heat generated in the blanket is removed by the coolant flowing in the properly arranged tubes. The breeder which consists of small pebbles of natural isotopic Li_2O is packed in the blanket vessel. A diameter of 1 mm was chosen for the pebbles in order to reduce the wall effect of the coolant tubes.

a) Reference Design

From the structural consideration that the PRPD should be as wide as possible and that the coolant tubes should be practicably arranged, the temperature range of 450°C ∿ 700°C was chosen for the NVDP for Li_2O.

Standard condition of the thermal gap layers is stagnant helium gas of 1 ata. from the viewpoint of structural simplicity, and heat transfer mode is heat conduction. The arrangement of coolant tubes is illustrated in Fig.VIII-4-72 for the case that the maximum temperature of the NVDP (T^N_{max}) is 700°C. Wall effect and thermal radiation effect of Li_2O pebbles are taken into consideration. The effective thermal conductivity of the breeder zone (Li_2O) is shown in Fig. VIII-4-71. The PRPD (Δp) for this NVDP is 86% ∿ 150% of the predicted power density.

Table VIII-4-15 summarizes the major specifications of the revised reference blanket. When taking the fabrication error of coolant tube pitch (1 mm), the packing error of Li_2O pebbles (5%), and the error of thermal conductivity for Li_2O (10%) into account, the maximum temperature of Li_2O (T^S_{max}) is 800°C and the PRPD (Δp) is the range of 86% ∿ 130%.

b) Methods to Expand PRPD

When the blanket operation beyond the Δp is required, it seems that the following measures should be considered in the blanket design.

i) In order to lower the temperature of breeder zone, beryllium (or zirconium) pebbles are homogeneously mixed with Li_2O pebbles (the volume ratio 1 : 1) and are packed in the blanket. In this case, if the tube arrangement is the same as the reference design, temperature of NVDP (T^N_{max}) becomes 620°C (or 650°C) from 700°C of the reference

design, and the PRPD (Δp) is improved to 86% ∿ 173% (or 86% ∿ 164%).

ii) In order to permit the blanket operation below the Δp, the thermal resistance of the gap is increased by obstructing the flow of helium, which is the standard condition of the gap in this case, and making the stagnant condition.

(5) Conclusions

Preliminary estimation of the margin for the power density variation was carried out on the tritium breeding blanket which used the Li_2O pebbles as a breeder, and the design was revised in order to permit the blanket operation in the wider range of power density. The results are summarized as follows:

i) When the Limits of Temperature Range during Reactor Operation (LTRO) for Li_2O was assumed to be 400°C ∿ 1,000°C, if the range 450°C ∿ 700°C was chosen for the Nominal Values of Design Parameters (NVDP) for Li_2O, it is possible to operate the blanket with the Permissible Range of Power Density variation (PRPD) of 86% ∿ 150%, without additional temperature control (i.e. active control).

ii) When the fabrication error of coolant tube pitch, the packing error of Li_2O pebbles, and the error of thermal conductivity for Li_2O were assumed to be 1 mm, 5%, and 10%, respectively, the maximum temperature of Li_2O rised by ∿100°C and the PRPD was 86% ∿ 130%.

iii) One method to lower the breeder temperature is a homogeneous mixture of Li_2O pebbles and beryllium (or zirconium) which is considered excellent in thermal and neutronic properties. If Li_2O and beryllium (or zirconium) were mixed in the ratio of 1:1 (volume), the maximum temperature of Li_2O was reduced by 80°C (or 50°C), and the PRPD was expanded to 86 ∿ 173% (or 86 ∿ 164%).

iv) For the blanket operation beyond the PRPD (Δp, 86 ∿ 150%) active control of temperature was required. The method to regulate the thermal resistance of gap layer was considered to be practicable.

From the viewpoint of minimizing the influence on the other systems, it seems reasonable to regulate the condition of helium in the gap (flow or stagnant). It permits the blanket operation in the range of 64 ∿ 126% for the NVDP of 450 ∿ 700°C.

v) Although the method to pass a mixture gas of He/Ar in a proper mixing ratio through the gap has the advantage that the thermal resistance can be regulated continuously, influence on the other systems must be examined.

In order to design more realistic reference blanket, further examination should be required on the following items:

i) definition of the range of power density variation anticipated in tritium breeding blanket operation.

ii) examination for fabrication errors, uncertainties of material properties and predicted power density by R&D.

iii) improvement of structural design for active control method, if necessary.

iv) improvement of effective thermal conductivity of breeder zone (e.g. mixing beryllium pebbles).

Table VIII-4-15 Major Specifications of Revised Tritium Breeding Blanket

Blanket Type		Breeder Out of Tube/ Non Moderator	
Breeder		Li_2O Pebbles (85% Theoretical Density)	
		Diameter	1 mm
		Packing Fraction	70 %
Tempearture Limits of Li_2O (LTRO[a])		Lower Limit	400°C
		Upper Limit	1000°C
Tempearture Control		Coolant Tube Arrangement according to Power Density/ Thermal Gap around the Tubes (stagnant He Gas)	
		100% Li_2O	50% Li_2O + 50% Be
Operation Temperature of Li_2O			
Nominal Temperature			
(NVDP[b], Tn)	min.	450°C	450°C
	max.	700°C	620°C
Systematic Temperature[c] (Ts)			
	max.	800°C	-----
Permissible Range of Power Density Variation ($\triangle$passive[d], PRPD)			
based on NVDP		86% ~ 150% of the standard power density	86% ~ 173%
based on Ts		86% ~ 129%	-----
Permissible Range of Power Density Variation ($\triangle$active[e], PRPD)			
Change of Thermal Resistance of Gap Layer			
He Sweep ⟶ stagnant He		64% ~ 126%	-----
Tritium Breeding Ratio (local) (Coolant for First wall : D_2O)		~1.0 (natural lithium)	~1.4 (30% ^6Li)

Table VIII-4-15 (cont'd)

Coolant Tube	10 mm O.D. Arrangement (see Fig. 3.5)
Coolant	Pressurized Water (1MPa)
Inlet Temperature	50°C
Outlet Temperature	90°C
Pressure Loss	0.3 MPa
Max. Velocity	4.5 m/sec
Tritium Purge Gas	Helium
Flow Rate	200 Nm^3/hr
Pressure Loss	0.015 MPa

Note : a. Limits of Temperature Range during Reactor Operation.
b. Nominal Values of the Design Parameters.
c. The following errors were considered in estimating the temperature : pitch of tube 1 mm, packing fraction of Li_2O 5 %, and thermal conductivity of Li_2O 10 %.
d. PRPD for passive control.
e. PRPD for active control.

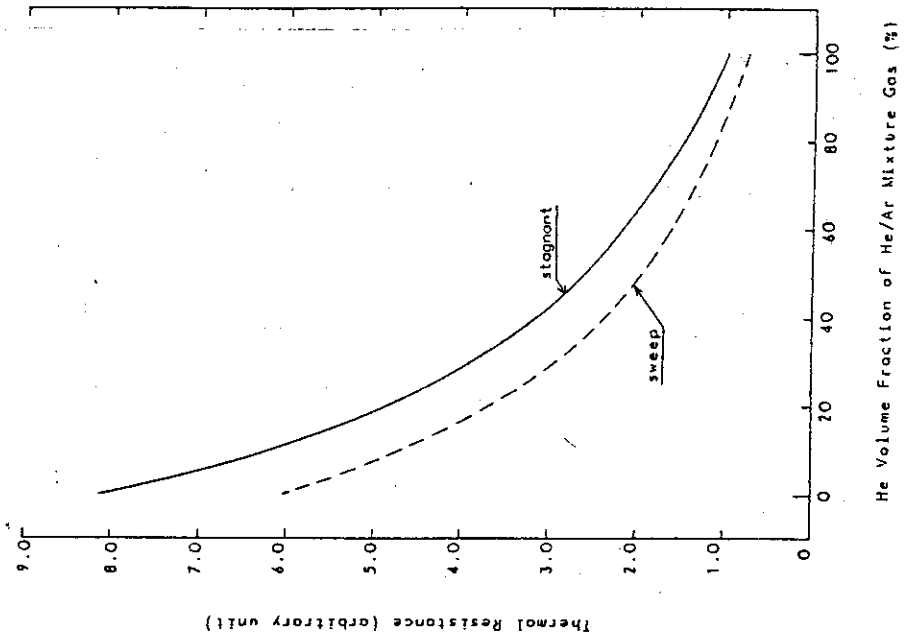

Fig. VIII-4-69 Thermal Resistance in Gas Layer

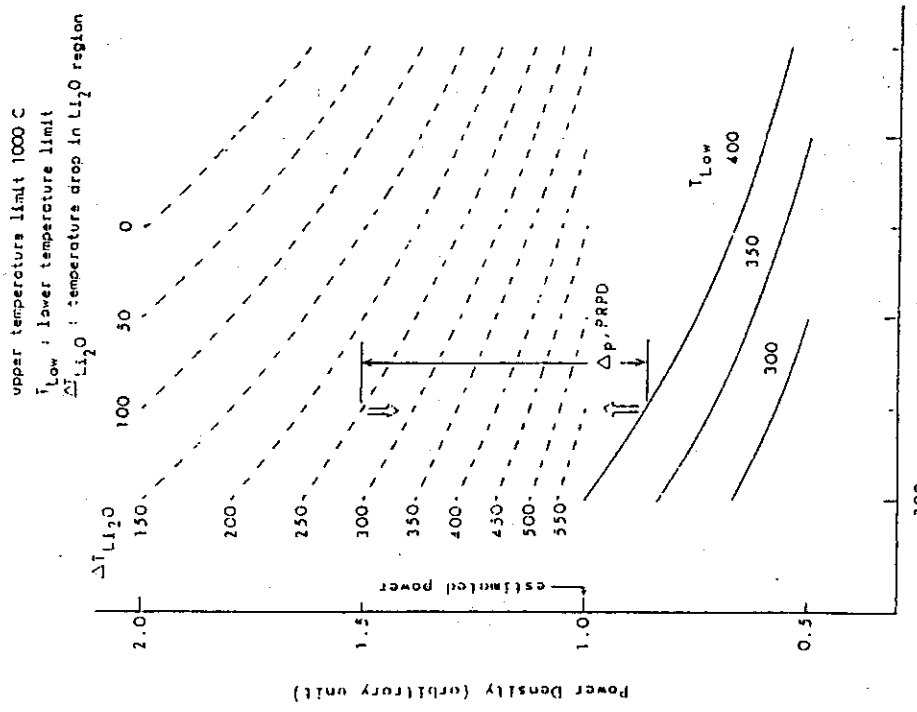

Fig. VIII-4-68 Permissible Range of Power Density Variation (PRPD) without Active Control

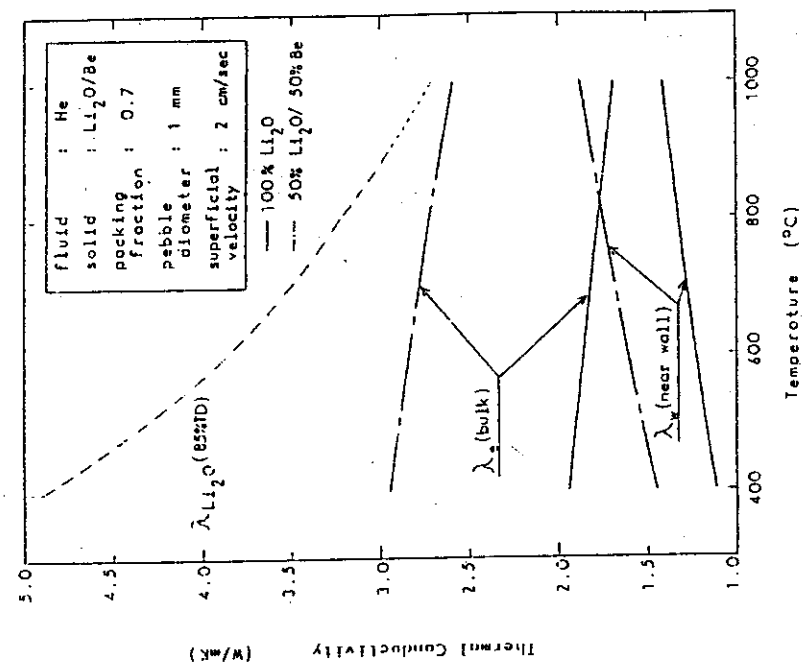

Fig. VIII-4-71 Effective Thermal Conductivity of Packed Column

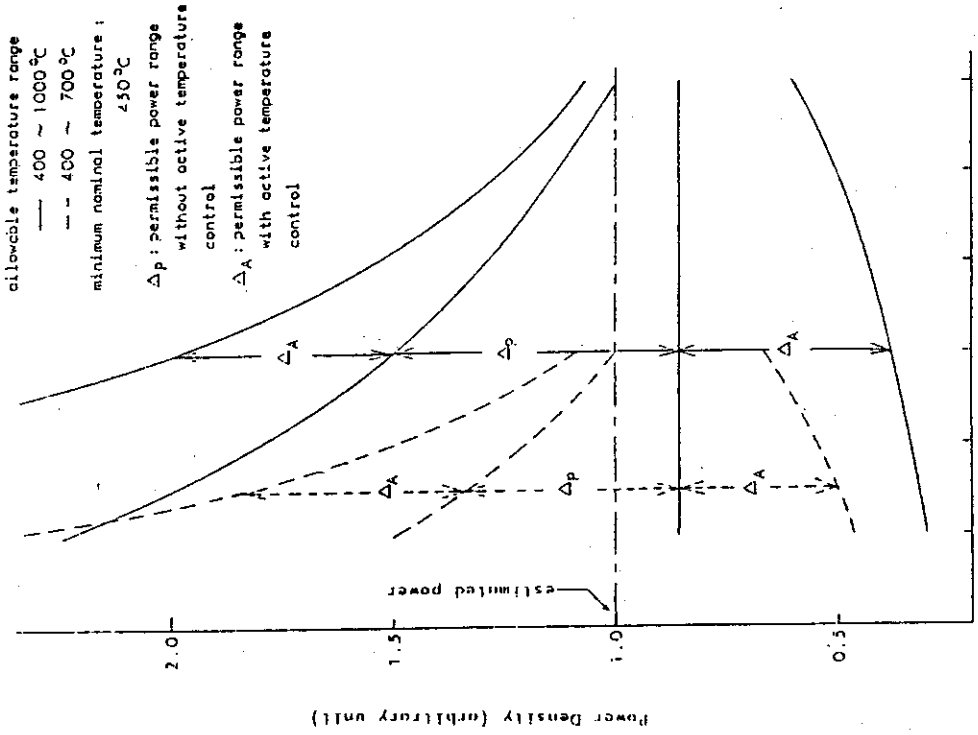

Fig. VIII-4-70 Ideal Permissible Range of Power Density Variation (FRPD)

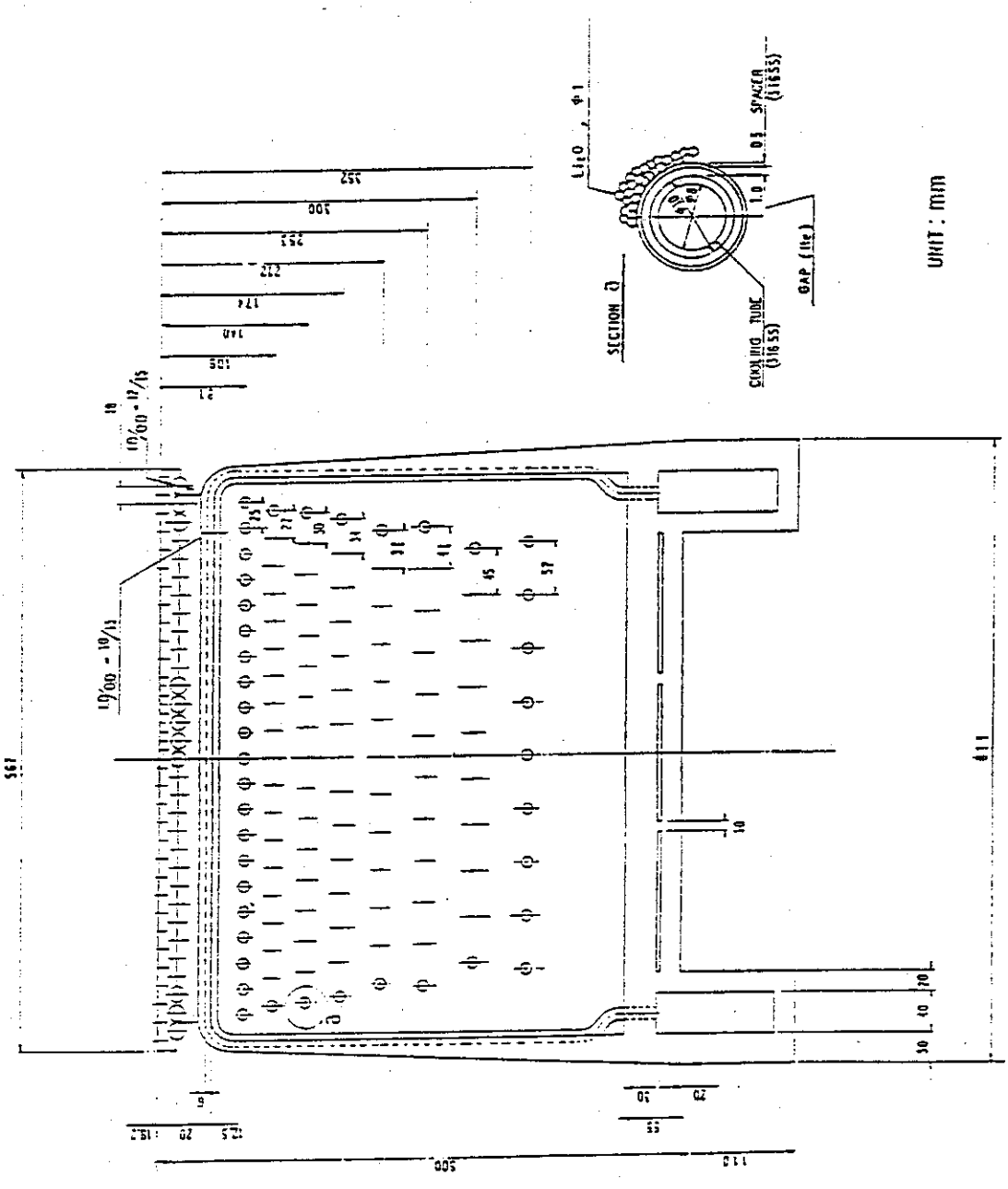

Fig. VIII-4-72 Cross-section of Tritium Producing Blanket (T_{min}/T_{max} = 450/700 °C)

4 1.6 Hydrogen Influence on Weldability

(a) Considerations of Hydrogen Influence on Weldability

In the first wall of nuclear fusion reactor, tritium is absorbed to the austenitic stainless steel such as type 316 S.S. which is one of the candidate structural materials. This tritium absorbed will be around five ppm in weight at most.

General characteristics of hydrogen embrittlement of austenitic stainless steel is described below. From the characteristics, ductility, one of the key factors in weldability, is not appreciably affected by the hydrogen amount around five ppm in weight as shown in Fig.VIII-4-73. And it is certain that δ ferrite in the weld metal of austenitic stainless steel decreases the ductility, as shown in Figs.VIII-4-75 and VIII-4-76. However, hydrogen amount absorbed in these figures is not clear. Therefore, it is necessary to make clear the effect of δ ferrite on the ductility under hydrogen amount around five ppm in weight. Further, it should be corroborated whether tritium has other serious effects on the austenitic stainless steel or not. From above-mentioned considerations, proper welding process must be selected in the repair work of first wall.

(1) General Considerations

It might be safely said that austenitic material such as austenitic stainless steel is far more insensitive to the hydrogen embrittlement than ferritic material for the reasons as follows[48].

① Hydrogen diffusion constant of austenitic material with F.C.C latice structure is remarkably smaller in itself than that of ferritic material with B.C.C. latice structure.

② Hydrogen solubility of austenitic material is several times as large as that of ferritic material. Therefore, the effect of diffusive hydrogen of small amount is not appreciable in the austenitic material.

In the first wall for nuclear fusion reactor, there will be the tritium absorption of rather large amount . In such a case, technological attention must be paid from the following points of view even if austenitic stainless steel is employed as the structural material.

① Hydrogen-induced α' martensite (B.C.C.) will be easily formed under these conditions. As a result, the material becomes sensitive to hydrogen embrittlement.

② α' martensite (B.C.C.) is said to be formed in the cold-worked austenitic stainless steel such as type 304 S.S. of metastable austenite. These phenomena also occur in the type 316 S.S. which is subjected to cold working during fabrication[49].

③ Conventional weld metal of austenitic stainless steel includes δ ferrite up to 10% approximately to prevent hot cracking during welding. This δ ferrite is sensitive to hydrogen embrittlement.

(2) Hydrogen Embrittlement of Austenitic Stainless Steel

As mentioned above, it is suspected that hydrogen embrittlement of the austenitic stainless steel will occur under such circumstances as fusion experimental reactor. Therefore, these phenomena were herein reviewed in the applications of other fields.

a) Effect of Hydrogen-induced Martensite on Embrittlement

Fig.VIII-4-73 shows the effect of hydrogen amount absorbed on the total elongation of type 304 S.S. in tensile test. This figure shows that there is remarkable embrittlement due to hydrogen absorption[50]. Fig.VIII-4-74 also shows the effect of Nieq* on embrittlement ratio for various stainless steel. From this

---

* Nieq. is given as follows;

$$Nieq. = Ni(\%) + 0.65Cr(\%) + 0.98Mo(\%) + 1.05Mn(\%) + 0.35Si(\%) + 12.6C(\%)$$

figure, notched material and sensitized one tend to show high sensitivity to hydrogen embrittlement [48]. This embrittlement is caused by hydrogen-induced α' martensite in the matrix and tensile properties result in low ductility, low tensile strength and high yield strength[50].

b) Effect of Strain-induced Martensite on Embrittlement

It is certain that strain-induced martensite increases hydrogen embrittlement[51,52]. However, it is doubtful whether this α' martensite plays a major role for embrittlement[53]. Because the austenitic matrix is also embrittled as shown above. Tables VIII-4-16 and VIII-4-17 show the effect of plastic deformation on fracture stresses[52].

c) Effect of δ Ferrite on Embrittlement

Figs. VIII-4-75 and VIII-4-76 show the effect of δ ferrite on the tensile test results[48,54]. It is surmised that weld metal of austenitic stainless steel is subjected to hydrogen embrittlement and that this embrittlement is especially accelerated by post-weld heat treatment during which σ phase precipitates in the weld metal zone.

Table VIII-4-16 Mechanical Properties of the Steels Tensile Tested at Room Temperature before and after Hydrogen Charging[51]

Material		Reference		Hydrogen charged	
	$R_{p0.2}$, N/mm^2	R_m, N/mm^2	A, o/o	R_m, N/mm^2	A, o/o
AISI 304	310	480	38	210	0
AISI 316	300	480	39	100	0
AISI 310	330	520	25	330	0

Table VIII-4-17 Effect of Plastic Deformation on Fracture Stresses of Hydrogen Charged Specimens[51]

Material	R_m, N/mm^2	Material	R_m, N/mm^2
AISI 304		AISI 316	
10 o/o deformation	150	10 o/o deformation	430
20 o/o deformation	190	20 o/o deformation	90
30 o/o deformation	250	30 o/o deformation	260
50 o/o deformation	420	50 o/o deformation	260
α'-martensite		AISI 310	
10 o/o	210	10 o/o deformation	480
20 o/o	70	30 o/o deformation	400
		50 o/o deformation	460

* : Design Condition of First Wall
= 0.56 (cc-H_2/10g-Fe)

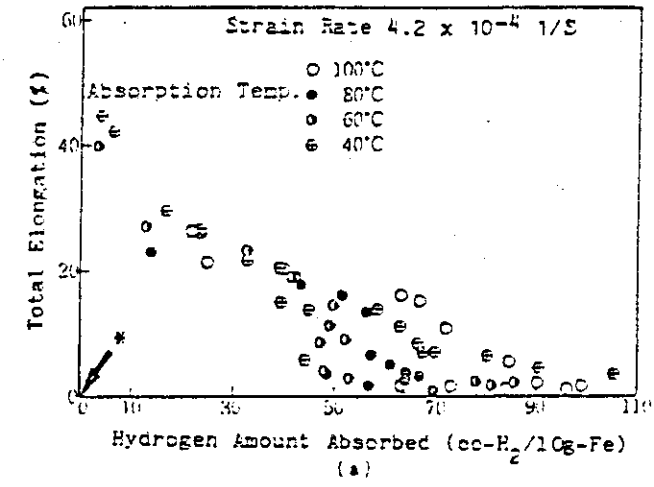

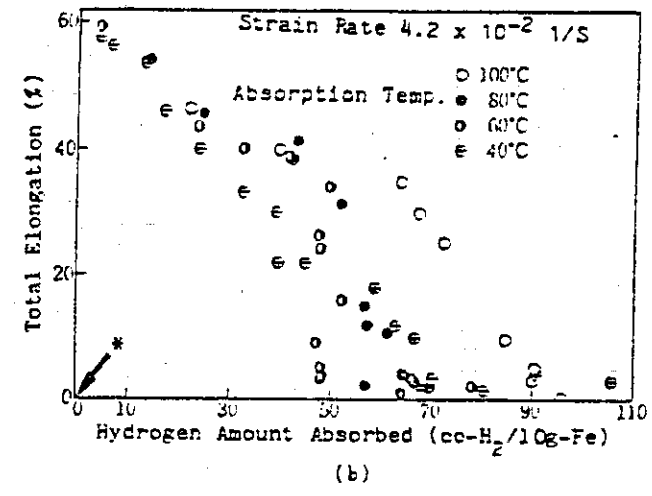

Fig. VIII-4-73 Effect of Hydrogen Amount Absorbed on Total Elongation[49]

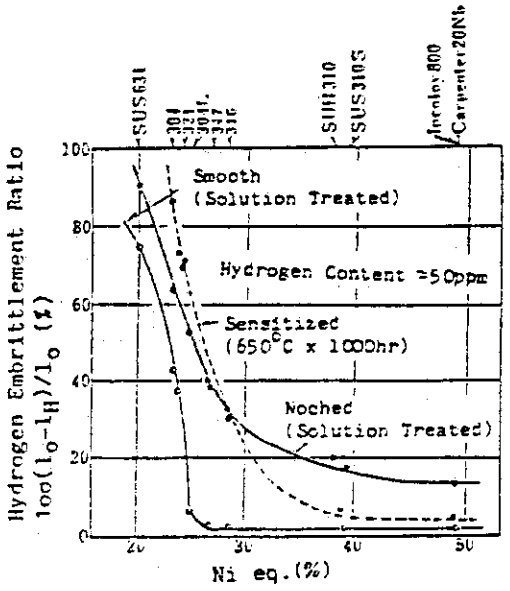

Fig. VIII-4-74 Effect of Ni eq. on Hydrogen Embrittlement of Austenitic Stainless Steel and Heat-resisted Steel [49]
(Hydrogen Treatment-condition : 400 °C , 280 atm)
(l_o: Total Elongation of Hydrogen Free Specimen,
l_H: Total Elongation of Hydrogen-charged Specimen)

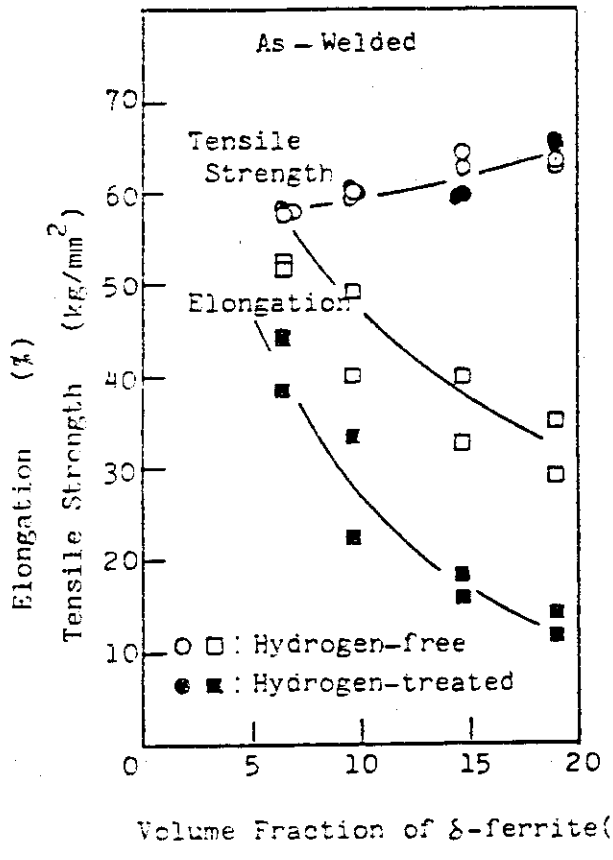

Fig. VIII-4-75 Effect of δ-ferrite on Hydrogen Embrittlement of As-welded Material[53]

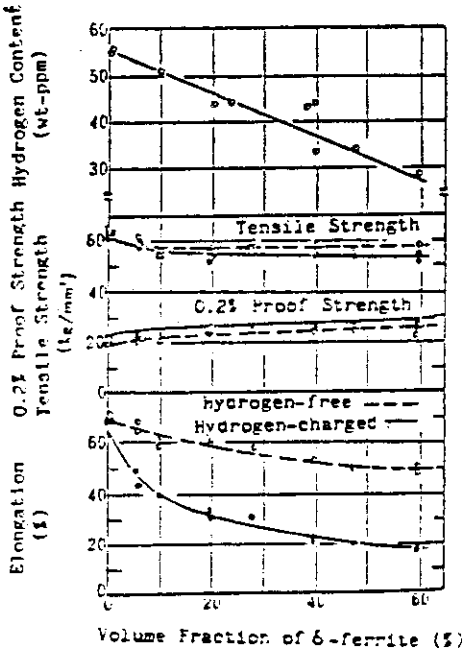

Fig. VIII-4-76 Effect of δ-ferrite Content on Hydrogen Embrittlement of Type 304L S.S. [47]
(Hydrogen Treatment Condition : 400 °C , 290 atm)

5. Tritium system

Tritium Systems in the INTOR are needed to (1) purify and recycle tritium for the plasma fuel cycle, (2) recover tritium from the breeding blanket, and (3) provide tritium containment and atmospheric cleanup, etc.

The main radioactive hazard will come from the use of tritium at these tritium systems.

Exposure of personnel due to released tritium is limited by proper containments and tritium removal systems.

The main criteria to provide guidance for the design of tritium system are as follows;

i) By the application of multiple containment system, tritium leakage from tritium system is decreased to safety level in the populational area, even if the accidental tritium release were taken place.

ii) A minimum tritium inventory is to be maintained in tritium system.

iii) Each tritium removal system can be used for multi-purpose.

iv) The primary containment system is made of materials which has been less effected by hydrogen embrittement and considered to apply welded joints as much as possible.

v) Tritium systems operate at temperature and pressure below those at which significant diffusion of tritium through metal wall occurs.

vi) All tritium systems are enclosed within containment structures which are equipped with Emergency Air Cleaning System.

Fig.VIII-5-1 shows the flow schematics of the tritium system.

5.1 Plasma reprocessing line

(a) Fuel Gas Circulation System

Conceptual design has been carried out for Fuel Gas Circulation System (FCS). The most important subject is to minimize tritium inventory. Tritium inventory of FCS is designed to be as minimum as technically possible. Table VIII-5-1 shows the tritium inventory of FCS.

a) FCS functions

The main functions of FCS are as follows.

i) Pumping out the burned fuel gas from the plasma chamber
ii) Removal of impurities and He from the exhaust stream
iii) Separation of hydrogen isotopes for reuse
iv) Adjustment of fuel gas composition for fuel supply

b) Major parameters

Table VIII-5-2 shows the major parameters of FCS.

c) System description

Fig. VIII-5-2 and Fig. VIII-5-3 show the flow diagram of Cryogenic Pumping Unit and main FCS.
Fig. VIII-5-4 shows the process flow diagram of FCS.

FCS consists of five units. The main characteristics of theses units are as follows.

i) Cryogenic pumping unit

Cryopumps pump out the burned fuel gas from chamber. Tritium is pumped out with cryocondasation panel. and helium is pumped out with cryosorption panel.

ii) Purification unit (I)

Impurities is removed from fuel gas with cold traps. Tritiated water is sent to the electrolysis cell of Breeding Blanket Tritium Recovery System (BRS). And the other impurities are sent to Effluent Tritium

Removal System (ERS).

iii) Purification unit (II)

Helium is removed from fuel gas with the palladium alloy permeaters and sent to ERS. Tritium inventory of the palladium alloy permeaters is not significant as shown in Table VIII-5-1.

iv) Isotope Separation unit

The fuel gas is separated to T_2, D_2, DT and H_2 with Isotope Separation unit.
Cryogenic distillation method is adopted for Isotope Separation unit, because it appears to be practicable.

The tritium inventory of Isotope Separation unit is about 100g as shown in Table VIII-5-1. In order to minimize tritium inventory, a more detailed investigation will be needed.

Fig.VIII-5-5 shows the layout of the FCS glove boxes.

v) Fuel Gas Adjustment unit

Having passed the Isotope seperation unit, the pure D_2, DT, and T_2 output is stored and mixed in the Fuel Gas Adjustment unit. The adjusted fuel mixture is then directed to the fuel injector where the needed fuel mixture are prepared for use in the reactor fuelling device.

Table Ⅷ-5-1 FCS Tritium Inventory

System		Tritium inventory	Remarks
FCS	Cryogenic pumping unit	117 g	six pumps
	Purification unit I II	8 g	nine permeaters
	Isotope Separation unit	93 g	four distillation collumns
	Fuel gas adjustment unit	23 g	
	Miscellaneous	25 g	
Total		266 g	
Main storage system		2320 g	a storage with a capacity of 30 days
Total		2590 g	

Table Ⅷ-5-2 FCS Major Parameters

Parameters	Unit Vlue	Remarks
Average flow rate of plasma exhausting gas	23.2 g-mol/hr	Power : 620MW Duty factor : 200/245 Burn rate : 0.05
Atom fraction of plasma exhausting gas	Hydrogen isotopes : 0.95 [H : 0.005 D : 0.4975 T : 0.4975] He: 0.05	
Average flow rate of NBI exhausting gas	1.37 g-mol/hr	
Atom fraction of NBI exhausting gas	H : 0.004 D : 0.995 T : 0.001	
Product D_2 gas purity	0.996	
Product T_2 gas purity	0.99	
Tritium permissible level in waste	1000 Ci/y	

5.2 Blanket reprocessing line

(a) Breeding Blanket Tritium Recovery System

Conceptual design of the Breeding Blanket Tritium Recovery System (BRS) has been carried out. The most important goal of the design is to minimize tritium inventory. Tritium inventory is designed as minimum as technically possible. Table VIII-5-3 summarizes the tritium inventory.

a) BRS functions

The main functions of BRS are as follows;

i) to extract trtium produced in breeding blanket with sweeping helium flow,

ii) to recover tritium as tritium oxide with absorbing on molecular sieve (MS) dryer,

iii) to decompose this recovered tritium oxide to trtium gas and to oxygen, and to pass this tritium gas to the purification unit of Fuel Gas Circuration System (FCS).

b) Major parameters

Major parameters of the BRS is summarized in Table VIII-5-4

c) System constructions

BRS consists of three units:

i) sweep gas circuration unit,

ii) MS dryer regeneration units, and

iii) electrolysis units.

d) Configuration

Components of the BRS are installed in four blocks of gloveboxes. Fig.VIII-5-6 shows the layout of glovebox blocks in BRS room. Fig.VIII-5-7 shows the layout of components in GBs.

e) System performance and system description

Fig.VIII-5-8 shows flow sheet of the BRS and Fig. VIII-5-9 shows process flow diagram of the BRS.

The BRS is designed to recycle 200Nm^3/hr of tritium-contained helium gas at atmospheric pressure. H_2O is assumed to leak through the coolant tube into the blanket atmosphere in a rate of one tenth of equivalent tritium produced in it.

Catalytic oxidizer converts tritium gas in sweeping helium gas to tritium oxide (T_2O) at 473K. Then helium gas is cooled to 323K and passed to MS dryer. T_2O and H_2O are

absorbed on MS dryer and water vapor pressure is decreased below 7.6×10^{-4} torr.

Four MS dryers are equipped and operated in shifts of tweleve hours to minimize adsorption time per dryer. Regeneration of MS dryer is carried out with regenerating helium gas of 573K. The desorbed water is condensed with cold traps of 288K and drained continuously.

Tritiated water recovered is then passed to electrolysis cell in continuous mode. The electrolysis cell is designed to be as small in volume as technically possible by means of high current density per unit electrode area and narrow spacing of electrodes.

Tritium gas produced in the electrolysis cell is sent to the purification unit of the Fuel Gas Circuration System (FCS). And oxygen also produced in it is sent to Effluent Tritium Removal System (ERS).

Table VIII-5-3 Tritium Inventory of BRS

Unit	Inventory	Remarks
Sweep Gas Recircuration Unit	33 g	Four MS Dryers
MS Dryer Regeneration Unit		
Electrolysis Unit	39 g	
Miscellaneous	15 g	
Total	87 g	

Table VIII-5-4 Major Parameters of BRS

Conditions	Value	Remarks
Average Tritium Extraction Rate from Blanket	0.469 g-mol/hr	BR 1.0 duty factor 100/140
Average H_2O Inleak Rate into Blanket	0.0469 g-mol/hr	
Flow Rate of Sweeping Helium Gas	200 Nm^3/hr	
Temperature of Sweeping Helium Gas	ambient	
Pressure of Sweeping Helium Gas	atmospheric	

5.3 Air detritiation

(a) Tritium Removal System

Conceptual design of the tritium removal system (TRS) has been carried. The TRS is designed to be used for multi-purpose. And the TRS is designed to apply multiple barrier containment concept.

a) TRS Functions

The TRS has four major functions:

i) to remove tritium from the atmosphere of secondary containments,

ii) to remove tritium from routinely generated gaseous effluent from tritium systems except the FCS and the BRS,

iii) to remove tritium from the air of the building atmosphere in the event of an accidental tritium release, and

iv) to regenerate dryers of the TRS and the ERS of the WTS.

b) System Construction

The TRS consists of four subsystems:

i) Inert Gas Purification System (GPS),

ii) Effluent Air Detritiation System (ADS),

iii) Emergency Air Cleaning System (ECS) and

iv) Dryer Regeneration System (DRS).

Conceptual flow sheet of these four subsystems is shown in Fig.Ⅷ-5-10

c) System Description

i) Inert Gas Purification System (GPS)

The GPS recirculates glovebox atmospheric inert gas and recover tritium so as to minimize tritium leak from the glovebox to the environment. The GPS is designed by the combination of catalytic oxidizer, MS dryers and cold trap to remove impurities and tritiated species.

ii) Effluent Air Detritiation System (ADS)

The ADS is designed to remove tritium in once-through mode from routinely generated gaseous effluent from tritium concerning systems except the FCS and the MS dryers.

iii) Emergency Air Cleaning System (ECS)

The ECS is designed to provide detritiation of building atmosphere for an accidental tritium release. The ECS, which consists of catalytic oxidizer and MS dryers, is designed to be automatically actuated and to be opetated to reduce the activity level of the contaminated room.

iv) Dryer Regeneration System (DRS)

The DRS is designed to regenerate dryers of TRS and ERS of WTS. The MS dryers are regenerated by means of recirculating heated gas and outgassed water is collected by means of condensation.

5.4 Waste processing line

(a) Tritium waste treatment system

Conceptual design of tritium waste treatment system (WTS) is carried out. The WTS is designed to handle all the liquid and solid, and specially gas exhausted from FCS and BRS, and to minimize contamination of personnel and surroundings.

a) WTS functions

The WTS has five major functions:

i) to remove tritium in exhaust gas of the primary containment (FCS and BRS etc.),
ii) to enrich tritiated liquid waste for packaging,
iii) to package tritiated liquid waste enriched,
iv) to package tritiated oil, and
v) to package tritiated solid waste for disposal.

b) System construction

The WTS consists of five sub-systems:

i) effluent tritium removal system (ERS),
ii) tritiated liquid waste enrichment system (LES),
iii) tritiated liquid waste packaging system (LPS),
iv) tritiated oil packaging system (OPS), and
v) tritiated solid waste packaging system (SPS).

Conceptual flow diagram of ERS and OPS is shown in Fig. VIII-5-11, and that of LES, LPS and SPS is shown in Fig. VIII-5-12.

c) System description

i) Effluent tritium removal system (ERS)

The ERS treats tritium-bearing waste gas originated from the FCS and BRS to reduce the tritium concentration to a level of dischargeable to the stack. The ERS is designed based on catalytic conversion and adsorption on molecular sieve.

ii) Tritiated liquid waste enrichment system (LES)

The LES enriches tritiated water by means of water distillation methods for packaging enriched tritiated water.

iii) Tritiated liquid waste packaging system (LPS)

The LPS packs high level tritiated water in a container with cement and absorbent. The packed container is sent to SPS.

iv) Tritiated oil packaging system (OPS)

The OPS packs tritiated oil originated mainly from mechanical pumpsof tritium system in a container with absorbent. The packed container is sent to the SPS.

v) Tritiated solid waste Packaging system (SPS)

The SPS packs tritiated solid waste with asphalt for disposal.

Notation

FCS	Fuel Gas Circulation System
BRS	Breeding Blanket Tritium Recovery System
PCS	Primary Cooling System
FRS	Fuel Receiver System
TSS	Tritium Storage System
WTS	Tritium Waste Treatment System
LES	Tritiated Liquid Waste Enrichment System
LPS	Tritiated Liquid Waste Packaging System
ERS	Effluent Tritium Removal System
SPS	Tritiated Solid Waste Packaging System
OPS	Tritiated Oil Packaging System
RPS	Radioactive Solid Waste Packaging System
WSS	Waste Storage System
LSS	Tritiated Liquid Waste Storage System
SSS	Tritiated Solid Waste Storage System
CSS	Tritiated Contaminated Component Storage System
RSS	Radioactive Solid Waste Storage System
TRS	Tritium Removal System
GPS	Inert Gas Purification System
ADS	Effluent Air Detritiation System
ECS	Emergency Air Cleaning System
DRS	Dryer Regeneration System

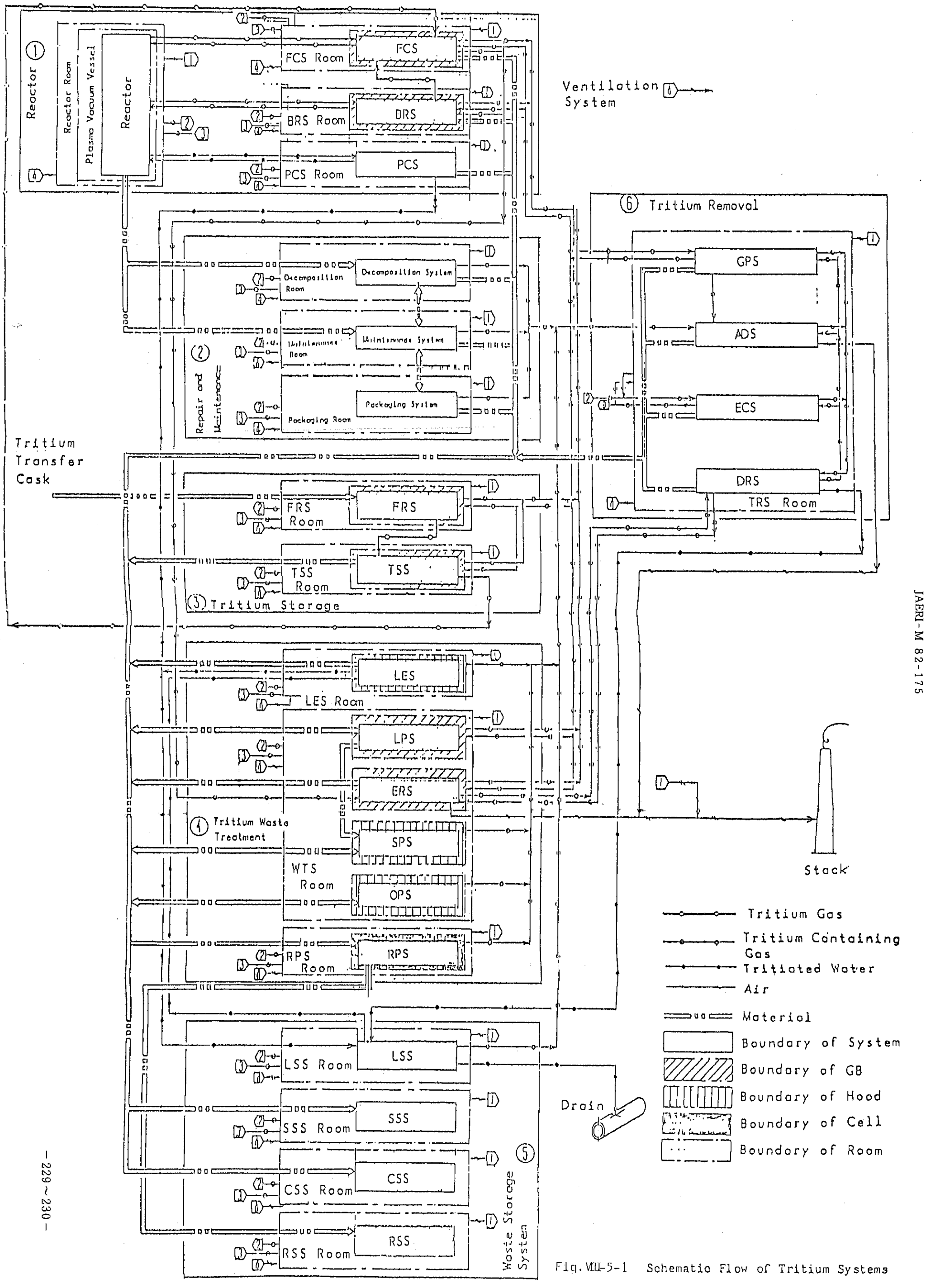

Fig. VIII-5-1 Schematic Flow of Tritium Systems

JAERI-M 82-175

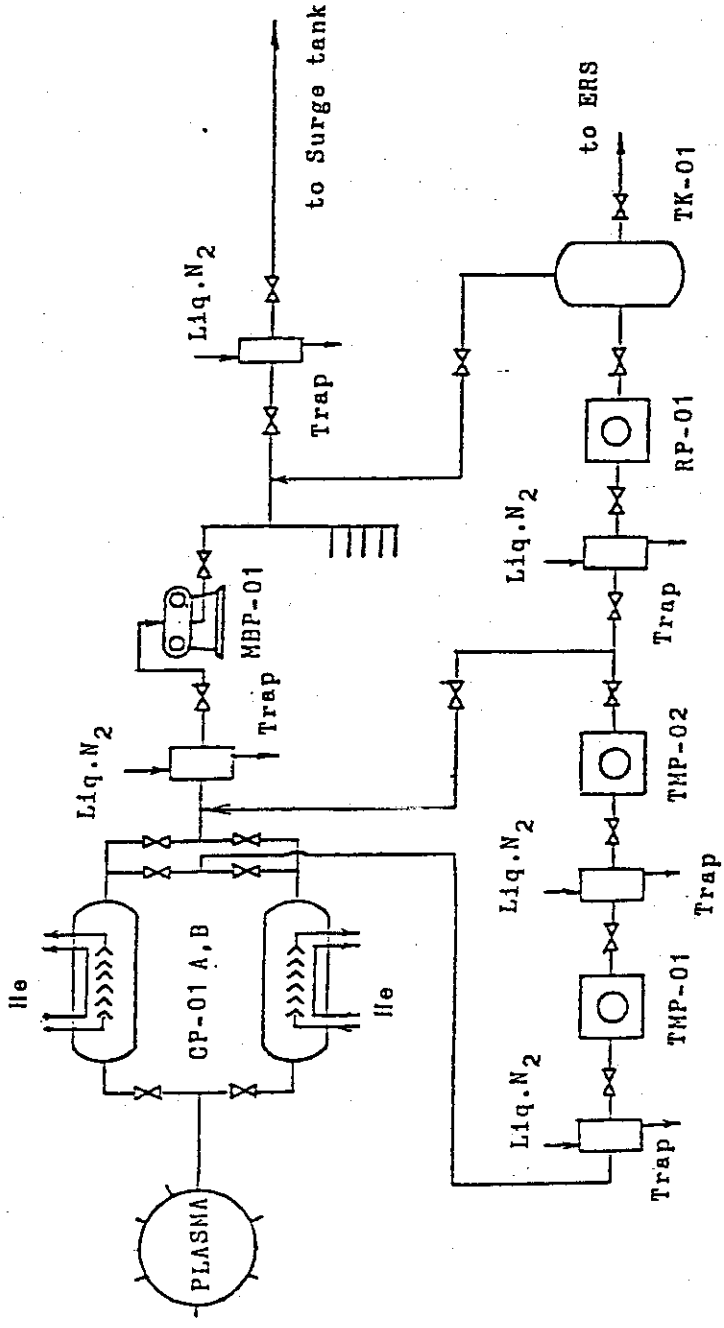

Fig.VIII-5-2 Flow Sheet of Cryogenic Pumping Unit

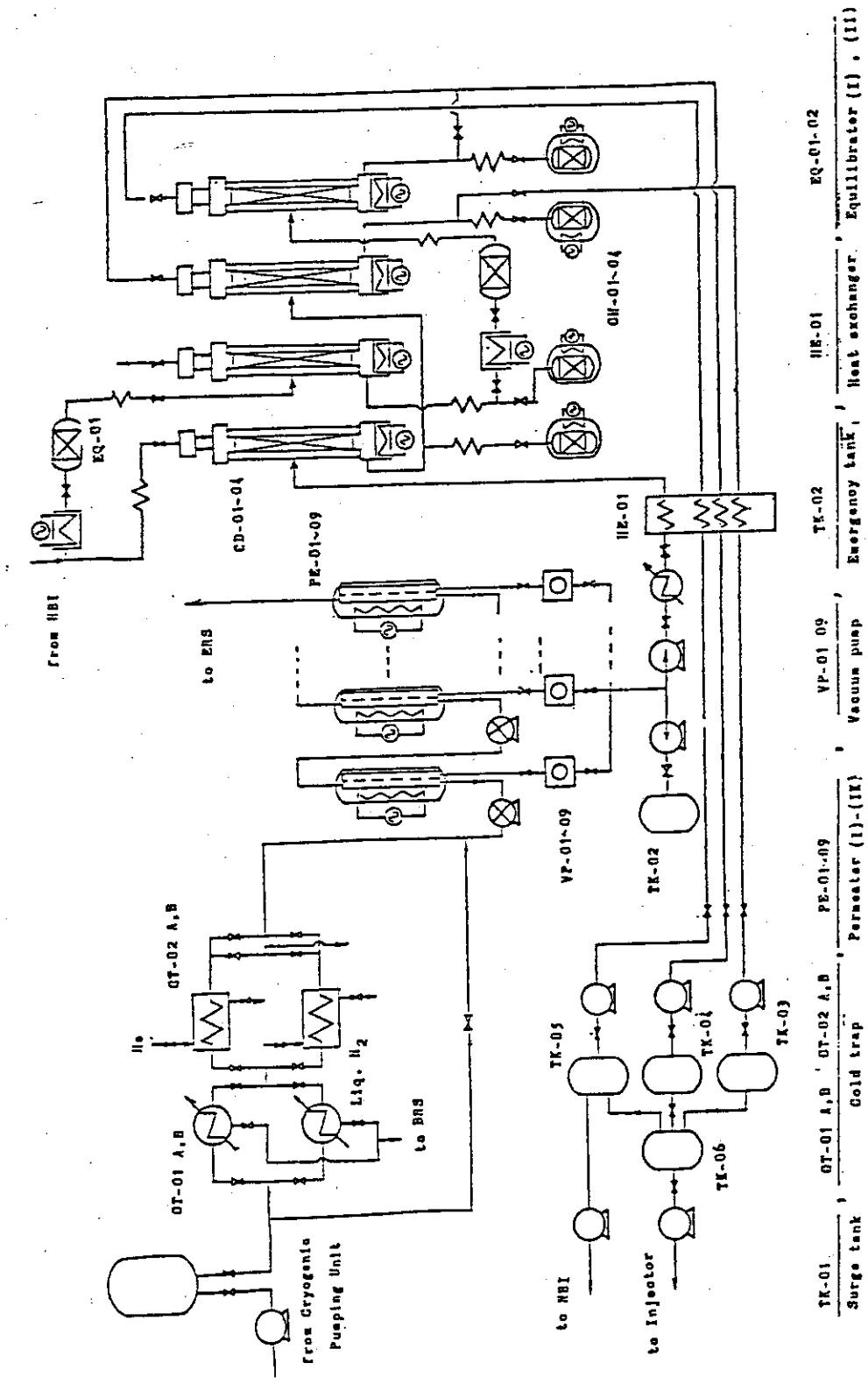

Fig. VII-5-3 Flow Sheet of FCS

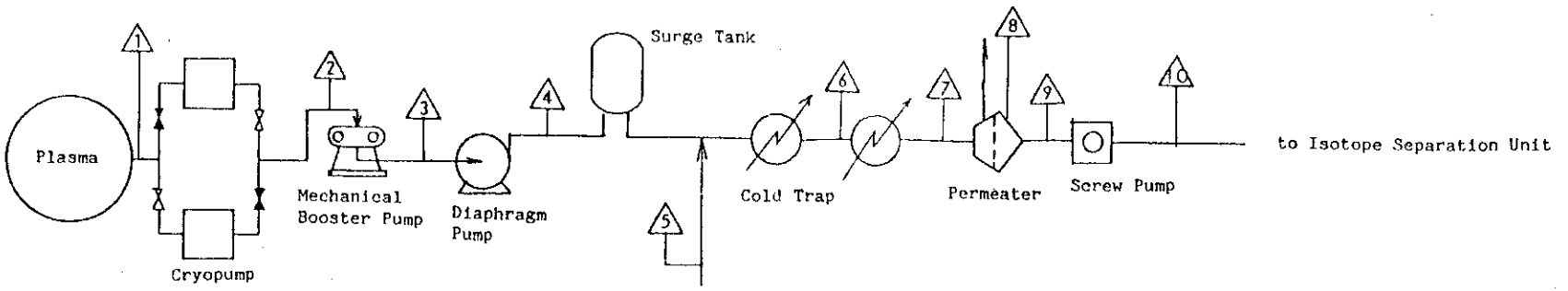

Flow No.		1	2	3	4	5	6	7	8	9	10
Flow Rate	(mol/hr)	22.07	←	←	←	0.52	22.58	22.58	1.10	21.48	21.48
Temp.	(K)	—	293	←	←	←	110	30	673	673	293
Press.	(Torr)	—	<20	760	1000	760	760	760	760	1 or 0.01	760
Atomic Fraction	H	0.005	←	←	←	0.0905	0.007	←	0	0.007	←
	D	0.473	←	←	←	0	0.462	←	7 (-6)	0.486	←
	T	0.473	←	←	←	0.905	0.482	←	7 (-6)	0.507	←
	He	0.05	←	←	←	0	0.049	←	≒1.0	0	←
	Impurities	—	—	—	—	0.005	9 (-5)	0	0	0	←

Fig. VIII-5-4 Process Flow Diagram of FCS (1/2)

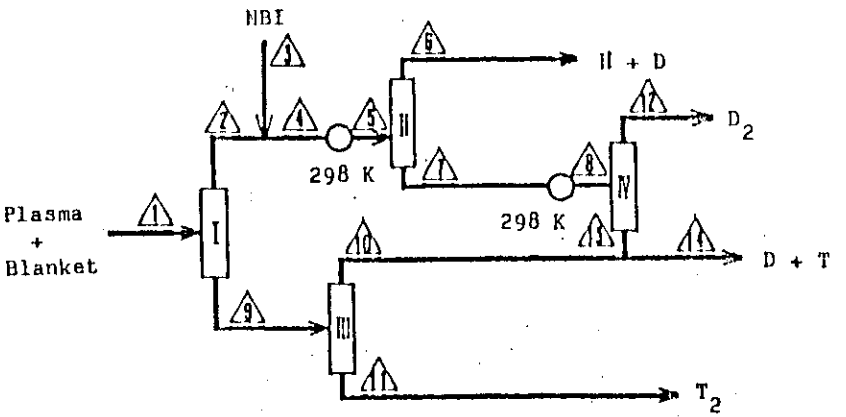

	Total Theoretical Stages	Feed Location	Reflux Ratio
Column I	70	35	25
Column II	70	45	200
Column III	70	35	10.5
Column IV	70	35	10

		1	2	3	4	5	6	7	8	9	10	11	12	13	14
Flow Rate, g-mol/hr		21.5	5.38	1.37	6.75	6.75	0.433	6.32	6.32	16.1	11.0	5.10	6.09	0.230	11.2
Molar Fraction	H_2	7.21 (-5)	2.88 (-4)	1.97 (-5)	2.33 (-4)	7.01 (-4)	1.09 (-2)	1.68 (-12)	3.04 (-20)	3.04 (-20)	4.45 (-20)	1.52 (-39)	6.62 (-12)	1.74 (-26)	4.36 (-20)
	HD	7.47 (-3)	2.98 (-2)	7.95 (-3)	2.54 (-2)	4.59 (-2)	0.716	4.49 (-5)	1.75 (-11)	1.75 (-11)	2.56 (-11)	4.53 (-24)	4.66 (-6)	7.61 (-14)	2.51 (-11)
	HT	6.94 (-3)	2.77 (-2)	7.28 (-6)	2.21 (-2)	6.01 (-4)	9.32 (-3)	5.98 (-8)	2.96 (-8)	2.96 (-8)	4.33 (-8)	1.27 (-17)	6.21 (-8)	2.10 (-12)	4.24 (-8)
	D_2	0.238	0.936	0.990	0.947	0.926	0.264	0.971	5.36 (-3)	5.36 (-3)	7.84 (-3)	7.07 (-9)	1.00	0.218	1.21 (-2)
	DT	0.487	6.45 (-3)	1.99 (-3)	5.54 (-3)	2.66 (-2)	2.78 (-7)	2.85 (-2)	0.647	0.647	0.946	2.35 (-3)	2.20 (-4)	0.776	0.943
	T_2	0.260	1.47 (-6)	1.05 (-6)	1.39 (-6)	2.00 (-4)	1.57 (-13)	2.18 (-4)	0.347	0.347	4.57 (-2)	0.998	1.03 (-9)	6.00 (-3)	4.49 (-2)
Atomic Fraction	H	7.28 (-3)	2.91 (-2)	0.004	2.40 (-2)	2.40 (-2)	0.374	2.27 (-6)	1.50 (-8)	1.50 (-8)	2.17 (-8)	6.37 (-18)	2.36 (-6)	1.09 (-12)	2.12 (-8)
	D	0.486	0.954	0.995	0.962	0.962	0.622	0.986	0.329	0.329	0.481	1.17 (-3)	1.00	0.606	0.484
	T	0.507	1.71 (-2)	0.001	1.38 (-2)	1.38 (-2)	3.01 (-4)	1.44 (-2)	0.671	0.671	0.519	0.999	1.10 (-4)	0.394	0.516

Fig.VIII-5-4 Process Flow Diagram of FCS (2/2)

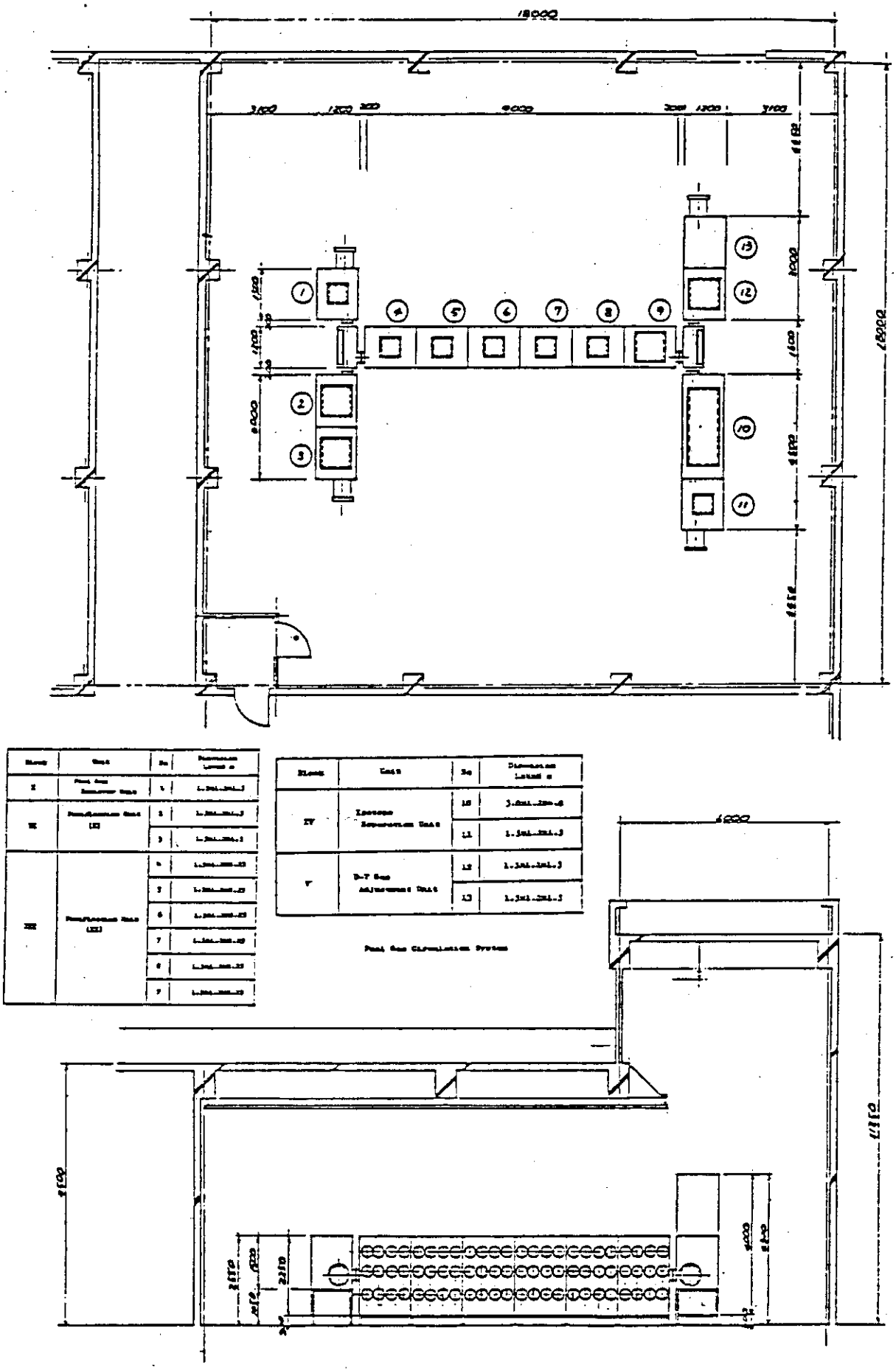

Fig. VIII-5-5-5 Layout of Glovebox Blocks in FCS Room

Glove Box			
Block	Unit	No	Dimension LxWxH m
I	Sweep Gas Recirculation Unit	1	1.5x1.2x1.5
		2	1.5x1.2x3.0
		3	1.5x1.2x1.5
		4	1.5x1.2x1.5
II	MS Dryer	5	1.5x1.2x1.5
		6	1.5x1.2x1.5
		7	1.5x1.2x1.5
III	MS Dryer Regeneration Unit	8	1.5x1.2x1.5
		9	1.5x1.2x1.5
		10	1.5x1.2x1.5
		11	1.5x1.2x3.0
IV	Electrolysis Cell Unit	12	0.75x1.2x1.5

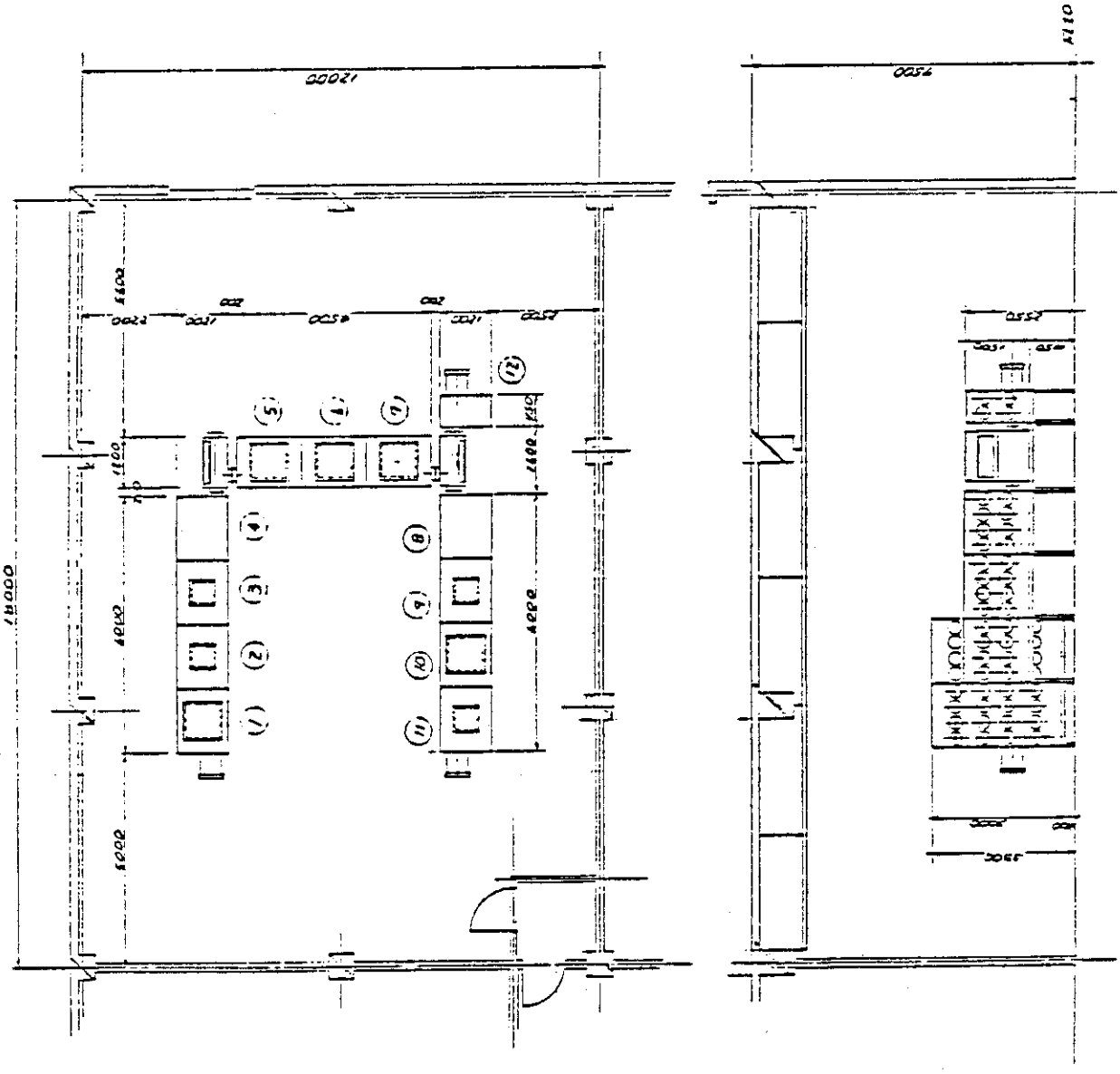

Fig. VII-5-6 Layout of Glovebox Blocks in BRS Room

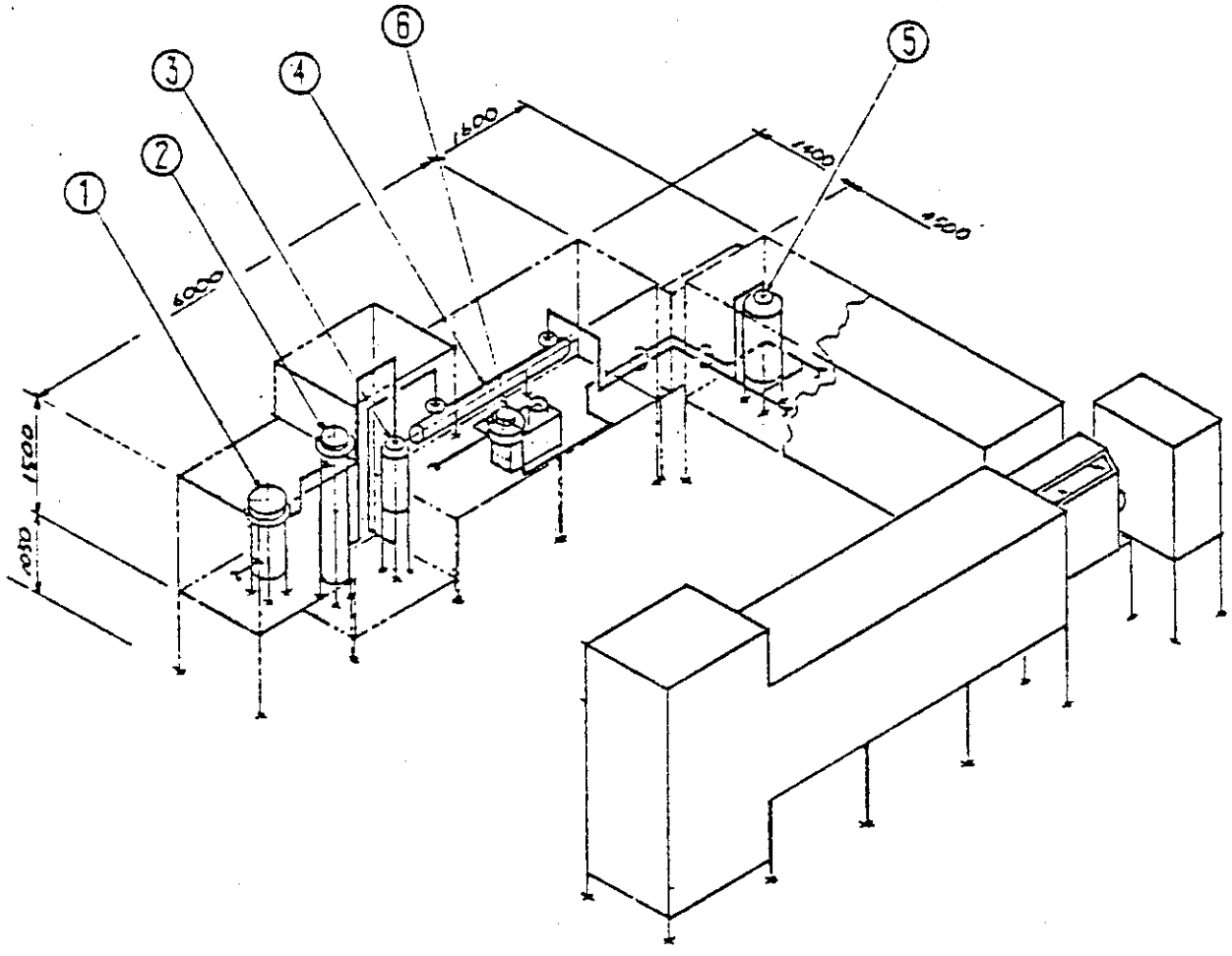

① Filter
② Heater
③ Oxidizer
④ Heat Exchanger
⑤ MS Dryer
⑥ Circulator

Fig.VIII-5-7 Layout of Components in GBs

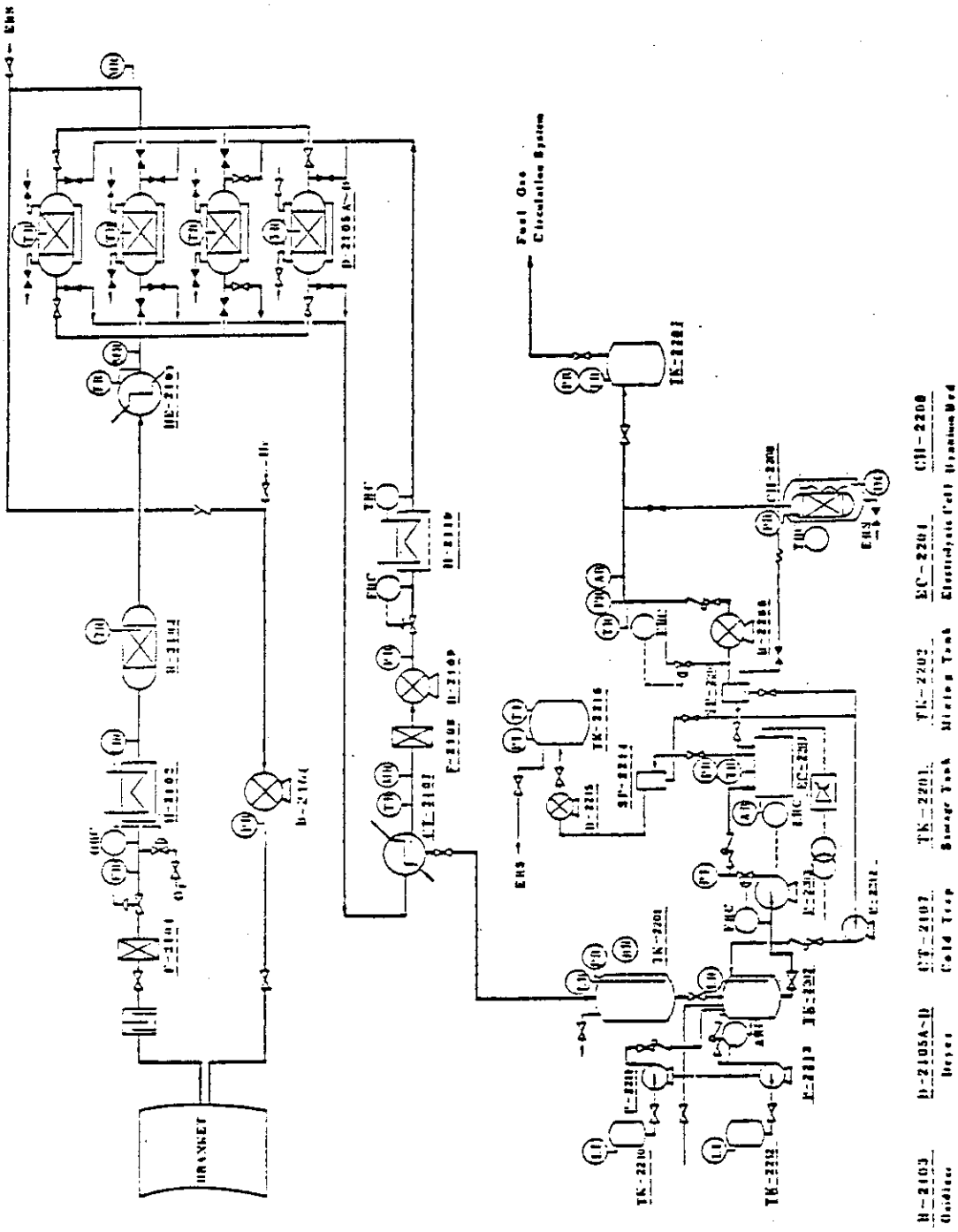

Fig. VII-5-8 Flow Sheet of BRS

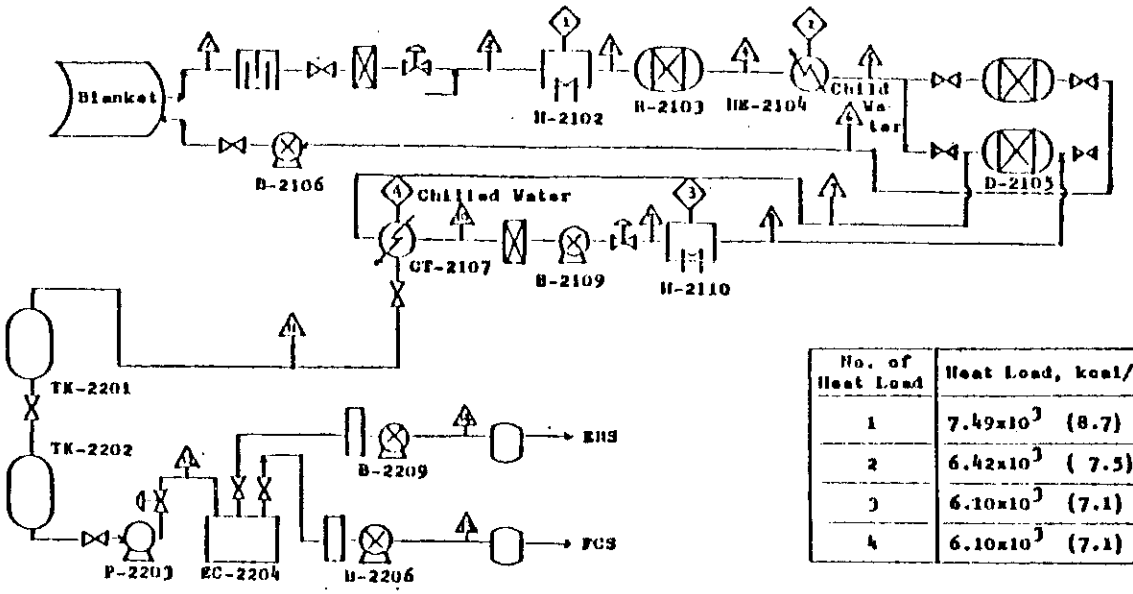

No. of Heat Load	Heat Load, kcal/hr (W)
1	7.49×10^{3} (8.7)
2	6.42×10^{3} (7.5)
3	6.10×10^{3} (7.1)
4	6.10×10^{3} (7.1)

B-2102 Heater
R-2103 Catalytic Oxidizer
HE-2104 Cooler
D-2105 MS Dryer
B-2106 Circulator
CT-2107 Cold Trap
B-2109 Circulator
B-2110 Heater
TK-2201 Holding Tank
TK-2202 Adjusting Tank
P-2203 Pump
EC-2204 Electrolysis Cell
B-2206 Blower
B-2209 Blower

Flow No.			①	②	③	④	⑤	⑥	⑦	⑧	⑨	⑩	⑪	⑫	⑬	⑭
Fluid			No Gas	←	←	←	←	←	←	←	←	←	Water (T_2O)	←	Hydrogen (T_2)	Oxygen
Flow Rate		g-mol/hr											max.			
		Nm^3/hr	200	←	←	←	←	←	100	←	←	←	2.4 (2) 4.3(-3)	0.516 9.3(-6)	0.516 1.16(-3)	0.258 5.78(-3)
Temperature		°C	25	←	200	←	50	←	15	300	←	15	25	←	←	←
Press.		ata	~1										~1		~1	
Composition	T_2	-	4.00(-3) Torr	←	←	4.00(-6) Torr	←	←	—	—	—	—	—	—	0.905	0.00901
	T_2O	-	3.60(-2) Torr	←	←	4.00(-2) Torr	←	6.84(-4) Torr	11.5	←	max. 47.9	11.5	0.90	0.90	~0	~0
	H_2	-	—	—	—	—	—	—	—	—	—	—	—	—	0.0905	9.01(-4)
		-	4.00(-3) Torr	←	←	←	←	7.60(-5) Torr	1.28	←	max. 5.33	1.28	0.10	0.10	~0	~0
	O_2	-	8.0(-3) Torr	1.0(-2) Torr	←	8.0(-3) Torr	←	←	—	—	—	—	—	—	0.005	0.99
Tritium Concentration		Ci/m^3	(1.4 -2)	←	←	←	←	2.3	1.9 (4)	←	max. 1.6 (5)	3.9 (4)	2.9 (9)	←	2.3 (5)	2.3 (4)

Fig.VIII-5-9 Process Flow Diagram of BRS

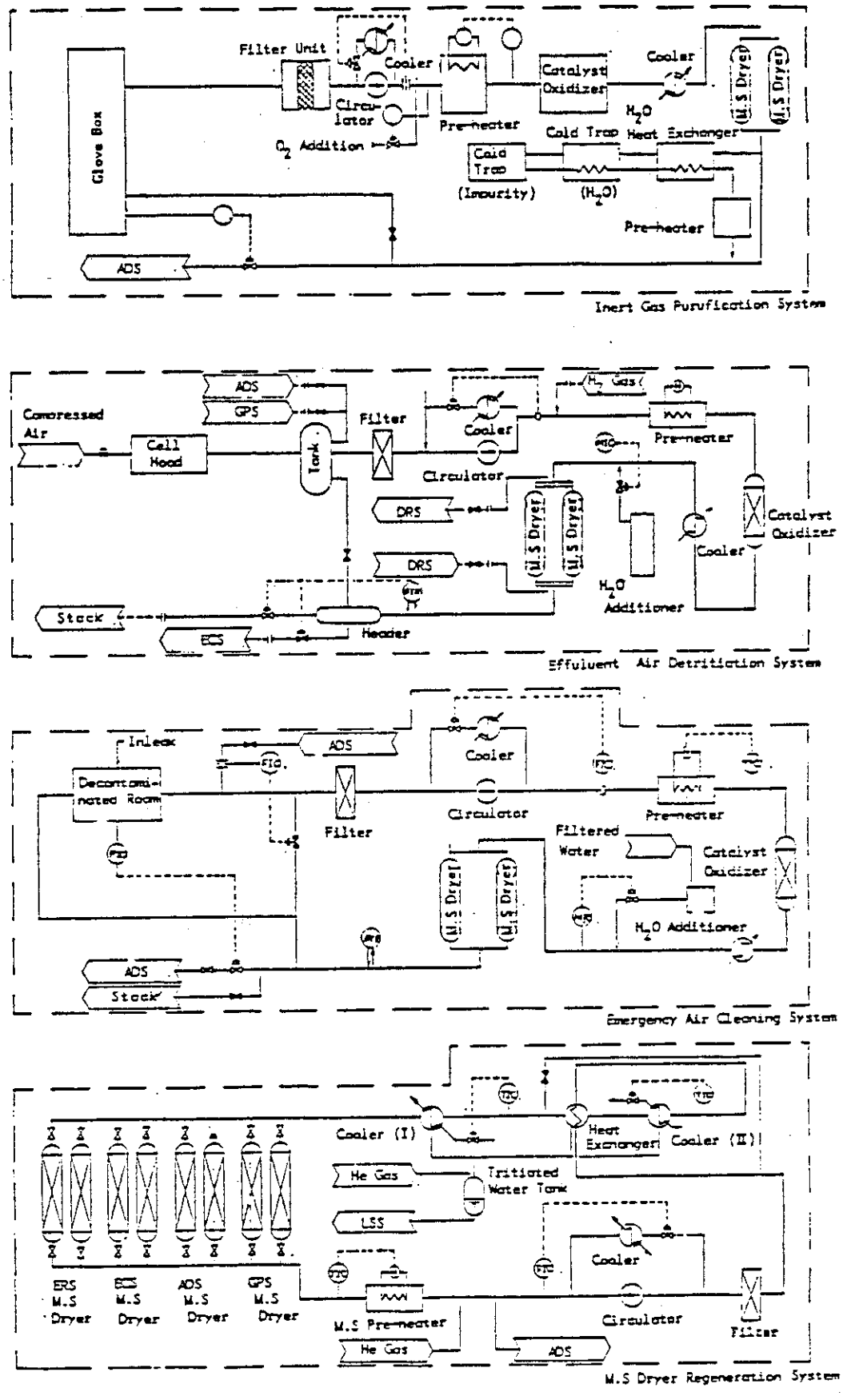

Fig. VIII-5-10 Conceptual Flow Sheet of TRS

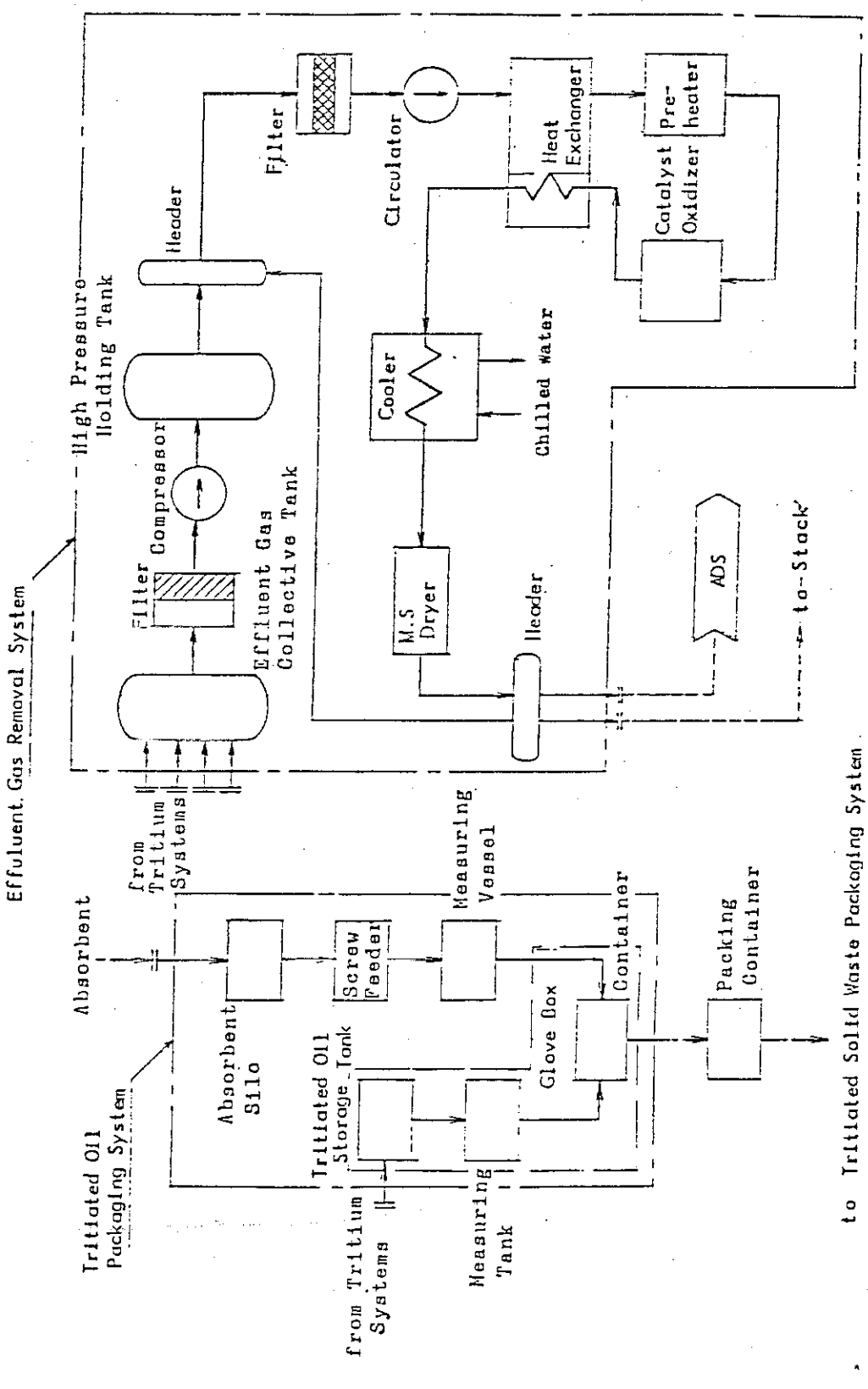

Fig. VII-5-11 Conceptual Flow Sheet of ERS and OPS

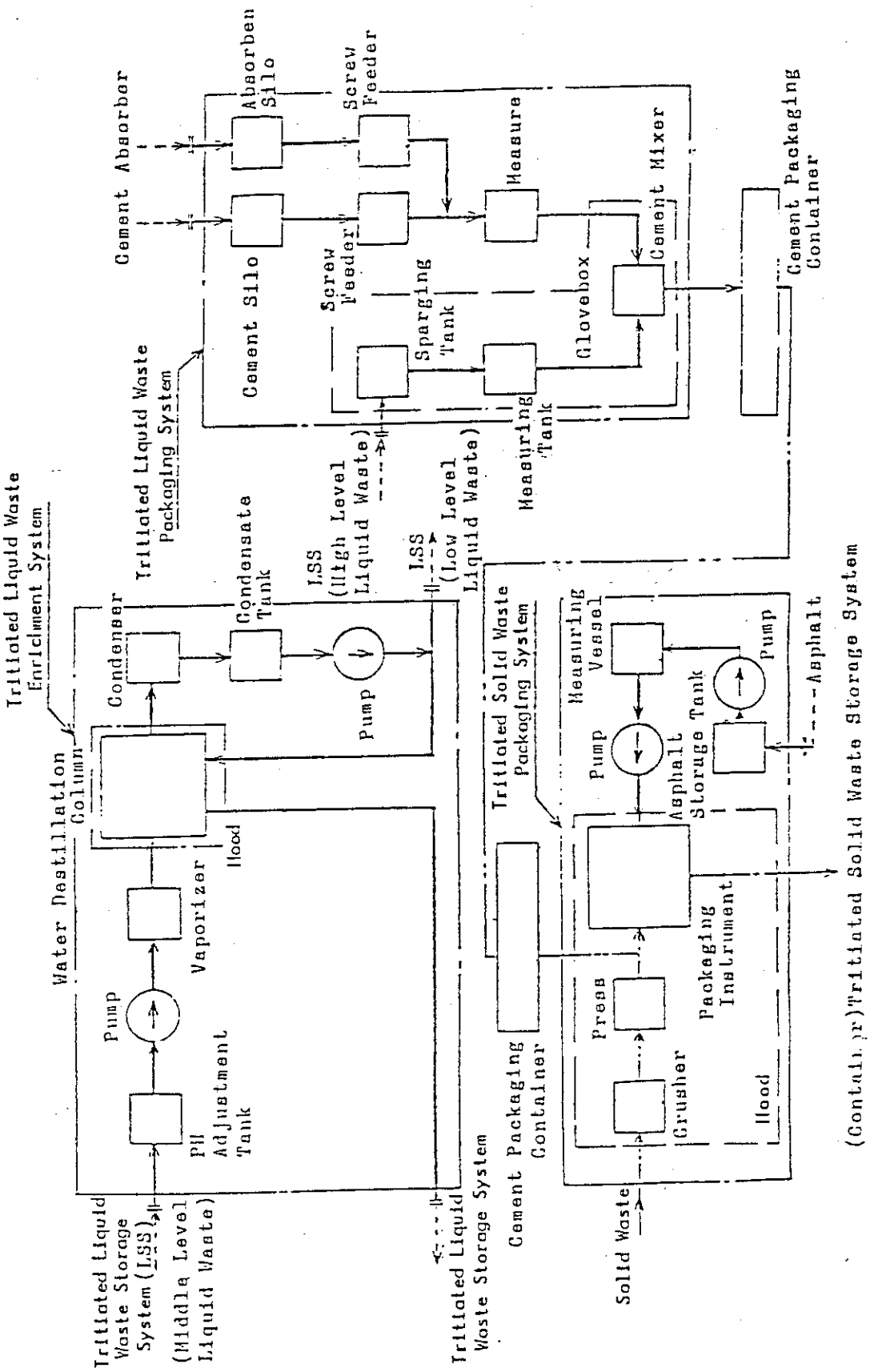

Fig. VIII-5-12 Conceptual Flow Sheet of LES, LPS and SPS Tritiated Solid Waste Storage System

6. Safety consideration

6.1 Accident analysis

(a) Accident Scenarios for the Tritium Systems

(1) Intorduction

Major potential tritium release hazards of tritium systems of INTOR are clarified critical failure mode and evaluated the adequacy of safety features of the design. Since fusion technology is not yet well-established, the more comprehensive criteria and standards must be provided.

In order to design adequate safety systems technically and practically, preliminary study on safety for potential tritium release accidents is carried out in this section. Failures leading to the release of tritium are categorized mainly with respect to the effect on the personnel and surroundings, and the probability of failure mode is not considered in this stage. As the tritium systems are designed based on the multiple barrier containment concept and the ECS is designed to remove released tritium into the terminal containment in the case of an accident, abnormal tritium release to the environment requires a three-fold failure of primary and secondary containments along with either a breach of containment room or a failure of the ECS. In this study, a three-fold failure is not assumed and the ECS is assumed to be actuated immediately.

And as a special safety matter inherent to fusion reactor, there exists a potential tritium decontamination problem after an accident. This problem has to be conducted in near future.

(2) Potential Source of Tritium Release

The most serious consequence results potentially from the accident of systems with great tritium inventory. Tritium inventories of the major systems are evaluated and summarized in Table VIII-6-1.

As is shown from Table VIII-6-1, most of tritium in the reactor room is accumulated in cryopumps in the form of tritium gas. So this system is assumed to be a major potential source of tritium release in the reactor room because of its great tritium inventory and of being contained in only double barriers. Although maximum permissible level of tritium oxide is two hundred times severer than that of tritium gas and the electrolysis cell unit of the BRS contains 39 g of tritium oxide,

it is not considered as the major tritium release source because of being contained in triple barriers.

(3) Identification of Potential Accident

Preliminary safety analysis only on failures of major components (critical to safety) of potential tritium release is carried out with a method of a Failure Modes and Effects Analysis (FMEA). The basis of the FMEA is to assume a single failure of a system component and to follow its effect through systems to determine the ultimate result of the failure.

Model of tritium systems is shown in Fig. VIII-6-1 depicting the potential accident.

The anticipated failure modes and their consequences for the tritium systems regarding to nine initiators are listed in Table VIII-6-2.

(4) Accident Sequences

According to nine initiators of FMEA table, accident progression sequences and the ultimate consequences are studied.

This accident progression sequences are shown in Fig. VIII-6-2. Accident initiators and event trees need to be defined in some details in order to facilitate assessment of the hazard potential and the appropriate mitigating design features. In every case, the released tritium is finally removed with the ECS. The capacity of the ECS is not yet decided. The required flow rate, which depends on the free volume of the reactor room, is assumed to be enormous. There exists a suggestion to compart the reactor room by some sub-rooms.

Table VIII-6-1 Tritium Inventories of Major Systems

	System	Tritium Inventory	Form	Remarks
(i)	Plasma Vacuum Vessel	8.1×10^{2} Ci (0.08 g)	Gas	
(ii)	Fuel Gas Circulation System (FCS)			
	Cryogenic Pumping Unit	1.1×10^{6} Ci (120 g)	Gas	2.3×10^{5} Ci (24 g)/cryopump
	Other Units	1.4×10^{6} Ci (150 g)	Gas	Isotope Separation Unit; 2.3×10^{5} Ci (24 g)
(iii)	Breeding Blanket Tritium Recovery System (BRS)	8.4×10^{5} Ci (87 g)	Oxide	Electrolysis Cell Unit; 3.7×10^{5} Ci (39 g)
(iv)	Primary Cooling System (PCS)	3.1×10^{4} Ci (3.2 g)	Oxide	assumed the tritium permeation rate to be 620 Ci per day and the tritiated water processing rate to be 2.0 % of water inventory per day
(v)	Tritium Storage System	2.2×10^{7} Ci (2300 g)	UT_3	

JAERI-M 82-175

Table VIII-6-2 Failure Mode and Effects Analysis for Tritium Systems (1/4)

No.	System	Component	Function	Failure Mode	Failure Effect
①	Reactor	Plasma vacuum vessel	Isolate reactor from environment	Rupture	i) Just after the rupture, air flows into the vacuum vessel, and so tritium is not releasad to environment. ii) After the pressure of the vacuum vessel and that of the reactor room get equilibrium, tritium in the vacuum vessel is released in the mechanism of thermal expansion and natural convection. iii) The amount of tritium released is estimated to be equal to the tritium quantity in vacuum vessel of 830 Ci (0.08 g). iv) Potential detonation of hydrogen-oxygen mixture may occur on cryopanels of cryopumps.
②	Blanket	Blanket vessel	Provide isolation between breeding material and plasma vacuum chamber	Rupture	Tritium produced in blanket is released to the plasma vacuum vessel. The amount of tritium released is about 400 Ci, that is equal to one seventy-seconds of total blanket tritium inventory because 72 blanket modules are placed in the plasma vacuum vessel.
③	Primary cooling system	Coolant piping in blanket	Cool breeding material	Rupture	i) Cooling water flows into the blanket and reacts with breeding material (Li_2O) Heat generation rate is evaluated to be about 2 kW in the condition of coolant flow rate of 0.3 kg/sec.

Table VIII-6-2 Failure Mode and Effects Analysis for Tritium Systems (2/4)

No.	System	Component	Function	Failure Mode	Failure Effect
					ii) Temperature in the blanket rises up and pressure in the blanket vessel exceeds the allowable one of 0.1 MPa.
					iii) The blanket vessel ruptures and tritium is released as in the case of the rupture at the blanket vessel (②).
					iv) Pressure in the vacuum vessel may increase and possible rupture of the vacuum vessel may occur. Tritium in the vacuum vessel is released to the reactor room.
					v) The amount of tritium released to the reactor room is estimated to be sum of tritium inventories in the vacuum vessel and the blanket vessel.
⑪	Primary cooling system	Coolant pipe equiped in plasma vacuum vessel	Cool breeding material	Rupture	i) Cooling water flows into the plasma vacuum vessel. And pressure in the vacuum vessel might rise up to about 0.5 MPa under the severest assumption.
					ii) As allowable internal pressure of vacuum vessel is estimated to be 0.2 to 0.3 MPa, it may be breached.

Table VIII-6-2 Failure Mode and Effects Analysis for Tritium Systems (3/4)

No.	System	Component	Function	Failure Mode	Failure Effect
					iii) The amount of tritium released is equal to that in the case of plasma vacuum vessel rupture (①), that is 830 Ci (0.08 g).
⑤	Vacuum system	Cryopump	Evacuate plasma vacuum vessel	Rupture due to hydrogen detonation	Release of at most 2.4×10^5 Ci (24 g) of tritium to reactor room.
⑥	Vacuum system	Cryopump gate valve	Isolate cryopump during regeneration	Rupture of gate valve during regeneration	Release of at most 2.4×10^5 Ci (24 g) of tritium to plasma vacuum vessel.
⑦	Fuel gas circulation system	Isotope separation unit	Separate hydrogen isotopes	Rupture of the distillation columns and surrounding vacuum jacket due to loss of refrigeration	Release of at most 8.9×10^5 Ci (93 g) of tritium to glovebox of 17.1 m^3.

Table VIII-6-2 Failure Mode and Effects Analysis for Tritium Systems (4/4)

No.	System	Component	Function	Failure Mode	Failure Effect
⑧	Breeding blanket tritium recovery system	Electrolysis cell	Convert T_2O to T_2	Rupture	3.7×10^5 Ci (39 g) of tritiated water flows out into the glovebox of 1.35 m^3. If four glove-ports are not covered and temperature of glovebox is 25 °C, tritium release rate to room is estimated to be 1.7×10^2 Ci/hr.
⑨	Tritium storage system	Uranium getter	Storage of tritium	Rupture	Possible release of 2.2×10^7 Ci (2300 g) of tritium into glovebox.

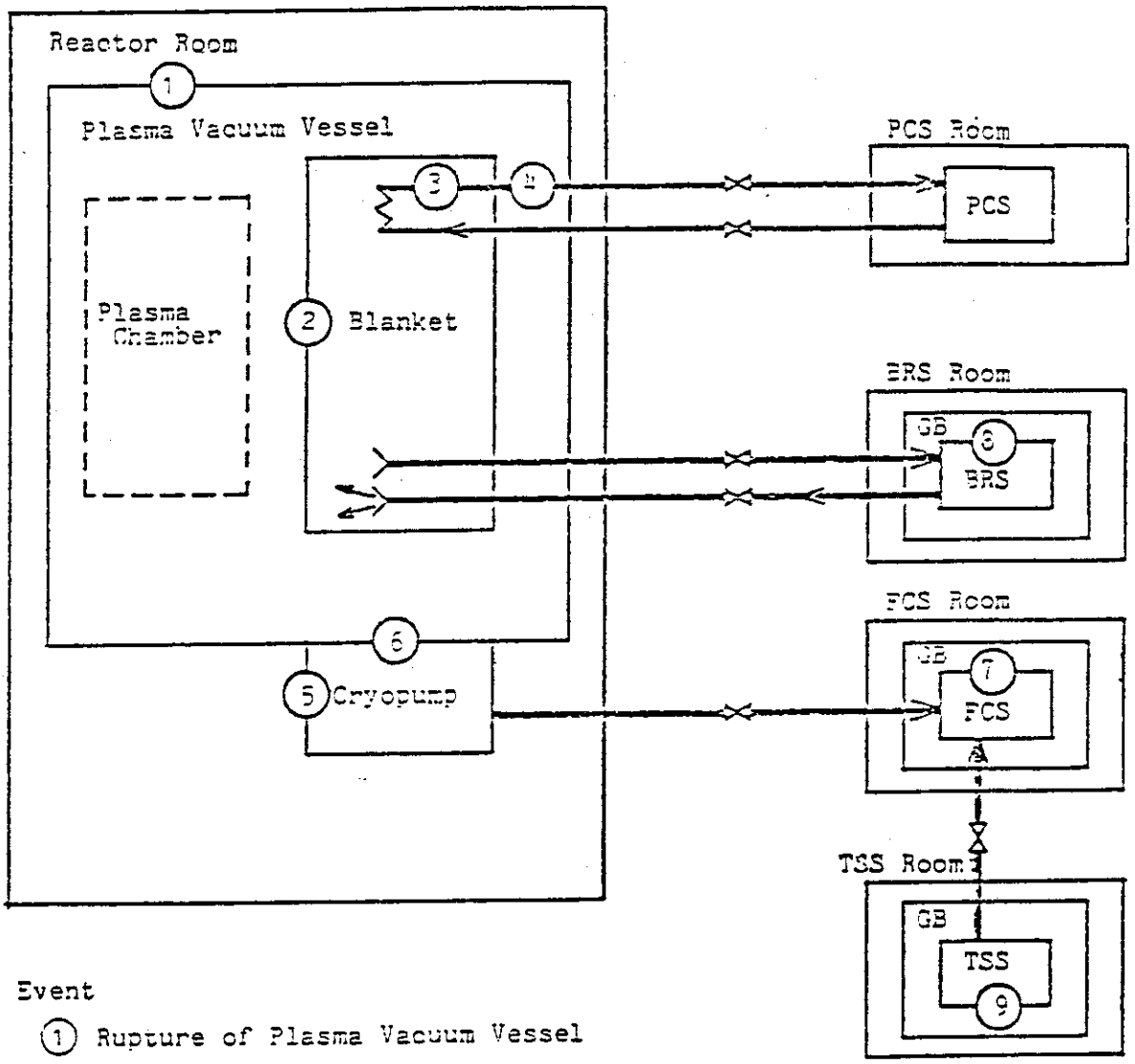

Event

① Rupture of Plasma Vacuum Vessel
② Rupture of Blanket Vessel
③ Rupture of Primary Coolant Pipe in Blanket
④ Rupture of Primary Coolant Pipe in Plasma Vacuum Vessel
⑤ Rupture of Cryopump
⑥ Rupture of Cryopump Gate Valve
⑦ Rupture of Fuel Gas Circulation System (FCS)
⑧ Rupture of Breeding Blanket Tritium Recovery System (BRS)
⑨ Rupture of Tritium Storage System (TSS)

Fig.VIII-6-1 Model of Failure Modes for Tritium Systems

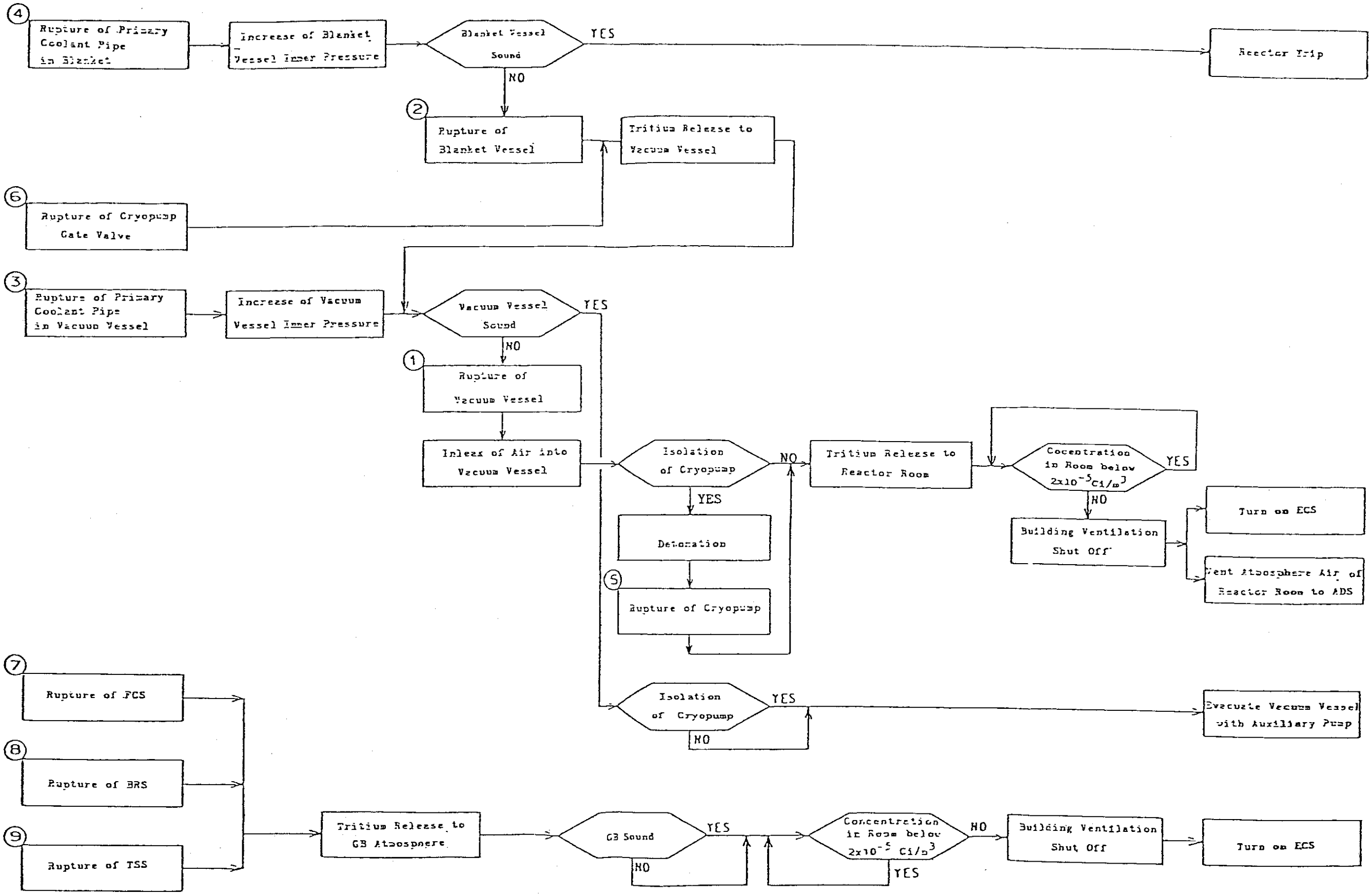

Fig.VIII-6-2 Accident Progression Sequences for Tritium Systems

(b) Pressure Response in Vacuum Vessel during Pipe Rupture Accidents

Pressure response in vacuum vessel was calculated to examine its integrity when a pipe was ruptured in it.

(1) Analytical Model

① The cooling system and the vacuum vessel are considered as a single volume, respectively.

② Discharge flow from the ruptured pipe is assumed to be critical flow into the vacuum vessel.

③ Steam and water in the volume are assumed to be in a condition of thermal equilibrium.

④ Decay heat in structural material is considered.

⑤ Residual heat of the first wall is considered.

⑥ If the pressure in the vacuum vessel is higher than the one in the cooling system, it is assumed that discharge flow from ruptured pipe is zero but reverse flow to the cooling system does not take place.

(2) Analytical Conditions

Analytical conditions are shown in Table VIII-6-3.

Primary cooling system is pressurized by surge tanks at normal operational condition. Its pressure and maximum temperature (temperature at outlet of reactor) are 1 MPa and 90°C, respectively. If surge tanks work after pipe rupture, the pressure in vacuum vessel does not rise so high as generated, steam is condensed since a large mount of water blows into the vacuum vessel.

On the other hand, if the surge tanks don't work, water flowing into the vacuum vessel is considered to evaporate by residual heat more than the former case and the pressure in the vacuum vessel will rise due to the steam generated. So this case is considered to be one of the most severe cases for the vacuum vessel. Therefore, in this analysis surge tanks are assumed not to work.

Rupture was assumed to take place either of a blanket pipe (200 mm I.D.) or a first wall cooling pipe (12 mm I.D.). Assumed rupture shape was a double-ended.

(3) Analytical Results

Pressure responses in the cooling system and the vacuum system are shown in Fig. VIII-6-3.

Pressures in the vacuum vessel rise up to about 5 kgf/cm^2 (0.51 MPa) in the case of the rupture of the blanket pipe, and about 6 kgf/cm^2 (0.61 MPa) in the case of the rupture of the first wall cooling tube.

As the allowable design pressure of the vessel is of the order of 2 $\sim$ 3 kgf/cm^2 (0.2 $\sim$ 0.3 MPa), the vacuum vessel may be failed. Therefore it is required to install a device to release the pressure, such as rupture disk.

It should be noted here however, it takes tens of second before the pressure builds up to such a high pressure.

Table VIII-6-3 Analytical Conditions

Surface Area of First Wall	380 m^2
Thickness of First Wall	20 mm
Initial Temperature of First Wall	350°C
Surface Area of Structure	7010 m^2
Surface Temperature of Structure	120°C
Surface Heat Transfer Coefficients	
Surface of First Wall	300 $kcal/m^2 \cdot hr \cdot °C$
Surface of Structure	10 $kcal/m^2 \cdot hr \cdot °C$
Volume in Primary Cooling System	500 m^3
Volume in Vacuum Vessel	850 m^3
Initial Temperature in Primary Cooling System	90°C

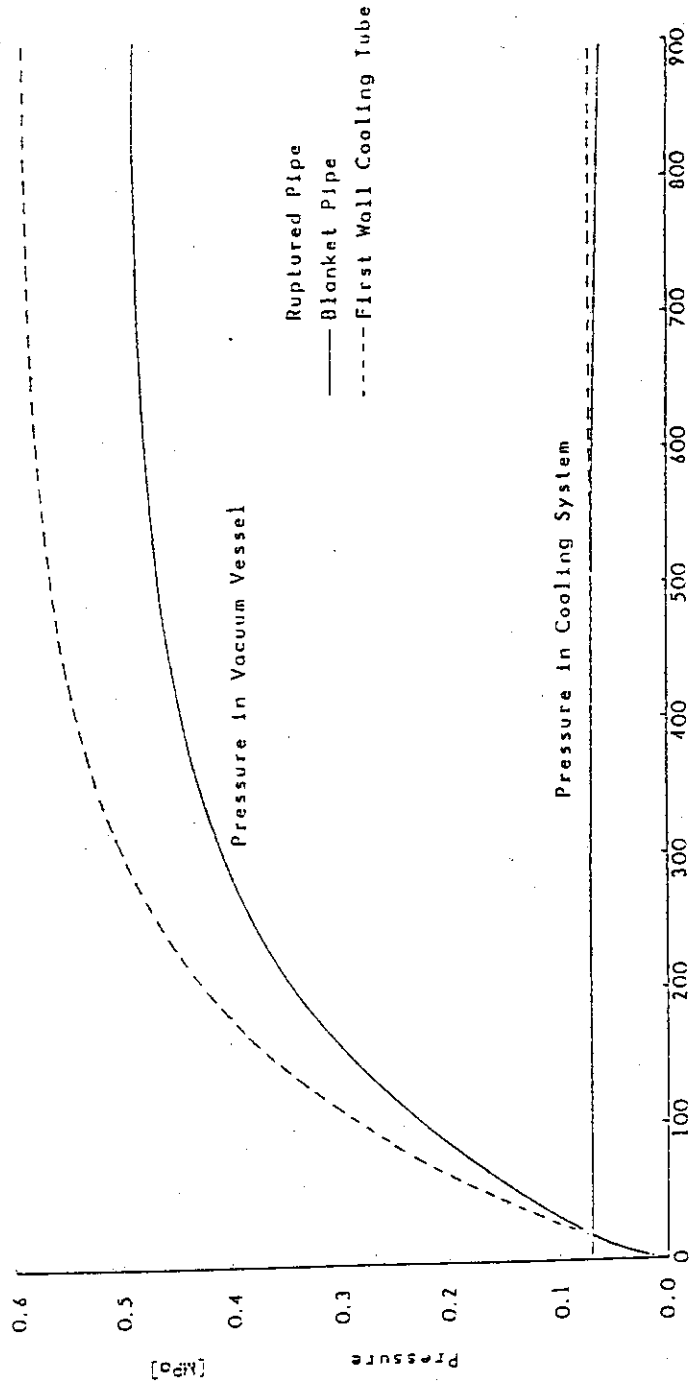

Fig. VIII-6-3 Pressure Response after Pipe Rupture

(c) Tritium Release due to Rupture of Bellows

Bellows structure is adopted to increase the electric resistance in toroidal direction of the vacuum vessel. An examination on tritium release due to rupture of bellows is carried out in this section.

As the inside of the vacuum vessel is vacuum and the outside of it is atmospheric, it is obvious that air flows into the vacuum vessel if bellows fails, and no tritium gas is released out of it. Therefore, in this section, an analysis is carried out on tritium release after both pressures become to be equalized.

The major processes for tritium release are considered as follows:

① Concentration diffusion

② Thermal expansion of air in vacuum vessel

③ Exchange between inside and outside of the vacuum vessel due to natural convection through the failure part.

The quantity of release due to natural convection (③) is largest if an upper part of vessel fails. Therefore, such a failure is considered in this study.

Tritium gas is assumed to be homogeneous in distribution in the vacuum vessel.

(1) Tritium Source for Release

Tritium gas in the vacuum vessel during the plant operation and in structural materials are considered as the tritium source for release. Tritium in the cryopump is not considered here.

(i) Quantity of Tritium in the Vacuum Vessel

Quantity of tritium in the vacuum vessel during the plant operation is about 830 Ci as shown in Table VIII-6-4. Conditions for calculation are shown in Table VIII-6-5.

(ii) Quantity of Tritium Released into the Vacuum Vessel

Once air flows into the vacuum vessel, plasma disappears and structures are heated by decay heat. However, since the cooling system continues to work, the temperature of the structure is assumed to be 50°C.

As described in 2.1.5, tritium released into the vacuum vessel is almost one from the divertor. Therefore, it is assumed that the tritium is released from only divertor.

(2) Analytical Method

(i) Tritium Release Rate due to Concentration Diffusion

Tritium concentrations of inside and outside of the vacuum vessel are assumed to be C [Ci/m^3] and 0 [Ci/m^3], respectively.

Then tritium release rate through ruptured part is obtained as follows with Fick's first law of diffusion.

$$G_{CD} = \frac{D'Ac}{l} \qquad \text{(VIII-6-1)}$$

where, G_{CD} : tritium release rate through ruptured part [Ci/sec]

D' : diffusion coefficient of T_2 - air system [m^2/sec]

l : length of ruptured part [m]

A : cross-sectional area of ruptured part [m^2]

Since the tritium concentration of inside of the vacuum vessel is described as

$$c = \frac{m}{V}$$

where, m : tritium quantity in the vaccum vessel [Ci]
V : free volume of the vacuum vessel [m^3]

tritium release rate due to concentration is obtained as

$$G_{CD} = \frac{D'A}{Vl} m \qquad \text{(VIII-6-2)}$$

By the way, diffusion coefficient of T_2-air system is obtained with Fujita's eq. described below.

$$D' = \frac{6.7 \times 10^{-8} \, T^{1.83}}{P\left[\left(\frac{T_c}{P_c}\right)_1^{1/3} + \left(\frac{T_c}{P_c}\right)_2^{1/3}\right]^3} \cdot \sqrt{\frac{1}{M_1} + \frac{1}{M_2}} \qquad \text{(VIII-6-3)}$$

where, P	:	pressure	[atm]
T_c	:	critical temperature	[K]
P_c	:	critical pressure	[atm]
T	:	temperature	[K]
M	:	molecular weight	[g/mol]
Subscript 1, 2 :		values for gas 1 and 2, respectively	

Physical properties are shown in Table VIII-6-6.

Using P = 1 [atm] and T = 50°C, diffusion coefficient is as follows:

$$D' = 5.29 \times 10^{-5} \quad [m^2/sec]$$

(ii) Tritium Release Rate due to Thermal Expansion of Air

The temperature of air of W [kg] heated by Q [kcal/sec] is derived with following equation.

$$wc_p \frac{dT}{dt} = Q \qquad \text{(VIII-6-4)}$$

where, C_p : isobaric specific heat capacity [kcal/kg·K]
T : temperature of air [K]
t : time [sec]

Assuming air to be ideal gas, following equation of states holds good,

$$pV = \frac{w}{M} RT \qquad \text{(VIII-6-5)}$$

where, p : pressure in vacuum vessel [kgf/m^2]
V : volume in vacuum vessel [m^3]
M : molecular weight of air [kg/kmol]
R : gas constant (=847.8) [kgf·m/kmol·K]

By the way, assuming that the cause of heating of air is heat transfer from component's surface to air due to natural convection, the heating rate Q is described as follows:

$$Q = \alpha(T_w - T)S' \qquad \text{(VIII-6-6)}$$

where, α : heat transfer coefficient [$kcal/m^2 \cdot sec \cdot K$]
T_w : surface temperature of components [K]
S' : heat transfer area [m^2]

The following equation is obtained from eqs. (VIII-6-5) - (VIII-6-6).

$$\frac{dw}{dt} = -\frac{\alpha S' R T_w}{p V c_p M}\left(w - \frac{pVM}{RT_w}\right) \qquad \text{(VIII-6-7)}$$

Integrating eq. (VIII-6-7)

$$w = \frac{pVM}{RT_w}\left[1 - \left(1 - \frac{T_w}{T_0}\right)e^{-\frac{t}{\tau}}\right] \qquad \text{(VIII-6-8)}$$

where,

$$\tau = \frac{p V c_p M}{\alpha S' R T_w}$$

T_0 : initial temperature of air [K]

As the air flow rate due to thermal expansion of air is -dw/dt, the tritium release rate G_{TE} [Ci/sec] due to thermal expansion is described as follows:

$$G_{TE} = \frac{-\frac{dw}{dt}}{w} m$$

$$= \frac{1}{\tau}\left[1 - \frac{1}{1 + (T_w/T_0 - 1)e^{-t/\tau}}\right] m \qquad \text{(VIII-6-9)}$$

(iii) Tritium Release Rate due to Natural Convection

A calculation model is shown in Fig. VIII-6-4.

Following equations hold with respect to flow path I (a path flowing out of the vacuum vessel) and flow path II (a path flowing into the vacuum vessel):

As the volume of the vacuum vessel,

$$A_I u_I = A_{II} u_{II} \qquad \text{(VIII-6-10)}$$

From pressure balance

$$\text{(Flow path I)} \qquad p_1 - p_2 = \zeta \frac{u_I^2}{2g v_1} + \frac{l}{v_1} \qquad \text{(VIII-6-11)}$$

$$\text{(Flow path II)} \qquad p_2 - p_1 = \zeta \frac{u_{II}^2}{2g v_2} - \frac{l}{v_2} \qquad \text{(VIII-6-12)}$$

As summation of flow areas of path I and II is constant,

$$A_I + A_{II} = A \qquad \text{(VIII-6-13)}$$

Assignment of flow area is decided such as to maximize the outflow rate:

$$\frac{d}{dA_I}\left(\frac{A_I u_I}{v_1}\right) = 0 \qquad \text{(VIII-6-14)}$$

where, A : flow area of ruptured part [m^2]
u : flow velocity [m/sec]
p : pressure [kgf/m^2]
ζ : inlet loss factor of pressure [-]
g : acceleration of gravity (=9.807) [m/sec^2]
v : specific volume [m^3/kgf]
l : length of flow path [m]

Subscript I : flow path I
II : flow path II
1 : inside of the vacuum vessel
2 : outside of the vacuum vessel

Airs in flow path I and II are assumed to be the same as ones in the inside and the outside of the vacuum vessel, respectively.

Flow area A_I and A_{II} and flow velocities u_I and u_{II} are obtained as follows from eqs. (VIII-6-10) - (VIII-6-13).

$$A_I = \frac{A}{1 + (v_1/v_2)^{1/3}} \qquad \text{(VIII-6-15)}$$

$$A_{II} = \frac{(v_1/v_2)^{1/3}}{1 + (v_1/v_2)^{1/3}} A \qquad \text{(VIII-6-16)}$$

$$u_I = \sqrt{\frac{2gl}{\zeta} \cdot \frac{(v_1/v_2) - 1}{1 + (v_1/v_2)^{1/3}}} \qquad \text{(VIII-6-17)}$$

$$u_{II} = (v_2/v_1)^{1/3} u_I \qquad \text{(VIII-6-18)}$$

Therefore, the tritium release rate G_{NC} [Ci/sec] is expressed as follows,

$$G_{NC} = \frac{A_I u_I}{V} m$$

$$= \frac{A}{V} \cdot \frac{m}{1+(v_1/v_2)^{1/3}} \sqrt{\frac{2gl}{\zeta} \cdot \frac{(v_1/v_2) - 1}{1+(v_1/v_2)^{1/3}}} \qquad \text{(VIII-6-19)}$$

(iv) Quantity of Tritium released

Quantity of tritium in the vacuum vessel is obtained by solving the following equation:

$$\frac{dm}{dt} = S_s \cdot \sqrt{\frac{D}{\pi t}} - G_{CD} - G_{TE} - G_{NC} \qquad \text{(VIII-6-20)}$$

Quantity of tritium m_{TR} [Ci] released into the reactor room from the vacuum vessel is obtained as follows by using m,

$$\frac{dm_{TR}}{dt} = G_{CD} + G_{TE} + G_{NC} \qquad \text{(VIII-6-21)}$$

(3) Analytical Results

Analytical conditions are shown in Table VIII-6-7.

As bellows are installed at the outside surface of the shield between two segments, width of the ruptured part is assumed to be the width of gap between two segments and its value to be 1 cm. Flow path length is assumed as the thickness of the shield.

Results of the analysis are shown in Fig. VIII-6-5. 70 Ci of tritium is released to the reactor room in about 30 seconds for all area of the ruptured bellows. Tritium release due to thermal expansion is dominant in this process.

After that, the release due to natural convection is dominant and the release quantity due to concentration diffusion is negligible small. If the length of the ruptured bellows is 10 cm, the tritium release rate is very small after that, while 400 Ci of the tritium is released within one hour if one circle bellows ruptured.

In the case of large scale rupture of the bellows, the tritium in the vacuum vessel is released to the reactor room in a relatively short time after the accident. But, as in the case of small scale rupture much tritium is remained in the vacuum vessel for a long time.

Table VIII-6-4 Quantities of Tritium in Vacuum Vessel

Region	Quantity of Tritium
Plasma	810 [Ci]
Plasma Chamber (Except Plasma)	2
Vacuum Vessel	19
Total	831

Table VIII-6-5 Conditions for Calculation

	Value	[Unit]
Plasma Volume	241	[m^3]
Volume of Plasma Chamber	320	[m^3]
Volume of Vacuum Vessel	850	[m^3]
Av. DT Ion Density (in Plasma)	1.4×10^{20}	[m^{-3}]
Partial Pressure of Tritium in Plasma Chamber	2×10^{-5}	[Torr]
Temperature in Plasma Chamber	350	[°C]
DT Pressure in Vacuum Vessel	1×10^{-5}	[Torr]
Temperature in Vacuum Vessel	50	[°C]

Table VIII-6-6 Physical Properties of T_2 and Air

T_2	Critical Temperature	Tc	43.7 [K]
	Critical Pressure	Pc	20.8 [atm]
	Molecular Weight	M	6.03 [g/mol]
Air	Critical Temperature	Tc	132.5 [K]
	Critical Pressure	Pc	37.2 [atm]
	Molecular Weight	M	28.96 [g/mol]

Table VIII-6-7 Analytical Conditions

Pressure in Vacuum Vessel, P_1	1 kgf/cm^2 (0.1 MPa)
Pressure in Reactor Room, P_2	1 kgf/cm^2 (0.1 MPa)
Temperature in Vacuum Vessel, T_1	50°C
Temperature in Reactor Room, T_2	20°C
Initial Temperature of Air, T_0	20°C
Surface Temperature of Components, Tw	50°C
Volume in Vacuum Vessel, V	850 m^3
Surface Area of Divertor, S	160 m^2
Surface Area of Components, S'	7010 m^2
Diffusion Coefficient of Divertor, D (Tungsten, 50°C)	1.93×10^{-9} cm^2/sec
Surface Heat Transfer Coefficient, α	10 kcal/m^2.hr.°C
Molecular Weight of Air, M	28.96 g/mol
Isobaric Specific Heat Capacity of Air, Cp (at 50°C)	0.240 kcal/kg.°C
Loss Factor, ζ	1.2
Length of Flow Path, ℓ	1.4 m

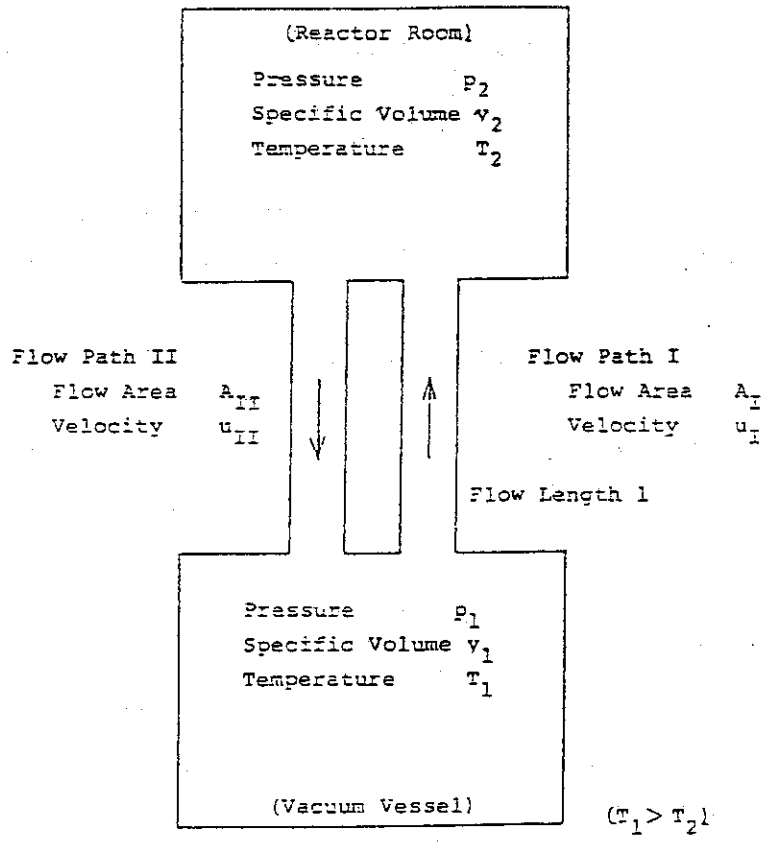

Fig. VIII-6-4 Model of Natural Convection

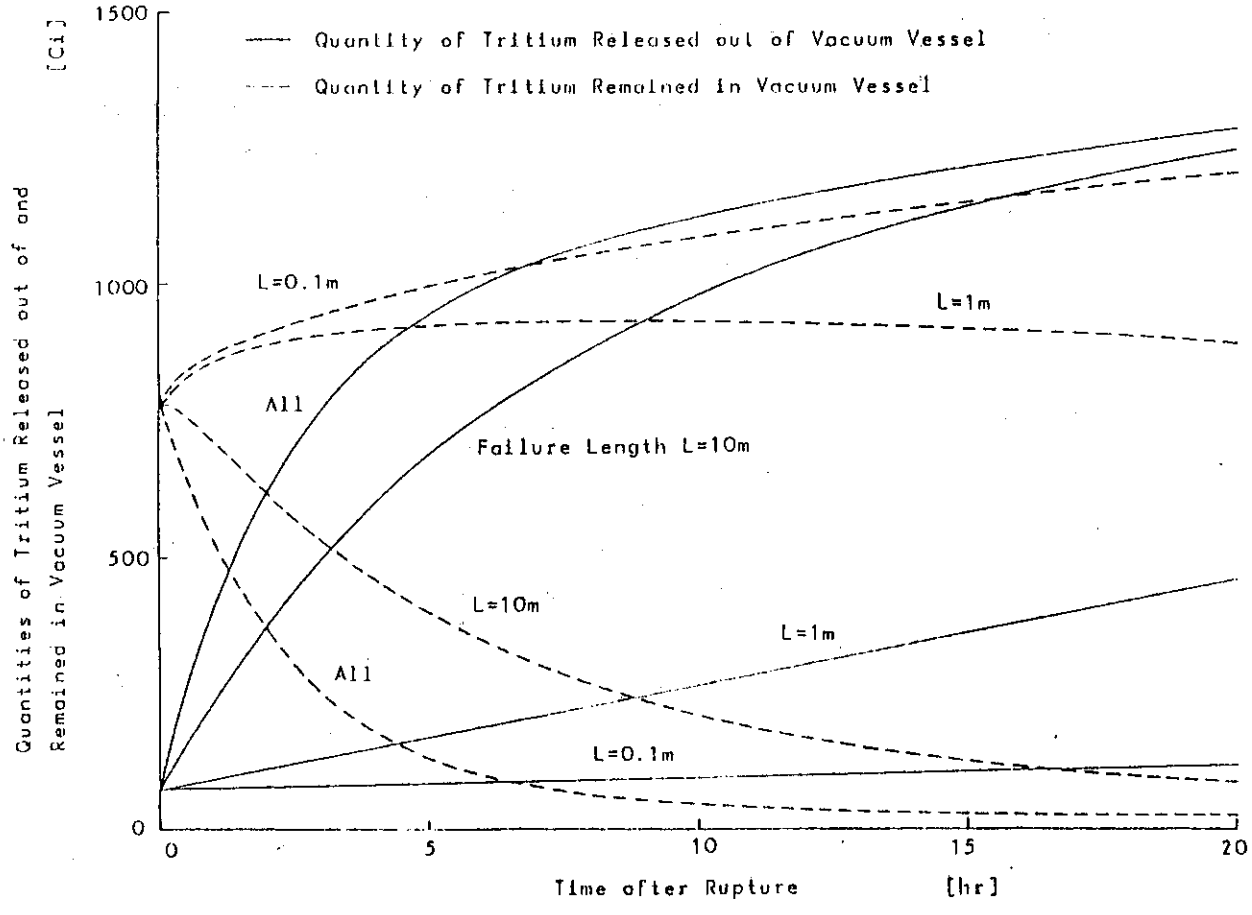

Fig.VIII-6-5 Quantities of Tritium Released out of and Remained in Vacuum Vessel

(d) Transient Analysis for Coolant Leakage in Blanket Module

(1) Objective

The objective of this analysis is to estimate the pressure response in the tritium breeding blanket following the leak of coolant in the blanket. The results of this analysis are used as preliminary data to evaluate integrity of the blanket structure.

(2) Analytical Model

1) Blanket Model

As illustrated in Fig. VIII-6-6, the blanket module is modeled as one node vessel whose free volume is assumed to be filled with helium gas of 1 kgf/cm^2, initially.

In the actual system, the blanket module is connected to the breeding blanket tritium recovery system through the tritium purge line.

2) Calculational Model for Leak Flow Rate

Assuming that the pressure of coolant supply system is constant and the effect of flushing can be neglected, the leak flow rate is expressed by the following equation.

$$G_{in} = A\sqrt{\frac{2g(P_w - P)}{\zeta V}}$$

where, G_{in} : leak flow rate [kg/sec]
A : leak area [m^2]
g : gravitational acceleration [m/sec^2]
P_w : coolant pressure [kgf/cm^2a]
P : blanket inner pressure [kgf/cm^2a]
ζ : loss coefficient
V : specific volume [m^3/kg]

3) Calculational Model for Heat Addition Rate

Possible heat supply sources for the blanket are:

① Surface heat load

② Nuclear heating rate

③ Reaction heat of $Li_2O - H_2O$

④ Decay heat

Among the above heat sources, ③ was not considered in this study because of difficulties of modeling at present. So, ① and ② were considered during the rated power operation, and ④ was considered following the reactor shutdown.

Heat addition rate to the leak flow from structural and breeder materials can be estimated as follows:

$$Q_e = G_{in} \times \{U_G(T_W) - U_L(T_C)\}$$

where, Q_e : heat addition rate to the leak flow [kcal/sec]
U_G : steam internal energy [kcal/kg]
T_W : temperature of the blanket module [°C]
U_L : leak water internal energy [kcal/kg]
T_C : leak water temperature [°C]

i) Heat Balance during the Rated Power Operation

$$mc \frac{dT_W}{dt} = Q_{rat} - Q_e - hs\ (T_W - T_{bulk})$$

where, mc : thermal capacity of the blanket module [kcal/°C]
Q_{rat} : rated thermal power (per one blanket module) [kcal/sec]

h : heat transfer rate (per one blanket module) [kcal/m^2·sec°C]

s : total heat trasnfer area of coolant tube (per one blanket module) [m^2]

T_{bulk} : bulk temperature of water coolant [°C]

ii) Heat Balance after the Reactor Shutdown

$$mc \frac{dT_W}{dt} = Q_{de} - Q_e - hs(T_W - T_{bulk})$$

where, Q_{de} : decay heat after the reactor shutdown [kcal/sec]

The computer code (BLOCK) is used in this analysis.

(3) Analytical Conditions

Main analytical conditions are shown in Table VIII-6-8. The analyses have been performed for three leak areas, two free volumes, and two modes of reactor operation.

(4) Results

1) Effects of the Leak Area and the Free Volume

Fig. VIII-6-7 shows the pressure responses in blanket after the leak of coolant tube during rated power operation. In this case, it was assumed that the leak could not be detected, and rated power operation was continued after the initiation of leak. Two cases of the free volume were considered. The first was blanket volume filled with helium (CASE A) and the second was 1 m^3 of volume in addition to the blanket volume (CASE B).

Naturally, the pressure response becomes more rapid as leak area becomes larger or free volume becomes smaller. The pressure increases to 3 kgf/cm^{2}a in 266 and 904 seconds after leak in the cases of A and B, respectively for leak area of 0.16 mm.

2) Effect of Reactor Shutdown

Figs. VIII-6-8 and VIII-6-9 show the pressure response in blanket module and temperature response of the structure after the reactor shutdown. The shutdown is initiated when blanket inner pressure is reached 1.2 kgf/cm^{2}a after the break of coolant tube.

In Fig. VIII-6-8 and VIII-6-9 show the pressure response in the leak area is 2 x 10^{-8}m^2 and 1m^2 is added to the free volume as the connected volume of the breeding blanket tritium recovery system.

3) Preliminary Conclusions

The following conclusions were obtained.

① When the leak area is relatively small (about 2 x 10^{-8} m^2), it may be possible to prevent the rupture of the blanket structure by the reactor shutdown.

② When the leak area is relatively large (2 x 10^{-7} m^2), the pressure response is too rapid to initiate the intentional reactor shutdown.

③ Large free volume is effective to ensure the sufficient margin of time for safety operation.

Table VIII-6-8 Major Analytical Conditions

Description	Unit	Value
Free Volume in a Blanket Module	m^3	0.4
Initial Pressure of Free Volume	Kgf/cm^2a	1.0
Initial Temperature of a Blanket Module (average)	℃	580
Break Area of Coolant Tube	m^2	$2\ 10^{-7} \sim 2\ 10^{-9}$
Loss Coefficient of Break Area		1.0
Pressure of Coolant	Kgf/cm^2a	10.0
Temperature of Coolant	℃	90
Thermal Capacity of a Blanket Module	Kcal/℃	1640
Rated Thermal Power in a Blanket Module	Kcal/sec	1240
Decay Heat after Plasma Shut Down	Kcal/sec	3.7

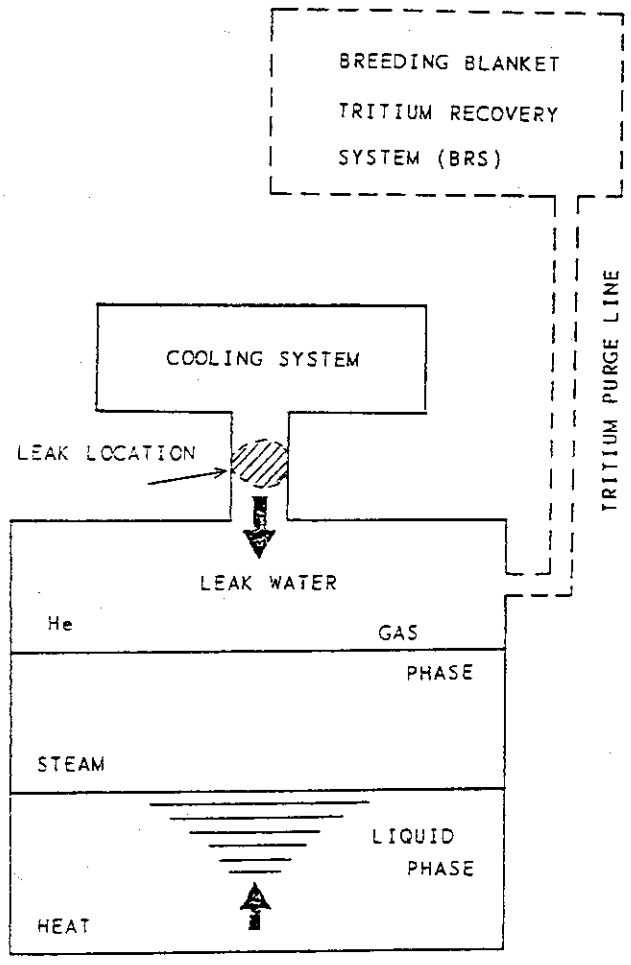

Fig. VIII-6-6 BLANKET MODEL

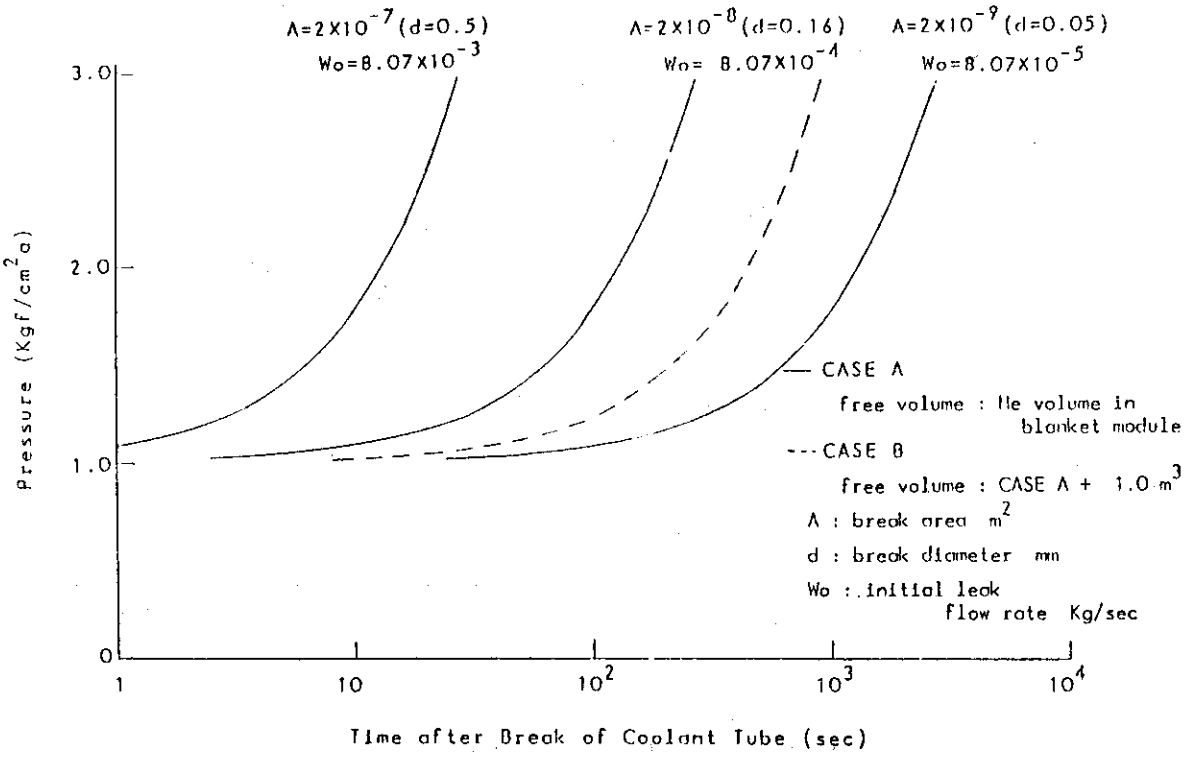

Fig. VIII-6-7 Pressure Response in Blanket after Break of Cooling Tube

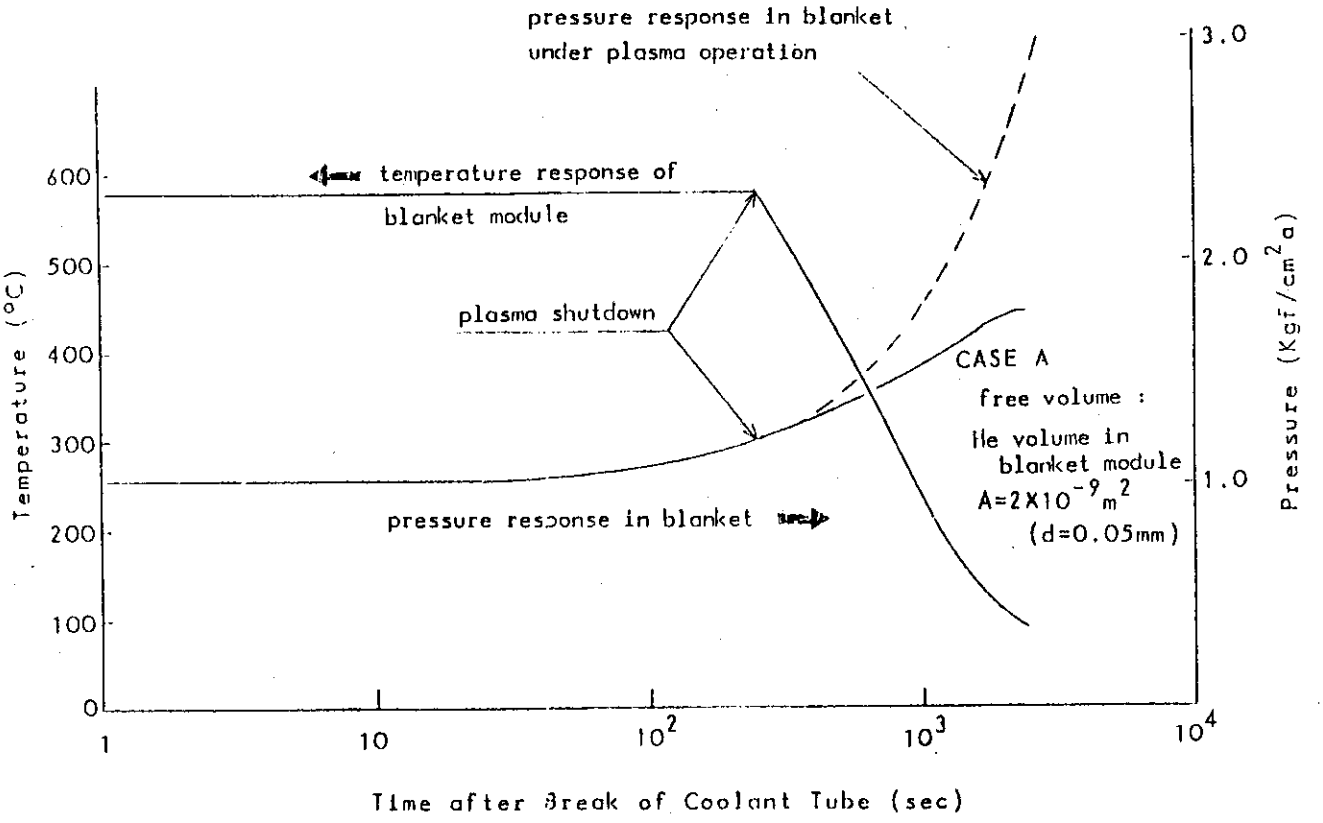

Fig. VIII-6-8 Pressure Response in Blanket and Temperature Response of Blanket Module after Break of Coolant Tube.

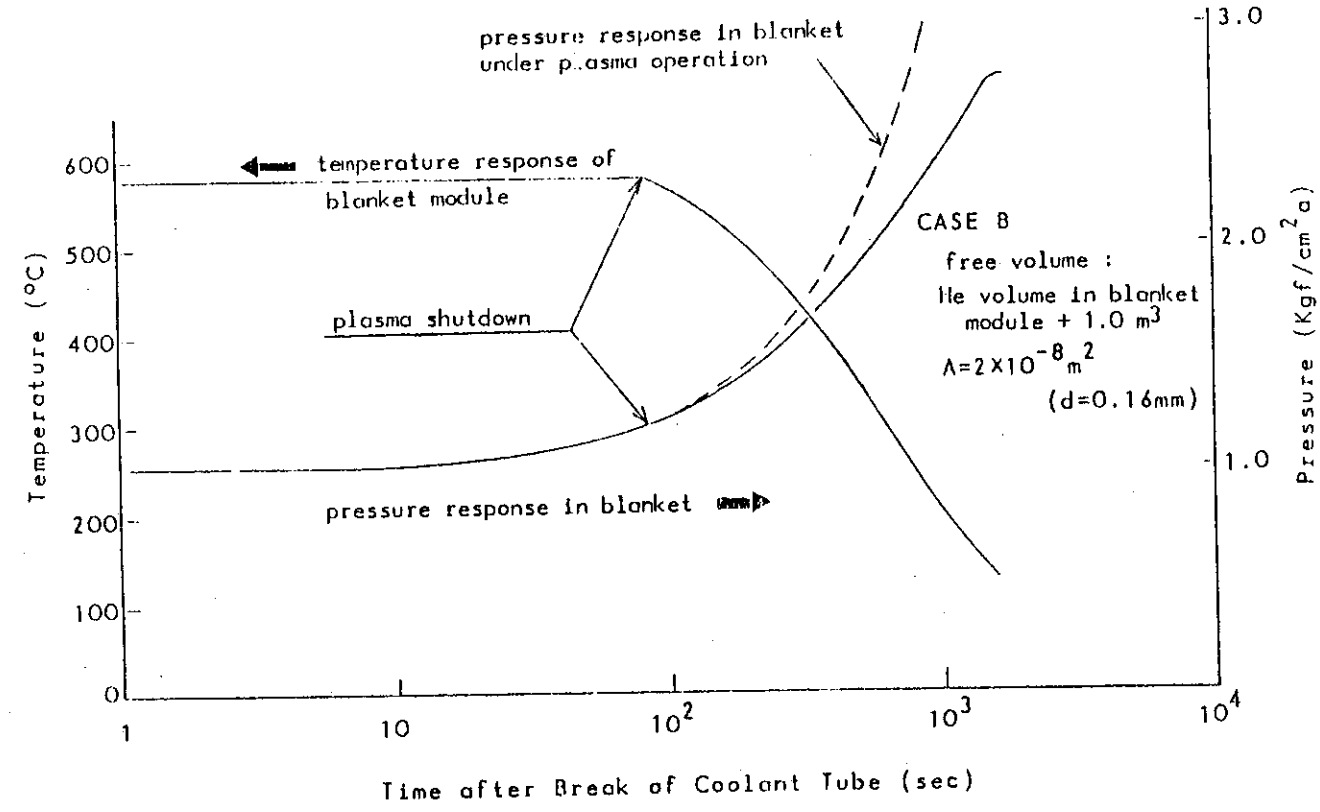

Fig. VIII-6-9 Pressure Response in Blanket and Temperature Response of Blanket Module after Break of Coolant Tube.

(e) Transient Analysis for Loss of Coolant Flow Accident due to Flow Blockage of the First Wall Cooling Tube

(1) Objectives

The transient analyses for a flow blockage of the first wall cooling tube have been carried out. The first wall is subjected to one of the most severe operating conditions due to the high surface heat load from the plasma and the high volumetric heat generation in the structure. Therefore the present study has been focused on the first wall. It is the purpose of this study to obtain the data for the evaluation of the first wall integrity in loss of coolant flow accident (LOFA) and the design of detection systems.

(2) Transient Analysis

The preliminary transient analyses for a flow blockage of the first wall cooling tube were carried out. The analyses were performed for two different scenarios of plasma operation. The first case considers that a flow blockage in a coolant channel could not be detected and normal operation of plasma would be still continuing after LOFA. The second case considers the automatic plasma shutdown is caused to prevent rupture of the blanket structure by detecting the malfunction.

The coolant flow rate is assumed to decrease instantaneously. The reduction rates of coolant flow are the parameters in this study.

It is assumed that LOFA can be detected when the coolant outlet temperature rises 10°C from its nominal value (90°C), and reactor is shut down so that plasma energy decays linearly to zero in 10 seconds. It was assumed that the volumetric heat generation in the structure due to decay heat after plasma shutdown was three percents of heating rates during normal operation.

These analyses have been carried out with a two-dimensional thermal analysis computer code. The model of the first wall analysed in this study is shown in Fig. VIII-6-10. Because of the limited capability of the program used in these analyses, no coolant boiling or coolant expulsion can be treated in the computer model. Principal conditions for the analyses are summarized in Table VIII-6-9.

(i) Flow Blockage with Continuous Plasma Operation

It was assumed in this analysis that a local flow blockage in a coolant channel of the first wall occurs but it could not be detected. Fig. VIII-6-11 shows the temperature response on the wall surface in the case of a flow blockage in a coolant channel. It is shown in this figure that the maximum temperature of the structure is kept under 350°C, even if the coolant mass flow rate reduces to 50% of the nominal value, due to the effect of adjacent normal coolant channels. Therefore the integrity of the first wall would be maintained in this condition. However, if the reduction rate of the coolant flow rate is larger than 50% or the flow blockages occur in two or more adjacent coolant channels, it seems to be difficult to maintain the integrity of the structure. Since the failure of a cooling tube would lead the introduction of the coolant into the vacuum vessel, a detection system for such a flow blockage is desirable.

(ii) Flow Blockage with Automatic Plasma Shutdown

Transient characteristics of the maximum temperature of the structure and the coolant outlet temperature are shown in Fig. VIII-6-12. In this analysis, the flow blockages in coolant channels are assumed to be detected by coolant temperature rise at the outlet and the automatic plasma shutdown is made by the

safety devices. This figure reveals that the temperature rise of the structure due to LOFA is below 20°C in every case, and the temperature decreases rapidly after plasma shutdown. Therefore the accident would be terminated without the failure of the blanket structure.

Table VIII-6-9 Analytical Conditions

Heat Load to First Wall		
Surface Heat Flux		
(plasma operation)	13.6	W/cm^2
(plasma shutdown)	none	
Volumetric Heat Generation		
(plasma operation)	13	W/cc
(plasma shutdown)	0.39	W/cc (3 %)
Coolant Conditions		
Inlet Temperature	50	°C
Outlet Temperature (normal operation)	90	°C
Coolant Velocity (normal operation)	1.8	m/sec
Heat Transfer Coefficient (normal operation)	11000	W/m^2K

*Heat transfer coefficient during LOFA is in proportion to $(W/W_0)^{0.8}$.

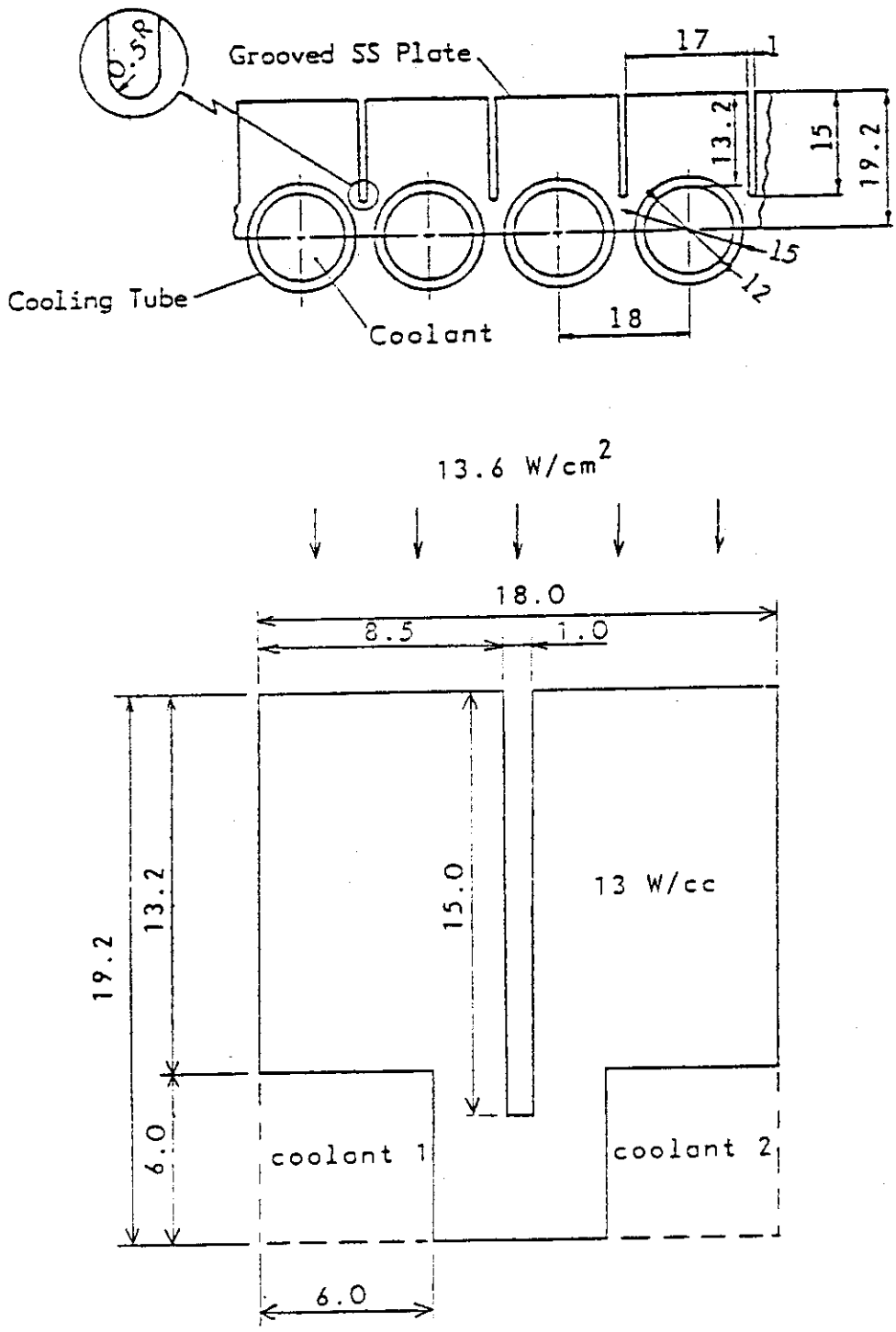

Fig. VIII-6-10 Analytical Model

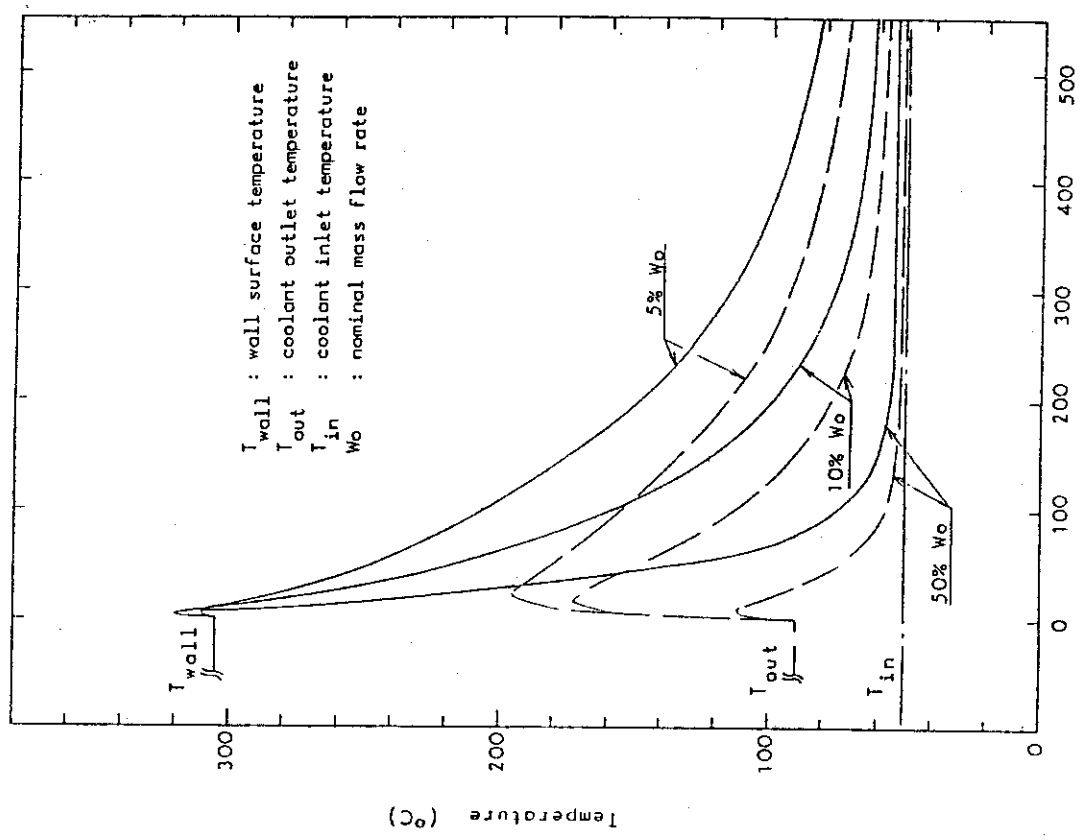

Fig. VIII-6-12 Temperature Response in Loss of Flow Accident with automatic Plasma Shutdown

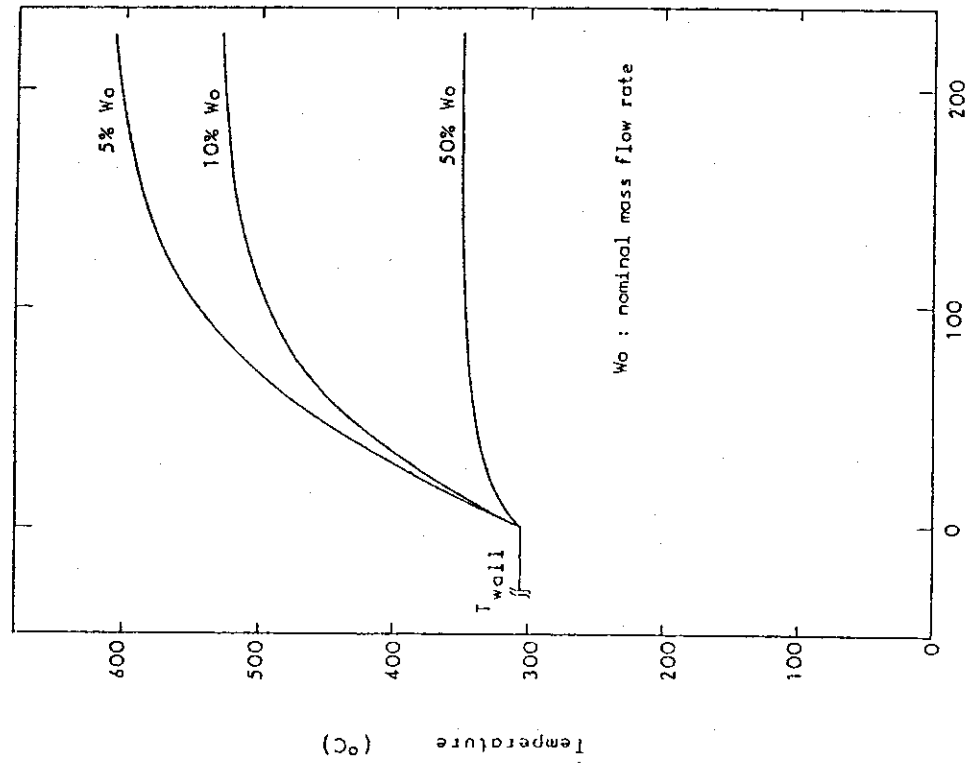

Fig. VIII-6-11 Temperature Response in Loss of Flow Accident with continuous Plasma Operation (single flow blockage)

6.2 Population dose

(a) Environmental Impact of the Tritium Released from the Stack

A case study of doses of radiation exposure to general population caused by tritium released from the stack was performed[55-58]. The major pathways of exposure with tritium were considered to be,

i) Internal exposure by inhalation and skin penetration of tritiated water vapor,

ii) Internal exposure by ingestion of vegetables, milk, and etc.,

iii) External radiation exposure by tritium β rays in air.

However, the 1st pathway seemed to be the biggest contribution in this evaluation(the doses from 2nd and 3rd pathways were about one-tenth of that of the 1st one), therefore, the evaluation was performed only the 1st pathway. Doses were also evaluated in two different cases; one is the ordinary release and the other is an accidental release. In order to evaluate dispersion, the meteorological data were obtained by the experiments using the meteorological tower, which is 90 high, placed 500 m away from the sea-shore and in the area flat land around. For the evaluation several weather conditions were assumed. In this evaluation all species released was regarded as tritiated water.

(1) The Evaluation of Tritium Concentration in Air

1) Average yearly concentration in normal operation

Assuming that the radioactive substance is continuously and constantly released, the geographical features around the release point is flat, and the decay of the tritium is neglected during dispersion, the concentration of the radioactive substance is expressed as eq. (VIII-6-22).

$$\chi(x, y, o) = \frac{Q}{\pi \cdot \sigma_Y \cdot \sigma_Z \cdot U} \cdot \exp\left(-\frac{y^2}{2\sigma_Y^2}\right) \cdot \exp\left(-\frac{H^2}{2\sigma_Z^2}\right) \quad \text{(VIII-6-22)}$$

where

$\chi(x, y, o)$: concentration of radioactive substance in the point(x, y, o) (Ci/m^3)

Q : release rate(Ci/h)

U : wind velocity (m/s)

H : height of effective release point (m)

σ_y : concentration cloud deviation parameters in the y direction

σ_z : concentration cloud deviation parameters in the z direction

The average yearly concentration in air above the ground level at the point receptor was calculated considering the concentration of one direction and the contribution of neighboring directions as shown in Fig. VIII-6-14.

$$\chi = \sum_{S=A}^{F} \left[\frac{Q}{3600\,\pi \cdot \sigma_{ys} \cdot \sigma_{zs} \cdot U_{S1}} \cdot \exp\left(-\frac{H_1^2}{2\sigma_{zs}^2}\right) \cdot Fs_1 \frac{Q}{3600 \cdot \pi \cdot \sigma_{ys} \cdot \sigma_{zs} \cdot U_{S2}} \right.$$

$$\left. \times \exp\left(-\frac{H_2^2}{2\sigma_{zs}^2}\right) \cdot F_{s2} + \frac{Q}{3600 \cdot \pi \cdot \sigma_{ys} \cdot \sigma_{zs} \cdot U_{S3}} \cdot \exp\left(-\frac{H_3^2}{2\sigma_{zs}^2}\right) \cdot F_{s3} \right]$$

(VIII-6-23)

where

σ_{ys} , σ_{zs} : σ_y, σ_z in atmospheric stability S

U_{S1} : wind velocity of wind direction in atmospheric stability S

U_{S2}, U_{S3} : wind velocity of neighboring directions in atmospheric stability S (m/s)

H_1 : effective height of release point for given direction (m)

H_2, H_3 : effective height of release point for neighboring directions (m)

F_{s1} : coefficient to obtain average value of the concentration in given direction at atmospheric stability S

F_{s2}, F_{s3} : coefficient to obtain average value of the concentration in neighboring directions at atmospheric stability S

where coefficients to obtain average value were induced following;

$$F_{s1} = \frac{\int_0^{y_1} \exp\left(-\frac{y^2}{2\sigma_{ys}^2}\right) dy}{y_1}$$

$$F_{s2} = F_{s3} = \frac{\int_0^{y_2} \exp\left(-\frac{y^2}{2\sigma_{ys}^2}\right) dy - \int_0^{y_1} \exp\left(-\frac{y^2}{2\sigma_{ys}^2}\right) dy}{y_2 - y_1}$$

(VIII-6-24)

$$y_1 = \frac{2\pi X}{16} \times \frac{1}{2} \pi x/16$$

$$y_2 = \frac{2\pi X}{16} \times \frac{3}{2} 3\pi x/16$$

X : distance of the point reciept from the release point (m)

The terms U_{S1}, U_{S2}, U_{S3} in (VIII-6-23) are the product of the inverse wind velocity and the wind direction for a given atmospheric stability each summed for an entire year. They are estimated by the following equation,

$$S_{d,s} = \sum_{i=1}^{N} \frac{{}_{d,s}\delta_i}{u_i}$$

where

N : number of data observed

u_i : wind velocity at time i (m/s)

${}_{d,s}\delta_i$: when wind direction is d and atmospheric stability S at time i, ${}_{d,s}\delta_i = 1$, except above ${}_{d,s}\delta_i = 0$.

The values of $S_{d,s}$ listed in Tables VIII-6-10 and VIII-6-11 were obtained respectively for a release at 40 m and 80 m at above ground level. The data in Tables VIII-6-12 and VIII-6-13 the frequency of a given wind direction at a given atmospheric stability, can be used to evaluate the effect of plume rise rate from the stack. In this evaluation the plume rise rate was assumed to be zero. The maximum average yearly concentration was shown in Fig. VIII-6-13 as a function of the distance of the point receptor X from the release point. The average concentration was evaluated in 16 directions with a release rate Q = 1 Ci/h(8760 Ci/y). The maximum average yearly dose 2.7×10^{-10} $\mu Ci/cm^3$ for a 40 m high stack occurred 400 m in down wind. For a 80 m high stack, the maximum average yearly dose 4.5×10^{-11} $\mu Ci/cm^3$ occurred 600 m in down wind. The concentration distribution in the down wind direction was shown in Fig. VIII-6-14 as a reference case assuming that the yearly weather condition was constant(u = 1, atmospheric stability : D in (VIII-6-22)). The maximum yearly dose was obtained assuming that the frequency of the wind direction was 15 %(the maximum value in Tables VIII-6-14 and VIII-6-15), that the release point was either 40 m

or 80 m above ground level, and that the wind velocity was 4 m/s or 6 m/s. The values are 7.2 X 10^{-10} μCi/cm^3 and 1.1 X 10^{-10} μCi/cm^3. These values compared with those obtained from meteorological data, while there is no big difference found.

2) Concentration Level for an Accidental Release

The concentration level in 16 directions from the release point was evaluated using meteorological data(wind direction, wind velocity, atmospheric stability) and the effective period of release. For this calculation, for a point receptor in a given direction was evaluated in the range 0.3 - 15 Km and then summed. The concentration level was assumed to be 97 % of the cumulateive yield. Eq. (VIII-6-25) was used to obtain the concentration level.

$$\chi/Q = \frac{1}{T} \sum_{i=1}^{T} (\chi/Q) \cdot d\delta_i \qquad \text{(VIII-6-25)}$$

where

χ/Q : concentration level during effective period of release

T : effective period of release

Q : release rate

$(\chi/Q)_i$: concentration level at time i

$d\delta_i$: if wind direction is given d direction, $d\delta_i = 1$, if wind direction is other than d direction, $d\delta_i = 0$

χ : concentration level on the axis of y = 0 in (VIII-6-22)

The maximum dose values at the point receptor X in 16 directions were shown as a function of distance from the release point in Fig. VIII-6-12 using observed meteorological data and assuming T = 1 in (VIII-6-25). The calculation was performed by the computor Code CQDQ developed in JAERI. The concentration level was 6.3 X 10^{-9} h/m^3 for a 40 m high stack, 800 m in down wind and 7.6 X 10^{-10} h/m^3 for a 80 m high stack, 2000 m in down wind.

(2) Doses by inhalation and by skin penetration

1) Yearly dose in normal operation

By assuming parameters given in ICRP, Pub. 2, the dose was calculated by (VIII-6-26).

$$D_m = \frac{K_1}{0.693\ m} \cdot f_a \cdot \varepsilon_m \cdot T_{em} \cdot M \cdot \bar{\chi}_i \qquad \text{(VIII-6-26)}$$

where

D_m : dose in organ(mrem/y, here body tissue)

K_1 : dose conversion factor, 1.87×10^7 (dis/MeV.q/ μCi· mrem/Y)

m : mass of body tissue, 4.3×10^4 g

f_a : ratio of incorporation of tritium in body tissue by inhalation 1

ε_m : effective energy of tritium radiation in body tissue 0.01 MeV

T_{em} : effective half life of tritium in body tissue 12 d

M : respiration rate, 2×10^7 cm^3/d

$\bar{\chi}$: average yearly concentration

The yearly dose in body tissue was obtained by (VIII-6-26) using average yearly concentration as calculated in sec. (1)-1). Results were tabulated in Table VIII-6-14.

2) Dose in an Accidental Release

Dose equivalent commitment in an accidental release was calculated by (VIII-6-27).

$$D_m = \frac{K_2}{0.693 \cdot m} \cdot f_a \cdot \epsilon_m \cdot T_{em} \cdot \left(\frac{\chi}{Q}\right) \cdot Q \cdot G \left(1 - e^{-\frac{0.693 \cdot T}{T_{em}}}\right) \qquad \text{(VIII-6-27)}$$

where

D_m : dose commitment for 50 years in body tissue(mrem)

K_2 : dose conversion coefficient, 2.1×10^9 (dis/MeV·q/ μCi· mrem/Y)

Q : amount of tritium released(Ci)
χ/Q : concentration level(h/m^3)

Other parameters than listed above were the same as those in sec. (2)-1). Dose commitment was calculated for 10000Ci tritium emission using the concentration level given in sec. (1)-2). Results were listed in Table VIII-6-15.

Calculated values of internal dose at the tritium release rate of 1 Ci/h for an entire year, were 0.82 mrem for a 40 m high stack and 0.14 mrem for a 80 m high stack, respectively. A design goal of INTOR-J aimed at the total release rate of gaseous effluent from the stack of the order of 1 Ci/d, internal dose of INTOR-J was considerably less than 500 mrem/y which is a limit dose in general population. If 10000Ci release occurres by an accidental release from the 40 m or 80 m high stack, the dose commitment was no more than 21.6 mrem or 2.6 mrem.

Table VIII-6-10 Sum of 1/(W,Spd) for Wind Direction and Stability (40 M)

Statistics from Jan. to Dec. (1978)

	NNE	NE	'ENE	E	ESE	SE	SSE	S	SSW	S*	*S*	W	*N*	N*	NNW	N	TOTL
A	4.28	2.77	5.60	19.61	10.17	8.18	8.17	3.03	3.21	8.12	5.70	5.77	3.75	8.74	4.77	3.53	105.59
B	48.89	57.85	60.94	74.04	41.56	56.07	43.12	33.72	28.40	44.76	35.72	21.29	44.54	71.87	81.08	59.83	803.86
C	7.93	29.97	17.30	5.98	5.27	9.09	20.26	5.17	8.31	19.68	13.67	9.09	5.73	7.42	13.05	10.40	186.56
D	101.07	149.55	69.80	33.58	15.80	26.33	40.19	37.46	34.70	73.46	43.41	31.06	43.08	78.56	126.24	82.48	988.78
E	17.02	15.28	6.38	2.53	2.03	2.70	7.92	9.16	14.36	11.01	10.27	3.37	2.24	2.28	7.45	9.60	118.72
F	121.08	99.41	67.10	62.17	31.25	51.11	65.62	50.98	75.72	75.20	75.83	63.30	99.08	128.33	214.75	197.42	1530.35
TOTL	295.30	354.83	247.12	197.91	106.09	152.99	185.28	142.11	164.70	232.43	184.63	133.87	196.60	297.20	507.37	323.26	

Table VIII-6-11 Sum of 1/(W,Spd) for Wind Direction and Stability (80 M)

Statistics from Jan. to Dec. (1978)

	NNE	NE	'ENE	E	ESE	SE	SSE	S	SSW	S*	*S*	W	*N*	N*	NNW	N	TOTL
A	1.54	4.51	3.91	8.57	10.10	8.86	10.06	3.37	3.31	4.73	3.08	1.45	5.71	6.07	3.05	4.55	81.12
B	17.92	30.87	35.05	52.41	37.66	36.57	44.56	24.83	10.64	14.12	31.28	29.93	36.96	49.99	47.88	37.35	536.02
C	4.28	16.30	17.84	8.95	4.23	3.75	12.73	8.83	3.24	14.07	14.31	5.40	6.41	4.80	4.21	11.46	141.03
D	53.96	98.03	54.59	27.00	15.94	16.58	17.36	25.51	26.47	41.43	42.43	24.49	21.23	46.09	55.92	66.93	633.99
E	7.11	9.41	8.12	3.95	1.80	0.78	2.50	5.08	12.77	8.43	8.25	3.69	1.68	1.45	2.26	5.86	83.11
F	90.48	57.87	51.84	42.91	25.94	24.04	27.86	28.61	41.38	51.22	57.39	38.06	33.78	97.32	93.33	116.96	899.18
TOTL	175.28	216.79	171.35	143.77	95.67	90.57	115.29	96.24	99.81	134.40	156.73	103.02	125.97	205.72	206.64	243.12	

Table VIII-6-12 Frequency(%) of Wind Direction and Stability (40 M)

Statistics from Jan. to Dec. (1978)

	NNE	NE	ENE	E	ESE	SE	SSE	S	SSW	SW	WSW	W	WNW	NW	NNW	N	TOTL
A	0.05	0.05	0.13	0.36	0.26	0.18	0.15	0.03	0.03	0.10	0.07	0.11	0.10	0.13	0.06	0.05	1.87
AB	0.34	0.37	0.61	0.79	0.60	0.70	0.41	0.20	0.21	0.24	0.34	0.23	0.38	0.37	0.51	0.33	6.04
B	0.44	0.79	0.89	0.75	0.47	0.83	0.76	0.31	0.23	0.36	0.40	0.29	0.36	0.47	0.57	0.48	8.39
BC	0.16	0.36	0.25	0.09	0.11	0.15	0.31	0.08	0.12	0.09	0.25	0.09	0.05	0.09	0.13	0.19	2.54
C	0.27	1.51	0.59	0.16	0.11	0.22	0.78	0.19	0.27	1.26	0.43	0.38	0.10	0.11	0.29	0.31	6.98
CD	0.15	0.06	0.25	0.0	0.0	0.0	0.41	0.11	0.08	0.27	0.20	0.11	0.05	0.07	0.11	0.08	2.77
D	4.08	8.60	2.63	0.87	0.25	0.49	1.11	1.51	1.11	3.15	1.31	0.76	0.89	1.34	2.47	2.47	33.05
E	0.70	0.92	0.34	0.14	0.07	0.11	0.37	0.53	0.72	0.63	0.60	0.19	0.12	0.12	0.28	0.37	6.27
F	0.43	0.58	0.38	0.20	0.13	0.12	0.23	0.36	0.60	0.62	0.48	0.11	0.22	0.14	0.30	0.35	5.65
-	2.37	1.70	1.30	0.73	0.35	0.61	0.81	0.74	1.32	1.60	1.39	1.00	1.47	1.64	4.54	3.62	25.62
TOTL	9.19	15.73	7.40	4.10	2.36	3.40	5.35	4.27	4.69	8.36	5.70	3.26	3.76	4.49	9.28	8.66	

Table VIII-6-13 Frequency(%) of Wind Direction and Stability (80 M)

Statistics from Jan. to Dec. (1978)

	NNE	NE	ENE	E	ESE	SE	SSE	S	SSW	SW	WSW	W	WNW	NW	NNW	N	TOTL
A	0.04	0.04	0.12	0.19	0.24	0.18	0.29	0.08	0.03	0.11	0.07	0.04	0.23	0.09	0.05	0.06	1.87
AB	0.27	0.32	0.40	0.70	0.64	0.64	0.68	0.30	0.08	0.12	0.36	0.37	0.65	0.46	0.48	0.43	6.91
B	0.31	0.51	0.91	0.76	0.39	0.57	1.09	0.27	0.16	0.27	0.51	0.33	0.53	0.57	0.49	0.58	8.49
BC	0.05	0.14	0.41	0.17	0.09	0.09	0.30	0.14	0.08	0.12	0.20	0.11	0.16	0.12	0.13	0.16	2.50
C	0.20	1.10	0.79	0.36	0.11	0.11	0.45	0.53	0.13	1.01	0.87	0.21	0.37	0.13	0.09	0.40	6.85
CD	0.08	0.74	0.37	0.07	0.0	0.0	0.08	0.25	0.08	0.21	0.43	0.07	0.17	0.04	0.07	0.08	2.72
D	3.33	7.84	3.70	1.08	0.49	0.44	0.66	1.07	1.54	2.70	2.05	1.16	0.84	1.03	1.55	3.24	32.72
E	0.56	0.70	0.56	0.26	0.09	0.04	0.16	0.37	0.93	0.68	0.67	0.32	0.16	0.09	0.12	0.47	6.16
F	0.46	0.93	0.46	0.29	0.21	0.13	0.11	0.21	0.68	0.57	0.67	0.24	0.08	0.18	0.28	0.60	5.61
-	4.02	2.00	1.29	0.73	0.46	0.39	0.62	0.62	1.02	1.60	1.88	1.18	1.51	2.06	1.88	4.97	26.23
TOTL	9.33	13.83	9.02	4.59	2.73	2.59	4.44	3.84	4.73	7.38	7.70	4.23	4.69	4.78	5.14	11.01	

Table VIII-6-14 Annual Dose Equivalent to Body Tissue due to Continous Release of HTO

Release Rate = 1 Ci/hr

	Stack Height (M)	Max. Conc. (μCi/cm^3)	Annual Dose (mrem)
Observed Meteorological Data	40	2.7×10^{-10}	0.82
	80	4.5×10^{-11}	0.14
Assumed Meteorological Data Stability = D Frequency Wind Direction = 15%	40 (W.S.) (4 m/s)	7.2×10^{-10}	2.2
	80 (W.S.) (6 m/s)	1.1×10^{-10}	0.33

Table VIII-6-15 Dose Equivalent to Body Tissue due to Accidental Release of HTO

Total Amount of Release = 10,000 Ci

Stack Height (M)	Max. Dispersion Factor χ/Q (h/m^3)	Dose Equivalent (mrem)
40	6.3×10^{-9}	21.4
80	7.6×10^{-10}	2.6

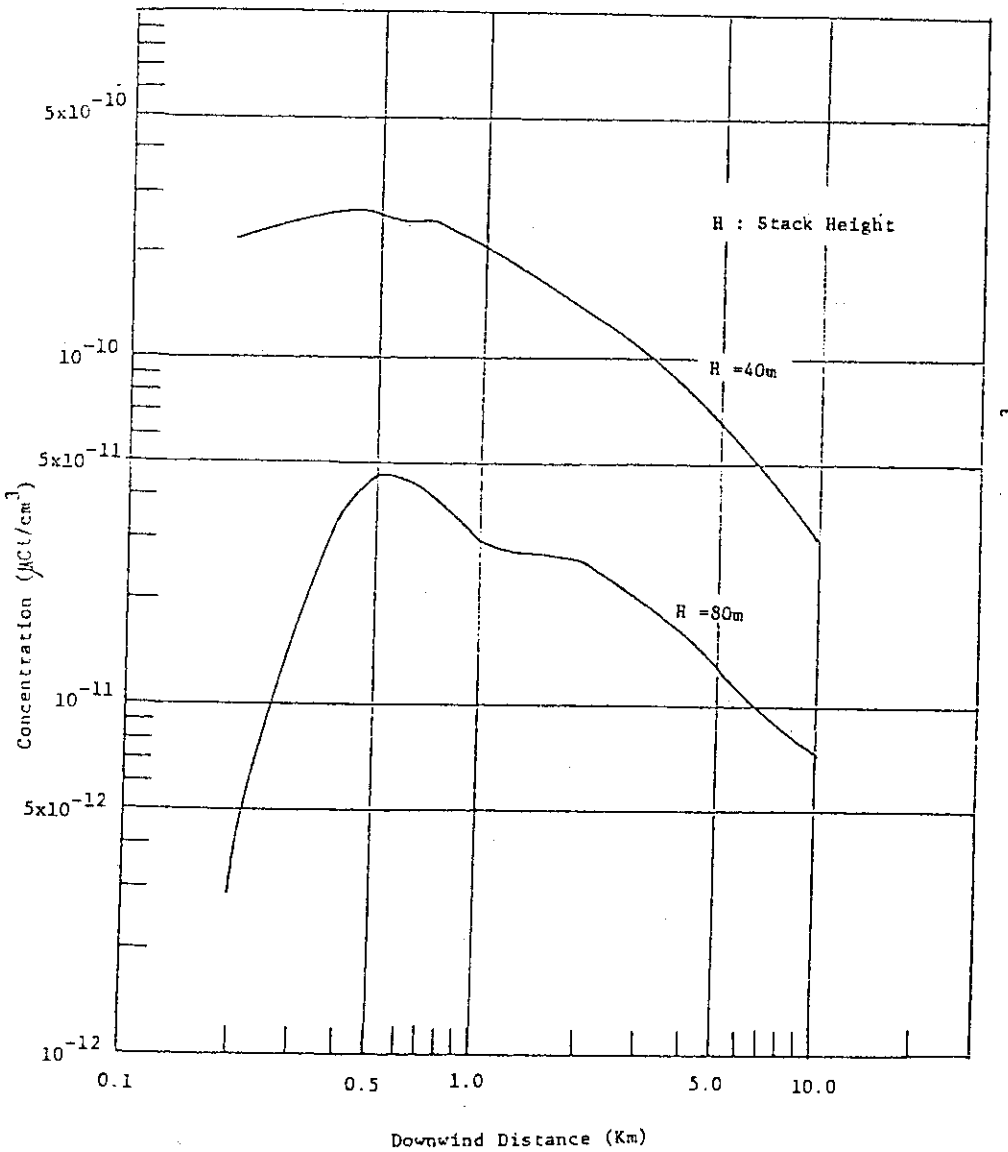

Fig. VIII-6-13 Yearly Mean concentration of HTO in the Air
Release Rate : 1 Ci/hr

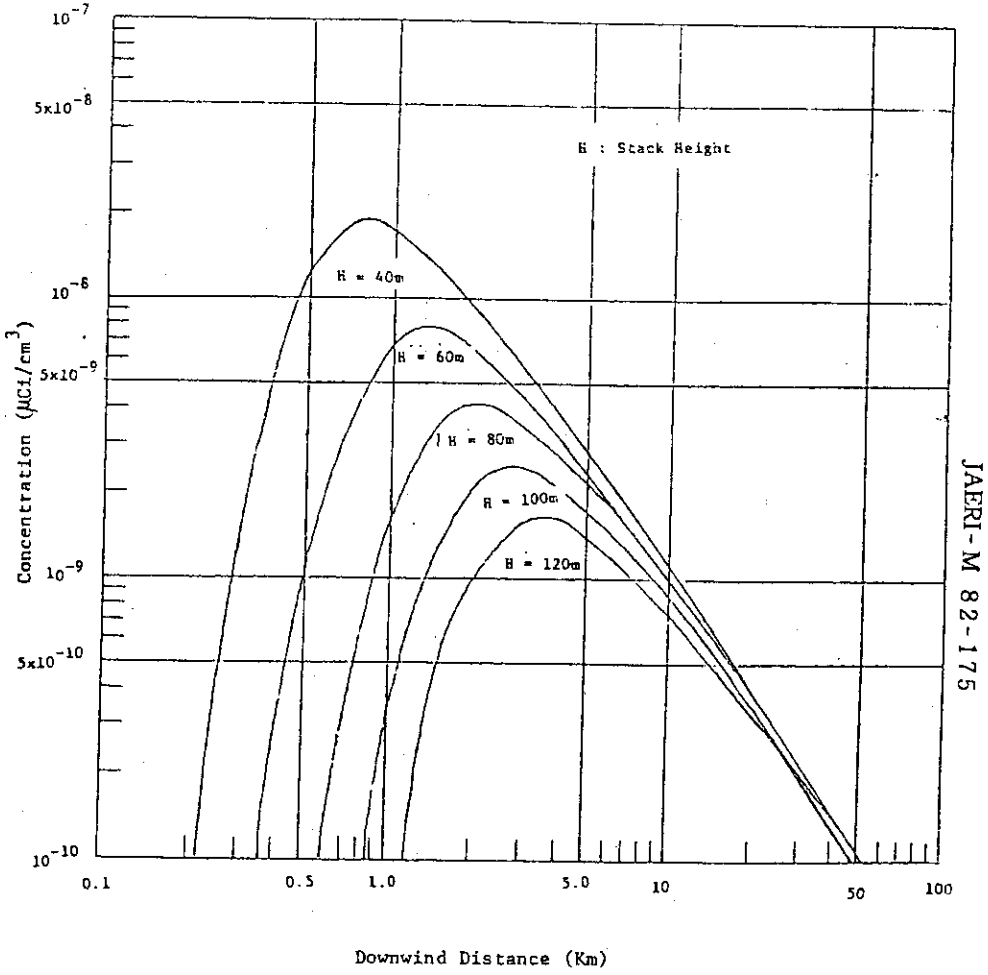

Fig. VIII-6-14 Distribution of Concentration in the Downwind

Stability : D

Wind Speed : 1 m/s

Release Rate : 1 Ci/hr

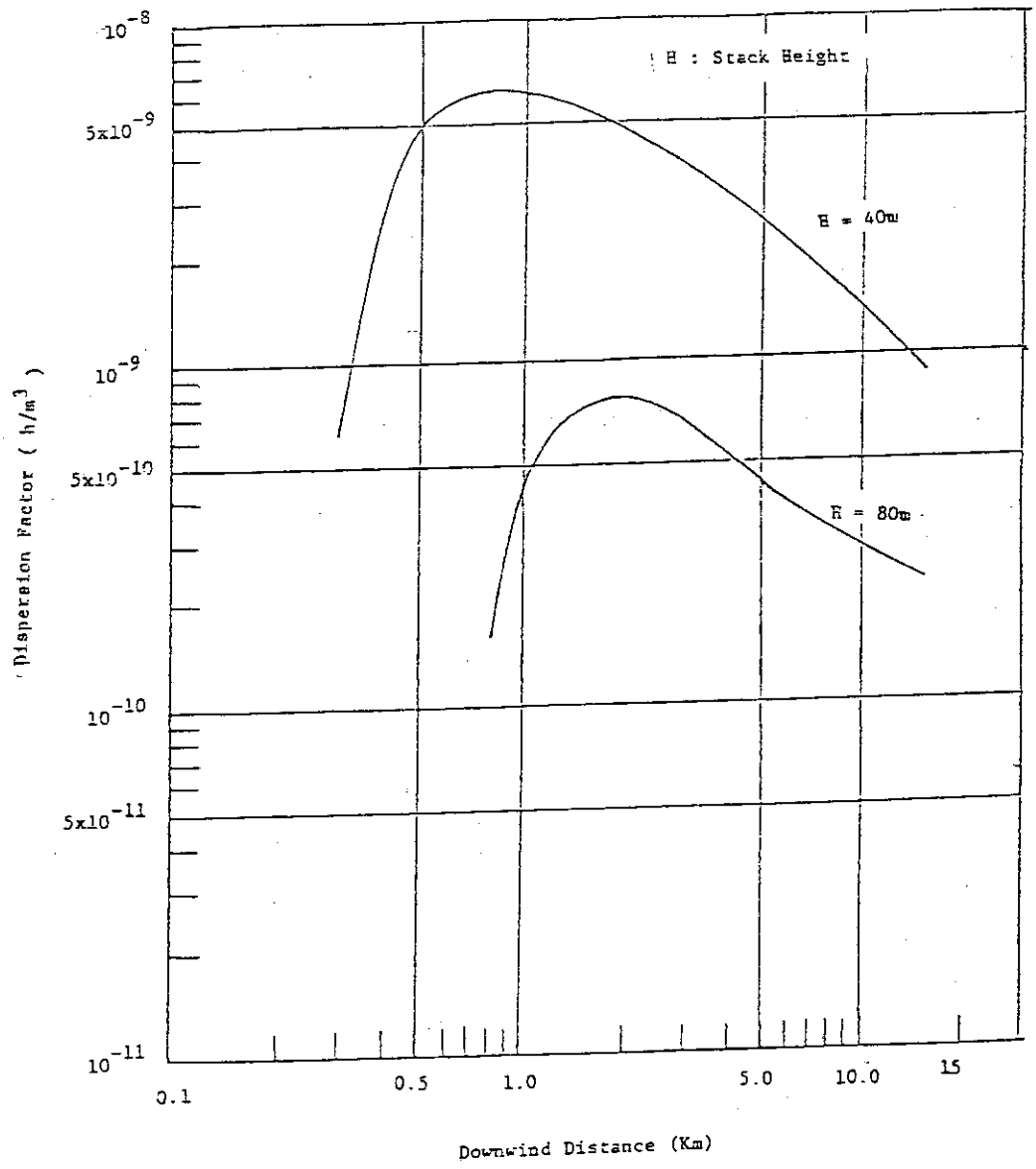

Fig. VIII-6-15 Dispersion Factor used for the Estimation of Accidental Release of HTO

Effective Release Time = 1hr

Acknowledgment

The authors are grateful to the people in Mitsubishi Atomic Power Industries for their contribution on the fabrication and inspection of sintered Li_2O pellets.

References

[1] Norval J. Hawkins, "Solubility of Hydrogen Isotopes in Nickel and Type 347 Stainless Steel to Hydrogen and Tritium ", KAPL-868 (April 13, 1953).

[2] D. Randall and O.N. Salmon, "Diffusion Studies I. The Permeability of Type 347 Stainless Steel to Hydrogen and Tritium ", KAPL-904 (August 24, 1953).

[3] G.W. Powell et al., "Solubility and Distribution of Tritium in Annealed and Cold Worked Stainless Steel in the 100 to 300°C Temperature Range", Corrosion NACE 26: 223-228 (1970).

[4] M.R. Louthan et al., "Tritium Adsorption in 304L Stainless Steel", DP-MS-74-25 (October 1974).

[5] K.F. Chaney and G.W. Powell, "The Diffusibity of Tritium in 304 Stainless Steel in the Temperature Range 100 to 300°C", Metallurgical Transactions 1: 2536-2537 (1970).

[6] J.H. Austin and T.S. Elleman, "Tritium Diffusion in 304 and 316 Stainless Steels in the Temperature Range 25 to 222°C", J. Nucl. Mater. 43 (1972) 119-125.

[7] R. Frauenfelder, "Solution and Diffusion of Hydrogen in Tungsten", Journal of Vacuum Science and Technology 6: 388-397 (1969).

[8] Mintz et al., "Tritium Diffusion", Nuclear Technology 31: 172 (1976).

[9] M.A. Abdou et al., "Tritium", FED-INTOR/TRIT/81-01, December 1981.

Acknowledgment

The authors are grateful to the people in Mitsubishi Atomic Power Industries for their contribution on the fabrication and inspection of sintered Li_2O pellets.

References

[1] Norval J. Hawkins, "Solubility of Hydrogen Isotopes in Nickel and Type 347 Stainless Steel to Hydrogen and Tritium ", KAPL-868 (April 13, 1953).

[2] D. Randall and O.N. Salmon, "Diffusion Studies I. The Permeability of Type 347 Stainless Steel to Hydrogen and Tritium ", KAPL-904 (August 24, 1953).

[3] G.W. Powell et al., "Solubility and Distribution of Tritium in Annealed and Cold Worked Stainless Steel in the 100 to 300°C Temperature Range", Corrosion NACE 26: 223-228 (1970).

[4] M.R. Louthan et al., "Tritium Adsorption in 304L Stainless Steel", DP-MS-74-25 (October 1974).

[5] K.F. Chaney and G.W. Powell, "The Diffusibity of Tritium in 304 Stainless Steel in the Temperature Range 100 to 300°C", Metallurgical Transactions 1: 2536-2537 (1970).

[6] J.H. Austin and T.S. Elleman, "Tritium Diffusion in 304 and 316 Stainless Steels in the Temperature Range 25 to 222°C", J. Nucl. Mater. 43 (1972) 119-125.

[7] R. Frauenfelder, "Solution and Diffusion of Hydrogen in Tungsten", Journal of Vacuum Science and Technology 6: 388-397 (1969).

[8] Mintz et al., "Tritium Diffusion", Nuclear Technology 31: 172 (1976).

[9] M.A. Abdou et al., "Tritium", FED-INTOR/TRIT/81-01, December 1981.

[10] T. Tanabe, N. Saito, Y. Etoh and S. Imoto, "Permeation and Reemission of Deuterium Implanted in First Wall Materials", J. Nucl. Mater. 103 & 104 (1981) 483-488.

[11] H. Katsuta and K. Furukawa, "Hydrogen and Deuterium Transport through Type 304 Stainless Steel at Elevated Temperatures", J. Nucl. Sci. Technol., 18, No.2 (Feb. 1981).

[12] C. Alender et al., "Tritium Diffusion in Nonmetallic Solids of Interest for Fusion Reactor", DOE/ET 52022-5.

[13] E.H. Van Deventer et al., "Hydrogen Permeation Characteristics of Aluminum-coated and Aluminum-modified Steels", J. Nucl. Mater., 88 (1980) 168-173.

[14] M. Ikeya, T. Miki, and M. Touge, Nature Vol. 292, 13 August 1981.

[15] T. Miki, M. Ikeya and M. Touge, J. Nucl. Mater. 101 (1981) 350-353.

[16] Y. Naruse et al., "Report for Group D: Tritium", Japan Contribution to INTOR Workshop, Session V, Phase IIA, July (1982).

[17] Koch-Sulzer Rectification Columns, Bulletin KS-1, Koch Engineering Company, INC., New York.

[18] N.J. Springfield, "Goodloe Column Packing", Packed Column Corporation.

[19] L.J. Wittenberg, "Experimental Verification of Tritium Control by Glovebox Containment", Nucl. Technl., vol. 38, May 1978.

[20] R.H. Land, V.A. Maroni, and M. Minkoff, "TSOAK-M1: A Computer Code to Determine Tritium Reaction/Release Parameters from Experimental Results of Air-Detritiation Tests", ANL Report ANL-79-82 (1980).

[21] P.A. Finn, R.G. Clemmer and B. Misra, "Tritium Management Requirements for D-T Fusion Reactors (ETF, INTOR, FED)", ANL-81-32 (1981).

[22] Technical Paper for MITI-AIE Nuclear Facility Decommissioning Meeting with Bechtel, Nov. 1981 (not for publication).

[23] S.K. Roy and R.L. Coble, "Solubility of Hydrogen in Porous Polyclystalline Aluminum Oxide", J. Am. Ceram. Soc., 50, (1967), 435.

[24] R.A. Causey, J.D. Fowler, C. Ravanbakht, T.S. Elleman and K. Verghese, "Hydrogen Diffusion and Solubility in Silicon Carbide", J. Am. Ceram. Soc., 61, (1978), 221.

[25] H. Katsuta and R.B. McLellan, "Diffusibity, Permeability and Solubility of Hydrogen in Platinum", J. Phys. Chem. Solids, 40, (1979), 697.

[26] H. Katsuta and R.B. McLellan, "Thermodynamics of Molybdenum-Niobium-Hydrogen Ternary Solid Solutions", J. Phys. Chem. Solids, 40, (1979), 845.

[27] D. Guggi, H.R. Ihle and U. Kurz, Proc. 9th Symp. on Fusion Technology, EUR 5602, (1976), 337.

[28] H. Kudo and K. Okuno, "Kinetic Stadies of Tritium Release Process in Newtron-Irradiated Li_2O and LiOH", J. Nucl. Mater., 101 (1981) 38-43.

[29] Y. Oishi, Y. Kamei, M. Akiyama and T. Yanagi, "Self Diffusion Coefficient of Lithium in Lithium Oxide", J. Nucl. Mater. 87, (1979), 341.

[30] K. Ando, Y. Oishi and T. Yoneda, "Determination of Oxygen Self-diffusion Coefficient in Polycrystalline Li_2O by gas-phase analysis", J. Nucl. Sci. Technol., 17, (1980), 269.

[31] T. Takahashi and T. Kikuchi, JAERI-M 7518 (1978).

[32] T. Takahashi and S. Nasu, Annual Meeting of the Atomic Energy Society of Japan, Tokyo (1981).

[33] N. Gregory and R. Mohr, J. Am. Chem. Soc. 77 (1955) 2142.

[34] K. Sako, M. Ohta, Y. Seki, H. Yamato, T. Hiraoka, K. Tanaka, N. Asami and S. Mori, JAERI-M 5502 (1973).

[35] V.G. Vasiliev, C.R. Borisov, N.N. Riapartseva and A.A. Vashman, US/USSR Workshop on Engineering and Economic Problems of EFT, Moscow and Leningrad (1979).

[36] K. Tanaka, H. Kudo and H. Amano, Proc. Radiation Effects and Tritium Technology for Fusion Reactors, CONF-750989, Vol. III (1976) p. 253.

[37] E.M. Larsen, S.I. Abdel-Khalik and M.S. Ortman, Nucl. Technol. 41 (1978) 12.

[38] K. Noda, K. Uchida, T. Tanifuji and S. Nasu, Phys. Rev. B 24 (1981) 3736.

[39] K. Noda, K. Uchida, T. Tanifuji and S. Nasu, J. Nucl. Mater. 91 (1980) 234.

[40] K. Uchida, K. Noda, T. Tanifuji, S. Nasu, T. Kirihara and A. Kikuchi, Phys. Status Solidi A 58 (1980) 557.

[41] I. Shindo, S. Kimura, K. Noda, T. Kurasawa and S. Nasu, J. Nucl. Mater. 79 (1979) 418.

[42] Y. Ueda, Y. Kasumata and M. Nishi, Japan, J. Appl. Phys. 16 (1977) 1743.

[43] Design and Fabrication of Reactor Pressure Vessel and Steam Generator 40 MWth HTGR (Peach Bottom - ANNEX - F), 1961.

[44] H. Kudo, C.H. Wu and H.R. Ihle, "Mass Spectrometric Study of the Vaporization of $Li_2O(s)$ and Thermochemistry of Gaseous LiO, Li_2O, Li_3O, and Li_2O_2", J. Nucl. Mater. 78 (1978) 380-389.

[45] H. Kimura, M. Asano and K. Kubo, "Thermochemical Study of the Vaporization of $Li_2O(c)$ by Mass Spectrometric Knudsen Effusion Method", J. Nucl. Mater. 92 (1980) 221-228.

[46] H. Watanabe et al., "Tritium Group Report-1", Japanese Contributions to INTOR Workshop, Phase II A, Session IV, 7-18 Dec. 1981.

[47] M. Hasegawa, "Hydrogen Damage of Stainless Steel as Structural Material (in Japanese)", JPI, Vol. 20, No.12, 1977, 36-41.

[48] K. Kamachi, "Hydrogen and Transformation in Metal (in Japanese)", Metal Physics Seminar, 3, No.5, 1978, 242-249.

[49] J. Saga et al., "Mechanical Properties of Hydrogen-absorbed Type 304 Stainless Steel (in Japanese)", Research Paper on Spring, No.24, 23-29.

[50] J.P. Bricout et al., "Study of retarded rupture of work-hardened austenitic stainless steel in cathodic hydrogen", Bull Carcel Etud Metaux, 14, No.9, 1980, 120-124.

[51] Hannu E. Haenninen and Tero J. Hakkarainen, "Influence of Metallurgical Factors on Hydrogen-induced Brittle Fracture in Austenitic Stainless Steel", Adv. Fract Rev, 4, 1982, 1881-1885.

[52] Hannu Haenninen and Tero Hakkarainen, "On the Effect of a Martensite in Hydrogen Embrittlement of Cathodically Charged AISI 304 Austenitic Stainless Steel", Corrosion, Vol.36, No.1, 1980, 47-51.

[53] E. Takahashi et al., "Hydrogen Embrittlement of Austenitic Stainless Steel Weld Metal (Report 2) (in Japanese)", Preprint of the National Meeting of the Japan Welding Society, No.28, 1981, 20-21.

[54] Y. Yoshida, Y. Naruse and T. Iijima, "Present Techniques for Control of Tritium Release and Experimental Monitoring in Fusion Research", J. Atom. Energy Soc. Japan, 21, 298 (1979).

[55] Japan AEC, "Guide for Meteorological Analysis for Safety Evaluation of Nuclear Reactors", (June, 1977).

[56] K. Imai, "A Computer Codes for Calculation of Relative Atmospheric Concentration, χ/Q and Relative Dose, D/Q in Potential Accident Consequence Assumed", to be published.

[57] M. Kakuta and T. Iijima, "Graphic Aid to Obtain Concentration of Materials Released from Nuclear plant to the Environment (Based on the English Method)": JAERI 1101 (1966).

[A1] H. Katsuta, S. Konishi and H. Yoshida, "Solubility and Diffusivity of Hydrogen in Li_2O Pellet", to be published in J. Nucl. Sci. Technol.

[A2] T. Takahashi and H. Watanabe, "Reaction of Li_2O with Moisture in He Atmosphere", to be published in JAERI-M.

[A3] K. Okuno and H. Kudo, "Rates of Tritium Release from Neutron-irradiated Sintered Li_2O Pellets", to be published in JAERI-M.

[N1] Japanese Contributions to IAEA INTOR Workshop, Phase IIA, Chapter I: Introduction, Chapter II: Summary and Recommendation, Chapter III: INTOR Concept, JAERI-M 82-170.

[N2] Japanese Contributions to IAEA INTOR Workshop, Phase IIA, Chapter IV: Plasma Confinement and Control, JAERI-M 82-171.

[N3] Japanese Contributions to IAEA INTOR Workshop, Phase IIA, Chapter V: RF heating and Current Drive, JAERI-M 82-172.

[N4] Japanese Contributions to IAEA INTOR Workshop, Phase IIA, Chapter VI: Impurity Control Physics, JAERI-M 82-173.

[N5] Japanese Contributions to IAEA INTOR Workshop, Phase IIA, Chapter VII: Impurity Control and First-Wall Engineering, JAERI-M 82-174.

[N6] Japanese Contributions to IAEA INTOR Workshop, Phase IIA, Chapter IX: Magnets, JAERI-M 82-176.

[N7] Japanese Contributions to IAEA INTOR Workshop, Phase IIA, Chapter X: Electromagnetics, JAERI-M 82-177.

[N8] Japanese Contributions to IAEA INTOR Workshop, Phase IIA, Chapter XI: Mechanical Configurations, JAERI-M 82-178.

[N9] Japanese Contributions to IAEA INTOR Workshop, Phase IIA, Chapter XII: Engineering Testing, JAERI-M 82-179.